uOttawa

L'Université canadienne
Canada's university

FACULTÉ DES ÉTUDES SUPÉRIEURES ET POSTOCTORALES

uOttawa

L'Université canadienne
Canada's university

FACULTY OF GRADUATE AND POSDOCTORAL STUDIES

Lei Gong

AUTEUR DE LA THÈSE / AUTHOR OF THESIS

Ph.D. (Civil Engineering)

GRADE / DEGREE

Department of Civil Engineering

FACULTÉ, ÉCOLE, DÉPARTEMENT / FACULTY, SCHOOL, DEPARTMENT

Dynamic Analysis of Long-Span Bridge Subjected to Traffic Loading

TITRE DE LA THÈSE / TITLE OF THESIS

Moe S. Cheung

DIRECTEUR (DIRECTRICE) DE LA THÈSE / THESIS SUPERVISOR

CO-DIRECTEUR (CO-DIRECTRICE) DE LA THÈSE / THESIS CO-SUPERVISOR

EXAMINATEURS (EXAMINATRICES) DE LA THÈSE / THESIS EXAMINERS

David Lau

Murat Saatchioglu

Ghyslaine McClure

Hiroshi Tanaka

Gary W. Slater

Le Doyen de la Faculté des études supérieures et postdoctorales / Dean of the Faculty of Graduate and Postdoctoral Studies

DYNAMIC ANALYSIS OF LONG-SPAN BRIDGE SUBJECTED TO TRAFFIC LOADING

Submitted by

Lei Gong, B.S., M.Eng

In fulfilment of the requirements for
The degree of Doctor of Philosophy

Thesis Supervisor: Professor M.S. Cheung

Department of Civil Engineering
University of Ottawa
Ottawa, Ontario, Canada
November 2008

Your file Votre référence
ISBN: 978-0-494-48654-2
Our file Notre référence
ISBN: 978-0-494-48654-2

ABSTRACT

Moving vehicle loads, associated with roadway traffic can induce significant dynamic effects in the structural behavior of bridges, especially for long-span bridges. The main objective of this research is to study traffic induced dynamic responses of long-span bridges, particular for box-girder bridges and cable-stayed bridges.

The finite element method has been employed in this study to obtain a three-dimensional mathematical model for the bridge system. For box-girder bridges, the deck, the box girders and the diaphragms are modeled as 8-node shell element. Linear elastic structural responses are considered. For cable-stayed bridges, the box-girder bridge deck and diaphragms are modeled as 8-node shell element, while the pylons are modeled as beam element. Stability functions are applied to both shell element and beam element to account for geometric nonlinearity. A two-node catenary cable element is adopted using exact analytical expressions for modeling stayed cables. Non-linear structural responses are considered.

For the present analytical study of the bridge-vehicle system, the vehicle is modeled as a three-axle six-wheel system. The equation derivations are described in details. The dynamic response is evaluated using the modal method and the step-by-step integration method. The natural frequencies and mode shapes of the bridge are obtained based on the deformed dead load tangent stiffness matrix. For cable-stayed bridge, an iterative scheme is utilized to obtain the deformed dead load tangent stiffness matrix due to its nonlinear characteristics.

The dynamic responses of bridges subjected to traffic loads are complicated because the dynamic effect induced by moving vehicles is basically influenced by the interaction between the bridge and the moving vehicle. The bridge-vehicle interaction is affected by many factors, such as vehicle speed, road roughness, damping of bridge and vehicle, dynamic characteristics

of bridge, and etc. Parametric study has been carried out to investigate those factors that influence the bridge-vehicle interaction.

The finite element computer program GLBA in FORTRAN 90 and MATLAB is developed to carry out the proposed research. GLBA includes four main modules: static linear analysis, static non-linear analysis, free vibration analysis and dynamic analysis due to traffic load.

ACKNOWLEDGEMENTS

I would like to take this opportunity to express my sincere gratitude to Professor Moe Cheung for his expert and patient guidance, encouragement and many valuable suggestions throughout the research program. The success of the present research would not be possible without his initiation and support.

Sincere appreciations are also expressed to Professor Hiroshi Tanaka and Professor David Lau for their sincerity and generosity in giving personal help and advice.

I wish to thank University of Ottawa and Department of Civil Engineering for providing the opportunity to carry on with my PhD's program. I also wish to thank Natural Science and Engineering Research Council of Canada for their financial support by providing me NSERC scholarship.

Finally, I express my deepest gratitude to my husband, my parents and my lovely daughter Sarah for their deep love, continued support and encouragement throughout my PhD. This thesis is dedicated to them.

TABLE OF CONTENTS

LIST OF FIGURES

LIST OF TABLES

Chapter 1

INTRODUCTION

1.1 Background of current Investigation

Bridges of increasing size and span have created phenomenal changes in the social patterns and economic conditions of areas by effectively eliminating water barriers between communities. They open new routes of communication between disintegrated and isolated communities, provide safe and efficient access to work, schools and recreation for people, and spur economic growth by facilitating trade within and between regions.

To meet the economic, social and recreational needs of the community for safe and efficient transportation systems, more and more long-span bridges have been built throughout the world. The volume of traffic and the speed of road vehicles over the bridge have increased tremendously. The ambition is to further increase the span length and use shallower and more slender girders for future bridges. To achieve this, accurate procedures need to be developed that can lead to a better understanding and a realistic prediction of the structural response due to not only wind and earthquake loading but also traffic loading.

1.2 Significance of the Present Research Work

The importance of vehicle-induced vibration with regard to the response and service life of bridges has long been recognized. In spite of the recognition of the importance and role of dynamic response in deterioration and fatigue damage, the use of current design practices can still result in bridges with undesirable dynamic response characteristics.

Heavy road vehicles moving on a long span bridge may significantly change the local dynamic behavior and affect the fatigue life of the bridge. The dynamic response amplifies both the deflections and the stresses induced in the bridge structure. Bridges should be designed to sustain such increased stresses and to keep the deflection within limits. On the other hand, the vibration of the bridge may in turn affect the running safety of road vehicles and the comfort of the passengers. The level of vibration should therefore be kept within the comfort zone.

The interaction between the bridge and road vehicles presents a complicated dynamic problem. A number of variables control the bridge – vehicle dynamic interaction. An insight into the mechanics of this problem is essential to develop an efficient numerical method for the analysis of bridge-vehicle response.

A number of analytical and experimental investigations have been carried out in the past to study the dynamic behavior of bridge decks traversed by moving vehicles. The vehicle has been modeled as moving load, moving mass, sprung mass or suspended rigid beam. A two-axle four-wheel 3-D vehicle model was presented in the analysis of box-girder bridge by Kashif (1992). A bridge was often modeled as continuous beam, two- dimensional plate, or three dimensional thin-walled beam / box girder. Cable-stayed bridges were usually modeled as beams and equivalent bar elements and the bridge – vehicle interaction analyses were carried out in 2-D models. However, long-span cable-stayed bridges built today are very flexible, they undergo large displacements, thus, should be analyzed using more refined models and accurate procedures.

The dynamic behavior of bridges subjected to moving vehicles is complicated. This is due to the fact that the dynamic effects induced by moving vehicles on the bridge are greatly influenced by the interaction between the vehicles and the bridge structure. A number of factors affect the vehicle-bridge interaction, such as vehicle speed, road roughness, damping of bridge and vehicle, dynamic characteristics of bridge, and etc. Although many investigations have been carried out in the past, there still remains a need for clearly identifying the important parameters that govern response. Due to the limitations of 2-D model in the analysis of long-span bridges, some important parameters such as multi lane effect need to be studied using 3-D model. Cable-stayed bridge systems, which are supported by cables instead of interval piers, have much more potential for nonlinear behavior than those of conventional continuous bridges. Although 2-D finite-element models have been widely studied, only the flexural mode has been considered. In order to estimate the importance of the lateral and torsional modes as well as their coupled modes for dynamic analysis, 3-D analysis should be called upon. In previous studies, the cables were modeled as tension-only truss elements with an equivalent modulus of elasticity, which only considers the sag effect but doesn't consider the stiffening effect due to large displacements. This approach results in softer cable response, especially for long-span bridges. In order to better study the cable nonlinearity due to its own sag and large displacements, the interaction between the cables and the bridge deck, and the interaction between the cables and the pylons, more accurate cable model should be developed.

1.3 Objectives of Research

The primary objective of the present research project is to develop suitable numerical models for handling both the vehicle and bridge responses that are of particular interest in long-span box-girder bridges and cable-stayed bridges. The finite element method is used to analyze the dynamic response of bridge structures. The following tasks will be carried out.

1. In this study, a more realistic 3-D vehicle model is developed, which consists of sprung and unsprung masses connected together by a system of springs and dash-pots. The vehicle is idealized as a three-axle, six -wheel system with a trailer pin connected to a

tractor, which is consistent to that specified by current bridge codes. The equations for bridge-vehicle interaction are derived and described in details.

2. For box-girder bridge modeling, 8-node isoparametric flat shell elements are adopted by combining existing membrane and bending elements. Free vibration analysis of two numerical examples, a cantilever beam and a simply supported thin flat plate, are presented to verify the reliability and accuracy of the proposed model.
3. Two box-girder bridges, Box-girder Bridge A and Confederation Bridge, are involved in the free vibration analysis and dynamic analysis subjected to traffic load. The results are compared with those obtained from previous research.
4. For cable-stayed bridges, due to the nonlinear characteristics, the pylons are modeled as three dimensional beam elements with stability functions to consider the coupling between axial and flexural stiffness; the cable elements are derived using the exact analytical expressions for the elastic catenary; and the bridge deck is modeled as 8-node isoparametric flat shell element with consideration of geometric nonlinearity. The stability functions of beam element are adopted from earlier studies. The geometric stiffness matrix of shell element is derived in the present study. The expressions of catenary cable element are derived according to the published algorithm. The natural frequencies and mode shapes of the bridge are obtained based on the deformed dead load tangent stiffness matrix. An iterative scheme is utilized to obtain the deformed dead load tangent stiffness matrix due to its geometric nonlinear characteristics.
5. To verify the proposed structural analysis model, a long-span box-girder cable-stayed bridge is studied with two types of cable arrangement, fan-type and harp-type.
6. Parametric studies will be carried out using 3-D bridge structure models and vehicle model. The following is a list of the important parameters.
    - Characteristics of the vehicle, which include: the number of axles, the axle spacing, axle loads, and the natural frequencies and damping of the vehicle.
    - Characteristics of the bridge structure, that is, its dimensions, support conditions, damping ratio and mass and stiffness distribution. These characteristics can be represented by the mode shapes and frequencies of the structure.

- Vehicle speed.
- The travel paths of vehicles on the bridge deck.
- The number of vehicles and their relative positions on the deck.

7. The finite element computer program GLBA is developed to carry out the proposed research, which is flexible to define a more realistic vehicle model and structural elements of the bridge. GLBA includes four main modules: static linear analysis, static non-linear analysis, free vibration analysis and dynamic analysis due to traffic load.

1.4 Outlines of the Thesis

The present work consists of three major parts, namely: (1) structural modeling of cable-stayed bridges and box-girder bridges, (2) vehicle modeling, and (3) bridge-vehicle interactions.

The outline of this report is given in the following:

- Chapter 1 introduces the problem to be investigated and the significance and scope of the present work.
- Chapter 2 is a literature review of the current investigations on the structure and vehicle modeling and the dynamic responses due to the bridge-vehicle interaction.
- Chapter 3 defines the box-girder bridge model. Formulations are also deduced in this chapter.
- Chapter 4 defines the cable-stayed bridge model. Formulations of stiffness matrix and mass matrix are derived.
- Chapter 5 defines the dynamic model of vehicle. Formulations of dynamic equations of vehicle and vehicle-bridge interaction are derived.
- Chapter 6 discussed the forced vibration of box-girder bridges subjected to vehicle transverse.
- Chapter 7 discussed the forced vibration of cable-stayed bridges subjected to vehicle transverse.
- Chapter 8 summarizes the conclusions and future work.

Chapter 2

LITERATURE REVIEW

2.1 Design Criteria

Most bridge codes specify the dynamic load as an additional static live load. The American Association of State Highway and Transportation Officials (AASHTO) Standard Specifications is the American bridge code that has been historically used for bridge design and construction. The AASHTO LRFD code was released in 1994. It is based on load and resistance factor limit states and was inspired by the Ontario Code. Both of these codes are still considered valid in the States. The AASHTO (1994) standard specifications formulated a simple empirical equation to relate the dynamic impact to the span length, where the span length is in feet as follows:

$$I = \frac{50}{L + 125} \tag{2.1}$$

The maximum value equals 0.30. This empirical equation was formulated decades ago and has been in effect since 1944. However, in the LRFD AASHTO (1998) bridge design specifications, live load is specified as a combination of HS20 truck and uniformly distributed load of 9.3 kN/m (640 lb/ft). The DLF equals 0.33 of the truck effect, with no dynamic load applied to the uniform loading.

The Ontario Highway Bridge Design Code (OHBDC 1983) specifies the dynamic load as a function of the first longitudinal natural frequency of the bridge. For a simply supported bridge with a uniform mass and flexural stiffness, the first natural frequency, f, is given by

$$f = \pi^2 \sqrt{\frac{EI}{mL^4}} \tag{2.2}$$

The dynamic responses are included by introducing Dynamic Load Allowance – an equivalent static load expressed as a fraction of the traffic load, which is considered to be equivalent to the dynamic and vibratory effects of the interaction of the moving vehicle and the bridge, including the vehicle response to irregularity in the riding surface. Values of the OHBDC 1991 dynamic load allowance fall between 0.2 and 0.4, with the higher values corresponding to frequencies between 2.5 and 4.5 Hz.

The Canadian Highway Bridge Design Code (CHBDC, CSA-S6-00) was published in 2000. It is based on limit states design. The truck models are defined according to statistical probability that the bridge structures will be overloaded. CHBDC 2000 specifies a constant value of 0.25 for medium- to long-span bridges and 0.4 for short span bridges. However, the CHBDC 2000 commentary in section C3.8.4.5 explains the background of the dynamic load allowance and the frequency approach adopted previously in OHBDC 1983 and 1991 stating that the reduction in dynamic load allowance was suggested during the code calibration process. However, the actual response of the structure seems to be characterized by a considerable degree of variation. This indicates to the importance of other factors, such as vehicle dynamics.

These design criteria provide safety and serviceability requirements of structures, but are based primarily on static loadings. They all adopted the impact factor for various dynamic responses, which is related to a single parameter, such as bridge span or natural frequency of vibration. Impact factor is defined as the ratio of dynamic response versus static response. In most cases, the response of bridge structures to static loadings can be determined satisfactorily by using simplified analysis. However, dynamic response depends on a number of factors. It is not so easy to predict while may be the major factor influencing bridge response. It has been reported that impact factor method according to current codes might oversimplified the complex physical phenomenon involved in the vehicle-bridge interaction, so that greatly underestimate

the actual bridge responses in many cases (Inbanathan and Wieland, 1987; Huang, et al, 1992; Galdos, et al, 1993; Chang and Lee, 1994; Nassif et. al., 2003). Therefore, it is important to develop formulas that reflect current situations.

2.2 Bridge – Vehicle Model

In the past years, there were many studies regarding the dynamic response of bridges subjected to moving vehicles. The early research can date back to the work of Jeffcott (1929). Many investigations have shown that the interaction between the vehicle and the bridge is a complex phenomenon governed by a large number of parameters.

Because of the complexity of bridge dynamics, it has not been possible to establish a clear correlation between the governing parameters and the bridge response even when sophisticated models are used in the analytical studies. In early studies, a moving vehicle traveling along a bridge was modeled as a moving load with the effect of inertia neglected (Tan and Shore 1968; Timoshenko et al. 1974; Warburton 1976; Sridharan and Mallik 1979). Such an assumption is valid for a wide range of problems encountered in bridge engineering, where the inertia of the vehicle is small enough compared to that of the bridge.

For those cases where the inertia of the vehicle cannot be ignored, a moving mass model has to be adopted instead (Blejwas et al. 1979; Inbanathan and Wieland 1987; Akin and Mofid 1989). The use of simplified models may be effective in identifying the important parameters as shown in Humar and Kashif (1992), in which they have carried out an analytical study of the beam model of a bridge. In that study, the response of the idealized beam structure is governed by three characterizing parameters: the speed parameter, the frequency ratio, and the mass ratio.

A beam model cannot truly represent a two-dimensional or three-dimensional behavior. On the other hand, the response of many bridge superstructures is multidimensional in nature, particularly under a moving vehicle whose path is not along the centerline of the bridge. Humar

and Kashif (1995) extended the beam model to a plate model. The bridge was idealized as an isotropic or orthotropic plate and the vehicle as a single sprung mass traveling along the deck in a direction parallel to span. Damping in both the bridge and the vehicle was ignored. It has concluded that the dynamic amplification factors for multiple presence of vehicles are, in general, lower than those for a single vehicle. It was also recognized that the model ignored certain important parameters which affect the response, such as the road roughness and vehicle configuration.

More sophisticated models that consider various dynamic characteristics of the moving vehicle have been used (Chu et al. 1986; Wang et al. 1991). In Hwang and Nowak(1991)'s study, models were developed for trucks, road surface (roughness) and the bridge. The statistical parameters were based on the results of surveys, tests and analysis. Truck parameters included the body (mass), suspensions, and tires. Road profiles were simulated using stochastic processes (power spectral density function). The Monte Carlo method was used to simulate the traffic on the bridge. Random variables including the truck type, total weight, axle distances, and speed were considered.

In the literature, Lagrange's equation with multipliers and constraint equations has been used in the analysis of vehicle-bridge systems (Blejwas et al. 1979). As it is well known, the use of Lagrange multipliers increases the number of unknowns. Therefore, Yang and Lin (1995) presented 'dynamic condensation method' to simulate the dynamic response of general vehicle-bridge systems. A typical vehicle-bridge model shown in Figure 2.1 was presented, in which a vehicle proceeding with speed v was idealized as a ridge beam resting on two suspension units, as represented by the springs and dashpots, and a bridge as a beamlike structure. In their study, an interaction element was defined such that it consisted of a bridge (beam) element and the suspension units of vehicles directly in contact with the element as shown in Figure 2.2, where the roughness of the road surface pavement was also indicated. For portions of the bridge that were not directly under the action of moving vehicles, only bridge elements were required. The composition of an interaction element and the parts of car bodies in contact was regarded as a substructure. By the dynamic condensation method, all the degrees of freedom associated with the car bodies existing within each substructure were eliminated. As the condensation was

performed on the element level, a conventional assembly process could be applied to form the structural equations. A road pavement profile was considered as a realization of a random process described by a power spectral density (PSD) function. As stated by the authors, the approach is suitable for the simulation of vehicle-bridge systems with various vehicle flow patterns.

The condensation method was also adopted in the analysis of railway bridges carrying high-speed trains, which consists of a number of cars in connection (Yang and Yau, 1997). A train was modeled as a series of sprung masses lumped at the bogie positions and a bridge with track irregularities by beam elements. Two sets of motion equations were coupled, one for the bridge and the other for each of the sprung masses. To solve the problem of coupling, the sprung mass equation was first discretized using Newmark's finite difference formulas and then condensed to that of the bridge element in contact. It has been concluded that high modes of vibration of the bridge affect more significantly the response of the vehicle than the bridge.

Hutton and Cheung (1979) studied the effects of vehicle and bridge parameters on the dynamic response of a box-girder bridge based on the finite-strip method. In their investigation, the vehicle was modeled as a plane rigid body supported at two points by suspension idealization. The road-surface profile was assumed to deviate from the horizontal by a sine wave of wavelength λ. However, the finite-strip-element method used in the study has some shortcomings. For example, it is not easy to isolate the effect of torsional and distortional warping on normal stresses from that of bending, to account for each type of structural action, to account for its relative significance in the overall behavior of the box, or to analyze the box-girder bridges with variable depth of cross section and complex boundary conditions. To improve it, Huang et al. (1995) presented a procedure for obtaining the dynamic response of thin-walled box-girder bridges due to truck loading. The box-girder bridge was divided into a number of thin-walled beam elements. Both warping torsion and distortion were considered in the study. The analytical vehicle was the AASHTO HS20-44 truck simulated as a nonlinear vehicle model with 11 independent degrees of freedom. Road-surface roughness was generated from power spectral density function. The analytical results showed that the dynamic response

of vertical bending moment was caused mainly by first several vibration modes, and that of torsion and distortion was greatly affected by the higher modes.

Finite-element method has also been used in the three-dimensional dynamic bridge analysis (Kou and DeWolf, 1997). Both two- and three-axle vehicle models were used in the study. The factors influencing the dynamic behavior were evaluated, which were the dimensions; the material properties; the section properties; the damping characteristics; the surface roughness; and the vehicular weights, speeds and locations.

Road traffic flow and composition are highly variable parameters, dependent upon the road type and the geo-economic conditions of the site in question. Its intrinsic complexity is further increased by changes over time, in particular, traffic conditions alternating from free-flowing to congested, which are quite difficult to predict theoretically. In order to be considered meaningful, traffic records must reproduce all the significant parameters of the traffic to be expected on the bridge in question; these are the yearly vehicular flow, vehicle weights and types, and their relative statistical distributions. A stochastic model (Croce and Salvatore 2001) was developed to reproduce the actual traffic while at the same time accounting for traffic interactions in one or several lanes. In the proposed model, real traffic was regarded as being made up of a set of standard vehicles, whose length and weight are stochastic variables distributed according to appropriate probability laws. The parameters of these laws could be deduced from traffic recordings, while the event of a single vehicle's arrival on the bridge was described through an equilibrium renewal stochastic process. In that way, an appropriate analytical-numerical procedure was derived, so that analysis of arbitrary mixtures of flowing and congested traffic could be performed under very general hypotheses, while also accounting for several loaded lanes, thereby arriving at extreme-value distributions of traffic effects.

Recently, the dynamic vehicle element (DVE) method was developed to solve the transient response of a vehicle–structure interaction system in time domain (Pan and Li, 2002). The DVE method treated the vehicle as a moving part of the entire system, which considered the vehicle influence at the element level by incorporating the detailed interaction between multiple vehicles and the structure induced by irregular road profiles. A simplified decoupled dynamic

nodal loading (DNL) method was proposed. The DNL method generated a time series of concentrated nodal loading which represented the vehicle reaction force on the structure. The DNL method accounted for the road irregularities and vehicle inertia effect, but neglected the interaction between the two subsystems.

2.3 Cable - Stayed Bridges

In recent years, some papers on the impact on cable-stayed bridges due to the vehicles have been published. Morris (1974, 1976) studied the dynamic response of a cable-stayed bridge subjected to stationary loads by using direct integration method. Fleming and Egeseli (1980) investigated the dynamic response of a cable-stayed bridge to seismic and wind loads and the load of a single moving force. Rasoul (1981) studied the dynamics of a cable-stayed bridge with two cables by the structural impedance algorithm.

Karoumi (1996) analyzed cable-stayed bridge dynamic response using a simple bridge model, namely a continuous beam on elastic supports and a simple vehicle model consisting of a single sprung mass shown in Figure 2.3. The vehicle model was a suspension model with two degrees of freedom. The author believed that it was adequate if the real vehicle length was small compared with the bridge length. The equation of motion of the vehicle was established as

$$\begin{aligned} &-(m_1+m_2)g-m_1\frac{d^2w_1}{dt^2}+k_s(w_2-w_1)+c_s(\frac{dw_2}{dt}-\frac{dw_1}{dt})+F(t)=0 \\ &m_2\frac{d^2w_2}{dt^2}+k_s(w_2-w_1)+c_s\left(\frac{dw_2}{dt}-\frac{dw_1}{dt}\right)=0 \end{aligned} \tag{2.3}$$

where $w_1(t)$ and $w_2(t)$ = the displacements of the vehicle unsprung mass m_1 and sprung mass m_2, respectively; k_s = stiffness of the spring connecting the two masses; c_s = damping coefficient of the viscous damper; and g = acceleration of gravity. The coupling equations for the point of contact between bridge deck and vehicle ($x(t) = x_v(t)$) were as

$$w_1(t)=y(x(t),t),\quad \dot{w}_1(t)=\frac{\partial y}{\partial x}v+\frac{\partial y}{\partial t},\quad \ddot{w}_1(t)=\frac{\partial^2 y}{\partial x^2}v^2+\frac{\partial^2 y}{\partial x\partial t}2v+\frac{\partial y}{\partial x}a+\frac{\partial^2 y}{\partial t^2} \tag{2.4}$$

where v = vehicle velocity; a = vehicle acceleration; and y(x(t),t) = bridge displacement. The self anchored fan-shaped cable-stayed bridge was defined with the following assumptions:

- uniform mass and flexural rigidity of the stiffening girder;
- cable forces under dead load were so adjusted that all displacements remained zero;
- axial girder forces had negligible effect on frequencies and mode shapes
- negligible cable mass
- bridge damping was small and therefore neglected
- bridge / vehicle system was at rest when the vehicle entered the main span of bridge
- road surface was in excellent shape, which meant the excitation of the dynamic system was caused only by the elastic displacement of the bridge
- the effects of rotation inertia and shear deformation were neglected

The governing equation of motion for vertical vibration of the bridge at any section of the stiffening girder was given by

$$E_g I_g \frac{\partial^4 y(x,t)}{\partial x^4} + k_c(x)\, y(x,t) + m_g \frac{\partial^2 y(x,t)}{\partial t^2} = -\delta(x - x_v)F(t) \qquad (2.5)$$

where δ = the Dirac delta function; E_g = modulus of elasticity; I_g = moment of inertia; m_g = mass per unit length; and k_c = spring stiffness.

Wang and Huang (1992) analyzed the cable-stayed bridge vibration due to the vehicle moving over different classes of roads with various speeds. A nonlinear vehicle model with seven degrees of freedom (DOF) was developed according to AASHTO HS20-44 truck, which is shown in Figure 2.4. The vehicle model consisted of five rigid masses as tractor, semi-trailer, steer wheel-axle set, tractor wheel-axle set, and trailer wheel-axle set. The tractor and semi-trailer were individually assigned two DOFs, corresponding to the vertical displacement (Y_{ti}) and rotation about the transverse axis (θ_{ti}). Each wheel-axle set was provided with one DOF in the vertical direction (Y_{ai}). Suspension force consisted of linear elastic spring force and constant interleaf friction force. The load-displacement relationship for friction force, suspension spring force, and the combination of the two forces are shown in Figure 2.5. The tire springs and all dampers were assumed to be linear. The equations of motion of the vehicle system were derived by using Lagrange's formulation:

$$\frac{d}{dt}\left(\frac{\partial T}{\partial \dot{q}_i}\right)-\frac{\partial T}{\partial \dot{q}_i}+\frac{\partial V}{\partial q_i}+\frac{\partial D}{\partial \dot{q}_i}=0 \tag{2.6}$$

where V = total potential energy of the system computed from the spring stiffness and relative displacements; T = total kinetic energy of the system calculated by using the masses and velocities of the system components; D = dissipation energy of the system obtained from the damping forces; and q_i and $\dot{q}$ = generalized displacements and velocities. The dynamic response of the cable-stayed bridge was analyzed with the finite-element method. The bridge deck was divided into beam elements. The node parameters were

$$\boldsymbol{\delta}^e=\begin{Bmatrix}\boldsymbol{\delta}_i\\ \boldsymbol{\delta}_j\end{Bmatrix} \tag{2.7}$$

in which $\boldsymbol{\delta}_i=[\theta_i\ u_i\ v_i]^T$; $\boldsymbol{\delta}_j=[\theta_j\ u_j\ v_j]^T$; u, v = transverse displacements in x- and y-direction, respectively; and θ = rotational displacement. The element stiffness matrix of a beam subjected to an axial force P was written in the form

$$\mathbf{K}_b=\mathbf{K}_{bl}+\mathbf{K}_{bg} \tag{2.8}$$

in which $\mathbf{K}_{bl}$ = the standard linear stiffness matrix and $\mathbf{K}_{bg}$ = the geometric stiffness matrix due to axial force P. P varied with both dead loads and vehicle loads. The element consistent mass matrix was used in the dynamic analysis. "Because the cable represents a flexible member with virtually no resistance to applied bending moments, its load-deformation relationship exhibits distinctly nonlinear behavior under normal design loads" (Wang and Huang, 1992). The authors considered an equivalent straight member with an equivalent modulus of elasticity to deal with the nonlinearity in the inclined cable stays.

$$E_{eq}=\frac{E_c}{\left[1+\dfrac{(wl_c)^2E_cA}{12P^3}\right]} \tag{2.9}$$

where E_c = cable material modulus of elasticity; l_c = horizontal projected length of the cable; w = weight per unit length of the cable; A = cross-sectional area; and P = cable tensile force. The element stiffness matrix for an inclined cable corresponding to the degrees-of-freedom shown in Equation 2.7 was written as

$$\mathbf{K}_c = \begin{bmatrix} 0 & 0 & 0 & 0 & 0 & 0 \\ 0 & R & 0 & 0 & -R & 0 \\ 0 & 0 & 0 & 0 & 0 & 0 \\ 0 & 0 & 0 & 0 & 0 & 0 \\ 0 & -R & 0 & 0 & R & 0 \\ 0 & 0 & 0 & 0 & 0 & 0 \end{bmatrix} \tag{2.10}$$

where $R = A\, E_{eq} / l_c$. The equation of motion of the bridge was

$$\mathbf{M}_B\ddot{\boldsymbol{\delta}} + \mathbf{D}_B\dot{\boldsymbol{\delta}} + \mathbf{K}_B\boldsymbol{\delta} = \mathbf{F}_{BT} \tag{2.11}$$

in which $\mathbf{M}_B$ = global mass matrix; $\mathbf{K}_B$ = global stiffness matrix; $\mathbf{D}_B$ = damping matrix; $\ddot{\boldsymbol{\delta}}$, $\dot{\boldsymbol{\delta}}$ and $\boldsymbol{\delta}$ = global nodal displacement, velocity and acceleration vectors; and $\mathbf{F}_{BT}$ = global nodal loading vector due to the interaction between the bridge and vehicle. The interaction force of the ith axle between the bridge and vehicle was given as

$$\mathbf{F}_{BT}^{i} = \mathbf{K}_{tyi}\mathbf{U}_{tyi} + \mathbf{D}_{tyi}\dot{\mathbf{U}}_{tyi} \tag{2.12}$$

in which $\mathbf{K}_{tyi}$ = tire stiffness of the ith axle; $\mathbf{D}_{tyi}$ = tire damping coefficient of the ith axle; $\mathbf{U}_{tyi}$ = relative displacement of the ith axle and bridge = $Y_{ai} - (-u_{sri}) - (-Y_{bi})$; Y_{ai} = vertical displacement of the ith axle; u_{sri} = road surface roughness under the ith axle; and Y_{bi} = bridge vertical displacement under the ith axle. The typical road surface was described by a periodically modulated random process.

Brownjohn and Xia (2000) also studied the dynamic responses of cable-stayed bridges using finite element (FE) model. After comparing the FE results with the measured results, it was found that the structure should be modeled with as much detail as possible to represent geometric and structural form for successful dynamic assessment of the structure.

The implementation of the finite-element model updating was recently presented for the Kap Shui Mun Bridge, a 430 m main span double-deck cable-stayed bridge in Hong Kong shown in Figure 2.6 (Zhang et al., 2001; Chang et al., 2001). Ambient vibration measurements were conducted. The dynamic characteristics of the bridge were studied through both three-dimensional finite-element prediction and field vibration measurement. The finite-element model was updated in an iterative fashion so as to minimize the differences between the

predicted and the measured natural frequencies. The results suggested that it might be possible to update the finite-element model so that the natural frequencies are reasonably close to the measured ones. Complete elimination of the frequency differences, however, seemed difficult at this time due to a few philosophical and practical assumptions introduced before and during the formulation of the model updating process.

A nonlinear analysis of cable-stayed bridge model has recently been carried out by George (1999). The three-dimensional finite-element model was formulated based on the geometric and material properties of the Quincy Bayview cable-stayed bridge, a three-span cable-stayed bridge crossing the Mississippi River and connecting Illinois and Missouri, in the United States. The complete finite model and the Quincy Bayview elevation are shown in Figure 2.7 and Figure 2.8, respectively. The author adopted the recent American and British bridge traffic live loads, which considered the static jam situation resulting from a stoppage of traffic. The effects of number and spacing cables as well as deck material were investigated. It was found that the choice of material for the deck could be greatly affected by the distribution of stays and by the intensity of the live load adopted.

Ren (1999) also investigated the nonlinear static and ultimate behavior of a long-span cable-stayed bridge up to failure and evaluated the overall safety of the bridge. The geometric nonlinearities were caused by the cable sag effect, axial force-bending interaction effect, and large displacement effect. Material nonlinearities arose when one or more bridge elements exceeded their individual elastic limits. The results showed that the overall safety of a long-span cable-stayed bridge was controlled primarily by the material nonlinear behavior of individual bridge elements. Live load uniformly distributed only in the central span was more harmful to the long-span cable-stayed bridge.

Techniques of dynamic tests and measurements for modal parameter identification on long-span bridges have been studied and developed in the past years. They can be generally classified into the three following types: (1) forced vibration tests; (2) ambient vibration tests; and (3) free vibration tests. In case of large and flexible bridges with significant natural frequencies in the range of 0–1 Hz, like cable-stayed or suspension bridges, it becomes difficult

and costly to provide controlled excitation at high enough levels. Alternatively, some researchers have been interested in ambient vibration method (Cunha et al. 2001; Zhang et al. 2001; and Chang et al. 2001). This method only requires the measurement of the structural response under ambient excitation, usually due to wind or traffic, and can lead to accurate estimates of the modal parameters quickly and inexpensively. Furthermore, it can provide the benefit of avoiding the shut-down of vehicle traffic during the tests caused by the installation of heavy shakers. The usual testing procedure consists of performing several measurements simultaneously at one or more reference points and at different other points along the structure.

2.4 Summary

Based on the published literature on the dynamic analysis of bridges, particularly long span and cable-stayed bridges, due to traffic loading, the following comments are made.

1. In all the aforementioned studies, the vehicle models can be categorized as 1) a moving load; 2) a moving mass; 3) sprung mass; and 4) suspended rigid beam, which are shown in Figure 2.9.
2. The bridges have been modeled as 1) continuous beam on elastic supports; 2) two-dimensional plate; and 3) three dimensional thin-walled beam / box girder.
3. For solving the vehicle-bridge interaction problems, the authors used Lagrange multiplier, condensation method and finite element /finite strip method for either linear analysis or nonlinear analysis. Among the refined methods, the finite-element method is probably the most involved and time consuming. However, it is still the most general and comprehensive technique for static and dynamic analysis, capturing all aspects affecting the structural response. The other methods proved to be adequate but limited in scope and applicability.

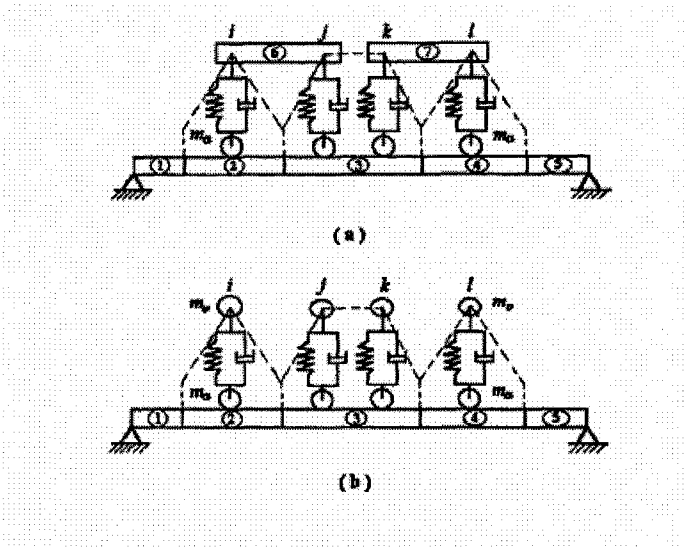

FIGURE 2.1 VEHICLE-BRIDGE SYSTEM: (A) GENERAL MODEL; (B) LUMPED MASS MODEL

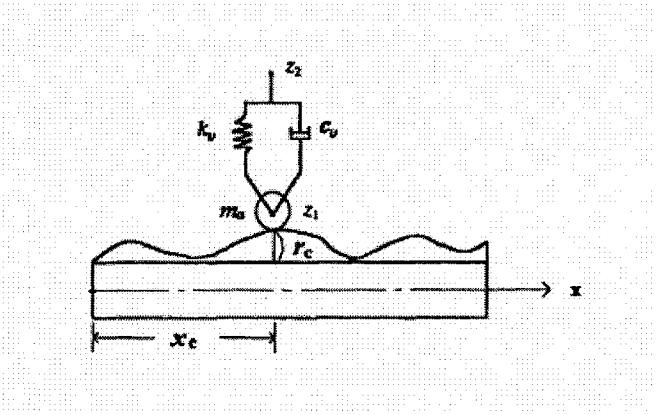

FIGURE 2.2 VEHICLE-BRIDGE INTERACTION ELEMENT

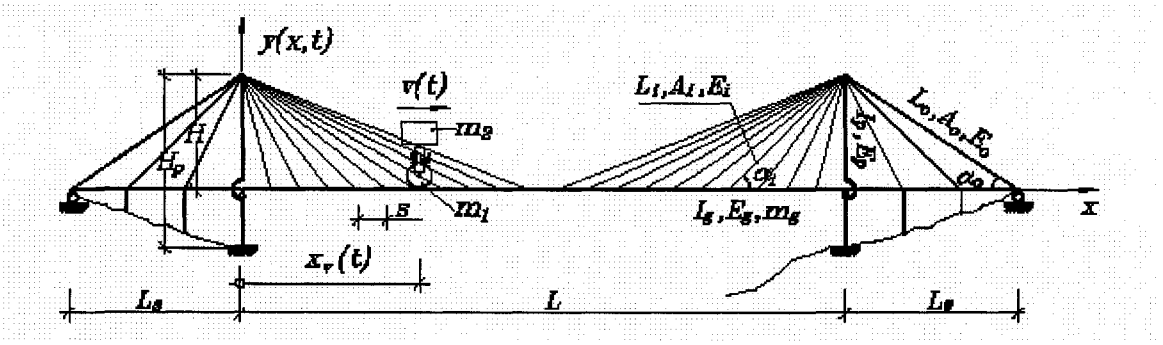

FIGURE 2.3 IDEALIZED VEHICLE IN CONTACT WITH A CABLE-STAYED BRIDGE

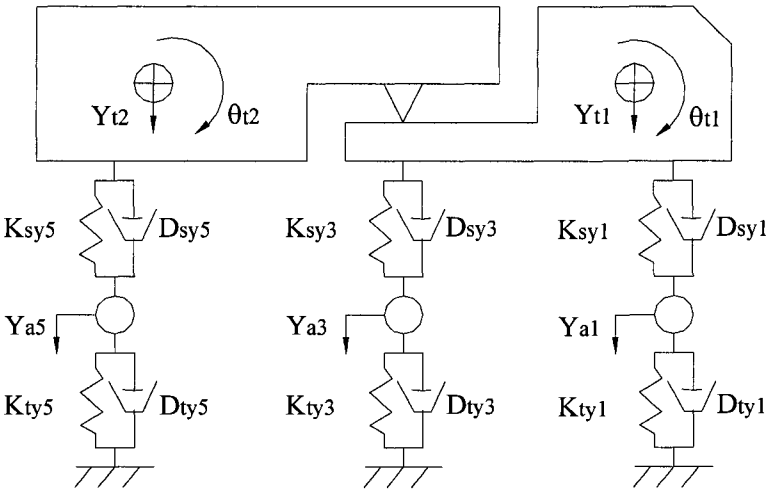

FIGURE 2.4 SIDE VIEW OF VEHICLE MODEL

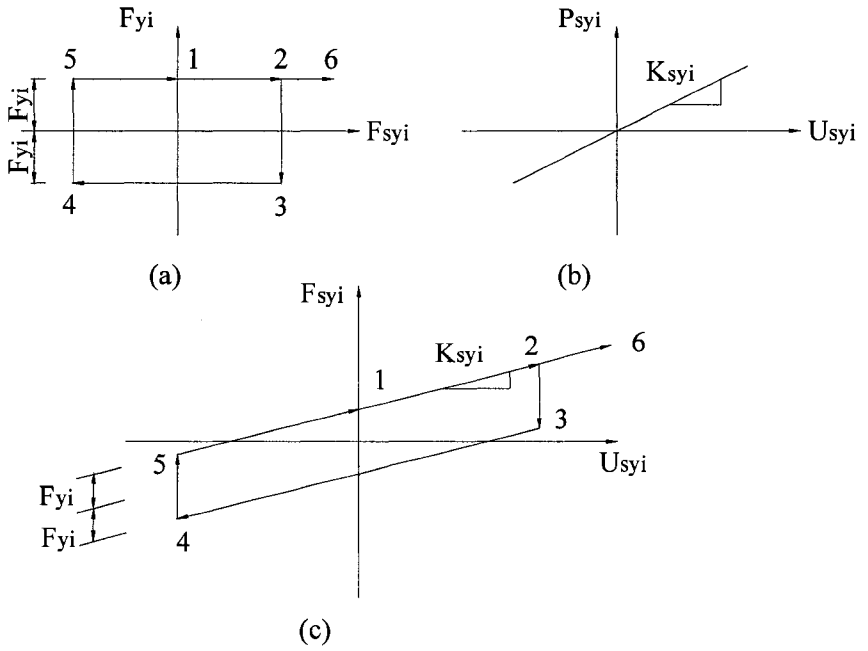

FIGURE 2.5 RELATIONSHIP BETWEEN FORCES AND DISPLACEMENTS IN VEHICLE SUSPENSION SYSTEM: (A) FRICTION FORCE; (B) SUSPENSION SPRING FORCE; (C) COMBINATION OF FRICTION AND SUSPENSION SPRING FORCES

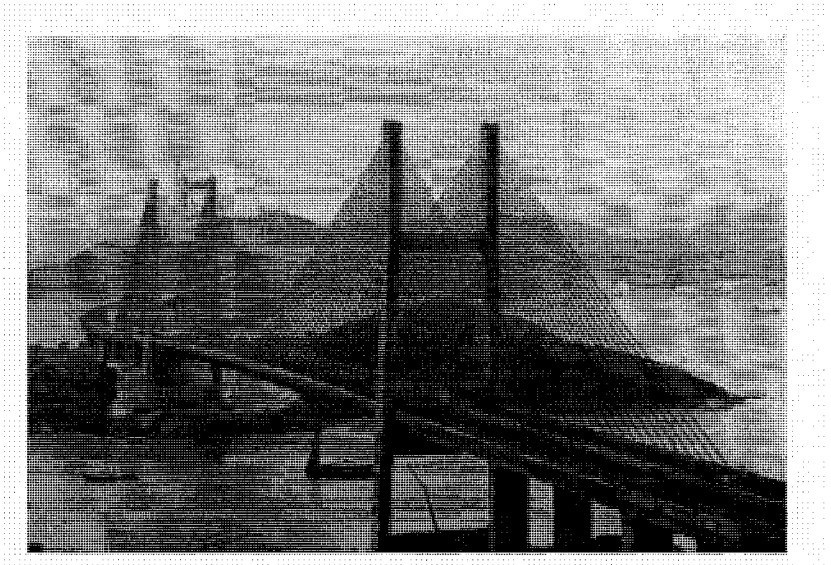

FIGURE 2.6 KAP SHUI MUN CABLE-STAYED BRIDGE IN HONG KONG

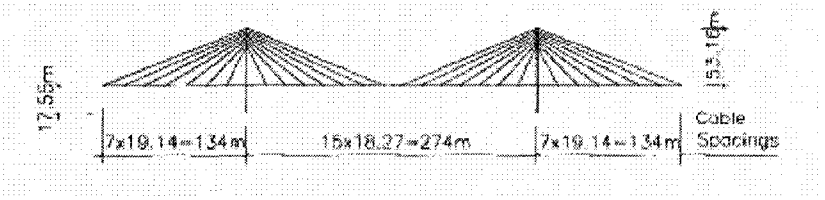

FIGURE 2.7 QUINCY BAYVIEW ELEVATION

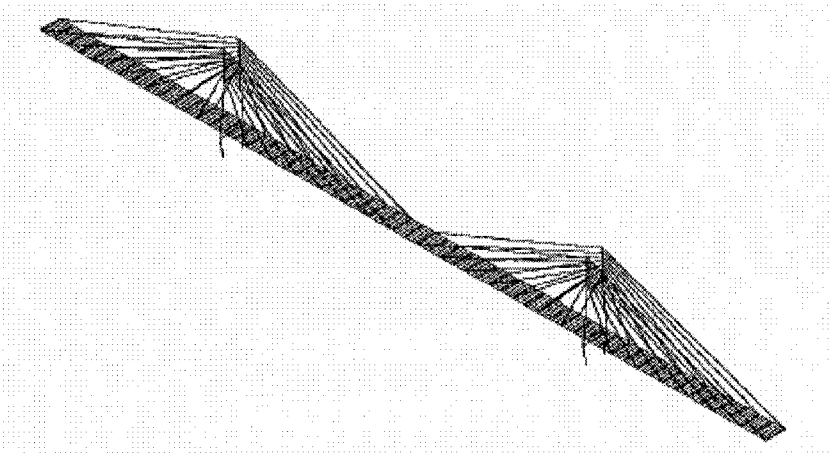

FIGURE 2.8 COMPLETE FINITE ELEMENT MODEL

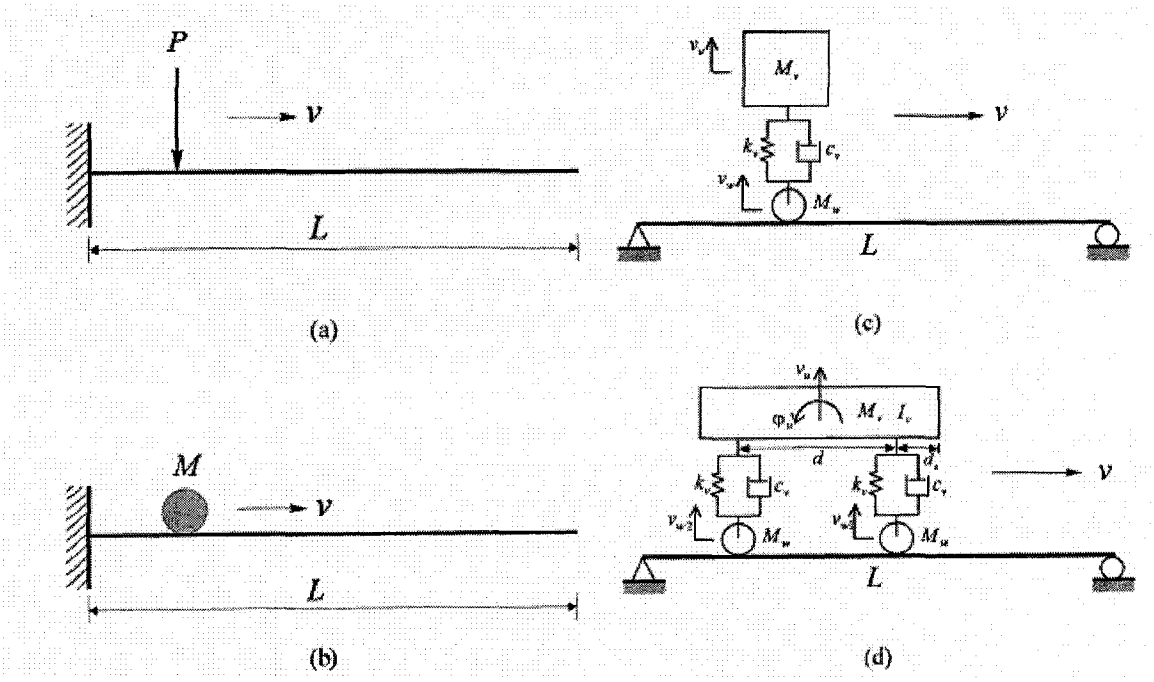

FIGURE 2.9 VEHICLE MODEL: (A) MOVING LOAD; (B) MOVING MASS; (C) SPRUNG MASS; (D) SUSPENDED RIGID BEAM

Chapter 3

STRUCTURAL ANALYSIS OF BOX-GIRDER BRIDGES

3.1 Introduction

Box-girder and deck type bridges have been proven to be very efficient structural forms for medium to long-span bridges. These bridges normally consist of interconnected plate elements of either prestressed or reinforced concrete, or structural steel, or a combination of them, which provide sufficient flexural and torsional strength to resist applied loads. Box-girder bridges can be easily constructed to follow any required alignment in plan and require relatively small amount of maintenance. They are usually aesthetically pleasing and are well suited to carrying pipes, cables, conduits and utilities.

The finite element method has been employed in this study to obtain an analytical model for the bridge system. Both the natural frequencies and the dynamic response of the box-girder bridge will be assessed using this analytical model.

The accuracy of mathematical model in predicting response is mostly based on the closeness of the proposed idealization to the realistic behavior of different components comprising the bridge system. Therefore a comparison study has been carried out to determine the suitable finite element model to represent the different components of the bridge.

The deck, the box girders and the diaphragms are the three main parts of the bridge structure. They usually have a small thickness compared with other dimensions of the bridges. A flat shell element is adopted in the proposed computer program GLBA and presented hereafter to model them all.

3.2 Stiffness and Mass Formulation

The flat shell formulation is based on the theory of plates with transverse shear deformations included. This theory, due to R. D. Mindlin (Hinton and Owen, 1984), uses the assumption that particles of the plate originally on a straight line that is normal to the undeformed middle surface remain on a straight line during deformation, but this line is not necessarily normal to the deformed middle surface. The detailed equation derivation presented hereafter has adopted the algorithm and procedure introduced by Hinton and Owen (1984) but followed the coordinate system shown in Figure 3.1.

3.2.1 Displacement Function and Isoparametric Transformation

The 8-node shell element shown in Figure 3.1 has 5 degrees of freedom for each node, i.e. two in-plane or membrane displacements along x and y axes, one transverse displacement and two rotations. With the above assumption, the displacement components of a point having coordinate (x, y, z) are, in the small displacement bending theory,

$$u(x,y,z) = u_0(x,y) - z \cdot \beta_x(x,y) \tag{3.1a}$$

$$v(x,y,z) = v_0(x,y) - z \cdot \beta_y(x,y) \tag{3.1b}$$

$$w(x,y,z) = w_0(x,y) \tag{3.1c}$$

where $u_0(x, y)$ and $v_0(x, y)$ are the membrane displacements in the x and y direction, $w_0(x, y)$ is the transverse displacement, and β_x and β_y are the rotations of the normal to the undeformed middle surface in the x, z and y, z planes, respectively.

The analyses of arbitrarily shaped shell elements are carried out on the ξ-η plane. For a typical element, the following Serendipity shape functions are defined for nodes 1 to 8 in terms of natural coordinate ξ and η (Figure 3.2):

For corner node $i = 1, 3, 5, 7$

$$N_i = \frac{1}{4}(1+\xi\cdot\xi_i)(1+\eta\cdot\eta_i)(\xi\cdot\xi_i+\eta\cdot\eta_i-1) \tag{3.2a}$$

and for middle node $i = 2, 4, 6, 8$

$$N_i = \frac{1}{2}\xi_i^2(1+\xi\cdot\xi_i)(1-\eta^2)+\frac{1}{2}\eta_i^2(1+\eta\cdot\eta_i)(1-\xi^2) \tag{3.2b}$$

An arbitrary point (x, y) in a typical isopametric 8-node element can be expressed as

$$\begin{aligned} x &= \sum_{i=1}^{8} N_i\cdot x_i \\ y &= \sum_{i=1}^{8} N_i\cdot y_i \end{aligned} \tag{3.3}$$

in which x_i and y_i are the coordinates of the i^{th} node in the x-y coordinate system.

From the above transformation, the Jacobian matrix of the element is defined as

$$\mathbf{J} = \begin{bmatrix} \dfrac{\partial x}{\partial \xi} & \dfrac{\partial y}{\partial \xi} \\ \dfrac{\partial x}{\partial \eta} & \dfrac{\partial y}{\partial \eta} \end{bmatrix} = \begin{bmatrix} \displaystyle\sum_{i=1}^{8}\frac{\partial N_i}{\partial \xi}x_i & \displaystyle\sum_{i=1}^{8}\frac{\partial N_i}{\partial \xi}y_i \\ \displaystyle\sum_{i=1}^{8}\frac{\partial N_i}{\partial \eta}x_i & \displaystyle\sum_{i=1}^{8}\frac{\partial N_i}{\partial \eta}y_i \end{bmatrix} \tag{3.4}$$

For any function $f(\xi, \eta)$, the following relationships hold:

$$\begin{Bmatrix} \dfrac{\partial f}{\partial \xi} \\ \dfrac{\partial f}{\partial \eta} \end{Bmatrix} = \begin{bmatrix} \dfrac{\partial x}{\partial \xi} & \dfrac{\partial y}{\partial \xi} \\ \dfrac{\partial x}{\partial \eta} & \dfrac{\partial y}{\partial \eta} \end{bmatrix} \begin{Bmatrix} \dfrac{\partial f}{\partial \xi} \\ \dfrac{\partial f}{\partial \eta} \end{Bmatrix} = \mathbf{J} \begin{Bmatrix} \dfrac{\partial f}{\partial x} \\ \dfrac{\partial f}{\partial y} \end{Bmatrix} \tag{3.5}$$

Thus, the derivatives of $f(\xi, \eta)$ with respect to x and y are obtained as

$$\begin{Bmatrix} \dfrac{\partial f}{\partial x} \\ \dfrac{\partial f}{\partial y} \end{Bmatrix} = \mathbf{J}^{-1} \begin{Bmatrix} \dfrac{\partial f}{\partial \xi} \\ \dfrac{\partial f}{\partial \eta} \end{Bmatrix} = \frac{1}{|\mathbf{J}|} \begin{bmatrix} \dfrac{\partial y}{\partial \eta} & -\dfrac{\partial y}{\partial \xi} \\ -\dfrac{\partial x}{\partial \eta} & \dfrac{\partial x}{\partial \xi} \end{bmatrix} \begin{Bmatrix} \dfrac{\partial f}{\partial \xi} \\ \dfrac{\partial f}{\partial \eta} \end{Bmatrix} \tag{3.6}$$

The displacements and normal rotations at any point (ξ, η) in a typical element can be expressed as

$$u_0(\xi,\eta) = \sum_{i=1}^{8} N_i \cdot u_i \tag{3.7a}$$

$$v_0(\xi,\eta) = \sum_{i=1}^{8} N_i \cdot v_i \tag{3.7b}$$

$$w_0(\xi,\eta) = \sum_{i=1}^{8} N_i \cdot w_i \tag{3.7c}$$

$$\beta_x(\xi,\eta) = -\sum_{i=1}^{8} N_i \cdot \theta_{yi} \tag{3.7d}$$

$$\beta_y(\xi,\eta) = \sum_{i=1}^{8} N_i \cdot \theta_{xi} \tag{3.7e}$$

in which u_i, v_i and w_i are the translations of the i^{th} node in the x, y and z direction, and θ_{xi} and θ_{yi} are the rotations of the i^{th} node about x and y axes respectively (i = 1, 2, 3, ..., 8). Substituting Equation 3.7 into 3.1, the total displacement can be expressed in the matrix form as

$$\begin{Bmatrix} u \\ v \\ w \end{Bmatrix} = \mathbf{N} \cdot \boldsymbol{\delta} \tag{3.8}$$

where **N** is the so-called displacement shape function as

$$\mathbf{N} = \begin{bmatrix} N_1 & 0 & 0 & 0 & zN_1 & N_2 & 0 & 0 & 0 & zN_2 & \cdots & N_8 & 0 & 0 & 0 & zN_8 \\ 0 & N_1 & 0 & -zN_1 & 0 & 0 & N_2 & 0 & -zN_2 & 0 & \cdots & 0 & N_8 & 0 & -zN_8 & 0 \\ 0 & 0 & N_1 & 0 & 0 & 0 & 0 & N_2 & 0 & 0 & \cdots & 0 & 0 & N_8 & 0 & 0 \end{bmatrix} \tag{3.9}$$

and $\boldsymbol{\delta}$ is the element displacement vector as

$$\boldsymbol{\delta} = \begin{bmatrix} u_1 & v_1 & w_1 & \theta_{x1} & \theta_{y1} & u_2 & v_2 & w_2 & \theta_{x2} & \theta_{y2} & \cdots u_8 & v_8 & w_8 & \theta_{x8} & \theta_{y8} \end{bmatrix}^T \tag{3.10}$$

3.2.2 Formulations of Stresses and Strains

The membrane strains $\boldsymbol{\varepsilon}_m$ in the shell element are given by

$$\boldsymbol{\varepsilon}_{\mathbf{m}} = \begin{bmatrix} \varepsilon_{xx} \\ \varepsilon_{yy} \\ \gamma_{xy} \end{bmatrix} = \begin{bmatrix} \dfrac{\partial u_0}{\partial x} \\ \dfrac{\partial v_0}{\partial y} \\ \dfrac{\partial u_0}{\partial y} + \dfrac{\partial v_0}{\partial x} \end{bmatrix} \tag{3.11}$$

The bending strains ε_{xx}, ε_{yy} and γ_{xy} vary linearly through the flat shell thickness and are given by the curvatures of the shell as

$$\boldsymbol{\varepsilon}_{\mathbf{b}} = \begin{bmatrix} \varepsilon_{xx} \\ \varepsilon_{yy} \\ \gamma_{xy} \end{bmatrix} = -z \begin{bmatrix} \dfrac{\partial \beta_x}{\partial x} \\ \dfrac{\partial \beta_y}{\partial y} \\ \dfrac{\partial \beta_x}{\partial y} + \dfrac{\partial \beta_y}{\partial x} \end{bmatrix} \tag{3.12}$$

The transverse shear strains are assumed to be constant through the thickness of the shell and can be expressed as

$$\boldsymbol{\varepsilon}_{\mathbf{s}} = \begin{bmatrix} \gamma_{xz} \\ \gamma_{yz} \end{bmatrix} = \begin{bmatrix} \dfrac{\partial w}{\partial x} - \beta_x \\ \dfrac{\partial w}{\partial y} - \beta_y \end{bmatrix} \tag{3.13}$$

Therefore, the total strains due to bending, shear and in-plane forces are

$$\boldsymbol{\varepsilon} = \begin{bmatrix} \varepsilon_{xx} \\ \varepsilon_{yy} \\ \gamma_{xy} \\ \gamma_{xz} \\ \gamma_{yz} \end{bmatrix} = \begin{bmatrix} \boldsymbol{\varepsilon}_{\mathbf{m}} \\ \mathbf{0} \end{bmatrix} + \begin{bmatrix} \boldsymbol{\varepsilon}_{\mathbf{b}} \\ \boldsymbol{\varepsilon}_{\mathbf{s}} \end{bmatrix} = \begin{bmatrix} \dfrac{\partial u_0}{\partial x} - z\dfrac{\partial \beta_x}{\partial x} \\ \dfrac{\partial v_0}{\partial y} - z\dfrac{\partial \beta_y}{\partial y} \\ \dfrac{\partial u_0}{\partial y} + \dfrac{\partial v_0}{\partial x} - z\dfrac{\partial \beta_x}{\partial y} - z\dfrac{\partial \beta_y}{\partial x} \\ \dfrac{\partial w_0}{\partial x} - \beta_x \\ \dfrac{\partial w_0}{\partial y} - \beta_y \end{bmatrix} \tag{3.14}$$

Substituting Equation 3.7 into Equations 3.11, 3.12 and 3.13, the strains can be expressed in terms of shape functions and nodal displacements as follows:

$$\boldsymbol{\varepsilon}_{\mathbf{m}} = \begin{bmatrix} \sum_{i=1}^{8} \frac{\partial N_i}{\partial x} u_i \\ \sum_{i=1}^{8} \frac{\partial N_i}{\partial y} v_i \\ \sum_{i=1}^{8} \frac{\partial N_i}{\partial y} u_i + \sum_{i=1}^{8} \frac{\partial N_i}{\partial x} v_i \end{bmatrix}$$

$$= \begin{bmatrix} \frac{\partial N_1}{\partial x} & 0 & \frac{\partial N_2}{\partial x} & 0 & \cdots & \frac{\partial N_8}{\partial x} & 0 \\ 0 & \frac{\partial N_1}{\partial y} & 0 & \frac{\partial N_2}{\partial y} & \cdots & 0 & \frac{\partial N_8}{\partial y} \\ \frac{\partial N_1}{\partial y} & \frac{\partial N_1}{\partial x} & \frac{\partial N_2}{\partial y} & \frac{\partial N_2}{\partial x} & \cdots & \frac{\partial N_8}{\partial y} & \frac{\partial N_8}{\partial x} \end{bmatrix} \cdot \begin{bmatrix} u_1 \\ v_1 \\ u_2 \\ v_2 \\ \vdots \\ u_8 \\ v_8 \end{bmatrix}$$

$$= \mathbf{B}_{\mathbf{m}} \cdot \boldsymbol{\delta}_{\mathbf{m}} \tag{3.15}$$

$$\boldsymbol{\varepsilon}_{\mathbf{b}} = z \begin{bmatrix} \sum_{i=1}^{8} \frac{\partial N_i}{\partial x} \theta_{yi} \\ -\sum_{i=1}^{8} \frac{\partial N_i}{\partial y} \theta_{xi} \\ \sum_{i=1}^{8} \frac{\partial N_i}{\partial y} \theta_{yi} - \sum_{i=1}^{8} \frac{\partial N_i}{\partial x} \theta_{xi} \end{bmatrix}$$

$$= z \begin{bmatrix} 0 & \frac{\partial N_1}{\partial y} & 0 & \frac{\partial N_2}{\partial y} & \cdots & 0 & \frac{\partial N_8}{\partial y} \\ -\frac{\partial N_1}{\partial x} & 0 & -\frac{\partial N_2}{\partial x} & 0 & \cdots & -\frac{\partial N_8}{\partial x} & 0 \\ \frac{\partial N_1}{\partial y} & -\frac{\partial N_1}{\partial x} & \frac{\partial N_2}{\partial y} & -\frac{\partial N_2}{\partial x} & \cdots & \frac{\partial N_8}{\partial y} & -\frac{\partial N_8}{\partial x} \end{bmatrix} \cdot \begin{bmatrix} \theta_{x1} \\ \theta_{y1} \\ \theta_{x2} \\ \theta_{y2} \\ \vdots \\ \theta_{x8} \\ \theta_{y8} \end{bmatrix}$$

$$= \mathbf{B}_{\mathbf{b}} \cdot \boldsymbol{\delta}_{\mathbf{b}} \tag{3.16}$$

$$\boldsymbol{\varepsilon}_s = \begin{bmatrix} \sum_{i=1}^{8} \frac{\partial N_i}{\partial x} w_i + \sum_{i=1}^{8} N_i \cdot \theta_{yi} \\ \sum_{i=1}^{8} \frac{\partial N_i}{\partial y} w_i - \sum_{i=1}^{8} N_i \cdot \theta_{xi} \end{bmatrix}$$

$$= \begin{bmatrix} \frac{\partial N_1}{\partial x} & 0 & N_1 & \frac{\partial N_2}{\partial x} & 0 & N_2 & \cdots & \frac{\partial N_8}{\partial x} & 0 & N_8 \\ \frac{\partial N_1}{\partial y} & -N_1 & 0 & \frac{\partial N_2}{\partial y} & -N_2 & 0 & \cdots & \frac{\partial N_8}{\partial y} & -N_8 & 0 \end{bmatrix} \cdot \begin{bmatrix} w_1 \\ \theta_{x1} \\ \theta_{y1} \\ w_2 \\ \theta_{x2} \\ \theta_{y2} \\ \vdots \\ w_8 \\ \theta_{x8} \\ \theta_{y8} \end{bmatrix}$$

$$= \mathbf{B}_s \cdot \boldsymbol{\delta}_s \tag{3.17}$$

The stresses are related to the strains as

$$\boldsymbol{\sigma}_m = \begin{Bmatrix} \sigma_{xx} \\ \sigma_{yy} \\ \tau_{xy} \end{Bmatrix} = \frac{E}{1-\nu^2} \begin{bmatrix} 1 & \nu & 0 \\ \nu & 1 & 0 \\ 0 & 0 & \frac{1-\nu}{2} \end{bmatrix} \cdot \boldsymbol{\varepsilon}_m \tag{3.18}$$

$$\boldsymbol{\sigma}_b = \begin{Bmatrix} \sigma_{xx} \\ \sigma_{yy} \\ \tau_{xy} \end{Bmatrix} = \frac{E}{1-\nu^2} \begin{bmatrix} 1 & \nu & 0 \\ \nu & 1 & 0 \\ 0 & 0 & \frac{1-\nu}{2} \end{bmatrix} \cdot \boldsymbol{\varepsilon}_b \tag{3.19}$$

$$\boldsymbol{\sigma}_s = \begin{Bmatrix} \tau_{xz} \\ \tau_{yz} \end{Bmatrix} = \frac{kE}{2(1+\nu)} \begin{bmatrix} 1 & 0 \\ 0 & 1 \end{bmatrix} \cdot \boldsymbol{\varepsilon}_s \tag{3.20}$$

where E is the material modulus of elasticity, ν is the Poisson's ratio and k is the shear correction factor to account for the actual non-uniformity of the shearing stresses which is taken as 5/6.

3.2.3 Formulations of Stiffness Matrix

The total potential energy for a typical flat shell element is given as

$$\begin{aligned}\pi &= \frac{1}{2}\int_{-\frac{h}{2}}^{\frac{h}{2}}\iint_A \boldsymbol{\sigma}_{\mathrm{m}}^{\mathrm{T}}\boldsymbol{\varepsilon}_{\mathrm{m}}\,dxdydz + \frac{1}{2}\int_{-\frac{h}{2}}^{\frac{h}{2}}\iint_A \boldsymbol{\sigma}_{\mathrm{s}}^{\mathrm{T}}\boldsymbol{\varepsilon}_{\mathrm{s}}\,dxdydz + \frac{1}{2}\int_{-\frac{h}{2}}^{\frac{h}{2}}\iint_A \boldsymbol{\sigma}_{\mathrm{b}}^{\mathrm{T}}\boldsymbol{\varepsilon}_{\mathrm{b}}\,dxdydz - \\ &\quad - \iint_A (F_x u_0 + F_y v_0 + F_z w_0)\,dxdy \\ &= \frac{1}{2}\iint_A \boldsymbol{\varepsilon}_{\mathrm{m}}^{\mathrm{T}}\mathbf{D}_{\mathrm{m}}\boldsymbol{\varepsilon}_{\mathrm{m}}\,dxdy + \frac{1}{2}\iint_A \boldsymbol{\varepsilon}_{\mathrm{s}}^{\mathrm{T}}\mathbf{D}_{\mathrm{s}}\boldsymbol{\varepsilon}_{\mathrm{s}}\,dxdy + \frac{1}{2}\iint_A \boldsymbol{\varepsilon}_{\mathrm{b}}^{\mathrm{T}}\mathbf{D}_{\mathrm{b}}\boldsymbol{\varepsilon}_{\mathrm{b}}\,dxdy - \\ &\quad - \iint_A (F_x u + F_y v + F_z w)\,dxdy\end{aligned} \tag{3.21}$$

in which F_x, F_y and F_z are the distributed load per unit area in the x, y and z directions respectively, h is the thickness of the shell element, and $\mathbf{D_m}$, $\mathbf{D_s}$ and $\mathbf{D_b}$ are elasticity matrices expressed as following:

$$\mathbf{D}_{\mathrm{m}} = \frac{E\cdot h}{1-\nu^2}\begin{bmatrix} 1 & \nu & 0 \\ \nu & 1 & 0 \\ 0 & 0 & \dfrac{1-\nu}{2} \end{bmatrix} \tag{3.22a}$$

$$\mathbf{D}_{\mathrm{b}} = \frac{E\cdot h^3}{12(1-\nu^2)}\begin{bmatrix} 1 & \nu & 0 \\ \nu & 1 & 0 \\ 0 & 0 & \dfrac{1-\nu}{2} \end{bmatrix} \tag{3.22b}$$

$$\mathbf{D}_{\mathrm{s}} = \frac{E\cdot h}{2.4(1+\nu)}\begin{bmatrix} 1 & 0 \\ 0 & 1 \end{bmatrix} \tag{3.22c}$$

The principle of virtual work says that the total work done by all forces acting on a system in static equilibrium is zero for any possible virtual displacement. Applying the principle on Equation 3.21 and letting $\delta\pi = 0$, the contributions to the stiffness matrices and load vector $\mathbf{P}$ may be written as

$$\mathbf{K}_{\mathrm{m}} = \int_{-1}^{1}\int_{1}^{1} \mathbf{B}_{\mathrm{m}}^{\mathrm{T}}\mathbf{D}_{\mathrm{m}}\mathbf{B}_{\mathrm{m}}\,\det\mathbf{J}\,d\xi d\eta \tag{3.23a}$$

$$\mathbf{K}_b = \int_{-1}^{1}\int_{1}^{1} \mathbf{B}_b^T \mathbf{D}_b \mathbf{B}_b \det \mathbf{J}\, d\xi d\eta \tag{3.23b}$$

$$\mathbf{K}_s = \int_{-1}^{1}\int_{1}^{1} \mathbf{B}_s^T \mathbf{D}_s \mathbf{B}_s \det \mathbf{J}\, d\xi d\eta \tag{3.23c}$$

$$\mathbf{P} = \int_{-1}^{1}\int_{1}^{1} \mathbf{N}^T \mathbf{q} \det \mathbf{J}\, d\xi d\eta \tag{3.23c}$$

where $\mathbf{K}_m$, $\mathbf{K}_b$ and $\mathbf{K}_s$ are the stiffness components respectively associated with the membrane, bending and shear strain energies; det **J** is the determinant of the Jacobian matrix; $dxdy$ = det **J** $d\xi d\eta$ is the area of the element; **N** is the displacement shape function defined in Equation 3.9; and $\mathbf{q} = [F_x \; F_y \; F_z]^T$.

3.2.4 Formulations of Mass Matrix

The mass matrix of a shell element can be obtained by using Equation 3.24, which is called consistent mass matrix (Humar, 1990).

$$\begin{aligned}\mathbf{M} &= \int_0^h \iint_A \rho \mathbf{N}^T \mathbf{N}\, dxdydz \\ &= \int_0^h \int_{-1}^{1}\int_{-1}^{1} \rho \mathbf{N}^T \mathbf{N}\, d\xi d\eta dz\end{aligned} \tag{3.24}$$

where ρ is the volume mass density of the element and h is the thickness of the shell.

3.3 Integration Scheme and Numerical Examples

The compatibility requirement of only continuity of displacements and independent rotations by the Mindlin formulation allows the use of a wide range of interpolation schemes. However, when exact numerical integration is used with standard Mindlin finite elements, poor results are obtained in application to thin plates, which is termed locking caused by the imposition of the constrains $\gamma_{xz} = \gamma_{xz} = 0$ by the shear strain energy terms in the total potential energy when limiting thin plate situations are approached. The imposition of these constrains leads to the deterioration of the stiffness matrix and over-stiff results.

Selective integration procedures are adopted in the present study. A reduced integration rule is used to evaluate the stiffness matrix associated with the shear strain energy in order to alleviate the over-constraining effects of this portion, while full integration is used on the remaining terms to retain the required rank of the overall stiffness matrix (Hinton and Owen, 1984).

To determine the suitability of the 8-node isoparametric shell element described above, two examples have been analyzed, in which both natural frequencies and dynamic responses have been assessed using this analytical model. The accuracy of a mathematical model in predicting response is mostly determined on the closeness of the proposed idealization to the realistic behavior of the bridge system. Therefore, the results obtained by the proposed model have been compared to the theoretical results, published results or those obtained by well-known commercial software, i.e. SAP2000.

3.3.1 A Simply Supported Thin Plate

Example 1 is a 15"×10"×1/8" aluminum rectangular plate with four edges simply supported shown in Figure 3.3 (Gorman, 1982), for which the properties is considered as follows:

Young's Modulus E = 1.0e7 lbs/in^2;

Poisson ratio υ = 0.333;

The mass per unit volume ρ = 2.527e-4 lb.sec^2/in^3.

The plate has been modeled by 25 proposed 8-node shell elements consisting of 96 integration points. The results of the analysis are presented in Table 3.1. For comparison purposes, the numerical results published by Gorman(1982) and the results of 75 4-node elements containing the same number of integration points (96 points) obtained by using SAP2000 are also shown in the table. Compared to the published results, the errors of the proposed 8-node element vary from 0.8% to 2.1 while the errors of the 4-node element were found to be much larger, which vary from 3.1% to 19.5%. It indicates that results of the proposed 8-node shell element are

much closer to the published solutions than those of the 4-node shell element. It also shows that lower frequencies are closer to the published results than higher frequencies in both cases. Generally, this example verified that the proposed shell element is fit for modeling plate-bending deformation.

3.3.2 Two Cantilever Beams

Two cantilever beams shown in Figure 3.4 (Kashif, 1992) have been analyzed to determine their response to static loads and their natural frequencies. The results of the analysis are presented in Tables 3.2 and 3.3 where the theoretical solution obtained by using the standard beam theory is also shown.

Table 3.2 shows the displacements at the free ends and stresses at the fix ends of the two beams subjected to two cases of loading. It can be seen from Table 3.2 that the displacements and shears of both beams are very close to theoretical results.

Table 3.3 shows the first 5 frequencies of the two beams. The results of Beam #1 with longer span are quite close to the theoretical results. For Beam #2 with shorter span, the frequency of the first mode is similar to the theoretical value, while those of higher modes have large errors. It indicates that the in-plane shear deformation is suitable for long-span beams using the proposed shell element.

3.4 Confederation Bridge

Completed in the summer of 1997, the Confederation Bridge provides a highway traffic link across the Northumberland Strait in eastern Canada, between Borden in Prince Edward Island and Cape Tormentine in the province of New Brunswick (Tadros, 1997 and Cheung, et., 1997). The 12.9 km long Confederation Bridge is the longest prestressed concrete box girder bridge in

the world built over salt water. The bridge consists of 11 approach spans and 45 main spans, each 250m in length, at a typical height of 40m above the mean sea level. For a typical main span, each two piers are rigidly connected together by the superstructure to form a portal frame of 250m span, with a 96m cantilever beyond each pier. Repeating these portal frames for all marine spans produces 21 frames. These frames are connected together by 60m simply supported drop-in spans.

A portal frame of the main spans is adopted in this analysis, as shown in Figure 3.5. The bridge cross-section is a prestressed single cell trapezoidal box. The total width of the bridge is 12m with 11m roadway. The depth of the superstructure varies from 4.5m at mid span to 14m at the pier location. The cross section is reinforced with steel "A" diaphragm at each pier to reduce torsional vibration at lower frequencies.

The first twelve mode shapes and the corresponding natural frequencies of the above analysis using the proposed model are presented in Table 3.4. Figure 3.7 illustrates the mode shapes and the corresponding deformation of cross section at mid-span. The first six mode shapes and the eighth mode shape are pure longitudinal flexure. The rest with higher frequencies are also longitudinal flexural but mixed with transverse flexure or torsion.

It is of special importance to compare the dynamic characteristics obtained in this study with measured vibrations published by Cheung, et al (1997). The first natural frequency from the analysis is 0.48Hz. It is close to the measured value of 0.5Hz, which is excited by vehicle traffic. The corresponding 1^{st} mode shape shown in Figure 3.7 is nearly identical to that obtained from measurement.

3.5 Summary

Summarized from the above discussions, in general, the proposed 8-node isoparametric shell element gives the best results. It is also the most efficient in convergence. Hence, the 8-node isoparametric shell element is chosen for the present study.

Box-girder bridges tend to be slender and more flexible than other types of bridges. Therefore, attention must be paid to the avoidance of excessive acceleration and dynamic deflection, which may cause pedestrian's discomfort and concern. Usually, dynamic deflections are more pronounced in bridges with torsional dominant modes, especially at sidewalk locations. Such modes tend to have more detrimental effects on human responses to vibrations and comfort level of pedestrians using the bridge. The acceleration level of a bridge is also directly related to the governing vibration mode. For bridges with a torsional dominant mode, the acceleration values are usually higher than those of flexural dominant modes. Since acceleration has a significant effect on human sensation and pedestrian comfort, the torsional mode must be avoided at all costs. For bridges with long span, the modes corresponding to low frequencies are pure longitudinal flexure. The governing deformation in higher modes is also longitudinal flexure but occasionally combined with lateral flexure and torsion.

TABLE 3.1 FREE VIBRATION OF ALUMINUM RECTANGULAR PLATE

Mode No.	Published [1] Frequency (Hz)	4-node shell element adopted by SAP2000		Proposed	
		Frequency (Hz)	Difference (%)	Frequency (Hz)	Difference (%)
1	172.8	167.5	3.1	171.4	0.8
2	332.2	311.9	6.1	334.3	0.6
3	531.6	509.4	4.2	532.9	0.2
4	598.0	547.2	8.5	605.8	1.3
5	691.0	609.9	11.7	701.5	1.5
6	970.1	780.8	19.5	990.0	2.1
Material Properties: $E = 1.0\times10^7$ psi, $\upsilon = 0.333$, $\rho = 2.527e{-}4$ lb.sec^2/in^3, thickness = 0.125in					

Note:

1. Results published by Gorman(1982).

TABLE 3.2 DISPLACEMENT AND STRESS OF CANTILEVER BEAMS

	Beam #1				Beam #2			
	Displacement at k		Stress at m		Displacement at k		Stress at m	
	Load A	Load B	Load A	Load B	Load A	Load B	Load A	Load B
Theory	0.135	0.202	90.00	90.00	1.000	1.000	16650.0	11112.0
Proposed	0.134	0.201	90.17	90.77	1.031	0.988	16700.0	11116.0
Material Properties: $E = 1.0 \times 10^5$, $\upsilon = 0.3$, $\rho = 0.1$, thickness = 1.0.								

TABLE 3.3 FREE VIBRATIONS OF CANTILEVER BEAMS

Mode No.	Natural Frequencies (Hz)			
	Beam #1		Beam #2	
	Theory	Proposed	Theory	Proposed
1	0.7	0.7	18.0	17.0
2	4.5	4.4	112.5	79.8
3	12.6	12.1	315.0	83.8
4	24.7	23.0	617.2	181.6
5	40.8	36.7	1020.3	250.5

TABLE 3.4 FREE VIBRATIONS OF CONFEDERATION BRIDGE

Mode No	Freq. (Hz)	Mode Shape
1	0.48	LF
2	0.55	LF
3	0.67	LF
4	1.05	LF
5	1.21	LF
6	1.25	LF
7	1.28	LF
8	1.79	LF
9	2.12	LF- TO
10	2.33	LF-TF
11	2.70	LF-TO
12	3.23	LF-TF
13	3.26	LF-TO
14	3.40	LF-TO
15	3.94	LF-TO
16	4.02	LF-TO
17	4.54	LF-TO-TF
18	4.57	LF-TF

Note:

1. LF – Longitudinal flexure
2. TF – Transverse flexure
3. TO – Torsion

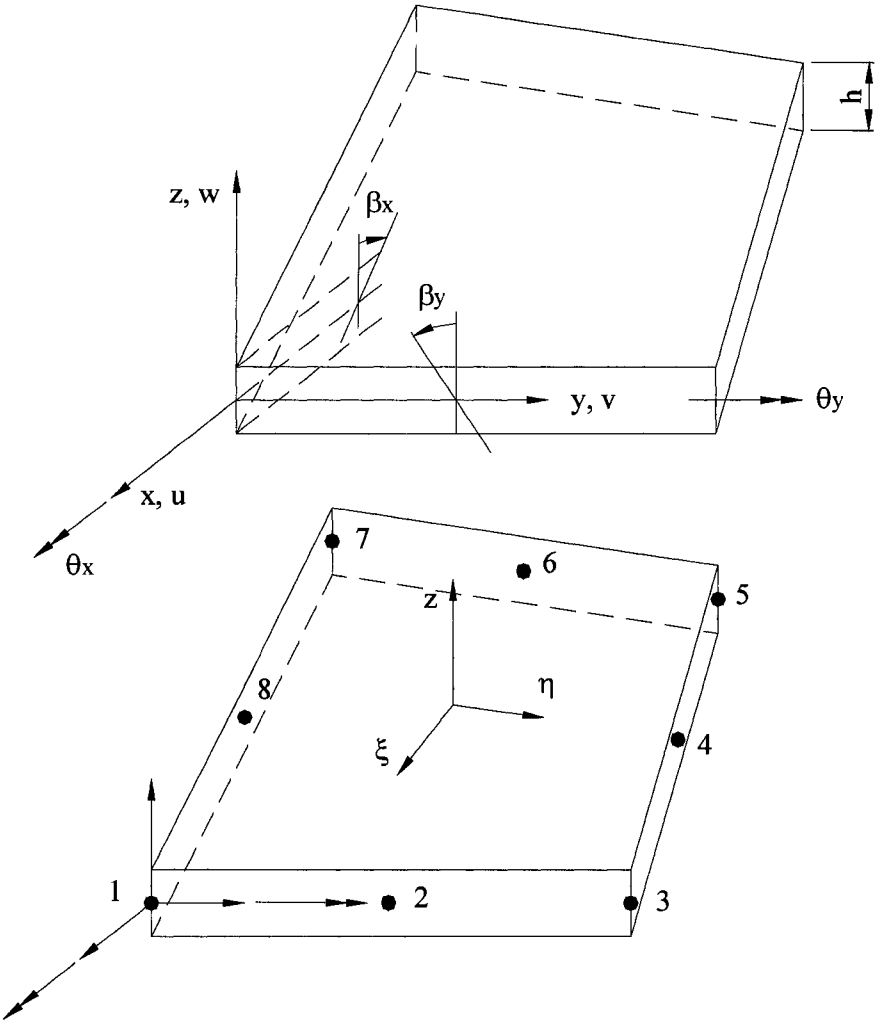

FIGURE 3.1 8-NODE SHELL ELEMENT

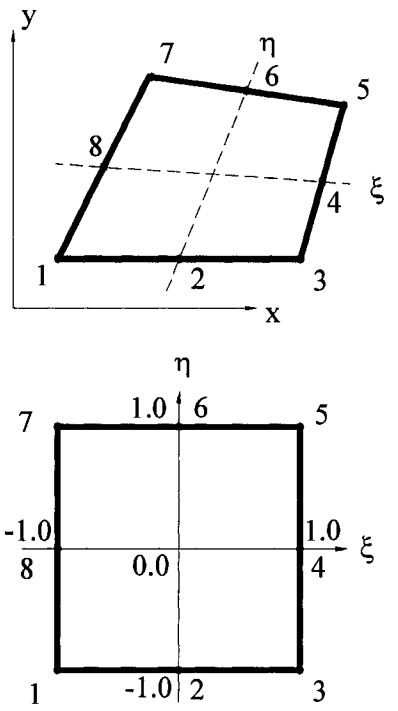

FIGURE 3.2 8-NODE SHELL ELEMENT COORDINATE TRANSFORMATION

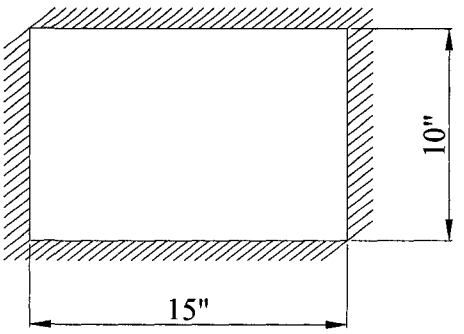

E = 1.0e7 psi, $\upsilon = 0.333$, $\rho = 2.527\text{e-}4$ lb.sec^2/ in^3
Thickness = 0.125"

FIGURE 3.3 ALUMINUM PLATE WITH SIMPLY SUPPORTED EDGES

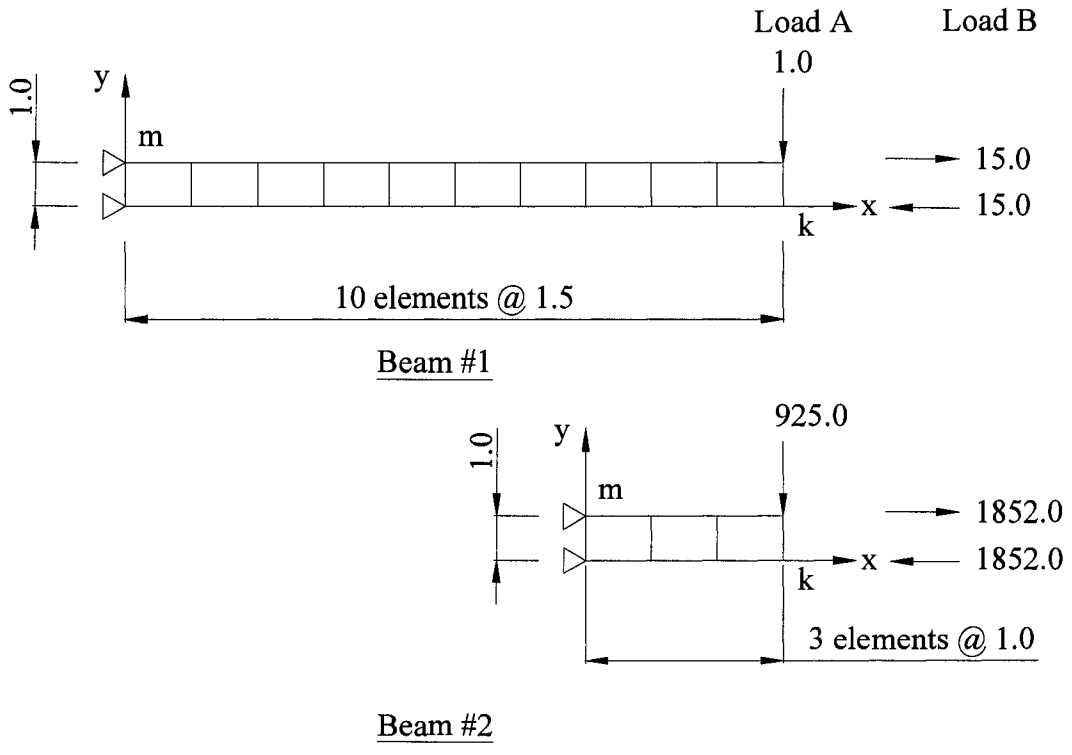

FIGURE 3.4 CANTILEVER BEAMS

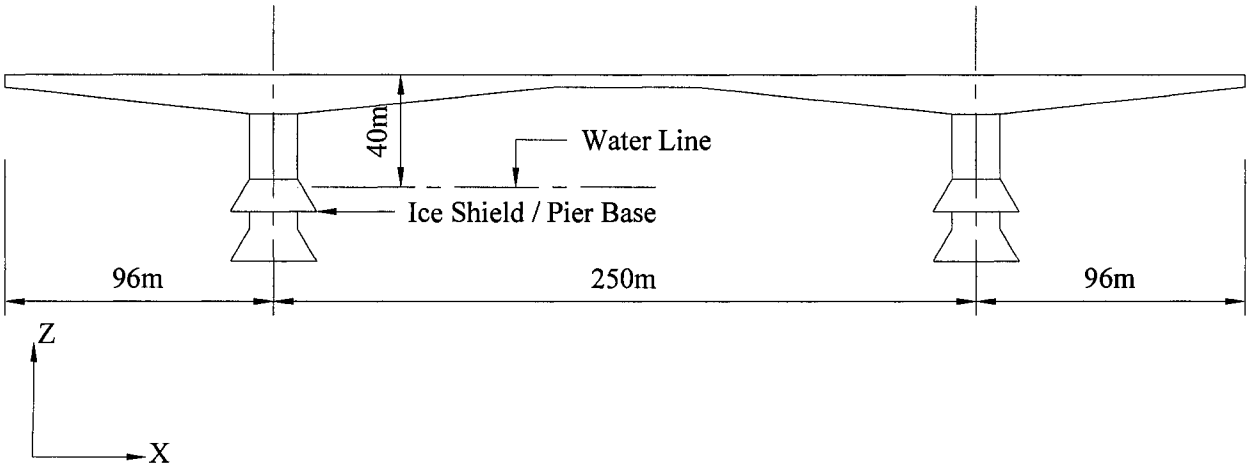

(a) Side View

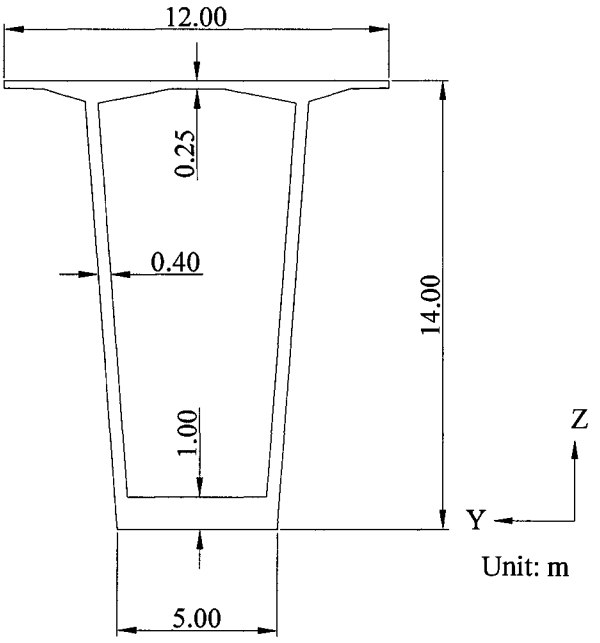

(2) Cross Section

FIGURE 3.5 CONFEDERATION BRIDGE

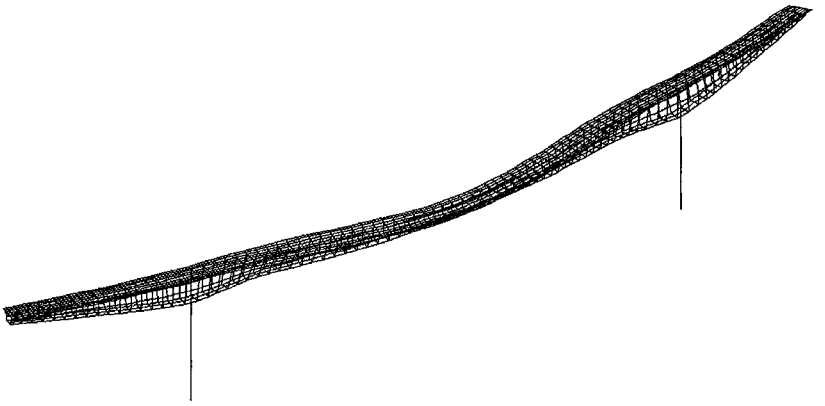

(1) Isometric View

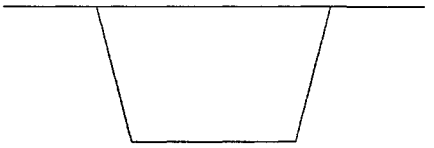

(2) Mid-span Cross Section

(a) Mode 1, Frequency = 0.48 Hz

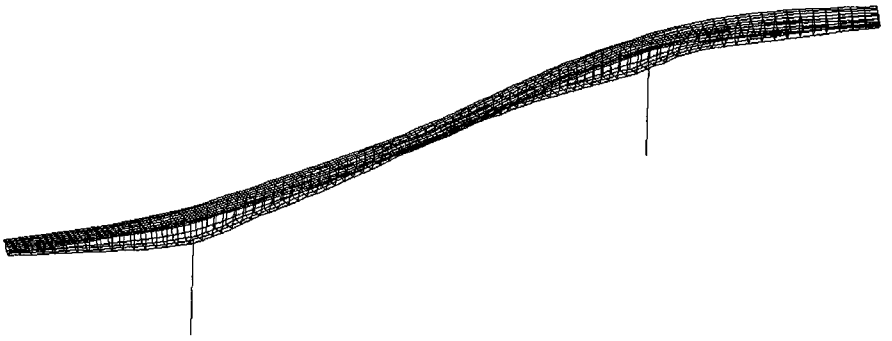

(1) Isometric View

(2) Mid-span Cross Section

(b) Mode 2, Frequency = 0.55 Hz

FIGURE 3.6 MODE SHAPES OF CONFEDERATION BRIDGE (CONTINUED)

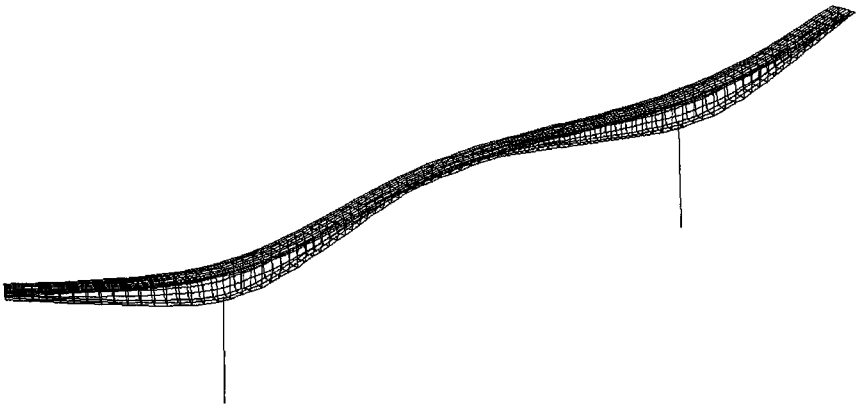

(1) Isometric View

(2) Mid-span Cross Section

(c) Mode 3, Frequency = 0.67 Hz

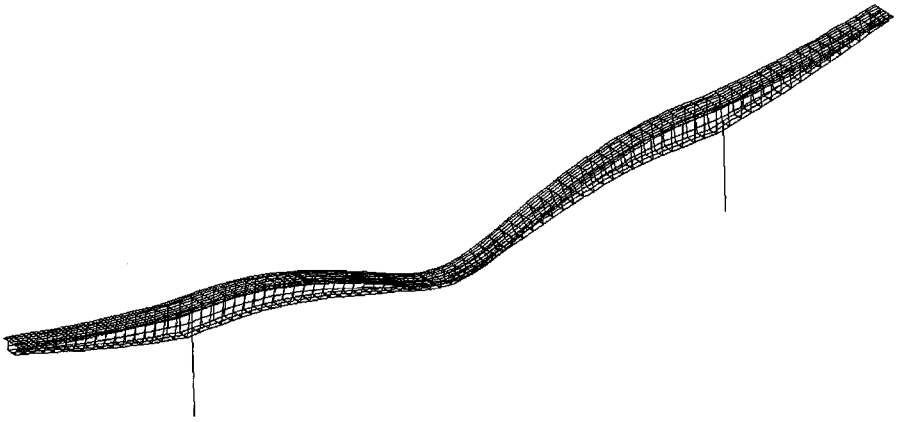

(1) Isometric View

(2) Mid-span Cross Section

(d) Mode 4, Frequency = 1.05 Hz

FIGURE 3.6 MODE SHAPES OF CONFEDERATION BRIDGE (CONTINUED)

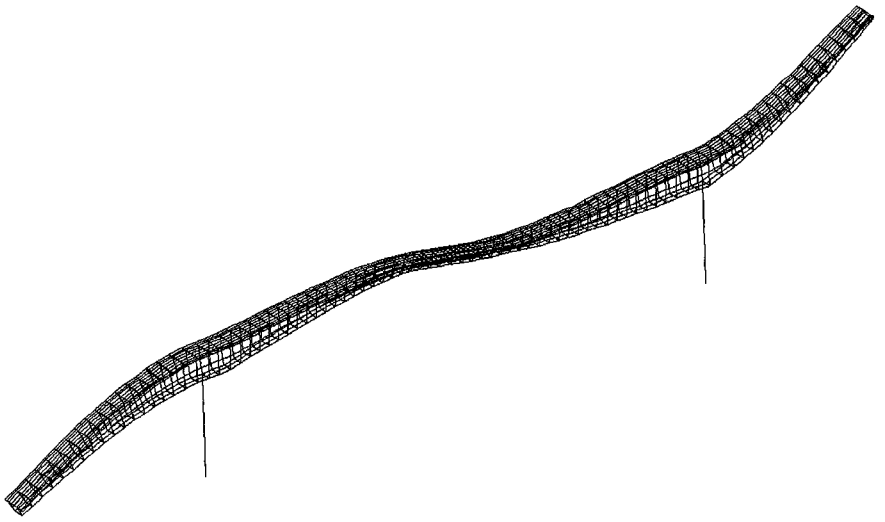

(1) Isometric View

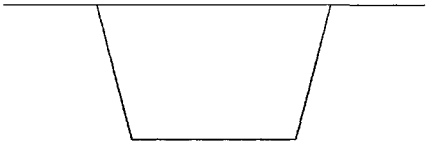

(2) Mid-span Cross Section

(e) Mode 5, Frequency = 1.21 Hz

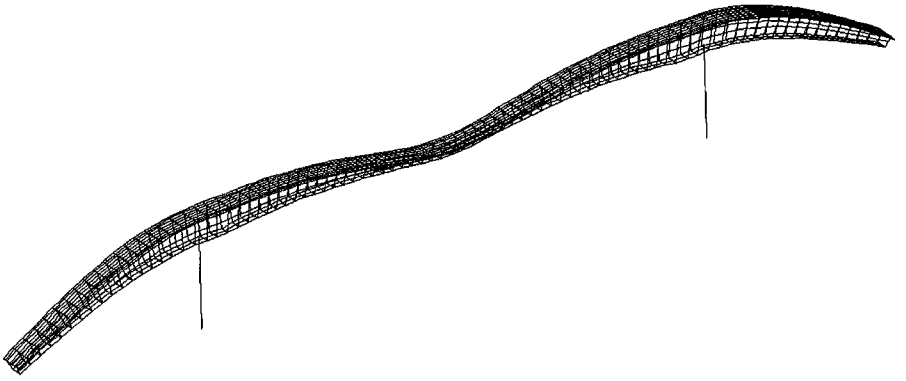

(1) Isometric View

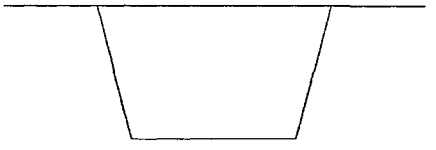

(2) Mid-span Cross Section

(f) Mode 6, Frequency = 1.25 Hz

FIGURE 3.6 MODE SHAPES OF CONFEDERATION BRIDGE (CONTINUED)

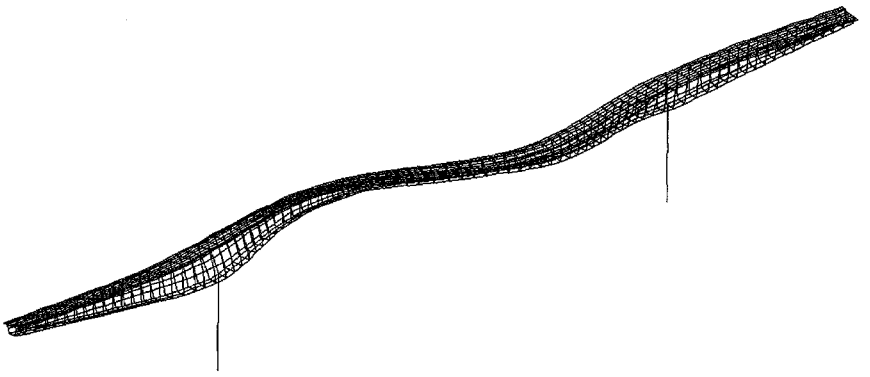

(1) Isometric View

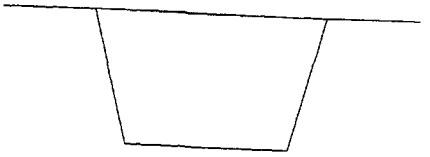

(2) Mid-span Cross Section

(g) Mode 7, Frequency = 1.28 Hz

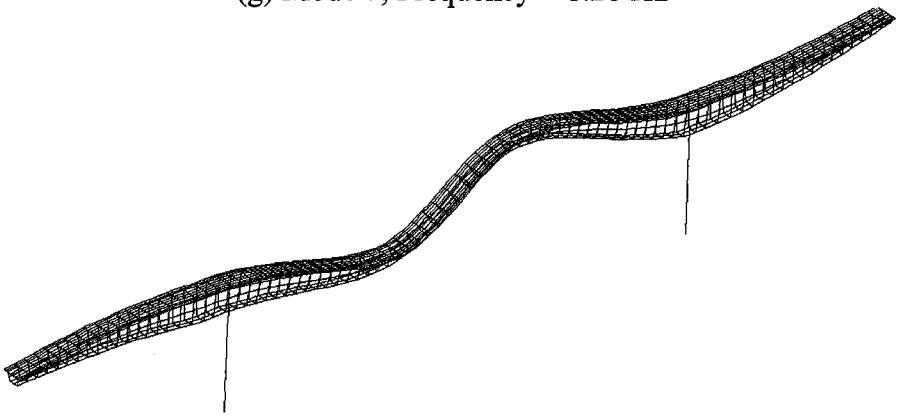

(1) Isometric View

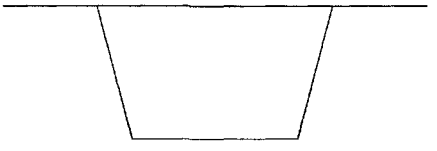

(2) Mid-span Cross Section

(h) Mode 8, Frequency = 1.79 Hz

FIGURE 3.6 MODE SHAPES OF CONFEDERATION BRIDGE (CONTINUED)

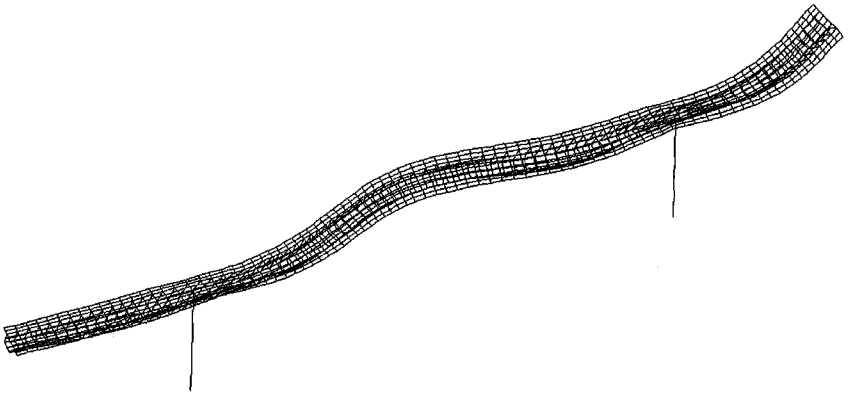

(1) Isometric View

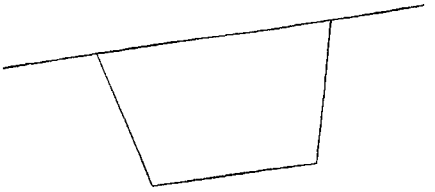

(2) Mid-span Cross Section

(i) Mode 9, Frequency = 2.12 Hz

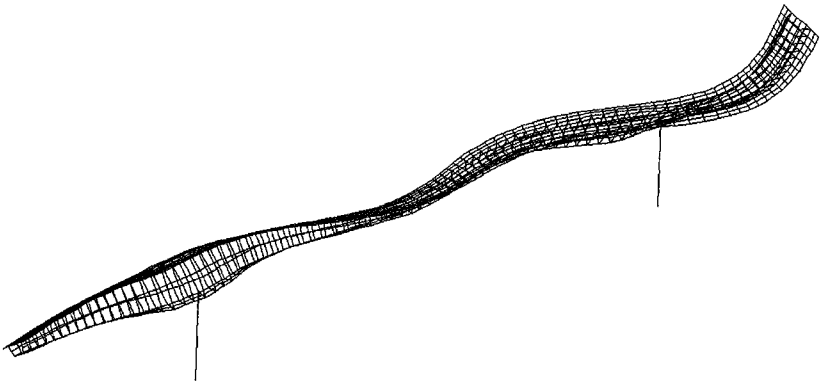

(1) Isometric View

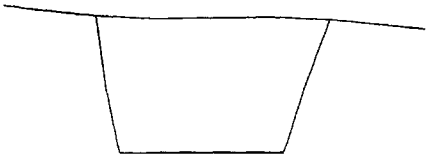

(2) Mid-span Cross Section

(j) Mode 10, Frequency = 2.33 Hz

FIGURE 3.6 MODE SHAPES OF CONFEDERATION BRIDGE (CONTINUED)

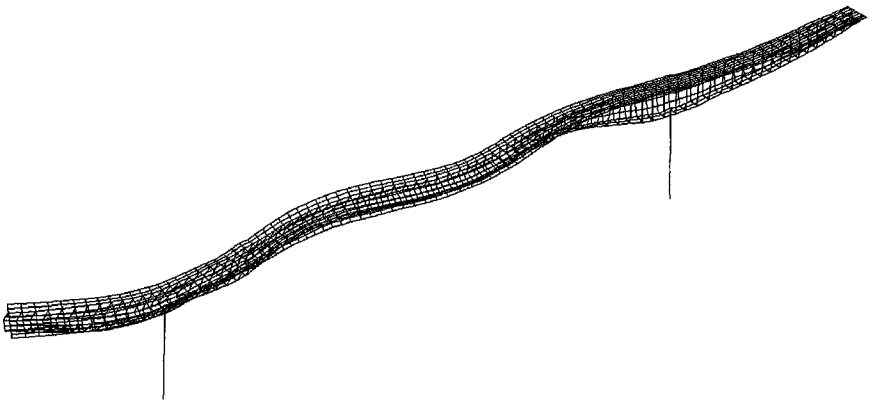

(1) Isometric View

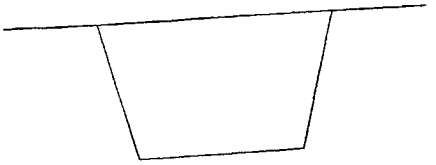

(2) Mid-span Cross Section

(k) Mode 11, Frequency = 2.70 Hz

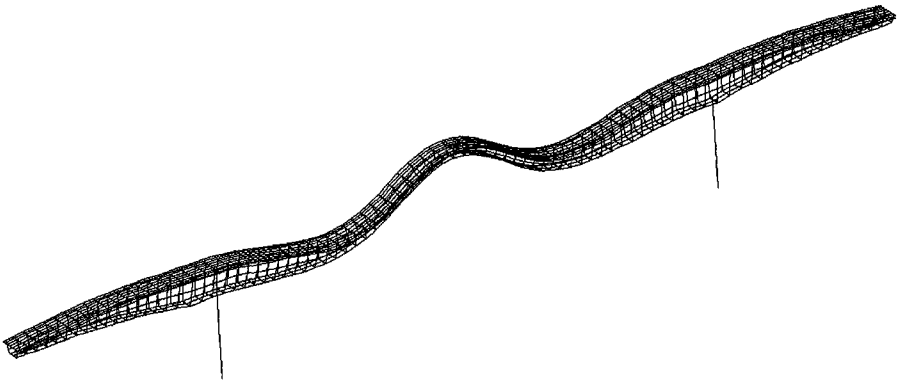

(1) Isometric View

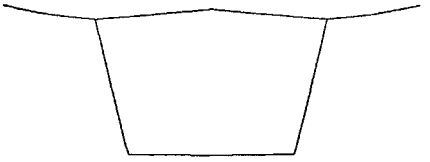

(2) Mid-span Cross Section

(l) Mode 12, Frequency = 3.23 Hz

FIGURE 3.6 MODE SHAPES OF CONFEDERATION BRIDGE (CONTINUED)

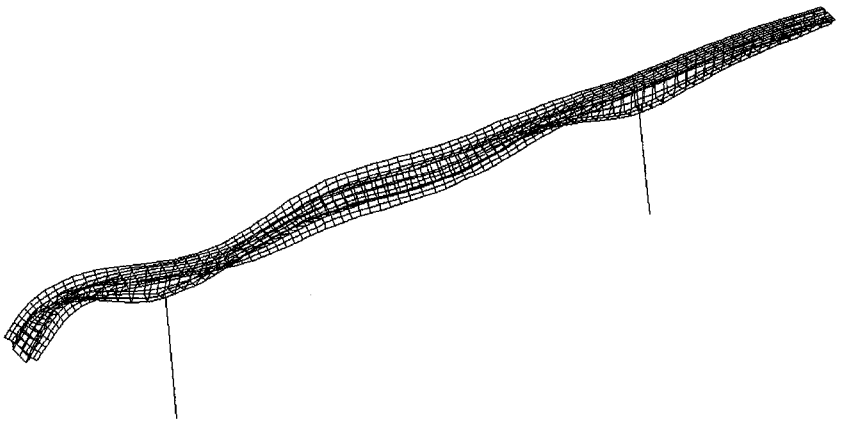

(1) Isometric View

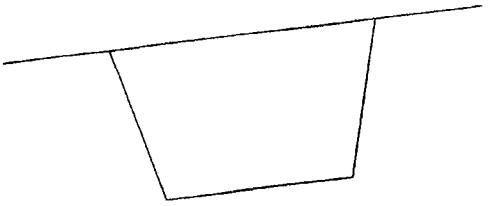

(2) Mid-span Cross Section

(m) Mode 13, Frequency = 3.26 Hz

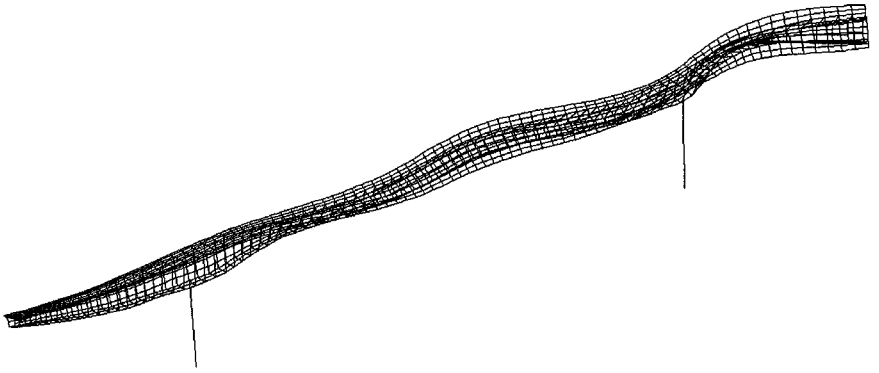

(1) Isometric View

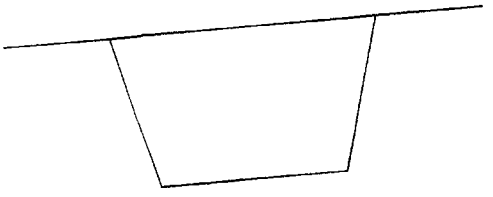

(2) Mid-span Cross Section

(n) Mode 14, Frequency = 3.40 Hz

FIGURE 3.6 MODE SHAPES OF CONFEDERATION BRIDGE (CONTINUED)

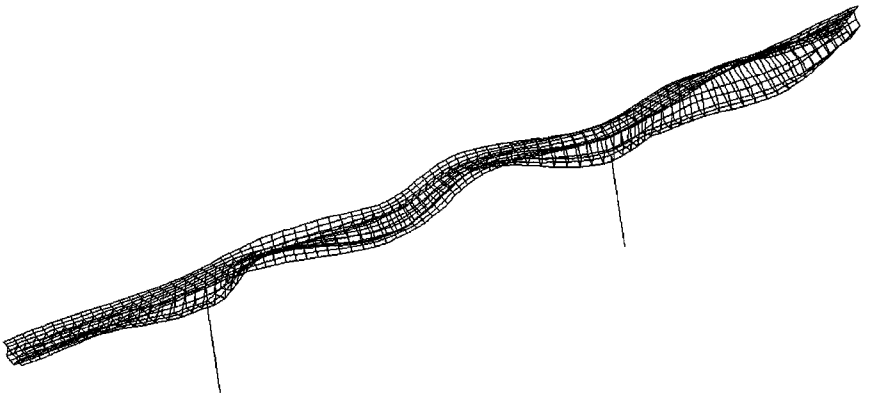

(1) Isometric View

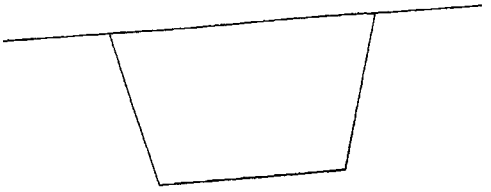

(2) Mid-span Cross Section

(o) Mode 15, Frequency = 3.94 Hz

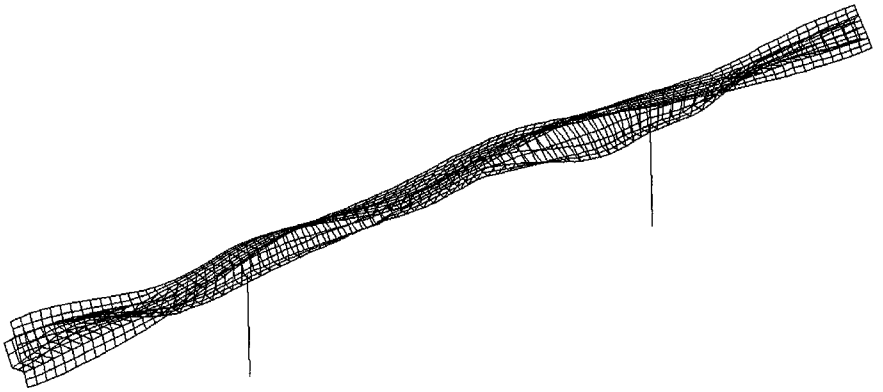

(1) Isometric View

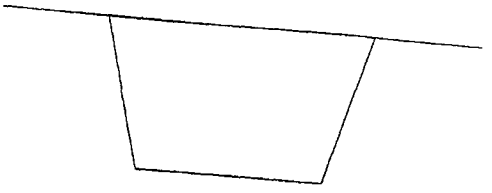

(2) Mid-span Cross Section

(p) Mode 16, Frequency = 4.02 Hz

FIGURE 3.6 MODE SHAPES OF CONFEDERATION BRIDGE (CONTINUED)

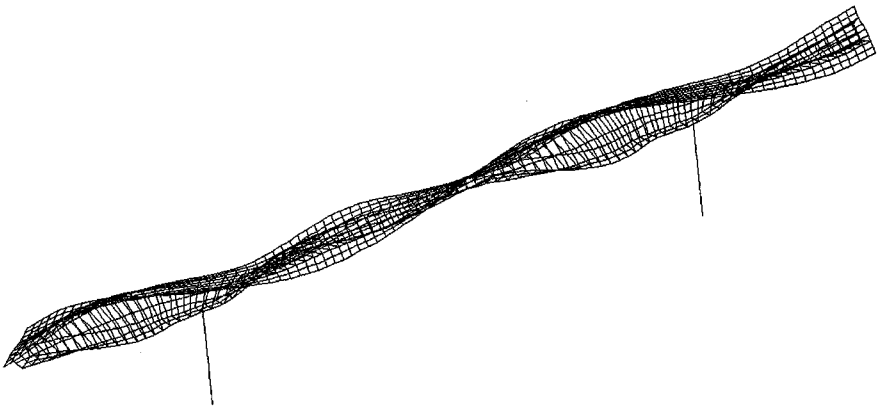

(1) Isometric View

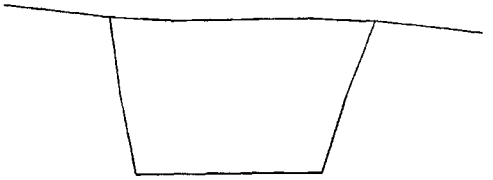

(2) Mid-span Cross Section

(q) Mode 17, Frequency = 4.54 Hz

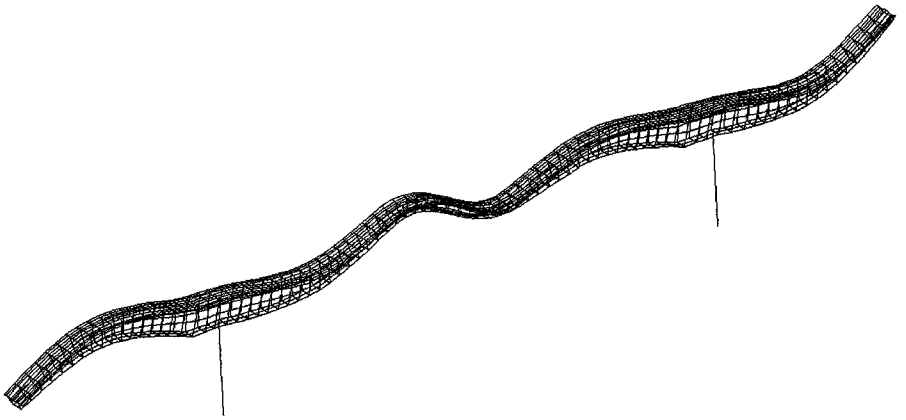

(1) Isometric View

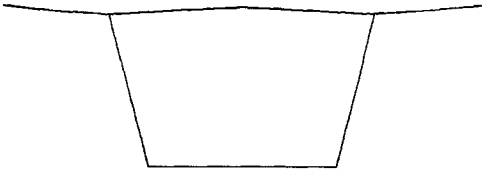

(2) Mid-span Cross Section

(r) Mode 18, Frequency = 4.57 Hz

FIGURE 3.6 MODE SHAPES OF CONFEDERATION BRIDGE (CONTINUED)

Chapter 4

STRUCTURAL ANALYSIS OF CABLE-STAYED BRIDGES

4.1 Introduction

Cable-stayed bridges have become very popular in recent decades due to the appealing aesthetics, the efficient utilization of structural materials, the efficient and fast mode of construction and other notable advantages. The recent developments in design technology, material qualities, and construction techniques in bridge engineering enable the construction of not only longer but also lighter and more slender bridges. A great number of elegant modern bridges are being built, and the ambition is to further increase the span length and use shallower and more slender girders for future bridges. To achieve this, accurate procedures need to be developed that can lead to a thorough understanding and a realistic prediction of the structural response due to traffic loading.

The basic components of cable-stayed bridges are cables, deck and pylons. Each of the three fundamental elements contributes in a definite way to the structural behavior of the whole. The deck, which can be modeled as girder or flat shell, resists bending moments and axial forces from the vertical dead load and live loads and the lateral loads induced by wind and earthquakes. The cables can only sustain axial load. The pylon resists the very large axial forces, and sometimes also bending moments, transmitted from the stay cables.

The dynamic characteristics of the cable-stayed bridges are very complicated. Due to the presence of the inclined cables, the swaying and torsional motions are strongly coupled together. Since determining the dynamic characteristics is the first step for the dynamic analysis, it is very important to have an accurate analytical model, which includes sufficient details of the dynamic behavior of the bridge, in order to ensure satisfactory results.

Although the material in the members in a cable-stayed bridge behaves in a linear- elastic fashion, the overall load-deformation relationships are non-linear under normal design loads. As the span length increases, the nonlinear characteristics of cable-stayed bridges become more important and complex. The primary sources of this overall non-linearity have been summarized as following by Nazmy and Abdel-Ghaffar (1990).

1. First, the nonlinear axial force-elongation relationship for the inclined cable stays results from the sag caused by their own weight. The axial stiffness of the cable varies non-linearly as a function of end displacements since part of the end moment occurs due to material deformation and another part occurs due to change in sag. As the axial tension increases in the cable stay, this latter part, i.e. the change in cable sag, becomes smaller and smaller, and the end movement occurs mainly due to material deformation. Accordingly, the apparent axial stiffness of the cable increases as its tensile stresses increase.
2. The second source is the nonlinear axial force – bending moment – deformation relationships for the towers and decks under combined bending and axial forces. When assuming small deformations in any structural system, the axial stiffness and flexural stiffness of bending members are usually considered to be uncoupled. But, when deformations are no longer small, there is an interaction between axial and flexural deformations in such members under the combined effect of axial forces and bending moments. The effective bending stiffness of the member decreases for a compressive axial force and increases for a tensile force. Similarly, the axial stiffness of the member will be affected due to an apparent shortening of the member caused by the bending deformation.

3. The geometry change caused by large displacements is the third contribution to the overall non-linearity. In cable-stayed bridges, displacements of several feet can occur under design loads, and correspondingly significant changes in the bridge geometry. In such a case the stiffness of the bridge in the deformed shape should be computed from the new geometry of the structure.

In this chapter, the finite element method is adopted to develop a mathematical model for the dynamic analysis of the cable-stayed bridges.

4.2 Stiffness and Mass Formulation of Tower and Girder

4.2.1 Displacement Function

The pylons and girders have been modeled as three dimensional beam elements as shown in Figure 4.1. Defining x, y and z as the axes of the local coordinate system of the beam element each node of element incorporate six degrees of freedom, i.e., translation u, v and w in the x, y and z directions and rotation θ_x, θ_y and θ_z about the x, y and z axes correspondingly.

$$\boldsymbol{\delta} = [u,\ v,\ w,\ \theta_x,\ \theta_y,\ \theta_z]^T \tag{4.1}$$

The nodal displacement vector of the beam element is therefore

$$\boldsymbol{\delta}_e = [u_i,\ v_i,\ w_i,\ \theta_{xi},\ \theta_{yi},\ \theta_{zi},\ u_j,\ v_j,\ w_j,\theta_{xj},\ \theta_{yj},\ \theta_{zj}]^T \tag{4.2}$$

The linear displacement u, v and w and rotation θ_x, θ_y and θ_z at an arbitrary point (x, y, z) within the beam element can be expressed as follows (Bathe, 1996)

$$
\begin{aligned}
u &= (1-\frac{x}{L})\cdot u_i + \frac{x}{L}\cdot u_j \\
v &= (1-\frac{3x^2}{L^2}+\frac{2x^3}{L^3})\cdot v_i + (x-\frac{2x^2}{L}+\frac{x^3}{L^2})\cdot \theta_{zi} + (\frac{3x^2}{L^2}-\frac{2x^3}{L^3})\cdot v_j + (-\frac{x^2}{L}+\frac{x^3}{L^2})\cdot \theta_{zj} \\
w &= (1-\frac{3x^2}{L^2}+\frac{2x^3}{L^3})\cdot w_i + (x-\frac{2x^2}{L}+\frac{x^3}{L^2})\cdot \theta_{yi} + (\frac{3x^2}{L^2}-\frac{2x^3}{L^3})\cdot w_j + (-\frac{x^2}{L}+\frac{x^3}{L^2})\cdot \theta_{yj} \\
\theta_x &= (1-\frac{x}{L})\cdot \theta_{xi} + \frac{x}{L}\cdot \theta_{xj} \\
\theta_y &= \frac{dw}{dx} \\
\theta_z &= \frac{dv}{dx}
\end{aligned}
\tag{4.3}
$$

Equation 4.3 can also be expressed in a matrix form as

$$
\begin{Bmatrix} u \\ v \\ w \\ \theta_x \end{Bmatrix} = \mathbf{N}\cdot\boldsymbol{\delta}_e \tag{4.4}
$$

in which **N** is the shape function matrix as

$$\mathbf{N}^T = \begin{bmatrix} 1-\frac{x}{L} & 0 & 0 & 0 \\ 0 & 1-\frac{3x^2}{L^2}+\frac{2x^3}{L^3} & 0 & 0 \\ 0 & 0 & 1-\frac{3x^2}{L^2}+\frac{2x^3}{L^3} & 0 \\ 0 & 0 & 0 & 1-\frac{x}{L} \\ 0 & 0 & (x-\frac{2x^2}{L}+\frac{x^3}{L^2}) & 0 \\ 0 & (x-\frac{2x^2}{L}+\frac{x^3}{L^2}) & 0 & 0 \\ \frac{x}{L} & 0 & 0 & 0 \\ 0 & \frac{3x^2}{L^2}-\frac{2x^3}{L^3} & 0 & 0 \\ 0 & 0 & \frac{3x^2}{L^2}-\frac{2x^3}{L^3} & 0 \\ 0 & 0 & 0 & \frac{x}{L} \\ 0 & 0 & -\frac{x^2}{L}+\frac{x^3}{L^2} & 0 \\ 0 & -\frac{x^2}{L}+\frac{x^3}{L^2} & 0 & 0 \end{bmatrix} \tag{4.5}$$

4.2.2 Stiffness Matrix of Beam Elements

The principle of virtual work is used to formulate the equilibrium condition. The principle is expressed as

$$\delta\pi = \delta U + \delta V = 0 \tag{4.6}$$

in which $\delta\pi$ is the variation of the total energy, δU is the variation of the internal strain energy stored and δV is the variation of the load potential energy (Trahair, 1993).

Internal strain energy due to longitudinal normal stresses is

$$U_n = \int_0^L \frac{1}{2}\left\{EA\left(\frac{du}{dx}\right)^2 + EI_y\left(\frac{d^2w}{dx^2}\right)^2 + EI_z\left(\frac{d^2v}{dx^2}\right)^2\right\}dx \tag{4.7}$$

where

E – the member material modulus of elasticity;

A – the cross section area;

I_y – the moment inertia of the cross section about the local principal y axis;

I_z – the moment inertia of the cross section about the local principal z axis.

Equation 4.8 expresses the internal strain energy stored due to St. Venant torsional effect as the beam deforms from its equilibrium position through an arbitrary angle of twist θ_x.

$$U_t = \int_0^L \frac{1}{2}GI_x\left(\frac{d\theta_x}{dx}\right)^2 dx \tag{4.8}$$

where

G – the member material shear modulus;

I_x – the moment inertia of the cross section about the local principal x axis.

Neglecting shear deformation the total internal energy is

$$U = U_n + U_t$$

$$= \int_0^L \frac{1}{2}\left\{EA\left(\frac{du}{dx}\right)^2 + EI_y\left(\frac{d^2w}{dx^2}\right)^2 + EI_z\left(\frac{d^2v}{dx^2}\right)^2 + GI_x\left(\frac{d\theta_x}{dx}\right)^2\right\}dx \tag{4.9}$$

The load potential energy component done by end forces is

$$V_L = -\boldsymbol{\delta}_e^T \cdot \mathbf{P}_e \tag{4.10}$$

where

$$\mathbf{P}_e = [N_{xi}, N_{yi}, N_{zi}, M_{xi}, M_{yi}, M_{zi}, N_{xj}, N_{yj}, N_{zj}, M_{xj}, M_{yj}, M_{zj}]^T \tag{4.11}$$

For a beam element that is buckled under an axial force P, the distance traveled by load P due to the bending moment about axis *y* and *z* is

$$\begin{aligned}\Delta_b &= \int_0^L \sqrt{dv^2 + dw^2 + dx^2} - L \\ &= \int_0^L \left[\sqrt{(\frac{dv}{dx})^2 + (\frac{dw}{dx})^2 + 1} \right] dx - L \\ &\approx \int_0^L \left[\frac{1}{2}(\frac{dv}{dx})^2 + \frac{1}{2}(\frac{dw}{dx})^2 + 1 \right] dx - L \\ &= \frac{1}{2} \int_0^L \left[(\frac{dv}{dx})^2 + (\frac{dw}{dx})^2 \right] dx\end{aligned} \tag{4.12}$$

Then, the load potential energy provided by axial force due to buckling is given as

$$V_p = P \cdot \Delta_b = \frac{P}{2} \int_0^L \left[(\frac{dv}{dx})^2 + (\frac{dw}{dx})^2 \right] dx \tag{4.13}$$

In which $P = N_j = -N_i$, P is positive for tension and negative for compression.

Therefore the total potential energy is

$$\begin{aligned}V &= V_p + V_L \\ &= \frac{P}{2} \int_0^L \left[(\frac{dv}{dx})^2 + (\frac{dw}{dx})^2 \right] dx - \boldsymbol{\delta}_e^T \cdot \mathbf{P}_e\end{aligned} \tag{4.14}$$

Substituting Equations 4.9 and 4.14 to 4.6, we get the following static equilibrium equation

$$\mathbf{K}_{E,b} \cdot \boldsymbol{\delta}_e + \mathbf{K}_{G,b} \cdot \boldsymbol{\delta}_e = \mathbf{P}_e \tag{4.15}$$

where $\mathbf{K}_{E,b}$ is the elastic stiffness matrix given by

$$\mathbf{K}_{E,b} = \begin{bmatrix}
\frac{EA}{L} & & & & & & & & & & & \\
0 & 12\frac{EI_z}{L^3} & & & & & & & & & & \\
0 & 0 & 12\frac{EI_y}{L^3} & & & & & & & & & \\
0 & 0 & 0 & \frac{GI_x}{L} & & & & & & & & \\
0 & 0 & 6\frac{EI_y}{L^2} & 0 & 4\frac{EI_y}{L} & & \textit{Symetric} & & & & & \\
0 & 6\frac{EI_z}{L^2} & 0 & 0 & 0 & 4\frac{EI_z}{L} & & & & & & \\
-\frac{EA}{L} & 0 & 0 & 0 & 0 & 0 & \frac{EA}{L} & & & & & \\
0 & -12\frac{EI_z}{L^3} & 0 & 0 & 0 & -6\frac{EI_z}{L^2} & 0 & 12\frac{EI_z}{L^3} & & & & \\
0 & 0 & -12\frac{EI_y}{L^3} & 0 & -6\frac{EI_y}{L^2} & 0 & 0 & 0 & 12\frac{EI_y}{L^3} & & & \\
0 & 0 & 0 & -\frac{GI_x}{L} & 0 & 0 & 0 & 0 & 0 & \frac{GI_x}{L} & & \\
0 & 0 & 6\frac{EI_y}{L^2} & 0 & 2\frac{EI_y}{L} & 0 & 0 & 0 & -6\frac{EI_y}{L^2} & 0 & 4\frac{EI_y}{L} & \\
0 & 6\frac{EI_z}{L^2} & 0 & 0 & 0 & 2\frac{EI_z}{L} & 0 & -6\frac{EI_z}{L^2} & 0 & 0 & 0 & 4\frac{EI_z}{L}
\end{bmatrix} \tag{4.16}$$

and $\mathbf{K}_{G,b}$ is the geometric stiffness matrix given by

$$\mathbf{K}_{G,b} = \frac{P}{L} \cdot \begin{bmatrix}
0 & & & & & & & & & & & \\
0 & \frac{6}{5} & & & & & & & & & & \\
0 & 0 & \frac{6}{5} & & & & & & & & & \\
0 & 0 & 0 & 0 & & & & & & & & \\
0 & 0 & -\frac{L}{10} & 0 & \frac{2}{15}L^2 & & & & \textit{Symetric} & & & \\
0 & \frac{L}{10} & 0 & 0 & 0 & \frac{2}{15}L^2 & & & & & & \\
0 & 0 & 0 & 0 & 0 & 0 & 0 & & & & & \\
0 & -\frac{6}{5} & 0 & 0 & 0 & -\frac{L}{10} & 0 & \frac{6}{5} & & & & \\
0 & 0 & -\frac{6}{5} & 0 & \frac{L}{10} & 0 & 0 & 0 & \frac{6}{5} & & & \\
0 & 0 & 0 & 0 & 0 & 0 & 0 & 0 & 0 & 0 & & \\
0 & 0 & -\frac{L}{10} & 0 & -\frac{L^2}{30} & 0 & 0 & 0 & \frac{L}{10} & 0 & \frac{2}{15}L^2 & \\
0 & \frac{L}{10} & 0 & 0 & 0 & -\frac{L^2}{30} & 0 & -\frac{L}{10} & 0 & 0 & 0 & \frac{2}{15}L^2
\end{bmatrix} \tag{4.17}$$

4.2.3 Stability Functions for Elastic Stiffness Matrix of Beam Elements

The large deformations that occur in the tower and girder elements of cable-stayed bridges generate a strong coupling between axial and flexural stiffness. This coupling can be considered in the refined nonlinear analysis by introducing the concept of stability functions, which are multiplication factors used to modify both the bending and axial stiffness of the member. Those stability functions have been derived in details by Weaver and Gere (1980) for the two-dimensional beam element. Nazmy and Abdel-Ghaffar (1990) extended the derivation to the three-dimensional beam-column elements shown in Figure 4.1. Equation 4.16 can be modified as

$$\mathbf{K}_{E,b}=\begin{bmatrix}
\frac{EA}{L}S_5 & & & & & & & & & & & & \\
0 & 12\frac{EI_z}{L^3}S_{z1} & & & & & & & & & & & \\
0 & 0 & 12\frac{EI_y}{L^3}S_{y1} & & & & & & & & & & \\
0 & 0 & 0 & \frac{GI_x}{L} & & & & & & & & & \\
0 & 0 & 6\frac{EI_y}{L^2}S_{y2} & 0 & 4\frac{EI_y}{L}S_{y3} & & & & & & & & \\
0 & 6\frac{EI_z}{L^2}S_{z2} & 0 & 0 & 0 & 4\frac{EI_z}{L}S_{z3} & & & & & & & \\
-\frac{EA}{L}S_5 & 0 & 0 & 0 & 0 & 0 & \frac{EA}{L}S_5 & & & & & & \\
0 & -12\frac{EI_z}{L^3}S_{z1} & 0 & 0 & 0 & -6\frac{EI_z}{L^2}S_{z2} & 0 & 12\frac{EI_z}{L^3}S_{z1} & & & & & \\
0 & 0 & -12\frac{EI_y}{L^3}S_{y1} & 0 & -6\frac{EI_y}{L^2}S_{y2} & 0 & 0 & 0 & 12\frac{EI_y}{L^3}S_{y1} & & & & \\
0 & 0 & 0 & -\frac{GI_x}{L} & 0 & 0 & 0 & 0 & 0 & \frac{GI_x}{L} & & & \\
0 & 0 & 6\frac{EI_y}{L^2}S_{y2} & 0 & 2\frac{EI_y}{L}S_{y4} & 0 & 0 & 0 & -6\frac{EI_y}{L^2}S_{y2} & 0 & 4\frac{EI_y}{L}S_{y3} & & \\
0 & 6\frac{EI_z}{L^2}S_{z2} & 0 & 0 & 0 & 2\frac{EI_z}{L}S_{z4} & 0 & -6\frac{EI_z}{L^2}S_{z2} & 0 & 0 & 0 & 4\frac{EI_z}{L}S_{z3}
\end{bmatrix} \quad \text{Symetric}$$

(4.18)

in which

$S_{y1} \sim S_{y4}$ – stability functions modifying the bending stiffness of the member about the local y axis,

$S_{z1} \sim S_{z4}$ – stability functions modifying the bending stiffness of the member about the local z axis,

S_5 – stability function modifying the axial stiffness.

For a tension member (axial force P is positive), the stability functions are

$$S_{y1} = \omega_y^3 \cdot \sinh\omega_y /(12R_{ty}) \tag{4.19a}$$

$$S_{y2} = \omega_y^2 \cdot (\cosh\omega_y - 1)/(6R_{ty}) \tag{4.19b}$$

$$S_{y3} = \omega_y \cdot (\omega_y \cdot \cosh\omega_y - \sinh\omega_y)/(4R_{ty}) \tag{4.19c}$$

$$S_{y4} = \omega_y \cdot (\sinh\omega_y - \omega_y)/(2R_{ty}) \quad (4.19d)$$

$$S_{z1} = \omega_z^3 \cdot \sinh\omega_z /(12R_{tz}) \quad (4.19e)$$

$$S_{z2} = \omega_z^2 \cdot (\cosh\omega_z - 1)/(6R_{tz}) \quad (4.19f)$$

$$S_{z3} = \omega_z \cdot (\omega_z \cdot \cosh\omega_z - \sinh\omega_z)/(4R_{tz}) \quad (4.19g)$$

$$S_{z4} = \omega_z \cdot (\sinh\omega_z - \omega_z)/(2R_{tz}) \quad (4.19h)$$

$$S_5 = 1/\{1 - EA(R_{tmy} + R_{tmz})/(4P^3L^2)\} \quad (4.19i)$$

where

$$\omega_y = \mu_y L \quad (4.20a)$$

$$\mu_y^2 = P/(EI_y) \quad (4.20b)$$

$$R_{ty} = 2 - 2\cosh\omega_y + \omega_y \sinh\omega_y \quad (4.20c)$$

$$\omega_z = \mu_z L \quad (4.20d)$$

$$\mu_z^2 = P/(EI_z) \quad (4.20e)$$

$$R_{tz} = 2 - 2\cosh\omega_z + \omega_z \sinh\omega_z \quad (4.20f)$$

$$R_{tmy} = \omega_y(M_{y1}^2 + M_{y2}^2)(\coth\omega_y + \omega_y \operatorname{cosech}^2\omega_y) - 2(M_{y1} + M_{y2})^2 + M_{y1} \cdot M_{y2} \cdot (1 + \omega_y \coth\omega_y)(2\omega_y \operatorname{cosech}\omega_y) \quad (4.20g)$$

$$R_{tmz} = \omega_z(M_{z1}^2 + M_{z2}^2)(\coth\omega_z + \omega_z \operatorname{cosech}^2\omega_z) - 2(M_{z1} + M_{z2})^2 + M_{z1} \cdot M_{z2} \cdot (1 + \omega_z \coth\omega_z)(2\omega_z \operatorname{cosech}\omega_z) \quad (4.20h)$$

For a compression member (axial force p is negative), the stability functions are

$$S_{y1} = \omega_y^3 \cdot \sin\omega_y /(12R_{cy}) \quad (4.21a)$$

$$S_{y2} = \omega_y^2 \cdot (1 - \cos\omega_y)/(6R_{cy}) \quad (4.21b)$$

$$S_{y3} = \omega_y \cdot (\sin\omega_y - \omega_y \cdot \cos\omega_y)/(4R_{cy}) \quad (4.21c)$$

$$S_{y4} = \omega_y \cdot (\omega_y - \sin\omega_y)/(2R_{cy}) \quad (4.21d)$$

$$S_{z1} = \omega_z^3 \cdot \sin\omega_z /(12R_{cz}) \quad (4.21e)$$

$$S_{z2} = \omega_z^2 \cdot (1 - \cos\omega_z)/(6R_{cz}) \quad (4.21f)$$

$$S_{z3} = \omega_z \cdot (\sin\omega_z - \omega_z \cdot \cos\omega_z)/(4R_{cz}) \quad (4.21g)$$

$$S_{z4} = \omega_z \cdot (\omega_z - \sin\omega_z)/(2R_{cz}) \quad (4.21h)$$

$$S_5 = 1/\{1 + EA(R_{cmy} + R_{cmz})/(4P^3L^2)\} \quad (4.21i)$$

where

$$\omega_y = \mu_y L \quad (4.22a)$$

$$\mu_y^2 = P/(EI_y) \quad (4.22b)$$

$$R_{cy} = 2 - 2\cos\omega_y - \omega_y \sin\omega_y \quad (4.22c)$$

$$\omega_z = \mu_z L \quad (4.22d)$$

$$\mu_z^2 = P/(EI_z) \quad (4.22e)$$

$$R_{cz} = 2 - 2\cos\omega_z - \omega_z \sin\omega_z \quad (4.22f)$$

$$R_{cmy} = \omega_y(M_{y1}^2 + M_{y2}^2)(\cot\omega_y + \omega_y \operatorname{cosec}^2\omega_y) - 2(M_{y1} + M_{y2})^2 + M_{y1} \cdot M_{y2} \cdot (1 + \omega_y \cot\omega_y)(2\omega_y \operatorname{cosec}\omega_y) \quad (4.22g)$$

$$R_{cmz} = \omega_z(M_{z1}^2 + M_{z2}^2)(\cot\omega_z + \omega_z \operatorname{cosec}^2\omega_z) - 2(M_{z1} + M_{z2})^2 + M_{z1} \cdot M_{z2} \cdot (1 + \omega_z \cot\omega_z)(2\omega_z \operatorname{cosec}\omega_z) \quad (4.22h)$$

4.2.4 Mass Matrix of Beam Elements

The mass matrix of a beam element can be obtained by using Equation 4.23.

$$\mathbf{M} = \int_0^L \rho \cdot A \cdot \mathbf{N}^T \cdot \mathbf{N}\, dx \quad (4.23)$$

in which ρ is the mass density of the beam and A is the area of cross-section. Substituting Equation 4.5 of shape function **N** into Equation 4.23, the mass matrix is given by

$$\mathbf{M}_b = \rho AL \cdot \begin{bmatrix}
\frac{1}{3} & & & & & & & & & & & \\
0 & \frac{13}{35} & & & & & & & & & & \\
0 & 0 & \frac{13}{35} & & & & & & & & & \\
0 & 0 & 0 & \frac{1}{3} & & & & & & & & \\
0 & 0 & \frac{11L}{210} & 0 & \frac{L^2}{105} & & & & & & & \\
0 & \frac{11L}{210} & 0 & 0 & 0 & \frac{L^2}{105} & & & & & & \\
\frac{1}{6} & 0 & 0 & 0 & 0 & 0 & \frac{1}{3} & & & & & \\
0 & \frac{9}{70} & 0 & 0 & 0 & \frac{13L}{420} & 0 & \frac{13}{35} & & & & \\
0 & 0 & \frac{9}{70} & 0 & \frac{13L}{420} & 0 & 0 & 0 & \frac{13}{35} & & & \\
0 & 0 & 0 & \frac{1}{6} & 0 & 0 & 0 & 0 & 0 & \frac{1}{3} & & \\
0 & 0 & -\frac{13L}{420} & 0 & -\frac{L^2}{140} & 0 & 0 & 0 & -\frac{11L}{210} & 0 & \frac{L^2}{105} & \\
0 & -\frac{13L}{420} & 0 & 0 & 0 & -\frac{L^2}{140} & 0 & -\frac{11L}{210} & 0 & 0 & 0 & \frac{L^2}{105}
\end{bmatrix} \quad \text{Symetric} \tag{4.24}$$

4.3 Stiffness and Mass Formulation of Cable Elements

4.3.1 Stiffness Matrix of Cable Elements Using Equivalent Modulus Method

Axial stiffness of a cable stay in a cable-stayed bridge is affected by the cable sag associated with the tension in the cable. With increase in the cable tension, the sag decreases and the axial stiffness of the inclined cable increases. A convenient method to consider the non-linearity in the inclined cable stays is to replace each cable by an equivalent chord member with an equivalent modulus of elasticity as shown in Figure 4.2, which was first introduced by Ernst (1965). The equivalent modulus of elasticity combines both the effects of material and

geometric deformations. As the cable represents a flexible member with virtually no resistance to applied moments, the idea of replacing each cable by a bar element with negligible moment of inertia has found wide acceptance and has been adopted by many researchers (Nazmy and Abdel-Ghaffar, 1990; Wang and Huang, 1992; Ren, 1999; Wang, 1999; Shu and Wang, 2001; Calcada and etc., 2005).

If the change of cable tension is negligible during a load increment, the equivalent modulus of elasticity can be considered constant and is given by

$$E_{eq} = \frac{E}{1+\left[\frac{(wL)^2 AE}{12T^3}\right]} \tag{4.25}$$

in which E is the cable material modulus of elasticity, L is the horizontal projected length of the cable, w is the weight per unit length of the cable, A is the area of the cross-section and T is the cable tension before the load increment is applied.

If the tension in the cable changes from T_i to T_j during a certain load increment, the equivalent modulus of elasticity is given by

$$E_{eq} = \frac{E}{1+\left[\frac{(wL)^2 (T_i + T_j) AE}{24 T_i^2 T_j^2}\right]} \tag{4.26}$$

The stiffness matrix of a cable stay shown in Figure 4.2 during a tension change in the cable from T_i to T_j is simply equal to

$$\mathbf{K}_{E,c} = \frac{AE_{eq}}{L_c}\begin{bmatrix} 1 & 0 & 0 & -1 & 0 & 0 \\ 0 & 0 & 0 & 0 & 0 & 0 \\ 0 & 0 & 0 & 0 & 0 & 0 \\ -1 & 0 & 0 & 1 & 0 & 0 \\ 0 & 0 & 0 & 0 & 0 & 0 \\ 0 & 0 & 0 & 0 & 0 & 0 \end{bmatrix} \tag{4.27}$$

where L_c is the chord length, A is the cross-sectional area and E_{eq} is the equivalent modulus of elasticity defined in Equation 4.26. The corresponding nodal displacement vector is

$$\boldsymbol{\delta}_e = [u_i, v_i, w_i, u_j, v_j, w_j]^T \tag{4.28}$$

where u_i, v_i, w_i, u_j, v_j *and* w_j are the translation of node i and j in the x, y and z direction correspondingly. The geometric stiffness matrix of truss element (Nazmy and Abdel-Ghaffar, 1990) is given by

$$\mathbf{K}_{G,c} = \frac{T}{L_c}\begin{bmatrix} 0 & 0 & 0 & 0 & 0 & 0 \\ 0 & 1 & 0 & 0 & -1 & 0 \\ 0 & 0 & 1 & 0 & 0 & -1 \\ 0 & 0 & 0 & 0 & 0 & 0 \\ 0 & -1 & 0 & 0 & 1 & 0 \\ 0 & 0 & -1 & 0 & 0 & 1 \end{bmatrix} \tag{4.29}$$

Therefore, the tangent stiffness matrix of a cable stay is

$$\mathbf{K}_{T,c} = \mathbf{K}_{E,c} + \mathbf{K}_{G,c} \tag{4.30}$$

Basically, the stay cables are modeled by truss elements whose nodal points are located at their supports in the deck and pylon. Each individual stay cable is treated as one element and the resulting modal configurations include the vibrating deck and pylons. Some researchers (Abdel-Ghaffar and Khalifa, 1991) paid further attention to cable vibration by modeling cable with multiple truss elements.

4.3.2 Stiffness Matrix of Cable Elements Using Refined Method

Although the equivalent modulus method has been adopted by several investigators, it has been shown that this approach results in softer cable response as it considers the sag effect but doesn't consider the stiffening effect due to large displacements. For cases such as short span cable-stayed bridges, analysis using equivalent modulus is often sufficient. However, long-span cable-stayed bridges built today are very flexible; they undergo large displacements, and should therefore be analyzed taking into account all sources of geometric nonlinearity. Today various other cable modeling techniques can be found in the literature. Gambhir and Batchelor (1977) developed a two-node curved finite element using cubic polynomial interpolation functions and used for the static and dynamic analysis of 3-D prestressed cable nets. Ozdemir(1979) developed another two-node curved finite element using Lagrangian functions for the interpolation of element geometry. Bathe(1996) presented an isoparametric cable element

including the element curvature. Ali and Abdel-Gaffar (1995) used a four-node isoparametric cable element for nonlinear seismic analysis of cable-stayed bridges.

O'Brien and Francis (1964) proposed a numerical trial and error method for cables under two-dimensional loads using basic elastic catenary equations. O'Brien (1967) generalized this method to include three-dimensional systems of loads, which accounted for the effects of superimposed concentrated loads, 3-D distributed loading acting over the full length or a part of the cable span, temperature change, and movement of the supports. This approach was later adopted by other investigators, and used for the analysis of simple cable structures (Peyrot and Goulois, 1979; Jayaraman and Knudson, 1981) and of power transmission lines (Peyrot and Goulois, 1978). The same approach was also suggested for the analysis of cable-stayed bridges (Karoumi, 1999; Xu and Guo, 2003). Yang and Fonder (1998) extended this method by modeling a stay cable with multiple catanary elements.

The cable element used in this study is derived using the exact analytical expressions for the elastic catenary. Detailed derivation is presented in the following section based on the algorithm suggested by O'Brien and Francis (1964). However, the analytical expressions for the elastic catenary adopted here are somewhat simpler and therefore easier to handle. The differences also occur in the method of initialization and iterative procedure for faster convergence and better precision.

4.3.2.1 Basic Equations of Elastic Catenary

The elastic cable element is considered as an elastic catenary with an unstressed length L_u, modulus of elasticity E, cross sectional area A, and weight per unit length w as shown in Figure 4.3(a). Assuming the cable is perfectly flexible and Hooke's law is applicable to the cable material, the equilibrium equations for the free body diagram of a cable segment are:

$$\begin{aligned} \sum F_x &= 0; \quad d(T \cdot \cos\phi) = 0 \\ \sum F_y &= 0; \quad d(T \cdot \sin\phi) = w \cdot ds \end{aligned} \tag{4.31}$$

From Equation 4.31

$$T \cdot \cos\phi = -N_{xi} = N_{xj} = const$$
$$d(N_{xi} \cdot \tan\phi) + w \cdot ds = 0 \tag{4.32}$$

where

$$\tan\phi = \frac{dy}{dx}$$
$$ds = \sqrt{dx^2 + dy^2} \tag{4.33}$$

Substituting Equation 4.33 into Equation 4.32, the basic differential equation is given by the usual expression

$$N_{xi}\frac{d^2y}{dx^2} + w \cdot \sqrt{1 + \frac{d^2y}{dx^2}} = 0 \tag{4.34}$$

Letting $p = \frac{dy}{dx}$, Equation 4.34 can be written as

$$\frac{dp}{\sqrt{1+p^2}} = -\frac{w}{N_{xi}} \cdot dx \tag{4.35}$$

Integrating Equation 4.35 gives

$$\int \frac{dp}{\sqrt{1+p^2}} = -\frac{w}{N_{xi}} \cdot x + \eta \tag{4.36}$$

Letting $p = \sinh\theta$, it gives

$$\int \frac{dp}{\sqrt{1+p^2}} = \int \frac{\cosh\theta}{\cosh\theta} \cdot d\theta = \theta = \sinh^{-1} p = -\frac{w}{N_{xi}} \cdot x + \eta \tag{4.37}$$

$$p = \frac{dy}{dx} = \sinh\left(-\frac{w}{N_{xi}} \cdot x + \eta\right) \tag{4.38}$$

Integrating Equation 4.38 gives

$$y(x) = -\frac{N_{xi}}{w}\cosh\left(-\frac{w}{N_{xi}} \cdot x + \eta\right) + \eta_1 \tag{4.39}$$

Inserting the conditions that y = 0 when x = 0 and y = L_y, it gives

$$\begin{aligned} y(x) &= -\frac{N_{xi}}{w}\cosh\left(-\frac{w}{N_{xi}} \cdot x + \eta\right) + \frac{N_{xi}}{w}\cosh(\eta) \\ &= -\frac{2N_{xi}}{w} \cdot \sinh\left(-\frac{w}{2N_{xi}} \cdot x + \eta\right) \cdot \sinh(\eta) \end{aligned} \tag{4.40}$$

where

$$\eta = -\alpha + \sinh^{-1}\left(\frac{L_y}{L_x}\cdot\frac{\alpha}{\sinh\alpha}\right) \tag{4.41}$$

$$\alpha = -\frac{wL_x}{2N_{xi}} \tag{4.42}$$

L_x – the horizontal projected length of the cable;

L_y – the vertical projected length of the cable;

To obtain the length of the cable

$$\begin{aligned} L_u &= \int ds = \int_0^{Lx}\sqrt{1+\left(\frac{dy}{dx}\right)^2}\,dx = \int_0^{Lx}\sqrt{1+\left[\sinh\left(-\frac{w}{N_{xi}}\cdot x+\eta\right)\right]^2}\,dx \\ &= -\frac{N_{xi}}{w}\left[\sinh\left(-\frac{w\cdot L_x}{N_{xi}}+\eta\right)-\sinh(\eta)\right] \\ &= -\frac{2N_{xi}}{w}\sinh(\alpha)\cdot\cosh(\alpha+\eta) \end{aligned} \tag{4.43}$$

Substituting Equation 4.41 into Equation 4.43

$$L_u = \sqrt{L_x^{\,2}\cdot\left(\frac{\sinh\alpha}{\alpha}\right)^2 + L_y^{\,2}} \tag{4.44}$$

To obtain vertical component of cable tension at each end of the cable

$$N_{yi} = N_{xi}\cdot\left(\frac{dy}{dx}\right)_{x=0} = N_{xi}\cdot\sinh\eta \tag{4.45}$$

From Equation 4.43 and 4.41

$$\cosh(\alpha+\eta) = -\frac{L_u\cdot w}{2N_{xi}\cdot\sinh\alpha}$$

$$\sinh(\alpha+\eta) = \frac{L_y}{L_x}\cdot\frac{\alpha}{\sinh\alpha} \tag{4.46}$$

$$\sinh\eta = \sinh(\alpha+\eta-\alpha) = \sinh(\alpha+\eta)\cosh\alpha - \cosh(\alpha+\eta)\sinh\alpha$$

Substituting Equation 4.46 into 4.45 yields on simplification

$$N_{yi} = \frac{w}{2}\left(L_u - L_y\frac{\cosh\alpha}{\sinh\alpha}\right) \tag{4.47}$$

$$N_{yj} = wLu - N_{yi}$$
$$= \frac{w}{2}\left(L_u + L_y \frac{\cosh\alpha}{\sinh\alpha}\right) \tag{4.48}$$

To obtain the cable tension at each end of the cable

$$T_i = \left|N_{xi}\left(\frac{ds}{dx}\right)_{x=0}\right| = \left(-N_{xi}\sqrt{1+\left(\frac{dy}{dx}\right)^2}\right)_{x=0} = -N_{xi}\cosh\eta$$
$$T_j = \left|N_{xj}\left(\frac{ds}{dx}\right)_{x=Lx}\right| = \left(-N_{xi}\sqrt{1+\left(\frac{dy}{dx}\right)^2}\right)_{x=Lx} = -N_{xi}\cosh(\eta+2\alpha) \tag{4.49}$$

From Equation 4.46

$$\cosh\eta = \cosh(\alpha+\eta-\alpha) = \cosh(\alpha+\eta)\cosh\alpha - \sinh(\alpha+\eta)\sinh\alpha$$
$$= -\frac{L_u w}{2N_{xi}}\frac{\cosh\alpha}{\sinh\alpha} + \frac{L_y}{L_x}\frac{wL_x}{2N_{xi}}$$
$$\cosh(\eta+2\alpha) = \cosh(\alpha+\eta+\alpha) = \cosh(\alpha+\eta)\cosh\alpha + \sinh(\alpha+\eta)\sinh\alpha \tag{4.50}$$
$$= -\frac{L_u w}{2N_{xi}}\frac{\cosh\alpha}{\sinh\alpha} - \frac{L_y}{L_x}\frac{wL_x}{2N_{xi}}$$

Substituting Equation 4.50 into 4.49

$$T_i = \frac{w}{2}\left(L_u \frac{\cosh\alpha}{\sinh\alpha} - L_y\right)$$
$$T_j = \frac{w}{2}\left(L_u \frac{\cosh\alpha}{\sinh\alpha} + L_y\right) \tag{4.51}$$

From Equation 4.51, an alternative expression for the vertical projection of the segment is obtained in terms of T_i and T_j

$$L_y = \frac{T_j - T_i}{w} \tag{4.52}$$

Also from Equation 4.51, an alternative expression for the horizontal projection of the segment is obtained as following

$$T_i + T_j = wL_u \frac{\cosh\alpha}{\sinh\alpha}$$

$$\alpha = \coth^{-1}\left(\frac{T_i + T_j}{wL_u}\right) = \frac{1}{2}\ln\frac{T_i + T_j + wL_u}{T_i + T_j - wL_u} = -\frac{wL_u}{2N_{xi}}$$

$$L_x = -\frac{N_{xi}}{w}\ln\frac{T_i + T_j + wL_u}{T_i + T_j - wL_u} \tag{4.53}$$

From Equations 4.47, 4.48 and 4.51

$$\frac{T_i + T_j + wL_u}{T_i + T_j + wL_u} = \frac{T_j + N_{yj}}{T_i - N_{yi}} = \frac{\sinh\alpha + \cosh\alpha}{\cosh\alpha - \sinh\alpha} \tag{4.54}$$

Therefore, Equation 4.53 can be written as

$$L_x = -\frac{N_{xi}}{w}\ln\frac{T_j + N_{yj}}{T_i - N_{yi}} \tag{4.55}$$

4.3.2.2 The Elastic Deformation of Cable

The elastic deformation of the cable is

$$\begin{aligned}(\Delta L_u)_E &= \int_s \frac{Tds}{EA} = \int_s |N_{xi}| \cdot \frac{ds}{dx}\cdot\frac{ds}{EA} = \int_0^{Lx} -\frac{N_{xi}}{EA}\left(1 + \left(\frac{dy}{dx}\right)^2\right)dx \\ &= -\frac{N_{xi}}{EA}\int_0^{Lx}\cosh^2\left(-\frac{w}{N_{xi}}\cdot x + \eta\right)dx \\ &= -\frac{N_{xi}}{2EA} + \frac{N_{xi}^2}{4EAw}(\sinh(4\alpha + 2\eta) - \sinh(2\eta)) \\ &= -\frac{N_{xi}}{2EA} + \frac{N_{xi}^2}{2EAw}\sinh(2\alpha)\cosh(2\alpha + 2\eta) \\ &= -\frac{N_{xi}}{2EA} + \frac{N_{xi}^2}{2EAw}\sinh(2\alpha)(2\cosh^2(\alpha + \eta) - 1)\end{aligned} \tag{4.56}$$

Substituting Equation 4.46, which on simplification yields

$$(\Delta L_u)_E = -\frac{N_{xi}}{2EA} + \frac{wL_u^2}{2EA}\frac{\cosh\alpha}{\sinh\alpha} - \frac{N_{xi}^2}{2EAw}\sinh(2\alpha) \tag{4.57}$$

To obtain horizontal component of the elastic deformation of the cable

$$(\Delta L_x)_E = \int_s \frac{Tds}{EA}\cos\phi = \int_s |N_{xi}| \cdot \frac{ds}{dx} \cdot \frac{ds}{EA} \cdot \frac{dx}{ds} = \int_0^{Lx} -\frac{N_{xi}}{EA}\sqrt{\left(1+\left(\frac{dy}{dx}\right)^2\right)}dx$$
$$= -\frac{N_{xi}L_u}{EA} \tag{4.58}$$

To obtain vertical component of the elastic deformation of the cable

$$(\Delta L_y)_E = \int_s \frac{Tds}{EA}\sin\phi = \int_s |N_{xi}| \cdot \frac{ds}{dx} \cdot \frac{ds}{EA} \cdot \frac{dy}{ds} = \int_0^{Lx} -\frac{N_{xi}}{EA}\frac{dy}{dx}\sqrt{\left(1+\left(\frac{dy}{dx}\right)^2\right)}dx$$
$$= -\frac{N_{xi}}{EA}\int_0^{Lx}\cosh(-\frac{w}{N_{xi}}x+\eta)\sinh(-\frac{w}{N_{xi}}x+\eta)dx$$
$$= -\frac{N_{xi}}{2EA}\int_0^{Lx}\sinh(-\frac{2w}{N_{xi}}x+2\eta)dx \tag{4.59}$$
$$= \frac{N_{xi}^2}{2EAw}[\cosh^2(-\frac{wL_x}{N_{xi}}+\eta)-\cosh^2\eta]$$

Substituting Equation 4.49 into Equation 4.57, it yields

$$(\Delta L_y)_E = \frac{1}{2EAw}(T_j^2 - T_i^2) \tag{4.60}$$

4.3.2.3 The Tangent Stiffness Matrix of Cable Element

From Equations 4.52, 4.55, 4.58 and 4.60, the exact relations between the element projections and cable force components at the ends of the element can be expressed as following, which includes the elastic catenary deformation

$$L_x = -N_{xi}\left(\frac{L_u}{EA} + \frac{1}{w}\ln\frac{T_j + N_{yj}}{T_i - N_{yi}}\right) \tag{4.61a}$$

$$L_y = \frac{1}{2EAw}(T_j^2 - T_i^2) + \frac{T_j - T_i}{w} \tag{4.61b}$$

By substituting the following relationships into Equation 4.61

$$\begin{aligned} N_{yj} &= wL_u - N_{yi} \\ N_{xj} &= -N_{xi} \\ T_i &= \sqrt{N_{xi}^2 + N_{yi}^2} \\ T_j &= \sqrt{N_{xj}^2 + N_{yj}^2} \end{aligned} \tag{4.62}$$

and differentiating the new expression of L_x and L_y with respect to N_{xi} and N_{yi}, we get

$$\begin{Bmatrix} dL_x \\ dL_y \end{Bmatrix} = \begin{bmatrix} \frac{\partial L_x}{\partial N_{xi}} & \frac{\partial L_x}{\partial N_{yi}} \\ \frac{\partial L_y}{\partial N_{xi}} & \frac{\partial L_y}{\partial N_{yi}} \end{bmatrix} \begin{Bmatrix} dN_{xi} \\ dN_{yi} \end{Bmatrix} = \mathbf{F} \begin{Bmatrix} dN_{xi} \\ dN_{yi} \end{Bmatrix} \tag{4.63}$$

where **F** is the flexibility matrix;

$$\frac{\partial L_x}{\partial N_{xi}} = \frac{Lx}{N_{xi}} - \frac{N_{xi}^2}{w}\left(\frac{1}{T_j(N_{yj}+T_j)} - \frac{1}{T_i(T_i - N_{yi})}\right) \tag{4.64a}$$

$$\frac{\partial L_x}{\partial N_{yi}} = \frac{\partial L_y}{\partial N_{xj}} = \frac{N_{xi}}{w}\left(\frac{1}{T_j} - \frac{1}{T_i}\right) \tag{4.64b}$$

$$\frac{\partial L_y}{\partial N_{yi}} = -\frac{L_u}{EA} - \frac{1}{w}\left(\frac{N_{yj}}{T_j} + \frac{N_{yi}}{T_i}\right) \tag{4.64c}$$

The stiffness matrix is obtained by the inverse of **F**, i.e. $\mathbf{K} = \mathbf{F}^{-1}$. The tangent stiffness matrix $\mathbf{K}_{T,\,c}$ and the corresponding internal force vector **P** for the element can now be expressed in terms of the six nodal degrees of freedom as

$$\mathbf{K}_{T,c} = \begin{bmatrix} -k_1 & & & & & \\ -k_2 & -k_3 & & & & \\ 0 & 0 & 0 & \textit{symetric} & & \\ k_1 & k_2 & 0 & -k_1 & & \\ k_2 & k_3 & 0 & -k_2 & -k_3 & \\ 0 & 0 & 0 & 0 & 0 & 0 \end{bmatrix} \tag{4.65a}$$

$$\mathbf{P} = \begin{bmatrix} N_{xi} \\ N_{yi} \\ 0 \\ N_{xj} \\ N_{yj} \\ 0 \end{bmatrix} \tag{4.65b}$$

where

$$k_1 = -\frac{1}{\det \mathbf{F}}\left[\frac{L_u}{EA} + \frac{1}{w}\left(\frac{N_{yj}}{T_j} + \frac{N_{yi}}{T_i}\right)\right] \tag{4.66a}$$

$$k_2 = -\frac{1}{\det \mathbf{F}}\left[\frac{N_{xi}}{w}\left(\frac{1}{T_j}-\frac{1}{T_i}\right)\right] \tag{4.66b}$$

$$k_3 = -\frac{1}{\det \mathbf{F}}\left[-\frac{Lx}{N_{xi}}+\frac{N_{xi}^2}{w}\left(\frac{1}{T_j(N_{yj}+T_j)}-\frac{1}{T_i(T_i-N_{yi})}\right)\right] \tag{4.66c}$$

$$\begin{aligned}\det \mathbf{F} = &\left[\frac{L_u}{EA}+\frac{1}{w}\left(\frac{N_{yj}}{T_j}+\frac{N_{yi}}{T_i}\right)\right]\cdot\left[\frac{Lx}{N_{xi}}+\frac{N_{xi}^2}{w}\left(\frac{1}{T_j(N_{yj}+T_j)}-\frac{1}{T_i(T_i-N_{yi})}\right)\right]\\ &-\left[\frac{N_{xi}}{w}\left(\frac{1}{T_j}-\frac{1}{T_i}\right)\right]^2\end{aligned} \tag{4.66d}$$

The element tangent stiffness matrix $\mathbf{K_{T,e}}$ relates the incremental element nodal force vector

$$\Delta\mathbf{P} = \{\Delta N_{xi}, \Delta N_{yi}, 0, \Delta N_{xj}, \Delta N_{yji}, 0\}^T \tag{4.67}$$

to the incremental nodal displacement vector

$$\Delta\boldsymbol{\delta} = [\,\Delta u_i,\ \Delta v_i,\ \Delta w_i, \Delta u_j,\ \Delta v_j,\ \Delta w_j]^T \tag{4.68}$$

4.3.2.4 Evaluation of the Tangent Stiffness Matrix and Internal Member Force

The following procedure is introduced to evaluate the tangent stiffness matrix and internal member force.

a) Evaluation of α And Initialization of N_{xi} and N_{yi}

To evaluate the tangent stiffness matrix $\mathbf{K_{T,e}}$ the end forces N_{xi} and N_{yi} must be determined. To initialize N_{xi} and N_{yi}, an important parameter α will be calculated first. Assuming the initial L_u, L_x and L_y are known, Equation 4.31a can be rewritten in the form

$$\frac{\sinh\alpha}{\alpha}-\frac{\sqrt{L_u^2-L_y^2}}{L_x}=0 \tag{4.69}$$

In order to get more accurate value of α, Newton-Raphson Method is introduced to solve Equation 4.69. Let

$$f(\alpha)=\frac{\sinh\alpha}{\alpha}-\frac{\sqrt{L_u^2-L_y^2}}{L_x} \tag{4.70}$$

The Taylor series of $f(\alpha)$ about the point $\alpha = \alpha_0 + \varepsilon$ is given by

$$f(\alpha_0+\varepsilon)=f(\alpha_0)+\frac{1}{1!}f'(\alpha_0)\varepsilon+\frac{1}{2!}f''(\alpha_0)\varepsilon^2+\cdots\infty \tag{4.71}$$

Keeping terms only to first order,

$$f(\alpha_0+\varepsilon)\approx f(\alpha_0)+f'(\alpha_0)\varepsilon \tag{4.72}$$

This expression can be used to estimate the amount of offset ε needed to land closer to the root starting from an initial guess ε. Setting $f(\alpha_0+\varepsilon)=0$ and solving for $\varepsilon \equiv \varepsilon_0$, it gives

$$\varepsilon_0=-\frac{f(\alpha_0)}{f'(\alpha_0)} \tag{4.73}$$

which is the first-order adjustment to the root's position. By letting $\alpha_1 = \alpha_0 + \varepsilon_0$, and so on, the process can be repeated until it converges to a root using

$$\varepsilon_n=-\frac{f(\alpha_n)}{f'(\alpha_n)} \tag{4.74}$$

With a good initial choice of the root's position, the algorithm can by applied iteratively to obtain

$$\alpha_{n+1}=\alpha_n-\frac{f(\alpha_n)}{f'(\alpha_n)} \tag{4.75}$$

According to the definition of Taylor expansion, any function $f(x)$ can be represented by the infinite series

$$f(x)=f(0)+\frac{1}{1!}f'(0)x+\frac{1}{2!}f''(0)x^2+\frac{1}{3!}f'''(0)x^3+\cdots\infty \tag{4.76}$$

The following expression is obtained for $\sinh\alpha$

$$\sinh\alpha=\alpha+\frac{1}{3!}\alpha^3+\frac{1}{5!}\alpha^5+\cdots+\infty\approx\alpha+\frac{1}{3!}\alpha^3 \tag{4.77}$$

Substituting Equation 4.77 into 4.69,

$$1+\frac{1}{3!}\alpha^2=\frac{\sqrt{L_u^2-L_y^2}}{L_x} \tag{4.78}$$

Therefore

$$\alpha = \sqrt{6\left(\frac{\sqrt{L_u^2 - L_y^2}}{L_x} - 1\right)} \tag{4.79}$$

which can be used as the initial trial α_0 that provides safe convergence.

For Cases where Equation 4.79 cannot be used because the unstressed cable length is less than the chord length, a conservative value of 0.2 for α is assumed.

Once the value of α is obtained, based on the catenary relationships, the initial values can be determined as

$$N_{xi} = -\frac{wL_x}{2\alpha} \tag{4.74}$$

and

$$N_{yi} = \frac{w}{2}\left(-L_y \frac{\cosh\alpha}{\sinh\alpha} + L_u\right) \tag{4.75}$$

Using Equation 4.32, N_{xj}, N_{yj}, T_i and T_j can also be obtained.

b) Evaluation of Tangent Stiffness Matrix $K_{T,c}$

From Section a, the end forces of cable element are obtained based on basic catenary equations. However, elastic deformation of cable element should be taken into account in order to get more accurate results. This can be achieved by the following procedure.

Newton-Raphson method is used to solve Equations 4.61a and 4.61b for the given L_u, L_x and L_y. Let

$$f_1(N_{xi}, N_{yi}) = -N_{xi}\left(\frac{L_u}{EA} + \frac{1}{w}\ln\frac{T_j + N_{yj}}{T_i - N_{yi}}\right) - L_x = 0 \tag{4.76a}$$

$$f_2(N_{xi}, N_{yi}) = \frac{1}{2EAw}(T_j^2 - T_i^2) + \frac{T_j - T_i}{w} - L_y = 0 \tag{4.76b}$$

The functions f_1 and f_2 can be expanded in Taylor series

$$f_1(N_{xi}+\delta N_{xi}, N_{yi}+\delta N_{yi}) = f_1(N_{xi}, N_{yi}) + \frac{\partial f_1}{\partial N_{xi}} dN_{xi} + \frac{\partial f_1}{\partial N_{yi}} dN_{yi} + o(\delta N_{xi}^2) + o(\delta N_{yi}^2) \tag{4.77a}$$

$$f_2(N_{xi}+\delta N_{xi}, N_{yi}+\delta N_{yi}) = f_2(N_{xi}, N_{yi}) + \frac{\partial f_2}{\partial N_{xi}} dN_{xi} + \frac{\partial f_2}{\partial N_{yi}} dN_{yi} + o(\delta N_{xi}^2) + o(\delta N_{yi}^2) \tag{4.77b}$$

By neglecting the terms of order δN_{xi}^2, δN_{yi}^2 and higher, and by setting

$$f_1(N_{xi}+\delta N_{xi}, N_{yi}+\delta N_{yi}) = 0$$

$$f_2(N_{xi}+\delta N_{xi}, N_{yi}+\delta N_{yi}) = 0$$

the following equations are obtained for the corrections δN_{xi} and δN_{yi} that move each function closer to zero simultaneously, namely

$$\begin{aligned} \frac{\partial f_1}{\partial N_{xi}} dN_{xi} + \frac{\partial f_1}{\partial N_{yi}} dN_{yi} &= -f_1(N_{xi}, N_{yi}) \\ \frac{\partial f_2}{\partial N_{xi}} dN_{xi} + \frac{\partial f_2}{\partial N_{yi}} dN_{yi} &= -f_2(N_{xi}, N_{yi}) \end{aligned} \tag{4.78}$$

Substituting the following relationship into Equation 4.78

$$\begin{aligned} &\frac{\partial f_1}{\partial N_{xi}} \equiv \frac{\partial L_x(N_{xi}, N_{yi})}{\partial N_{xi}}, \quad \frac{\partial f_1}{\partial N_{yi}} \equiv \frac{\partial L_x(N_{xi}, N_{yi})}{\partial N_{yi}} \\ &\frac{\partial f_2}{\partial N_{xi}} \equiv \frac{\partial L_y(N_{xi}, N_{yi})}{\partial N_{xi}}, \quad \frac{\partial f_2}{\partial N_{yi}} \equiv \frac{\partial L_y(N_{xi}, N_{yi})}{\partial N_{yi}} \\ &dL_x \equiv L_x - L_x(N_{xi}, N_{yi}) \equiv -f_1(N_{xi}, N_{yi}) \\ &dL_y \equiv L_y - L_y(N_{xi}, N_{yi}) \equiv -f_2(N_{xi}, N_{yi}) \end{aligned} \tag{4.79}$$

it can obtain the same expression as Equation 4.63. The results got from the previous section can be used as the initial trial. By solving Equation 4.63, the corrections are added to the solution vector,

$$\begin{Bmatrix} N_{xi} \\ N_{yi} \end{Bmatrix}_{new} = \begin{Bmatrix} N_{xi} \\ N_{yi} \end{Bmatrix}_{old} + \begin{Bmatrix} dN_{xi} \\ dN_{yi} \end{Bmatrix} \tag{4.80}$$

and the process iterated to convergence. The member force **P** and tangent stiffness matrix $\mathbf{K}_{T,e}$ are also obtained from Equation 4.65. In general it is a good idea to check the degree to which

both functions and variables have converged. Once either reaches machine accuracy, the other won't change.

c) Summary of the Iteration Procedure of Cable Element

To evaluate the tangent stiffness matrix $\mathbf{K}_{T,c}$ and internal force vector **P** for the given L_u, L_x and L_y, the following iteration procedure is summarized as following:

1. Set tolerant $tol = 1.0\times10^{-5}$.
2. Assuming L_u, L_x and L_y are given, calculate α. If $L_u < \sqrt{L_x^2 + L_y^2}$, α is equal to 0.2.
3. Initialize N_{xi}, N_{yi}, N_{xj}, N_{yj}, T_i and T_j.
4. From Equation 4.61, calculate $L_x(N_{xi}, N_{yi})$ and $L_y(N_{xi}, N_{yi})$.
   If $L_u < \sqrt{L_x^2(N_{xi},N_{yi}) + L_y^2(N_{xi},N_{yi})}$, go to step 8.
5. Calculate dL_x and dL_y. If $dL_x<tol$ and $dL_y<tol$, go to step 8.
6. Calculate flexibility matrix **F** and the inverse of **F**, **K**.
7. Calculate dN_{xi} and dN_{yi}. If $dL_x<tol$ and $dL_y<tol$, go to step 8; otherwise, update N_{xi} and N_{yi} from Equation 4.80, and go back to step 4.
8. Calculate member force **P** and tangent stiffness matrix $\mathbf{K}_{T,c}$.

4.3.3 Mass Matrix of Cable Elements

For the dynamic analysis, mass discretization is simply done by static lumping of the element mass at both ends giving the following lumped mass matrix (ρ is the mass density of the cable):

$$\mathbf{M} = \frac{\rho A L_u}{2}\begin{bmatrix} 1 & 0 & 0 & 0 \\ 0 & 1 & 0 & 0 \\ 0 & 0 & 1 & 0 \\ 0 & 0 & 0 & 1 \end{bmatrix} \tag{4.81}$$

4.3.4 Natural Frequency of Inclined Cables

For the out-of-plane motion (swinging modes, the z direction in Figure 4.3), the natural circular frequency of vibration of an inclined stay cable is (Irvine, 1981)

$$\omega_n = \frac{n\pi}{L_c}\sqrt{\frac{N_{xj}\cdot L_c}{m\cdot L_x}} \quad (n=1,2,3,\cdots) \tag{4.82}$$

The anti-symmetric in-plane modes (the x-y plane) consist of anti-symmetric vertical components and symmetric longitudinal components, while the symmetric in-plane modes consist of symmetric vertical components and anti-symmetric longitudinal components. In the case of anti-symmetric motion, the circular natural frequency is

$$\omega_n = \frac{2n\pi}{L_c}\sqrt{\frac{N_{xj}\cdot L_c}{m\cdot L_x}} \quad (n=1,2,3,\cdots) \tag{4.83}$$

while the circular frequency for symmetric motion may be found from the following equation:

$$\omega = \frac{\omega^*}{L_c}\sqrt{\frac{N_{xj}\cdot L_c}{m\cdot L_x}} \tag{4.84a}$$

$$\tan(\frac{\omega^*}{2}) = \frac{\omega^*}{2} - \frac{4}{\lambda^2}(\frac{\omega^*}{2})^3 \tag{4.84b}$$

$$\lambda^2 = \left(\frac{mgL_x^{\ 2}}{N_{xj}\cdot L_c}\right)^2 \cdot \frac{L_x\cdot EA}{N_{xj}\cdot L_e} \tag{4.84c}$$

$$L_e = L_c\left(1+\frac{1}{8}\left(\frac{mgL_x^{\ 2}}{N_{xj}L_c}\right)^2\right) \tag{4.84d}$$

in which g is the gravitational acceleration and L_c is the chord length equal to $\sqrt{L_x^2+L_y^2}$.

4.4 Stiffness Formulation of Deck

The deck is modeled as 8-node flat shells which have been described in the previous Chapter. However, due to the nonlinear characteristics of cable-stayed bridge, linear stability features will be considered in the analysis. So far, the bending and in-plane deformation of plates is

assumed to be uncoupled. In fact, if the deflection of a plate is large in comparison with the plate thickness, especially for long-span bridges, the deflection will cause in-plane strains, and interaction begins. Because the existing in-plane stresses have significant magnitude, it is possible to assume that the in-plane stresses are not affected by bending deformation. The derivation of the geometric stiffness matrix is presented as follows.

From the texts on continuum mechanics, the general strain-displacement relations for thin two-dimensional bodies are

$$\varepsilon_{xx} = \frac{\partial u}{\partial x} + \frac{1}{2}\left[\left(\frac{\partial u}{\partial x}\right)^2 + \left(\frac{\partial v}{\partial x}\right)^2 + \left(\frac{\partial w}{\partial x}\right)^2\right] \tag{4.85a}$$

$$\varepsilon_{yy} = \frac{\partial v}{\partial y} + \frac{1}{2}\left[\left(\frac{\partial u}{\partial y}\right)^2 + \left(\frac{\partial v}{\partial y}\right)^2 + \left(\frac{\partial w}{\partial y}\right)^2\right] \tag{4.85b}$$

$$\gamma_{xy} = \frac{\partial u}{\partial y} + \frac{\partial v}{\partial x} + \left(\frac{\partial u}{\partial x}\cdot\frac{\partial u}{\partial y} + \frac{\partial v}{\partial x}\cdot\frac{\partial v}{\partial y} + \frac{\partial w}{\partial x}\cdot\frac{\partial w}{\partial y}\right) \tag{4.85c}$$

$$\gamma_{xz} = \frac{\partial u}{\partial z} + \frac{\partial w}{\partial x} + \left(\frac{\partial u}{\partial x}\cdot\frac{\partial u}{\partial z} + \frac{\partial v}{\partial x}\cdot\frac{\partial v}{\partial z} + \frac{\partial w}{\partial x}\cdot\frac{\partial w}{\partial z}\right) \tag{4.85d}$$

$$\gamma_{yz} = \frac{\partial v}{\partial z} + \frac{\partial w}{\partial y} + \left(\frac{\partial u}{\partial z}\cdot\frac{\partial u}{\partial y} + \frac{\partial v}{\partial z}\cdot\frac{\partial v}{\partial y} + \frac{\partial w}{\partial z}\cdot\frac{\partial w}{\partial y}\right) \tag{4.85e}$$

Assuming the in-plane stresses are not affected by bending deformation, Equation 4.85a-e can be simplified as

$$\varepsilon_{xx} = \frac{\partial u}{\partial x} + \frac{1}{2}\left(\frac{\partial w}{\partial x}\right)^2 \tag{4.86a}$$

$$\varepsilon_{yy} = \frac{\partial v}{\partial y} + \frac{1}{2}\left(\frac{\partial w}{\partial y}\right)^2 \tag{4.86b}$$

$$\gamma_{xy} = \frac{\partial u}{\partial y} + \frac{\partial v}{\partial x} + \frac{\partial w}{\partial x}\cdot\frac{\partial w}{\partial y} \tag{4.86c}$$

$$\gamma_{xz} = \frac{\partial u}{\partial z} + \frac{\partial w}{\partial x} + \frac{\partial w}{\partial x}\cdot\frac{\partial w}{\partial z} \tag{4.86d}$$

$$\gamma_{yz} = \frac{\partial v}{\partial z} + \frac{\partial w}{\partial y} + \frac{\partial w}{\partial z}\cdot\frac{\partial w}{\partial y} \tag{4.86e}$$

Therefore, the geometric stiffness is given by

$$\mathbf{K}_{G,s} = \int_{-h/2}^{h/2} \iint_{A} \left[\sigma_{xx}^{0} \Phi^{T} \Phi + \sigma_{yy}^{0} \Gamma^{T} \Gamma + 2\tau_{xy}^{0} \Phi^{T} \Gamma\right] dxdydz \tag{4.94}$$

The tangent stiffness matrix is

$$\mathbf{K}_{T,s} = \mathbf{K}_{E,s} + \mathbf{K}_{G,s} \tag{4.95}$$

in which $\mathbf{K}_{E,s}$ is the elastic stiffnes matrix defined by Equation 3.23a-c.

4.5 Iteration Procedure

A computer program has been developed to perform the nonlinear static analysis of three-dimensional cable-stayed bridges assuming that the initial unstressed length L_u is given for each cable. A combination of the incremental and Newton-Raphson iterative scheme is adopted in this study (Nazmy and Abdel-Ghaffar, 1990). The iteration procedure is summarized in what follows:

A. Initialization

1. For beam elements, initialize all member stability functions; set all values equal to 1.0.
2. For all the elements, initialize internal member forces **P** and tangent stiffness matrix $\mathbf{K}_m$.
3. Obtain global internal member forces vector $\mathbf{P}_{int}$ and tangent stiffness matrix $\mathbf{K}_T$ by the standard assembly procedure.
4. Compute initial unbalanced joint loads $\mathbf{F}^{(1)} = \mathbf{P}_{ext} - \mathbf{P}_{int}$, where $\mathbf{P}_{ext}$ is the externally applied joint load vector, and $\mathbf{P}_{ext} = \{0\}$ for static dead loading analysis.
5. Initialize nodal displacement vector $\mathbf{D}^{(i)} = \{0\}$, i=0
6. Assume tolerance Tol ≤ 0.001 and maximum number of iterations nitem ≥ 10.

B. Start Iteration

1. i = i+1
2. Divide the unbalanced joint load $\mathbf{F}^{(i)}$ into the required number of load increments. Each increment is given by $\Delta\mathbf{F}^{(i)} = \mathbf{F}^{(i)} / nl$, where *nl* is the number of load increments in each load cycle.

3. For each load step n,
   a. Solve $\Delta\mathbf{F}^{(i)} = \mathbf{K}_T \cdot \Delta\mathbf{D}_{(n)}^{(i)}$ to get $\Delta\mathbf{D}_{(n)}^{(i)}$.
   b. Update displacements by $\mathbf{D}_{(n+1)}^{(i)} = \mathbf{D}_{(n)}^{(i)} + \Delta\mathbf{D}_{(n)}^{(i)}$
   c. Compute member internal forces $\mathbf{P}_{(n+1)}^{(i)} = \mathbf{P}_{(n)}^{(i)} + \mathbf{K}_m \Delta\mathbf{d}_{(n)}^{(i)}$.
   d. According to the new member internal forces, calculate the tangent stiffness matrix.
   e. Assemble new global stiffness matrix $\mathbf{K}_T$
   f. Repeat steps a ~ d until the last load step is finished, then $\mathbf{D}^{(i)} = \mathbf{D}_{(n+1)}^{(i)}$.
4. Compute new global internal member forces vector $\mathbf{P}_{\text{int}}$.
5. Compute unbalanced forces $\mathbf{F}^{(i+1)} = \mathbf{P}_{\text{ext}} - \mathbf{P}_{\text{int}}$
6. Check convergence: If $\left\|\mathbf{F}^{(i+1)}\right\|_\infty < Tol$, convergence has occurred, the final displacement $\mathbf{D}_{\text{final}} = \mathbf{D}^{(i)}$; otherwise, go to step 1. *Tol* is the tolerant which is taken as 10^{-5} in the present study.

4.6 Analytical Verification of Cable Element

In this section, two Examples have been studied to verify the cable element and the iteration procedure described in Section 4.3 and Section 4.5.

4.6.1 Example 1: Horizontal Cable

A cable hanging under its own weight and subjected to a tensile force at one end along its chord, as shown in Figure 4.4, has the following given properties:

Unstressed length $L_u = 312.7$ m;

Cross section area $A = 5.48\times10^{-4}$ m^2;

Weight per unit length $w = 46.11$ N/m;

Modulus of elasticity $E = 1.31\times10^{11}$ N/m^2.

According to the theory of catenary, a horizontal force of $H_0 = 1.7794\times10^4$ N is needed to span the distance of $L_{x0} = 304.8$m using a cable with the above given properties. This force gave a

mid point cable sag of 30.48m and is adopted as initial force when calculating the curves in Figure 4.5.

Two different models have been studied. For the two models: the cable was replaced by one catenary cable element and one bar element with an equivalent modulus of elasticity. The horizontal displacement dL_x along the chord of the cable was determined for different values of the tensile force H and the results are plotted in Figure 4.5. For comparison purposes, the results calculated directly by using the theory of catenary are also presented. Good agreement is observed when comparing the catenary cable element curve with the theory curve. A significant difference can be observed when comparing the bar element curve with the theory curve. This difference is due to the fact that the equivalent modulus approach accounts for the sag effect but does not account for the stiffening effect due to large displacements, which leads to a softer cable model.

4.6.2 Example 2: Inclined Cable

To further demonstrate the capability and accuracy of the proposed method, an inclined cable shown in Figure 4.6 has been studied. It has the same physical properties as Example 1. A horizontal tension of $H_0 = 1.228\times10^3$ N is needed for the initial condition displayed in the figure. Both theoretical analysis and finite element analysis using catenary cable element are carried out to obtain the relationship between horizontal displacement dL_x and horizontal tension H. The vertical dimension L_y remains constant while the horizontal force increases from H_0 to 10 times of H_0. The horizontal displacement and horizontal tension are normalized by the initial horizontal dimension of L_{x0} and tension H_0 respectively and plotted in Figure 4.7. Evidently, the results obtained by catenary model matches the theoretical values. It indicates that the approach of catenary model is practical in the cable analysis.

4.7 Case Study – Free Vibration of Long-Span Cable-Stayed Bridge

Cable-stayed bridges consist of three main parts: the pylons, the deck and the stayed cables. For nonlinear characteristics, cable-stayed bridges include a number of considerations such as span lengths, material of superstructure, longitudinal cable configurations, number of cables, frame of pylons, and etc. In order to investigate the nonlinear characteristics and free vibrations, a wide range of various bridge profiles have been studies.

4.7.1 Bridge Description

A 3D model of cable-stayed bridge shown in Figure 4.8 was adopted for this investigation, which is similar in configuration to an existing bridge in Japan – the Meiko-Nishi Bridge in Nagoya with a few modifications in dimension as well as replacing the original steel girder deck by the current box-girder deck. The bridge with total length of 627.8m comprises three spans: a 350 m central span between the two pylons, and two side spans each with a length of 146.4 m. The bridge deck is a closed steel box-girder 23.5m wide and 5.0m high. The total height of the reinforcement concrete pylon is 91.4 m with 30.4 m from pier top to bridge deck and 61 m above the top level of bridge deck. A horizontal beam near the top of each pylon has been added to improve the pylon behavior under both static and dynamic loads. The properties of structural members are listed in Table 4.1. Figure 4.9 shows the typical cross sections of the bridge deck and the pylons. To improve torsional resistance of bridge deck, solid plate diaphragms of thickness 20mm are provided at both ends of the bridge within each box.

4.7.2 Finite Element Model

The bridges are discredited as 3-D finite element model including three types of element: beam, shell and catenary cable. First, the pylons have been modeled as three dimensional beam

elements with stability function. Next, the bridge decks have been modeled as shell element with geometry stiffness consideration. Each nodes of both shell and bean elements incorporate six degrees of freedom, i.e., translation in the x, y and z directions as well as rotation about the x, y and z axes. Last, the stayed cables have been modeled as catenary cable elements.

In developing the model, a coordinate system is chosen such that the bridge deck is parallel to the XY-plane of the coordinate system with the X-axis along the longitudinal direction of the bridge. The Z-axis is perpendicular to the bridge deck surface.

The pylons were assumed to be rigidly fixed to the piers to reduce the overall structural deformations. The bridge decks were assumed to be simply supported at the end piers or abutments in order to reduce the redundancy of the structural system. Further more, the decks were also assumed to be elastically connected to each pylon by two vertical links and two horizontal links rather than being fixed to them. It has been found from previous researches that the response of a cable-stayed bridge to applied loads is highly dependent on the manner in which the bridge deck is connected to the pylons. If the deck swings freely at the pylons, the induced member forces due to wind and earthquake loads will be kept to minimum values. But the bridge may be very flexible under service loading condition such as dead loads and traffic loads. On the other hand, rigid connections between deck and pylons will reduce movements under service loads but increase internal forces caused by wind and seismic loads. Therefore, it is very important to provide elastic connections between the deck and pylons to control the bridge structural vibration.

Based on the above properties, five cases have been studied accounting for various parameters as follows:

	Cable Arrangement	Number of Cables	Solid Plate Diaphragms of 20 mm thickness	Deck Height (m)
Case 1	Fan	48	At two ends	2.5
Case 2	Harp	48	At two ends	2.5

Case 3	Fan	48	At two ends, at two pylons and at mid-span	2.5
Case 4	Fan	48	At two ends	1.25
Case 5	Fan	24	At two ends	2.5

4.7.3 Static Non-linear Analysis under Dead Load

Geometrically non-linear static analysis of cable-stayed bridges, in which large displacements occur under service loads, is essential to start linear or non-linear dynamic analyses from the dead load deformed state. The performance of the followed free vibration analysis and forced dynamic analysis are basically relied on the accuracy of the tangent stiffness matrix of the bridge obtained under gravity load condition. The static analysis under dead load were carried out for the five cases described above and the results are presented in Figures 4.10 through 4.15 and organized as follows:

- Figure 4.10: the overall deformation of the bridge for Cases 1, 2 and 5;
- Figure 4.11: normalized horizontal cable force of Cable #1 through Cable #12; the horizontal component of the external cable reaction (Cable #1) of Case 1 is considered as unity;
- Figure 4.12: normalized cable tension at pylon; the horizontal component of the external cable reaction (Cable #1) of Case 1 is considered as unity;
- Figure 4.13: normalized maximum cable stress; the cable stress is normalized by the maximum permissible stress, which is defined as 45% of the rupture stress of cable (Walther et al. 1985). The rupture stress is assumed to be 1700 N/mm^2 in the present study;
- Figure 4.14: normalized cumulative axial forces acting on bridge deck; the horizontal component of the external cable reaction (Cable #1) of Case 1 is considered as unity;
- Figure 4.15: vertical displacement of mid-span.

4.7.3.1 Influence of Cable Arrangement

The influence of the cable arrangement is analyzed by means of the fan pattern and harp pattern shown in Figures 4.8a and 4.8b. It can be seen that the maximum normal axial force acting on the bridge deck for Case 2 is much larger than that for Case 1, which indicates that the deck is more heavily stressed in a bridge of harp pattern than in a bridge of fan pattern. In the particular case of this study, the difference is about 16.5%. It can be observed that horizontal tension of cable for Case 2 is generally larger than that for Case 1, which contributes to the larger normal axial force in deck of harp arrangement. The value of normal stress is associated with both strength and stability of bridge deck. As a result, the harp cable arrangement appears less suitable than the fan cable arrangement, especially for long-span bridges. Whatever cable layout is considered, it can be noted that there is little difference in the level of deformation.

4.7.3.2 Influence of Number of Cables

The influence of number of cables has been studied by comparing the results for Case 1 (48 cables) and Case 5 (24 cables). It can be observed that the maximum cable tension increases with the decrease in the number of cables. However, Figure 4.14 indicates that the cumulative axial force increases as the number of cables increases. The structural stiffness may be changed if the axial force increases. For the two-pylon bridge, the bridge girder around the pylon is subjected to more compressive axial loads in Case 1 than in Case 5. Large compressive axial forces may reduce the stiffness of the bridge girder and lead to stability problems. On the other hand, the midpoint of the main span of the bridge is subjected to stronger tensile axial forces in Case 1 than in Case 5. Strongly tensile axial forces may enhance the stiffness at the midpoint of the main span. As a result, the mid-span deformation in Case 5 is larger than that in Case 1.

4.7.3.3 Influence of Diaphragm in Deck

The influence of diaphragm in deck has been investigated by Case 1 with diaphragms at two ends and Case 3 with diaphragms at two ends, two pylons and mid-span. Little difference is

observed for cable tension. However, providing extra solid plate diaphragms at pylons and mid-span within each box can reduce the mid-span vertical displacement as well as the transverse flexure deformation.

4.7.3.4 Influence of Deck Inertia

The influence of deck inertia has been studied by Case 1 and Case 4. The inertia of deck in Case 4 is approximately 25% of that in Case 1 by reducing the height of deck from 2.5 meters to 1.25 meters. It can be noted that the cable tension in Case 4 is slightly reduced due to the less heavy steel deck. Although the inertia of the deck is reduced by 75%, the deformation of the steel deck only increases to a limited extent of 28%, which is not proportional to the decrease of deck inertia. These observations may lead to the conclusion that a deck with higher inertia will attract considerable bending moments without appreciably reducing the forces in the cables and the deformation of mid-span. These also emphasize the importance of the role played by the cable stays.

4.7.4 Free Vibration Analysis

Vibrations of cable-stayed bridges become harmful when a predominant excitation frequency is in the vicinity of a natural frequency of the structural system or structural members such as stay cables, which can vibrate with the deck and the tower or independently from the main bridge. Traffic loads contain a broad spectrum of excitation frequencies and may cause large dynamic amplification of the structural response. Most vulnerable to such vibrations are the high-strength cables, which have damping ratios in the range of 0.05-4.0%.

The dynamic characteristics of a cable-stayed bridge, including its natural frequencies, vibration mode shapes and mechanical damping properties are important factors which can significantly affect its stability behavior under traffic loads. The Natural frequency module of the program GLBA is employed to perform the free vibration analysis of the cable-stayed

bridges described above. The free vibration analysis is based on the stiffness obtained by the foregoing dead load iteration procedure. The first eighteen natural vibration modes are calculated. Table 4.3 presents the first eighteen natural vibration frequencies and nature of the vibration modes of the bridge for the five cases defined in Section 4.7.2. The typical mode shapes of Cases 1 through 3 and Case 5 are illustrated in Figures 14.16 through 4.19 respectively.

Table 4.2 presents the natural frequencies of selected cables corresponding to out-of-plane motion, anti-symmetric in-plane motion and symmetric in-plane motion obtained from Equations 4.82 through 4.84d. The natural frequency of cable vibration depends on the parameters including: 1) horizontal component of cable tension; 2) cable dimension; and 3) mass of cable per unit length. It should be noted that the frequencies are the initial pure cable modes and the calculation will in no way predict the combination of these individual cables as viewed on the bridge as well as the dynamic interaction between the vibrating cables and the vibrating deck-tower system. Cable vibrations are basically classified into three categories: vortex shedding, rain vibration and wake galloping (Ohashi 1991). Vortex shedding is caused by alternate vortexes behind a cable and vortexes are equal. Rain vibration is caused by water rivulets either on the upper or lower side of a cable surface when a cable has a smooth surface. Wake galloping may occur in the backward stay which is excited by the wind stream of the forward stay. Cable vibrations can be suppressed by several methods, such as: connecting stays with wires; inserting spacers between two adjacent stays to prevent wake galloping; attaching oil dampers to the stays at deck level; and attaching fins on the circular surface of cable to increase surface roughness and prevent the occurrence of water rivulets. These methods are not intended to increase structural damping but to restrain the stay movements. Few observation of cable vibration excited by traffic loads were reported in the literature. Therefore, dynamic interaction between the vibrating cables and the vibrating deck-tower system are not considered in the present study. Further studies will be conducted in the future to account for the combination effects of cable vibration coupled with deck-tower system by modeling each cable with multiple catenary elements.

From Table 4.3 as well as Figures 4.16 through 4.19, the following observations can be drawn:

1. There is strong coupling in the three orthogonal directions, especially for torsion and flexure. It indicates that a three dimensional model can better reflect the dynamic characteristics of cable-stayed bridges than a two dimensional model. It is also evident that the close spacing of the natural frequencies is another feature in each case.
2. The fundamental mode is longitudinal flexure for all five cases.
3. The first torsional mode occurs at the third mode for all cases with only two diaphragms at the ends. Providing additional diaphragms at pylon and mid-span in Case 3 results in a significant improvement in the torsional resistance of the bridge, where the first torsional mode moves from the 3^{rd} to the 7^{th} position. In comparison with Case 1, the natural frequencies of case 3 are increased and the total number of torsional mode is reduced. Therefore, extra diaphragms in bridge deck will improve torsional resistance of the bridge system.
4. For lower modes, the natural frequencies in Case 2 (harp type) are lower than in Case 1 (fan type), while for higher modes, both natural frequencies and mode shapes appear similar for the two cases. Moreover, the harp type appears to have more torsional modes for lower frequencies.
5. Comparing the results of Case 1 and Case 5, the frequencies and mode shapes are only slightly different. In other words, the number of stayed cables has minor influence on the dynamic characteristics of cable-stayed bridges.
6. Although the stiffness of deck for Case 4 has decreased 75% compared to Case 1, the natural frequencies of Case 4 only decrease 20%. It indicates that the tension of stays play an important role for the stiffness of the entire structural system. It also reflects the non-linear characteristics of cable-stayed bridges.

4.8 Summary

In this chapter, the analytical model of cable-stayed bridge is developed by using finite element method. Due to the large deformation occurred in cable-stayed bridge, geometric nonlinearity has been taken into account. Stability functions are introduced to the stiffness of beam elements

to model the pylons. Geometric stiffness matrix is derived for shell element to model the bridge deck. The cable element is derived using the exact analytical expressions for the elastic catenary. The iterative procedure for obtaining the stiffness matrix and internal forces of cable element is presented. The numerical examples of a horizontal cable and an inclined cable verify the reliability and accuracy of the proposed model and method.

The free vibration analysis is based on the deformed dead load tangent stiffness matrix. The iterative scheme is utilized to obtain the deformed dead load tangent stiffness matrix due to its nonlinear characteristics. A cable-stayed bridge with various parameters shown in 4.7.2 has been studied on the responses under dead load and free vibrations.

The following conclusions can be drawn from the results obtained in the current studies:

1. The elastic catenary cable element realistically reflects the dynamic characteristics of a stayed cable.
2. There is strong coupling in the three orthogonal directions, especially for torsion and flexure. It indicates that a three dimensional model can better reflect the dynamic characteristics of cable-stayed bridges than a two dimensional model. It is also evident that the close spacing of the natural frequencies is another feature in each case.
3. Solid plate diaphragms play an important role on the structural behavior of box-girder cable-stayed bridge. Providing diaphragms not only at ends but also at pylons and mid-span within the box can improve the torsional and lateral resistance, decrease the mid-span deflection and increase the torsional frequency.
4. Cable arrangement is an important parameter for cable-stayed bridge. The deck is more heavily stressed in a bridge of harp pattern than in a bridge of fan pattern under dead load. For lower modes, the natural frequencies in harp type are lower than in fan type, while for higher modes, both natural frequencies and mode shapes appear similar. Moreover, the harp type appears to have more torsional modes for lower frequencies.
5. The cumulative axial force under dead load increases as the number of cables increases. The structural stiffness may be changed if the axial force increases. For the two-pylon bridge, the bridge girder around the pylon is subjected to more compressive axial loads with more cables. Large compressive axial forces may reduce the stiffness of the bridge

girder and lead to stability problems. On the other hand, the midpoint of the main span of the bridge is subjected to stronger tensile axial forces with the increase of number of cables. Strongly tensile axial forces may enhance the stiffness at the midpoint of the main span. However the number of stayed cables has minor influence on the dynamic characteristics of cable-stayed bridges.

6. Increasing deck inertia will attract considerable bending moments without appreciably reducing the forces in the cables and the deformation of mid-span under dead load. The natural frequencies do not increase proportionally with the increase of deck inertia. It indicates that the tension of stays play an important role for the stiffness of the entire structural system. It also reflects the non-linear characteristics of cable-stayed bridges.
7. Cable vibrations are basically induced by vortex shedding, rain vibration and wake galloping. Several methods can be adopted to restrain the stay movements. Few observation of cable vibration excited by traffic loads were reported in the literature. Therefore, dynamic interaction between the vibrating cables and the vibrating deck-tower system are not considered in the present study. Further studies will be conducted in the future to account for the combination effects of cable vibration coupled with deck-tower system by modeling each cable with multiple catenary elements.

TABLE 4.1 PHYSICAL PROPERTIES OF STRUCTURAL MEMBERS

Pylon (R.C.)	E (N/m^2)	G (N/m^2)	A (m^2)	I_x (m^4) (1)	I_y (m^4) (1)	I_z (m^4) (1)	ρ (kg/m^3)
Vertical Members	3.0×10^{10}	1.2×10^{10}	9.29	64.73	43.15	43.15	2320
Horizontal Members	3.0×10^{10}	1.2×10^{10}	5.57	8.68	1.73	1.73	2320
Steel	E (N/m^2)	G (N/m^2)	A (m^2)	I_x (m^4) (1)	I_y (m^4) (1)	I_z (m^4) (1)	ρ (kg/m^3)
Deck	2.0×10^{11}	7.7×10^{10}	-	-	-	-	7860
Steel Links	2.0×10^{11}	7.7×10^{10}	0.28	8.63×10^{-6}	0.052	0.052	7860
Cable No.	E (N/m^2)	G (N/m^2)	A (m^2)	I_x (m^4) (1)	I_y (m^4) (1)	I_z (m^4) (1)	ρ (kg/m^3)
1,24,25,48	2.0×10^{11}	7.7×10^{10}	0.0181	-	-	-	11000
2,11,14,23, 26,35,38,47	2.0×10^{11}	7.7×10^{10}	0.0116	-	-	-	11000
3,10,15,22, 27,34,39,46	2.0×10^{11}	7.7×10^{10}	0.0102	-	-	-	11000
4,9,16,21, 28,33,40,45	2.0×10^{11}	7.7×10^{10}	0.0088	-	-	-	11000
5,8,17,20, 29,32,41,44	2.0×10^{11}	7.7×10^{10}	0.0070	-	-	-	11000
6,7,18,19, 30,31,42,43	2.0×10^{11}	7.7×10^{10}	0.0057	-	-	-	11000
12,13,36,37	2.0×10^{11}	7.7×10^{10}	0.0186	-	-	-	11000

Note:

1. I_x, I_y and I_z : moment inertia of the cross section about the local principal x, y and axes of beam members.

TABLE 4.2 FUNDAMENTAL NATURAL FREQUENCY OF SELECTED CABLES FOR FREE VIBRATION (Hz)

Out-of-plane Motion					
Cable No	Case 1	Case 2	Case 3	Case 4	Case 5
1	0.657	0.657	0.657	0.653	0.733
3	0.763	0.805	0.763	0.755	0.844
5	0.886	1.131	0.886	0.879	0.987
8	0.886	1.131	0.886	0.879	0.987
10	0.763	0.805	0.763	0.755	0.844
12	0.657	0.657	0.657	0.655	0.734
Anti-symmetric In-plane Motion					
Cable No	Case 1	Case 2	Case 3	Case 4	Case 5
1	1.314	1.314	1.314	1.306	1.466
3	1.525	1.611	1.525	1.509	1.689
5	1.771	2.263	1.771	1.759	1.973
8	1.771	2.263	1.771	1.759	1.973
10	1.525	1.611	1.525	1.509	1.689
12	1.315	1.315	1.315	1.310	1.468
Symmetric In-plane Motion					
Cable No	Case 1	Case 2	Case 3	Case 4	Case 5
1	1.874	1.874	1.874	1.862	2.091
3	2.175	2.297	2.175	2.152	2.408
5	2.526	3.227	2.526	2.508	2.814
8	2.526	3.227	2.526	2.508	2.814
10	2.175	2.297	2.175	2.152	2.408
12	1.875	1.875	1.875	1.868	2.093

TABLE 4.3 FREE VIBRATIONS OF CABLE-STAYED BRIDGES

No.	Case 1		Case 2		Case 3		Case 4		Case 5	
	Fre. (Hz)	Mode Shape	Fre. (Hz)	Mode Shape	Fre. (Hz)	Mode Shape	Fre. (Hz)	Mode Shape	Fre. (Hz)	Mode Shape
1	0.31	LF	0.29	LF	0.31	LF	0.25	LF	0.33	LF
2	0.42	LF	0.38	LF	0.43	LF	0.34	LF	0.44	LF
3	0.56	TF-TO	0.52	TF-TO	0.62	LF	0.44	TF-TO	0.57	TF-TO
4	0.61	LF	0.57	LF	0.62	LF	0.48	LF	0.63	LF
5	0.62	LF	0.60	TF-TO	0.63	LF	0.50	LF	0.64	LF
6	0.62	LF	0.60	LF	0.67	LF	0.50	LF	0.64	LF
7	0.66	LF	0.64	TF-TO	0.72	TF-TO	0.52	LF	0.66	LF
8	0.70	TF-TO	0.68	TF-TO	0.73	TF-TO	0.56	TF-TO	0.73	TF-TO
9	0.83	TF	0.75	LF	0.88	TF-TO	0.68	TF	0.85	TF
10	0.86	TF-TO	0.84	LF	0.90	TF	0.72	TF-TO	0.89	TF-TO
11	0.91	LF	0.91	LF	0.94	LF	0.74	LF	0.92	LF
12	1.01	TF-TO	1.01	TF-TO	1.11	TF	0.80	TF-TO	1.03	TF-TO
13	1.03	LF-TO	1.03	TF-TO	1.47	LF	0.83	LF-TO	1.05	TF-TO
14	1.25	LF	1.24	LF-TF	1.54	TF-TO	0.98	LF	1.28	LF
15	1.42	LF	1.41	LF	1.62	TF-TO	1.16	LF	1.44	LF
16	1.47	TF-TO	1.46	TF-TO	1.72	LF	1.19	TF-TO	1.52	TF-TO
17	1.50	TF	1.50	TF	1.72	LF	1.23	TF	1.55	TF
18	1.69	LF	1.67	LF	1.90	LF	1.34	LF	1.72	LF

Note:

1. LF – Longitudinal flexure;
2. TF – Transverse flexure;
3. TO – Torsion.

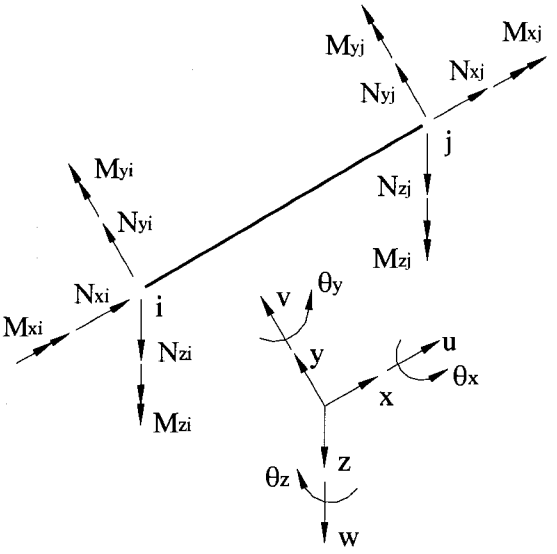

FIGURE 4.1 AXIAL FORCES AND END MOMENT FOR A BEAM ELEMENT

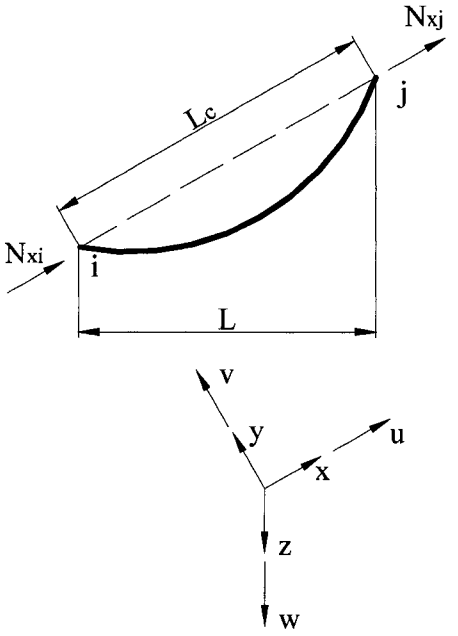

FIGURE 4.2 CABLE ELEMENT WITH EQUIVALENT MODULUS

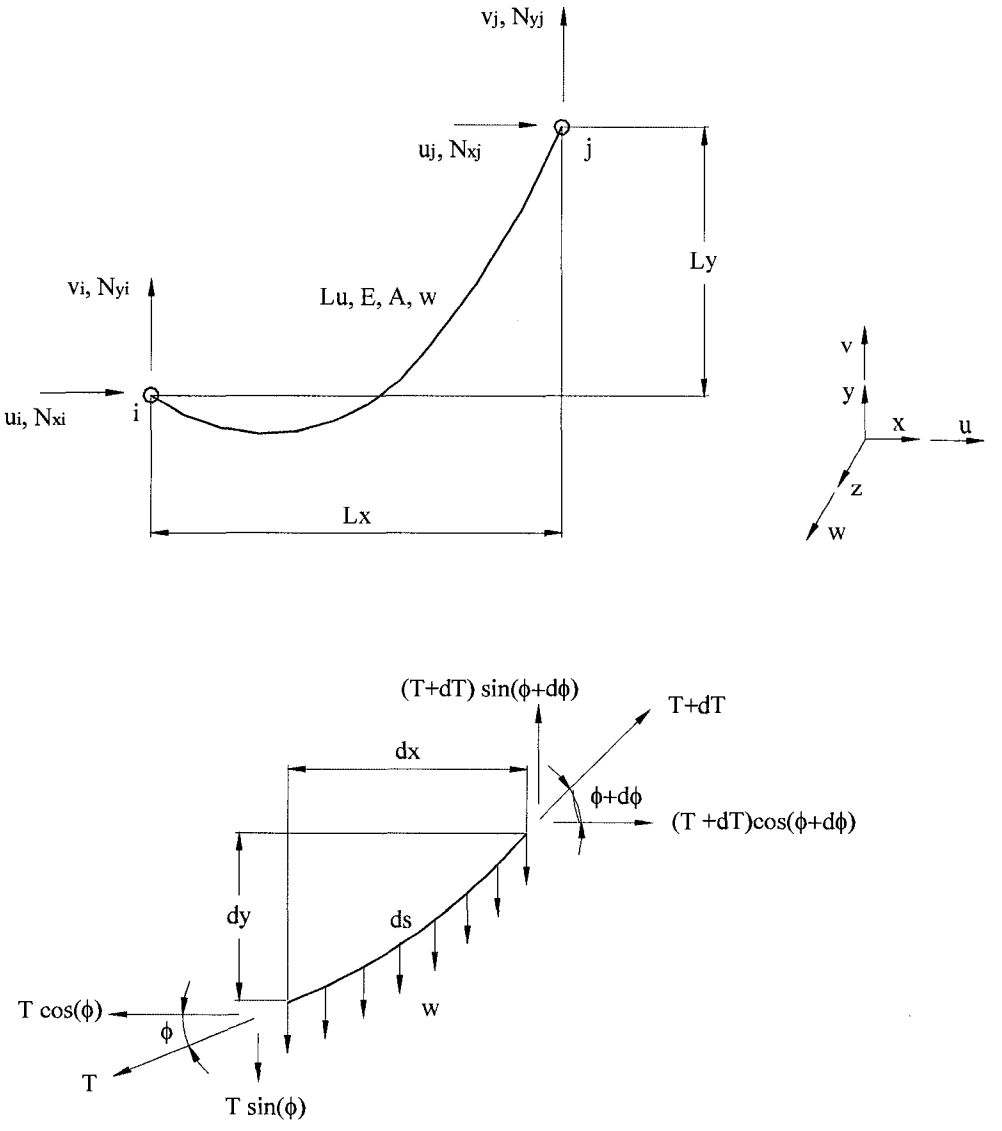

FIGURE 4.3 CATENARY CABLE ELEMENT

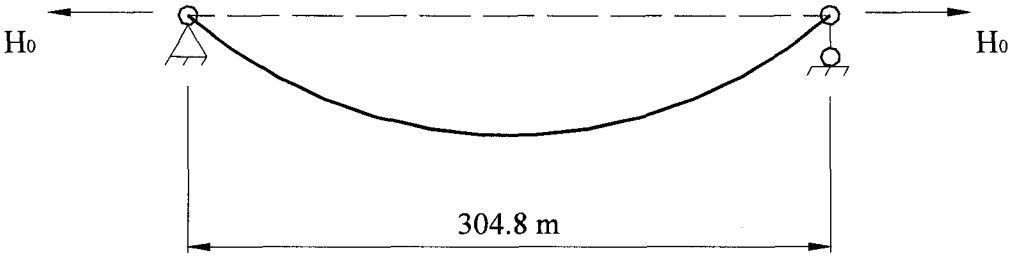

Lu = 312.7 m, E = 1.31×10^{11} N/m^2
A = 5.48×10^{-4} m^2, w = 46.11 N/m

FIGURE 4.4 EXAMPLE 1: HORIZONTAL CABLE

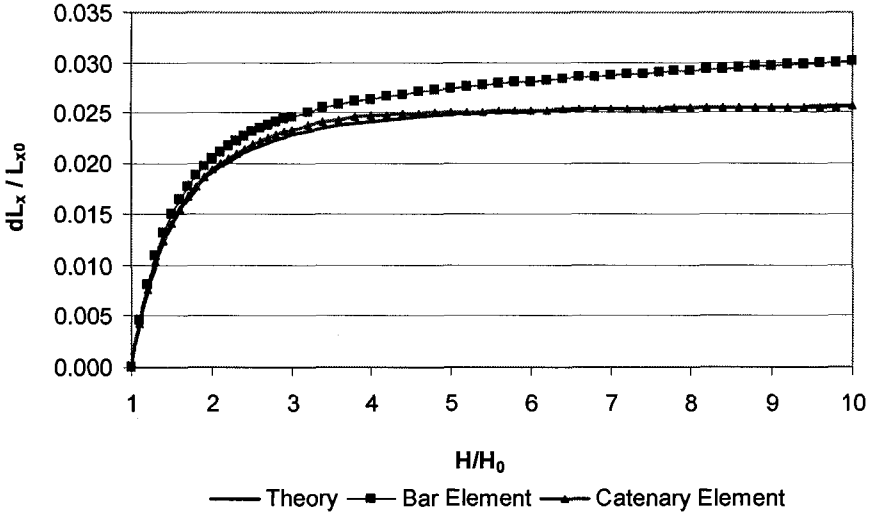

FIGURE 4.5 EXAMPLE 1: NORMALIZED HORIZONTAL DISPLACEMENT WITH RESPECT TO NORMALIZED HORIZONTAL TENSILE FORCE

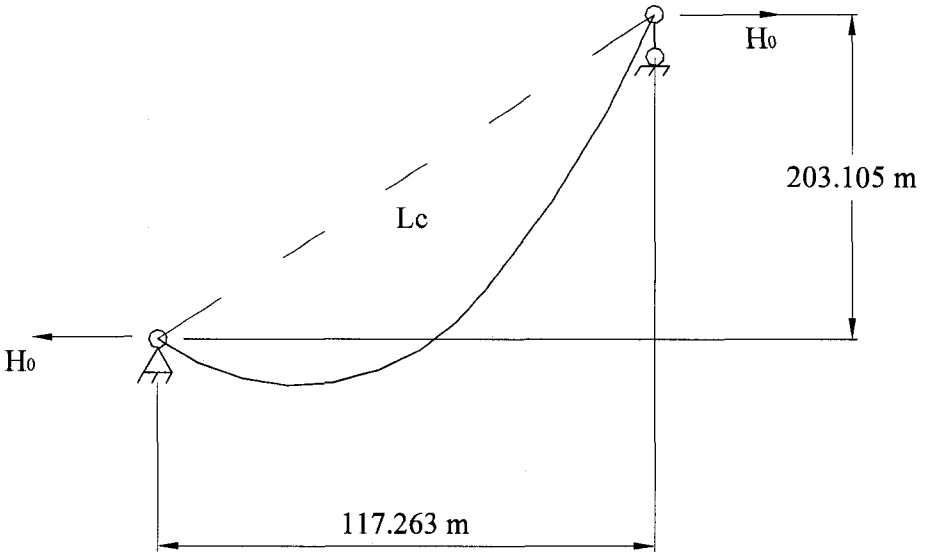

FIGURE 4.6 EXAMPLE 2: INCLINED CABLE

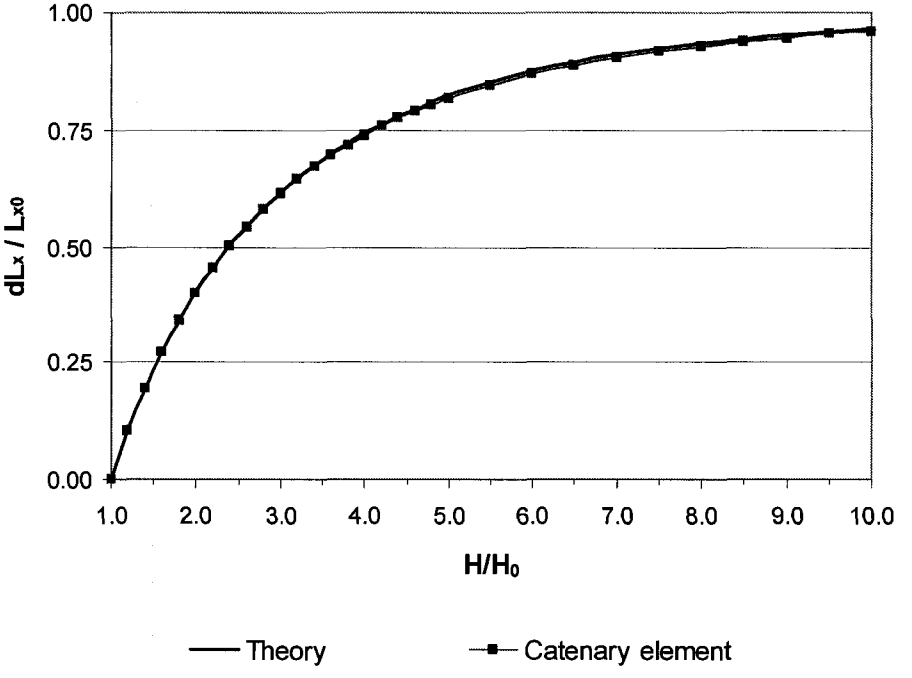

FIGURE 4.7 EXAMPLE 2: NORMALIZED HORIZONTAL DISPLACEMENT WITH RESPECT TO NORMALIZED HORIZONTAL TENSILE FORCE

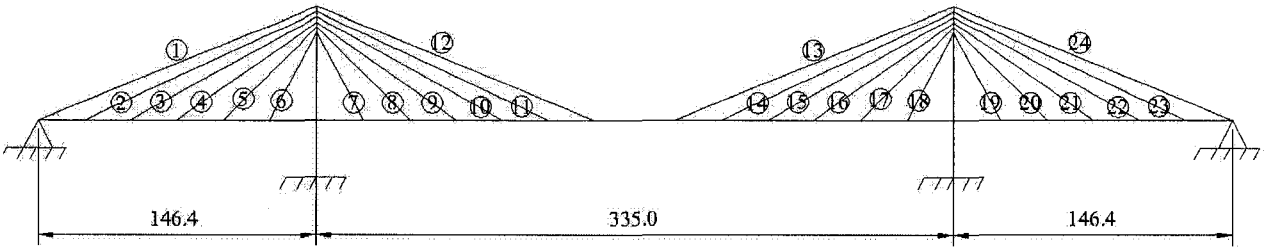

(a) Case 1 – Fan-type with 48 Cables

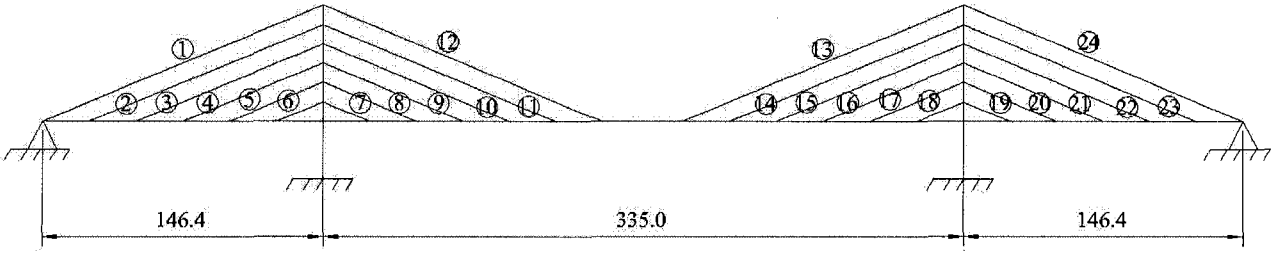

(b) Case 2 – Harp-type with 48 Cables

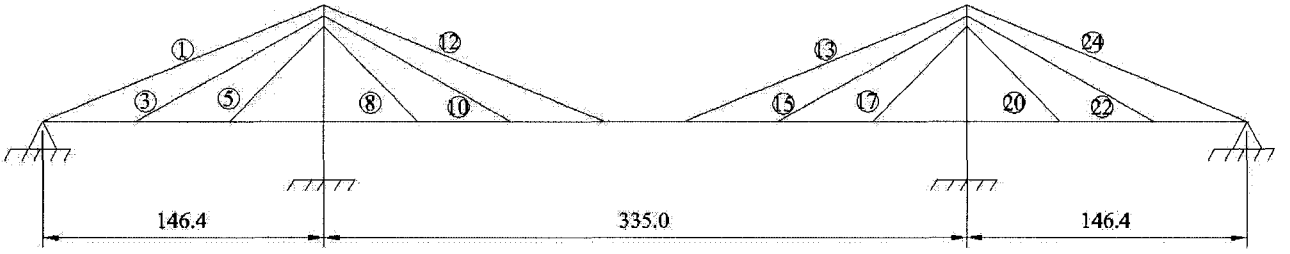

(c) Case 5 – Fan-type with 24 Cables

FIGURE 4.8 OVERALL CONFIGURATION OF CABLE-STAYED BRIDGE

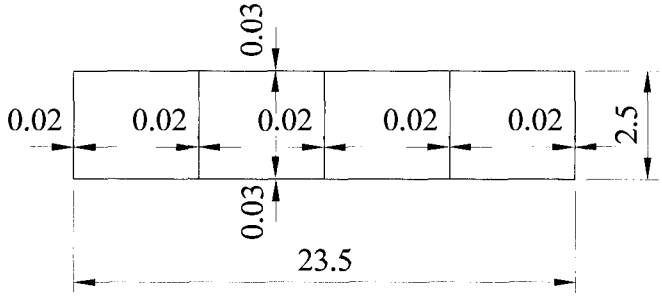

Unit: meter

(a) Cross-section of Bridge Deck

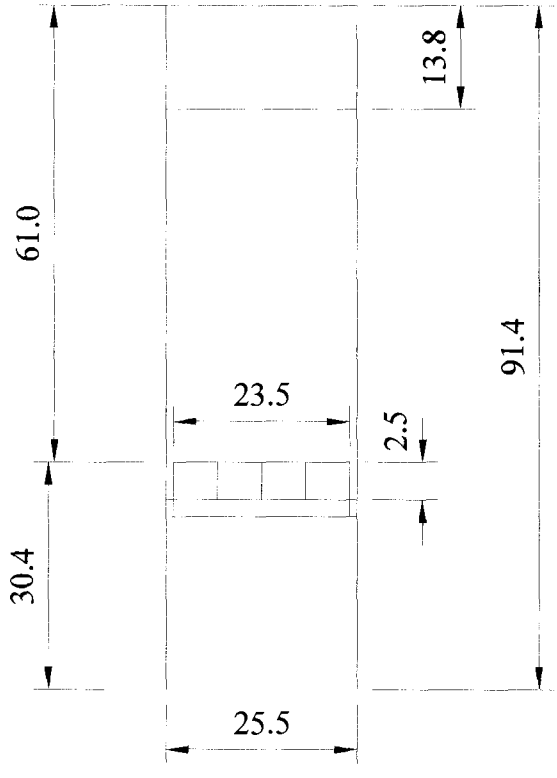

Unit: meter

(b) Pylon structure

FIGURE 4.9 TYPICAL CROSS-SECTION OF BRIDGE DECK AND PYLON STRUCTURE

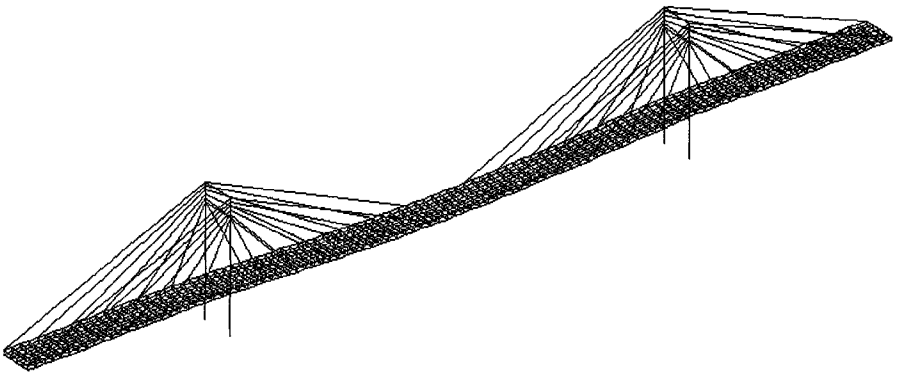

(a) Case 1

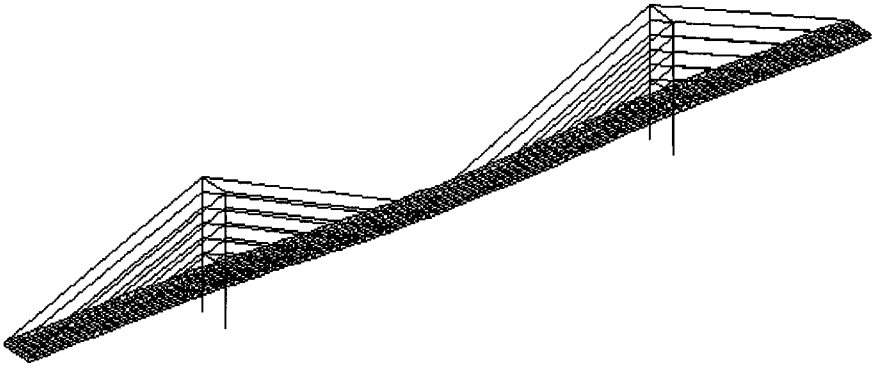

(b) Case 2

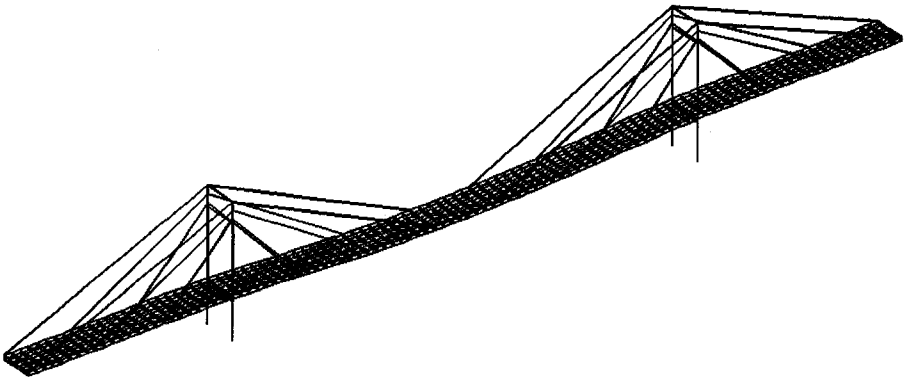

(c) Case 5

FIGURE 4.10 DEFOMATION OF CABLE-STAYED BRIDGE UNDER DEAD LOAD

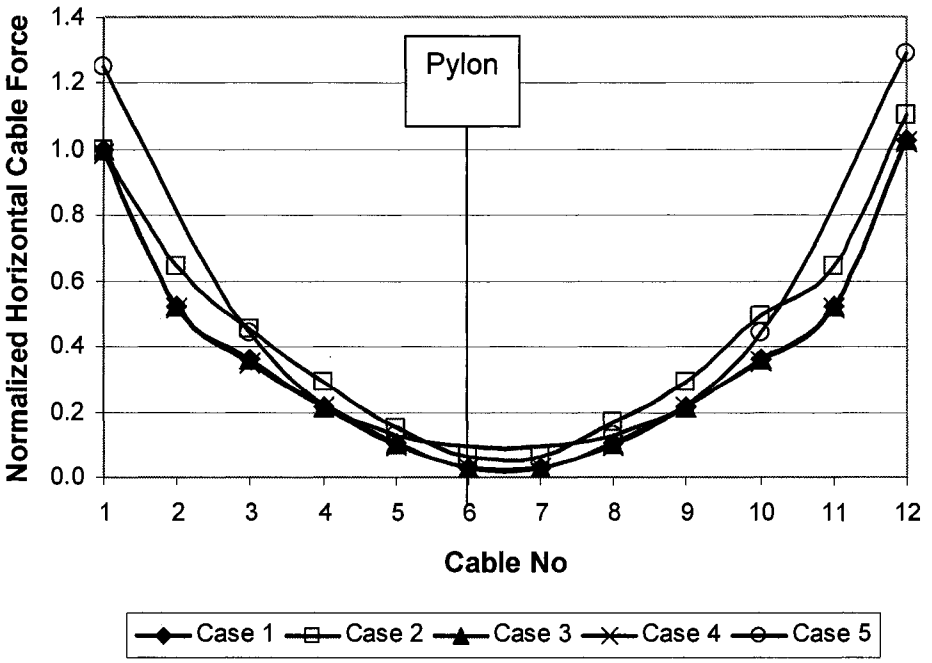

FIGURE 4.11 NORMALIZED HORIZONTAL CABLE FORCE UNDER DEAD LOAD

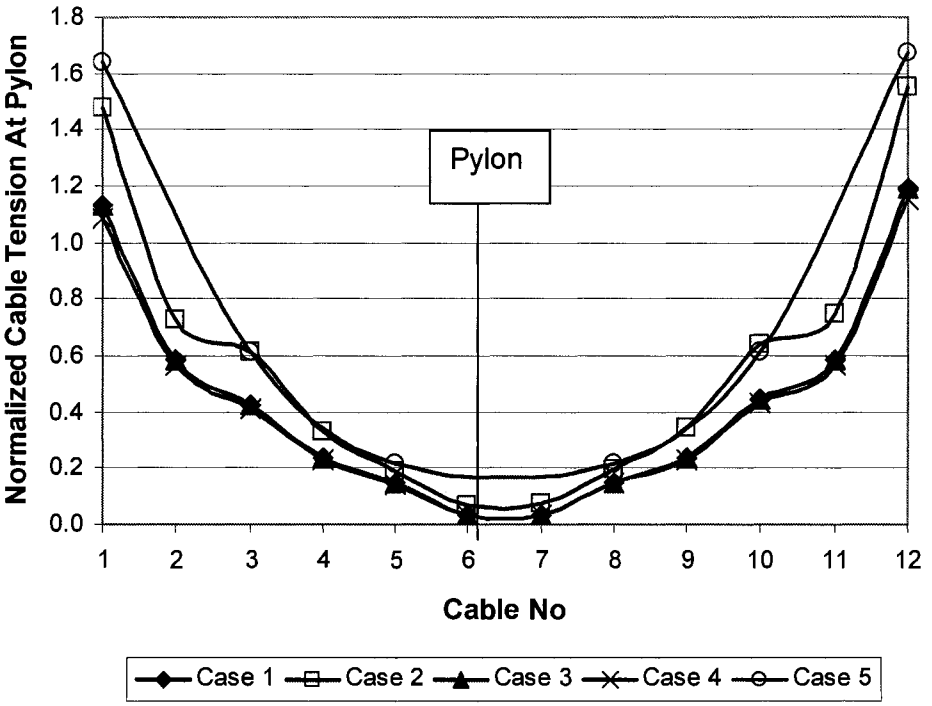

FIGURE 4.12 NORMALIZED CABLE TENSION AT PYLON UNDER DEAD LOAD

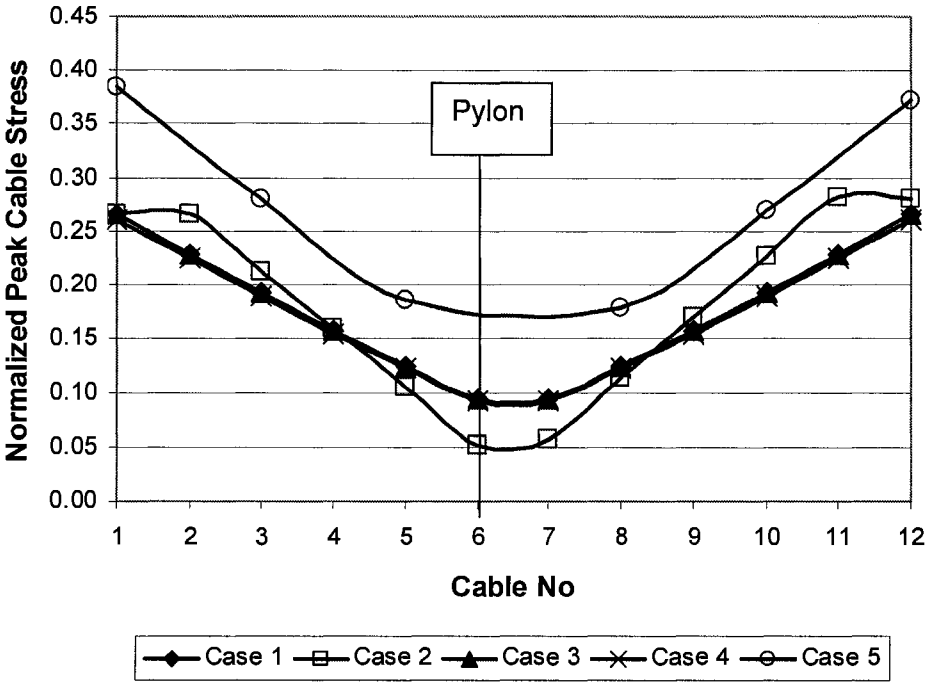

FIGURE 4.13 NORMALIZED PEAK CABLE STRESS UNDER DEAD LOAD

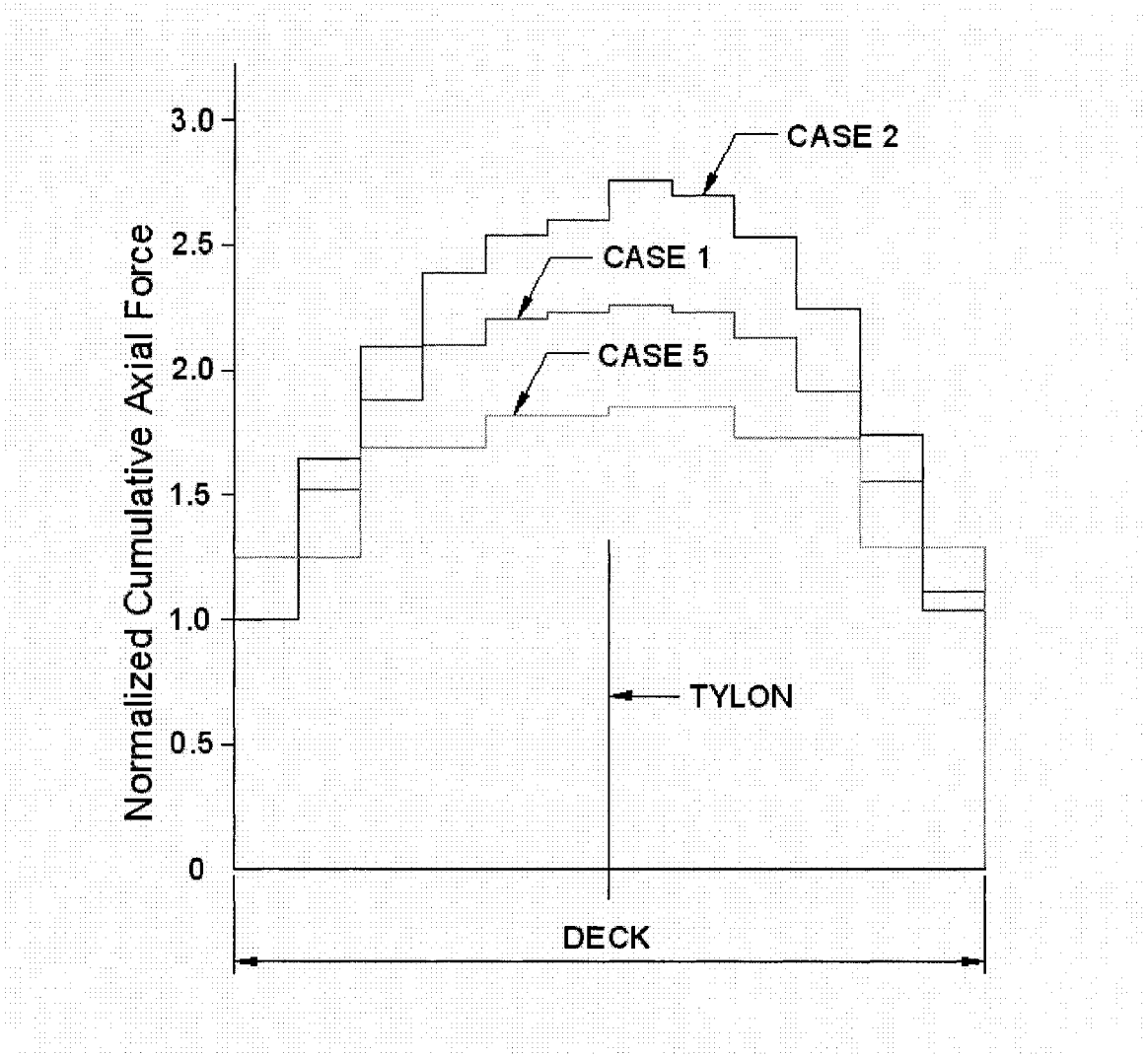

FIGURE 4.14 NORMALIZED CUMULATIVE AXIAL FORCES ACTING ON BRIDGE DECK UNDER DEAD LOAD

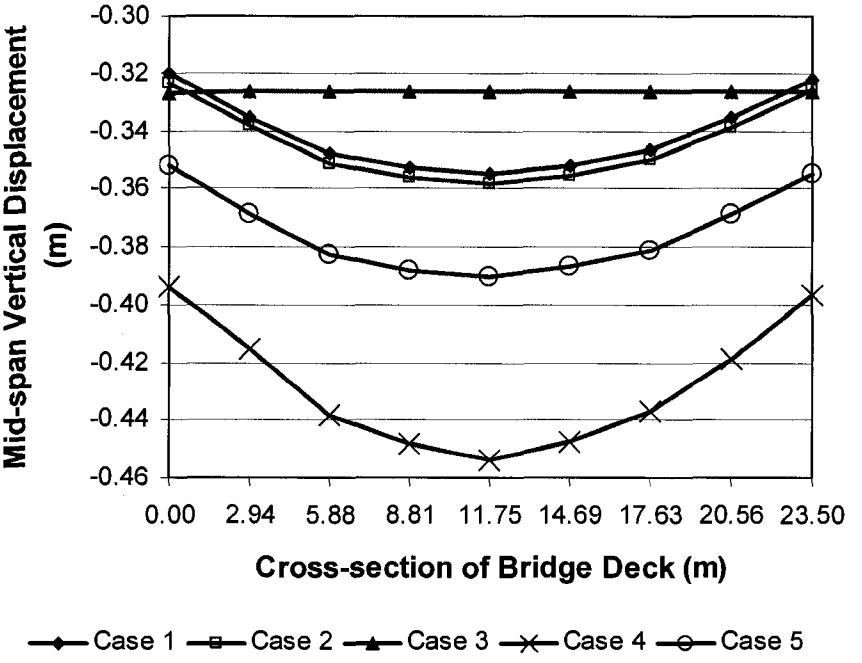

FIGURE 4.15 VERTICAL DISPLACEMENTS OF MID-SPAN UNDER DEAD LOAD

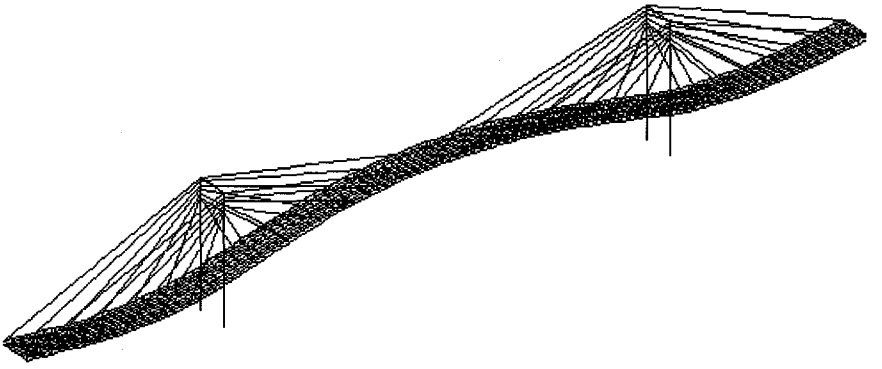

(a) Mode 1, Frequency = 0.31 Hz

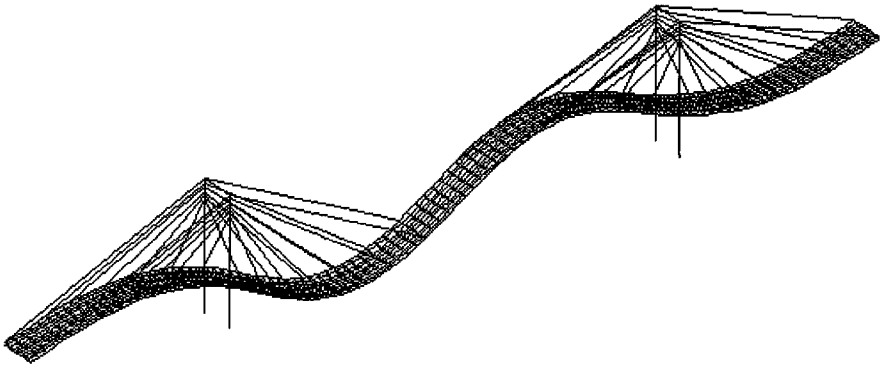

(b) Mode 2, Frequency = 0.42 Hz

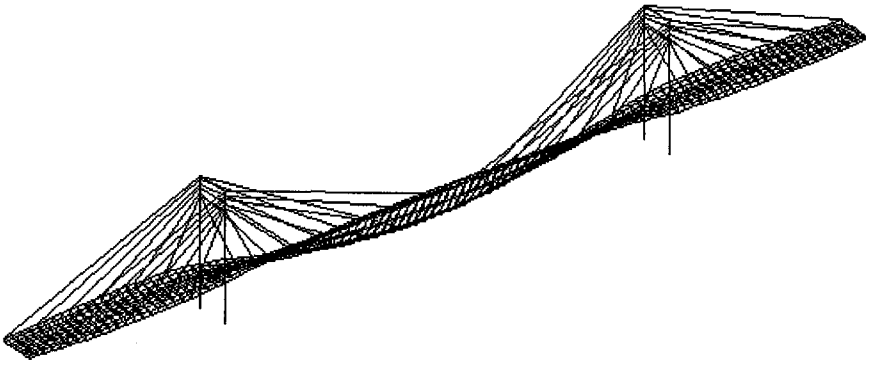

(c) Mode 3, Frequency = 0.56 Hz

FIGURE 4.16 MODE SHAPES OF CABLE-STAYED BRIDGE FOR CASE 1

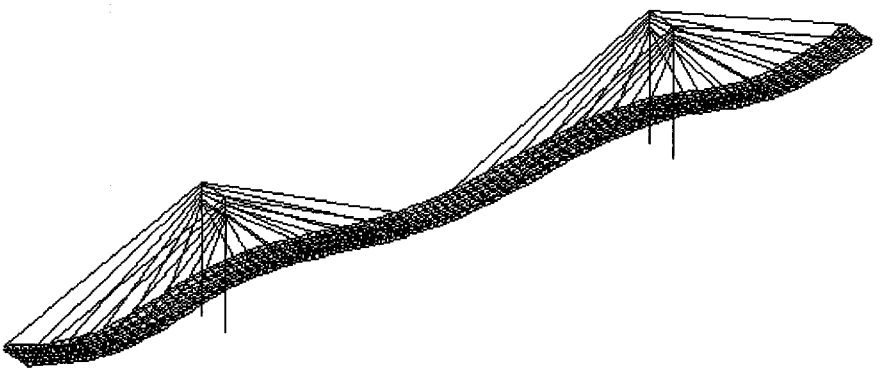

(d) Mode 4, Frequency = 0.61 Hz

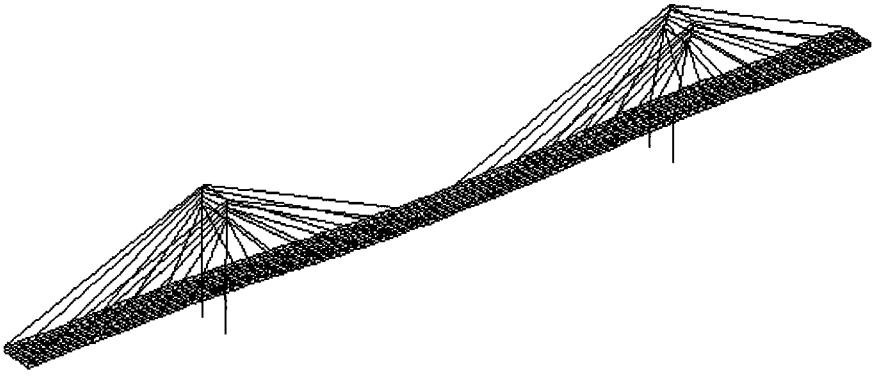

(e) Mode 5, Frequency = 0.62 Hz

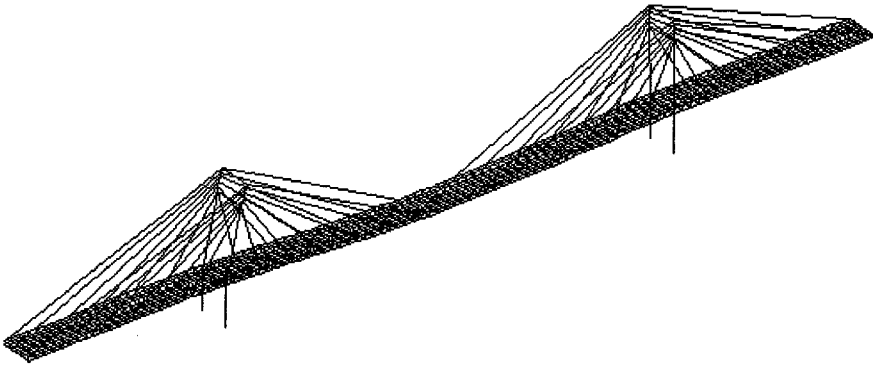

(f) Mode 6, Frequency = 0.62 Hz

FIGURE 4.16 MODE SHAPES OF CABLE-STAYED BRIDGE FOR CASE 1 (CONTINUED)

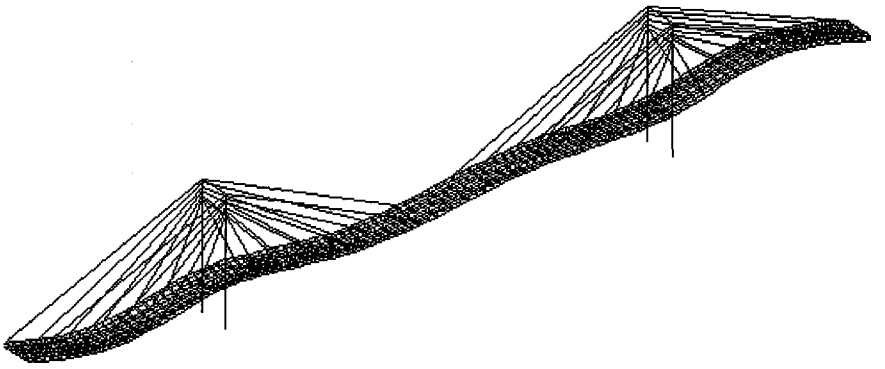

(g) Mode 7, Frequency = 0.66 Hz

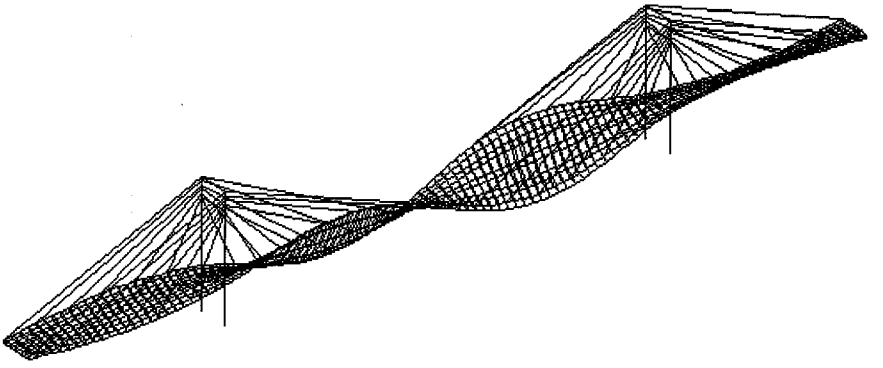

(h) Mode 8, Frequency = 0.70 Hz

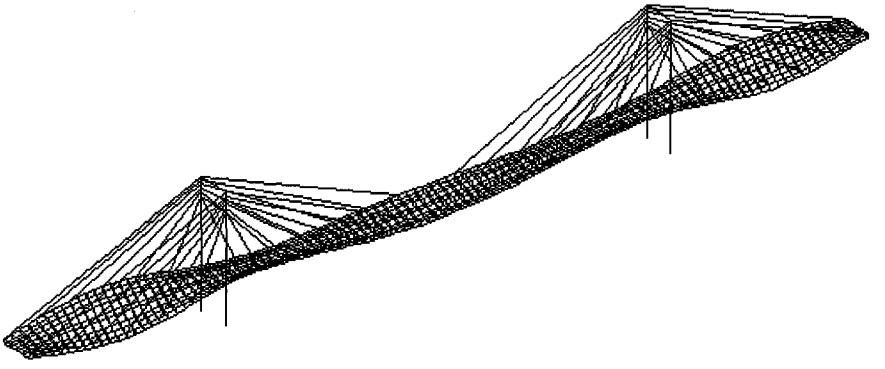

(i) Mode 9, Frequency = 0.83 Hz

FIGURE 4.16 MODE SHAPES OF CABLE-STAYED BRIDGE FOR CASE 1 (CONTINUED)

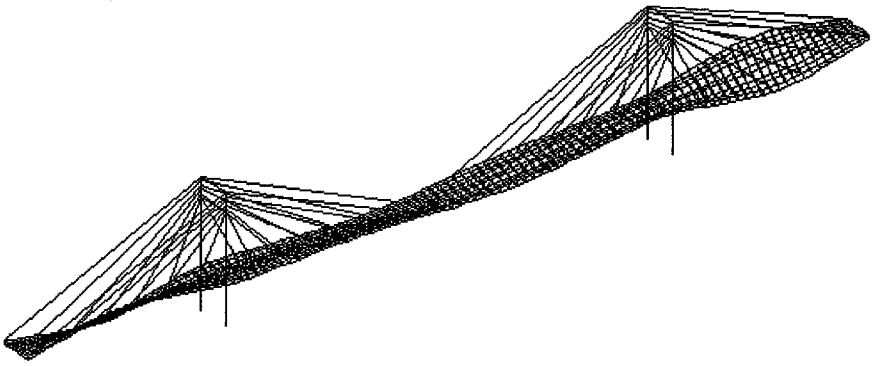

(j) Mode 10, Frequency = 0.86 Hz

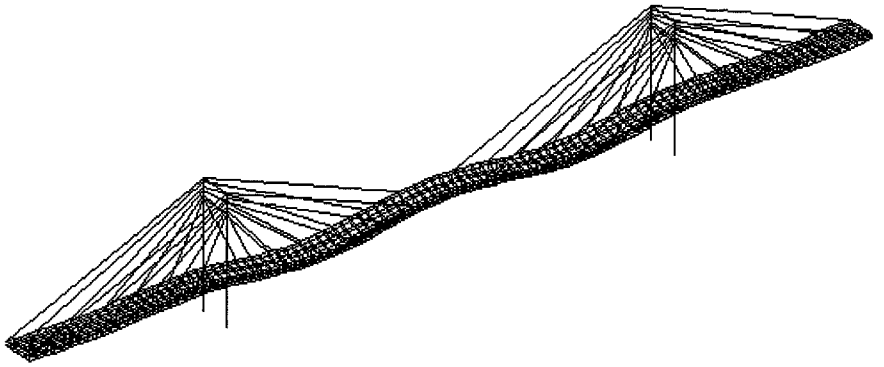

(k) Mode 11, Frequency = 0.91 Hz

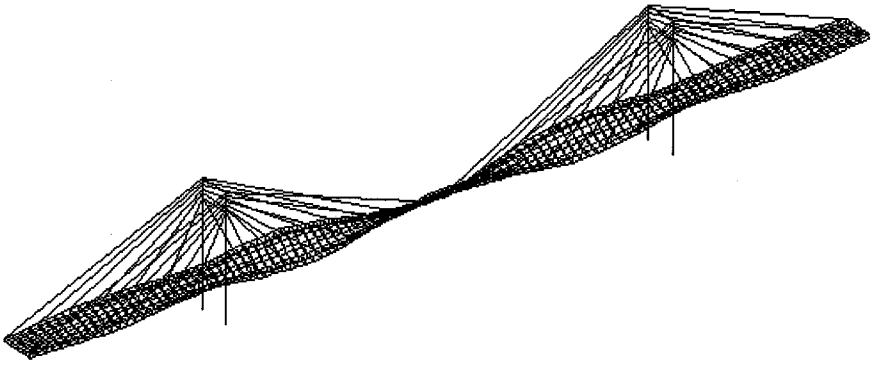

(l) Mode 12, Frequency = 1.01 Hz

FIGURE 4.16 MODE SHAPES OF CABLE-STAYED BRIDGE FOR CASE 1 (CONTINUED)

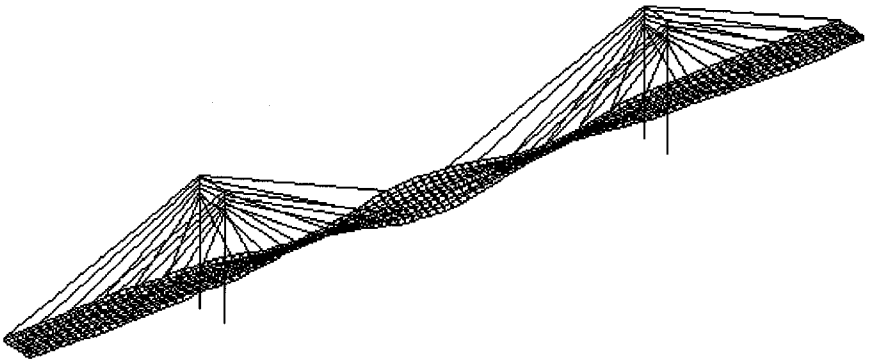

(m) Mode 13, Frequency = 1.03 Hz

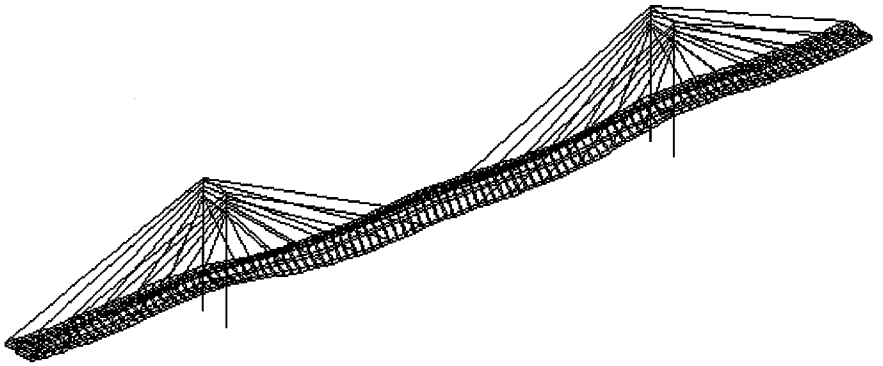

(n) Mode 14, Frequency = 1.25 Hz

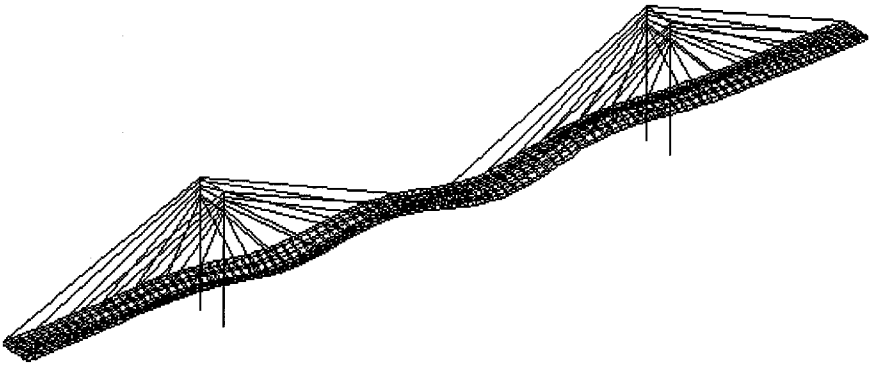

(o) Mode 15, Frequency = 1.42 Hz

FIGURE 4.16 MODE SHAPES OF CABLE-STAYED BRIDGE FOR CASE 1 (CONTINUED)

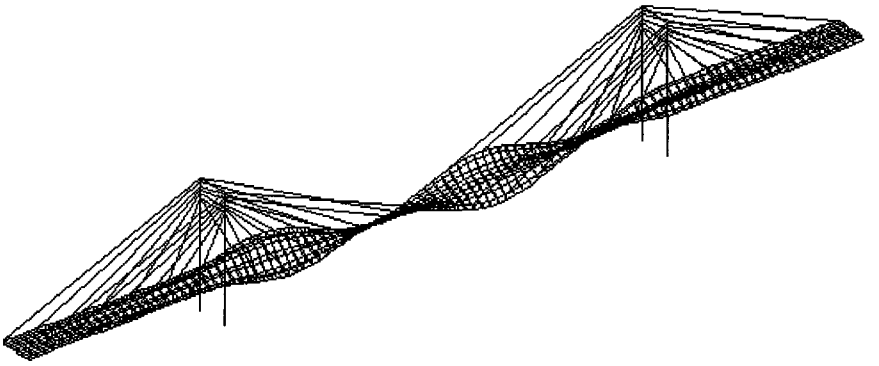

(p) Mode 16, Frequency = 1.47 Hz

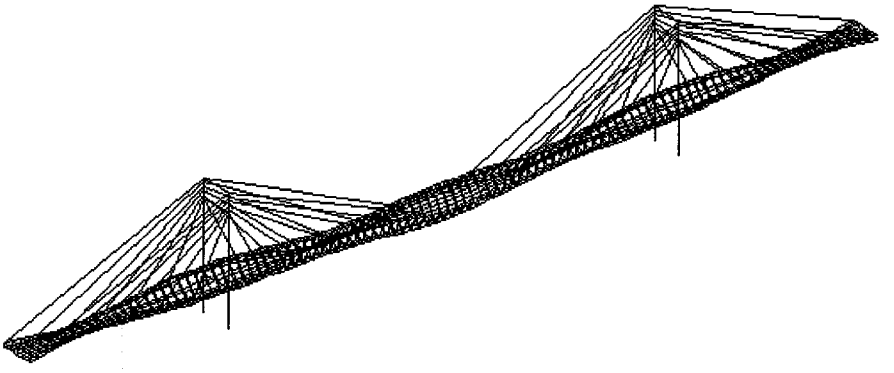

(q) Mode 17, Frequency = 1.50 Hz

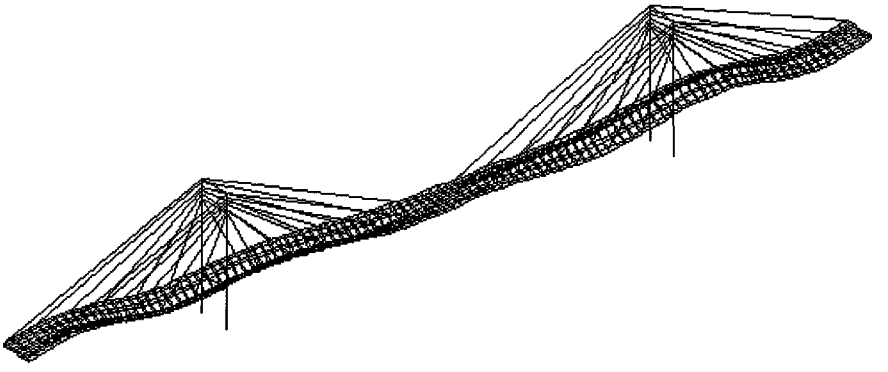

(r) Mode 18, Frequency = 1.69 Hz

FIGURE 4.16 MODE SHAPES OF CABLE-STAYED BRIDGE FOR CASE 1 (CONTINUED)

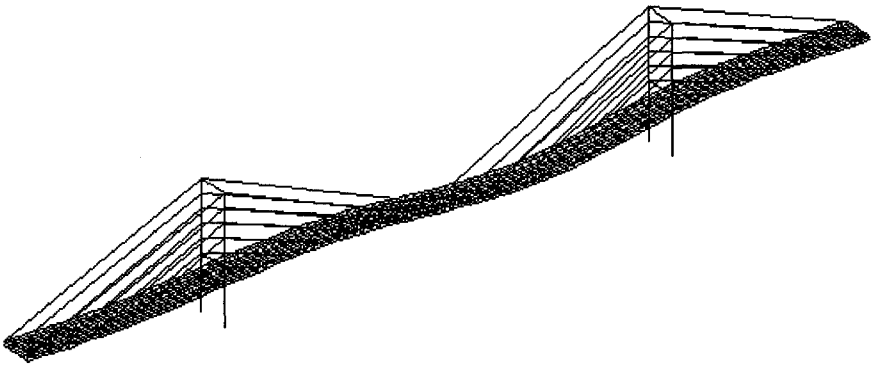

(a) Mode 1, Frequency = 0.29 Hz

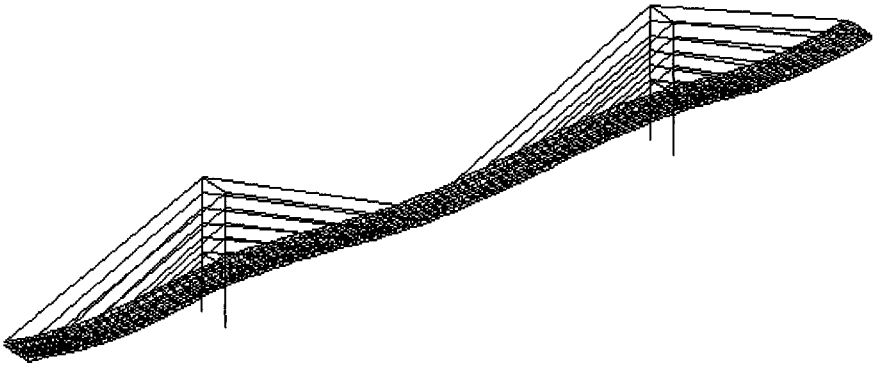

(b) Mode 2, Frequency = 0.38 Hz

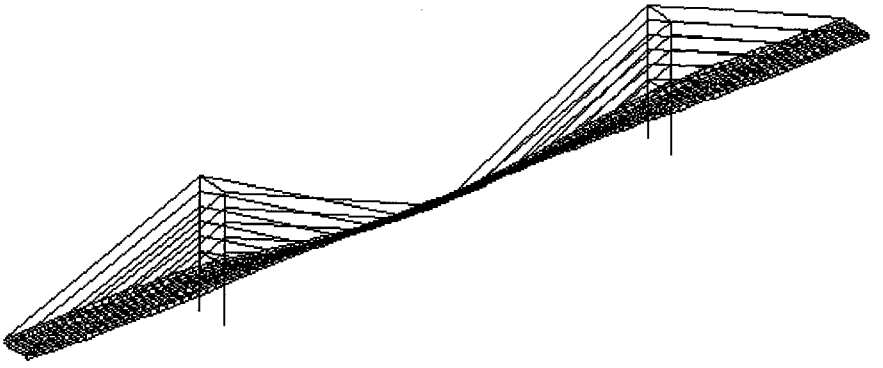

(c) Mode 3, Frequency = 0.52 Hz

FIGURE 4.17 MODE SHAPES OF CABLE-STAYED BRIDGE FOR CASE 2

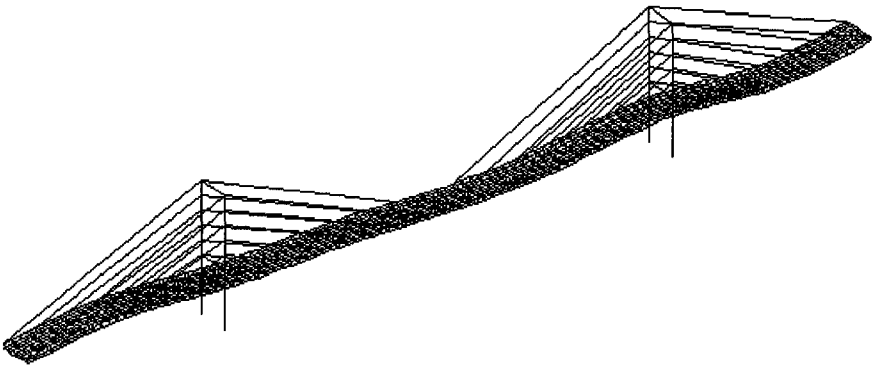

(d) Mode 4, Frequency = 0.57 Hz

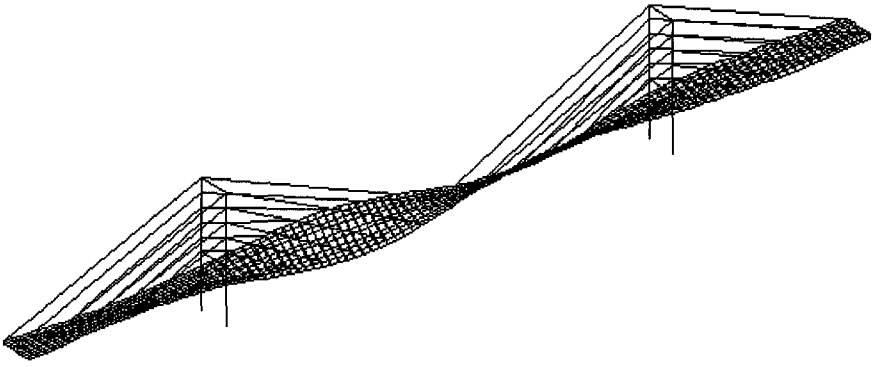

(e) Mode 5, Frequency = 0.60 Hz

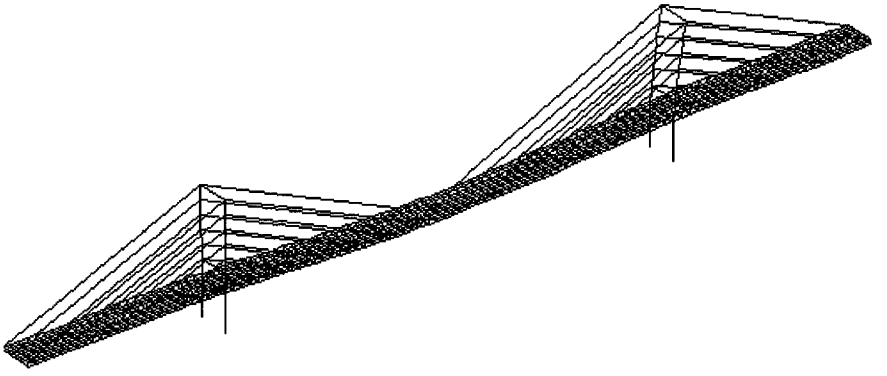

(f) Mode 6, Frequency = 0.60 Hz

FIGURE 4.17 MODE SHAPES OF CABLE-STAYED BRIDGE FOR CASE 2 (CONTINUED)

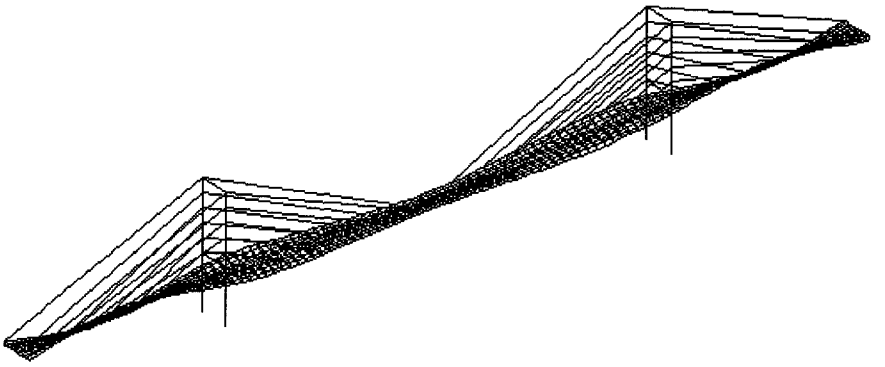

(g) Mode 7, Frequency = 0.64 Hz

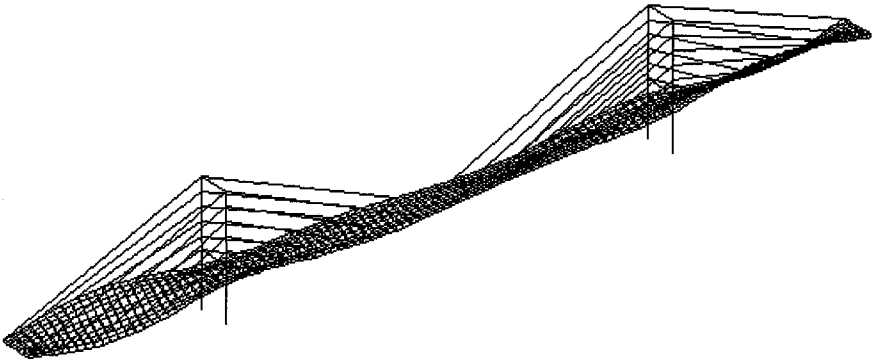

(h) Mode 8, Frequency = 0.68Hz

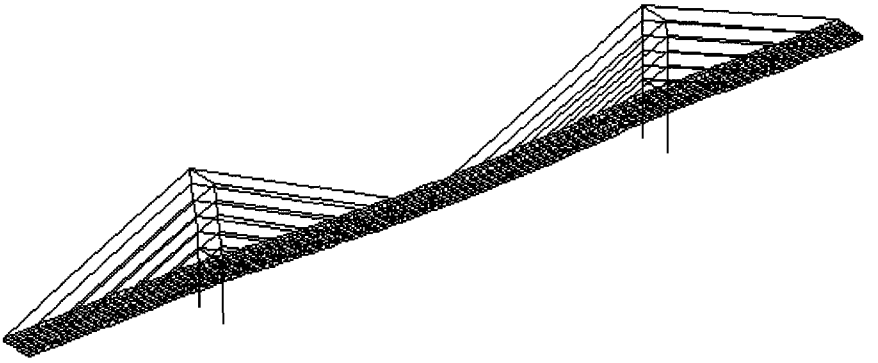

(i) Mode 9, Frequency = 0.75 Hz

FIGURE 4.17 MODE SHAPES OF CABLE-STAYED BRIDGE FOR CASE 2 (CONTINUED)

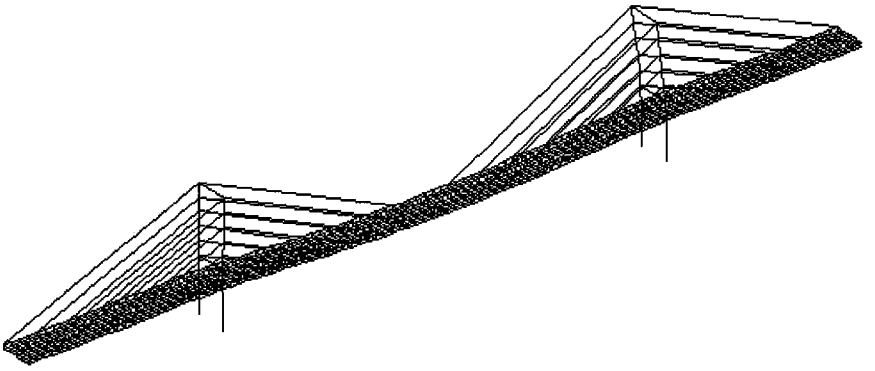

(j) Mode 10, Frequency = 0.84 Hz

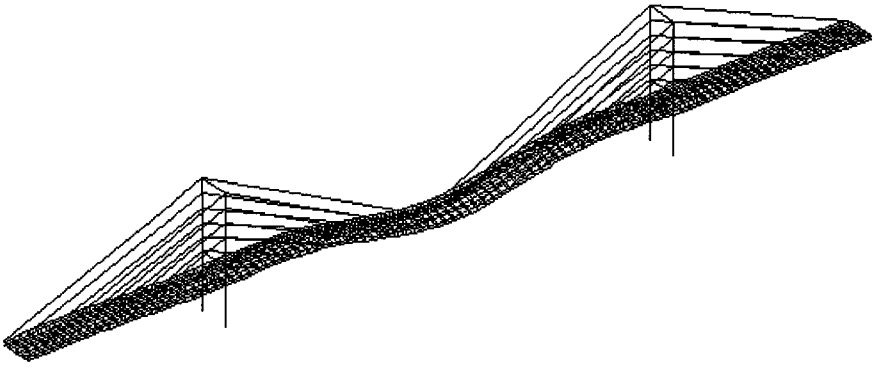

(k) Mode 11, Frequency = 0.91 Hz

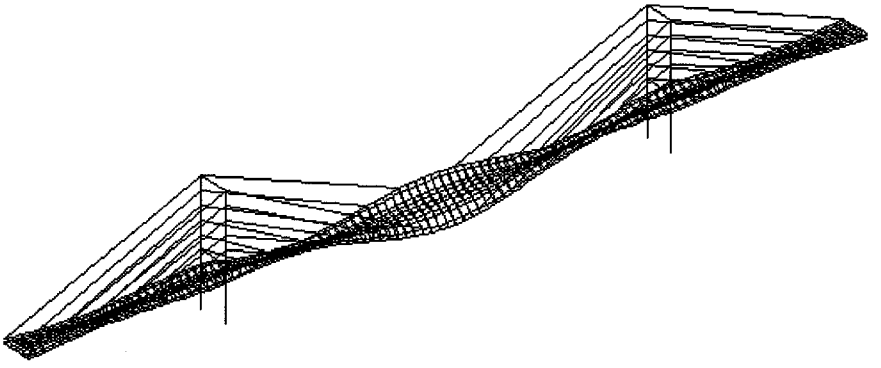

(l) Mode 12, Frequency = 1.01 Hz

FIGURE 4.17 MODE SHAPES OF CABLE-STAYED BRIDGE FOR CASE 2 (CONTINUED)

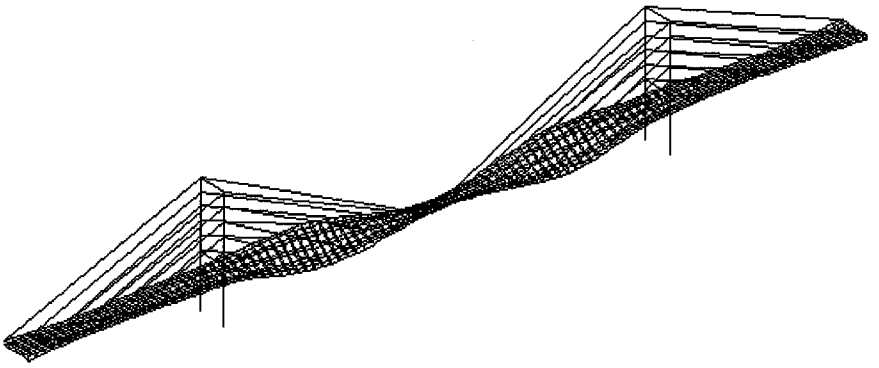

(m) Mode 13, Frequency = 1.03 Hz

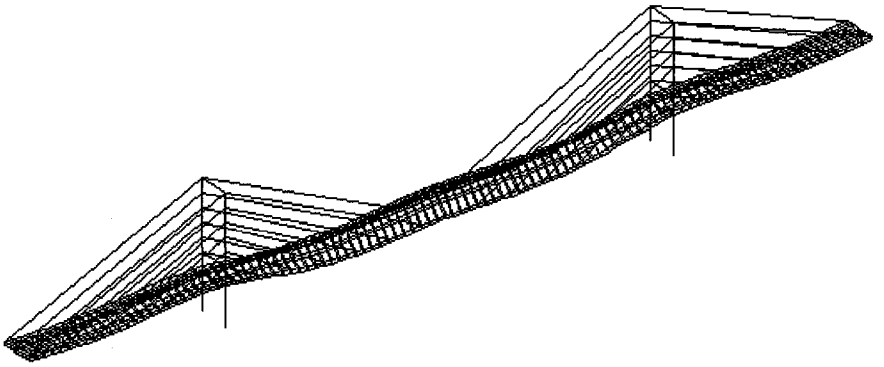

(n) Mode 14, Frequency = 1.24 Hz

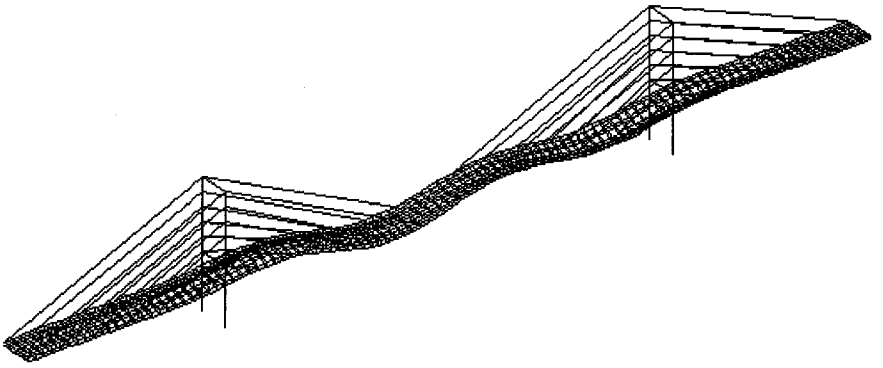

(o) Mode 15, Frequency = 1.41 Hz

FIGURE 4.17 MODE SHAPES OF CABLE-STAYED BRIDGE FOR CASE 2 (CONTINUED)

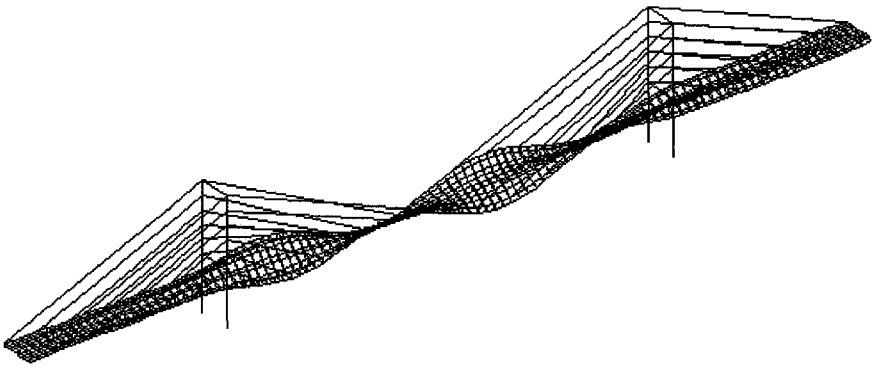

(p) Mode 16, Frequency = 1.46 Hz

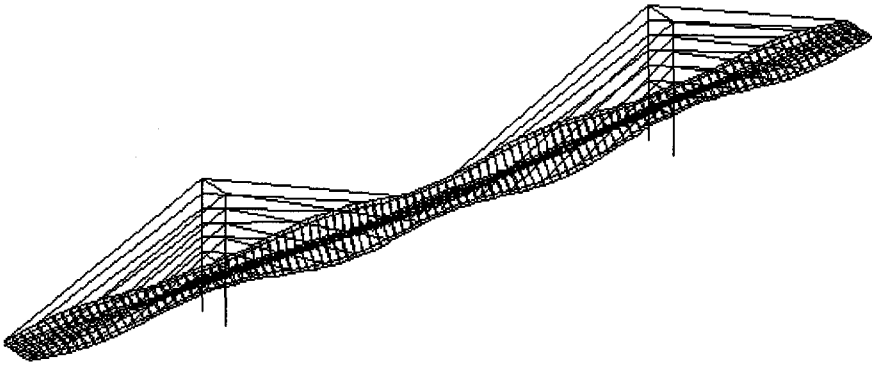

(q) Mode 17, Frequency = 1.50 Hz

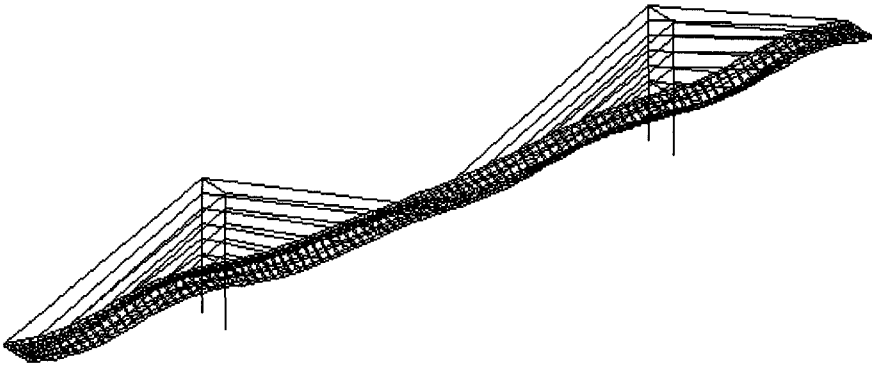

(r) Mode 18, Frequency = 1.67 Hz

FIGURE 4.17 MODE SHAPES OF CABLE-STAYED BRIDGE FOR CASE 2 (CONTINUED)

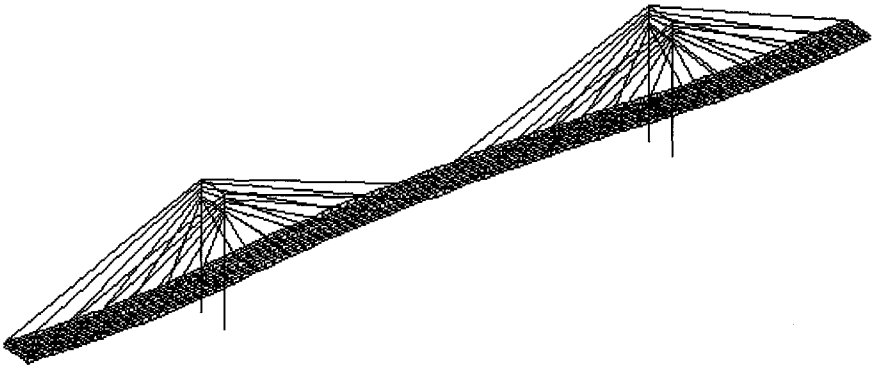

(a) Mode 1, Frequency = 0.31 Hz

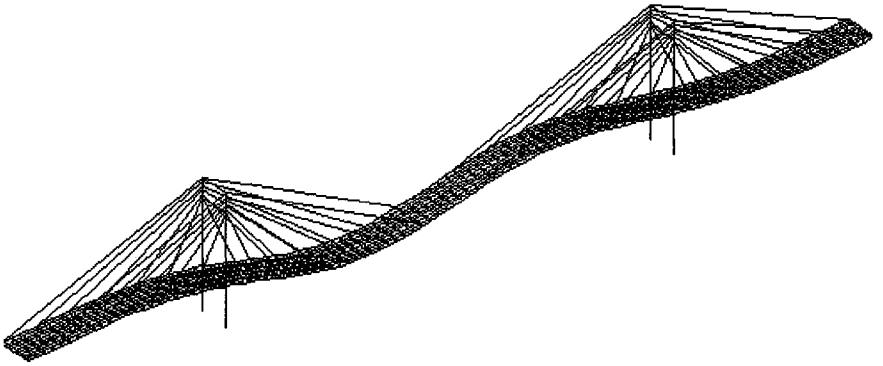

(b) Mode 2, Frequency = 0.43 Hz

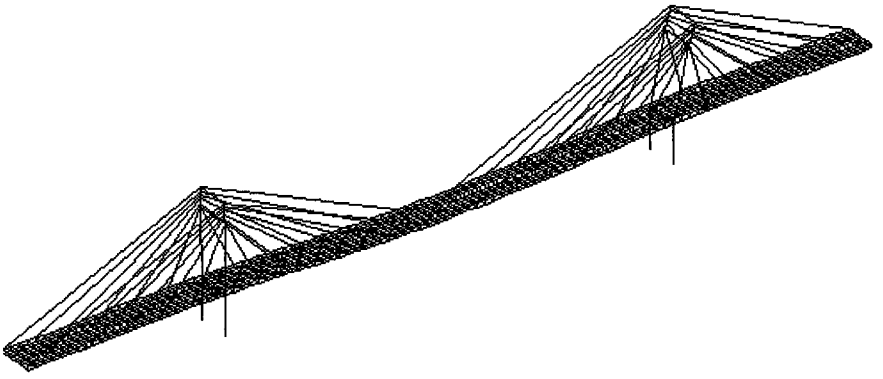

(c) Mode 3, Frequency = 0.62 Hz

FIGURE 4.18 MODE SHAPES OF CABLE-STAYED BRIDGE FOR CASE 3

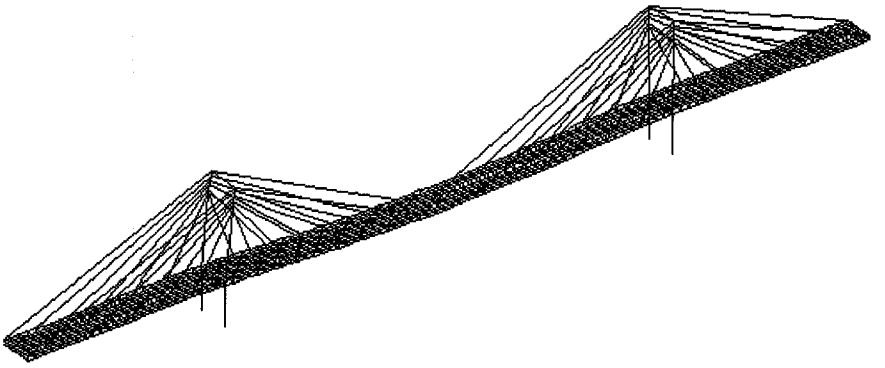

(d) Mode 4, Frequency = 0.62 Hz

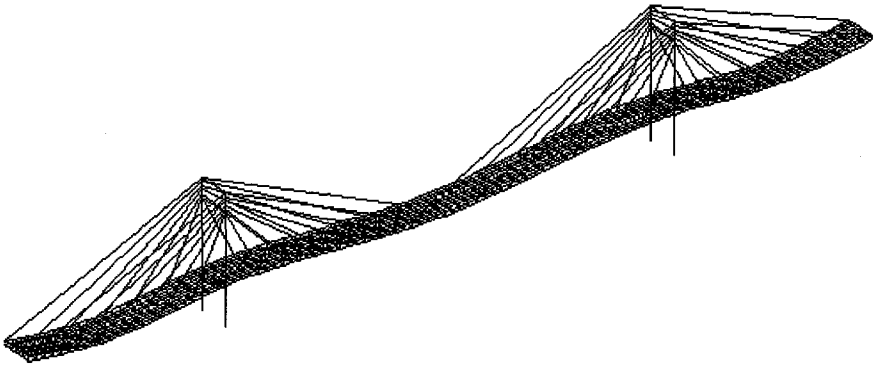

(e) Mode 5, Frequency = 0.63 Hz

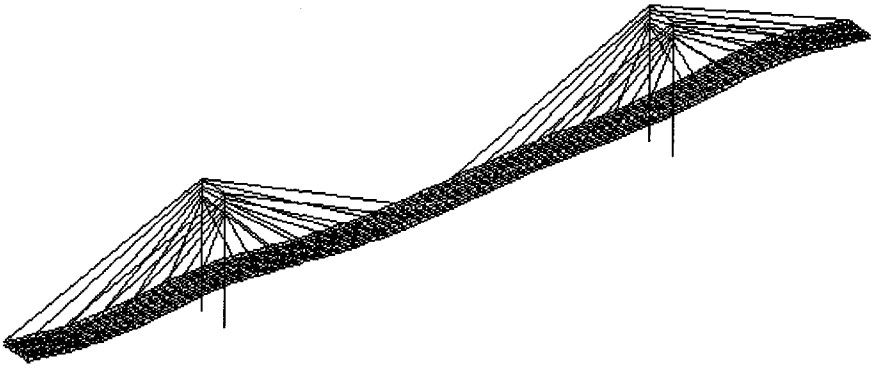

(f) Mode 6, Frequency = 0.67 Hz

FIGURE 4.18 MODE SHAPES OF CABLE-STAYED BRIDGE FOR CASE 3 (CONTINUED)

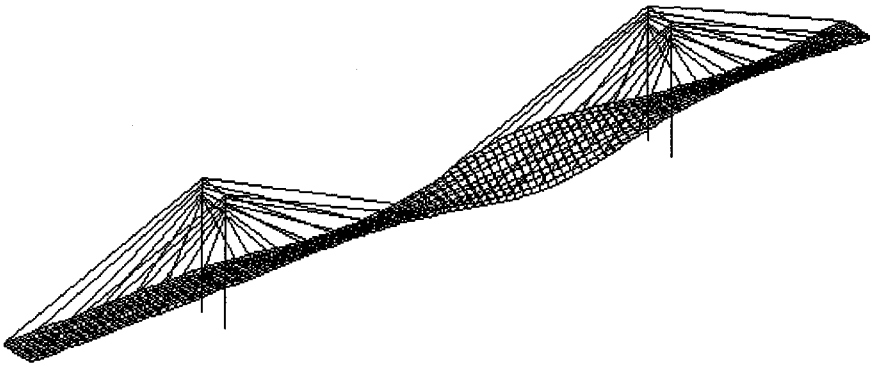

(g) Mode 7, Frequency = 0.72 Hz

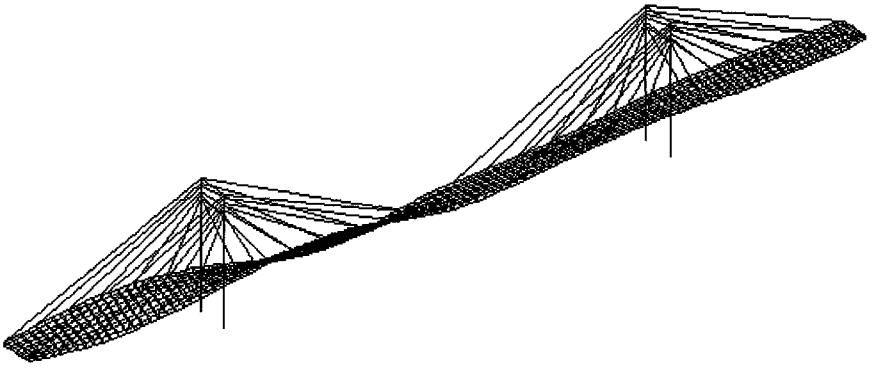

(h) Mode 8, Frequency = 0.73 Hz

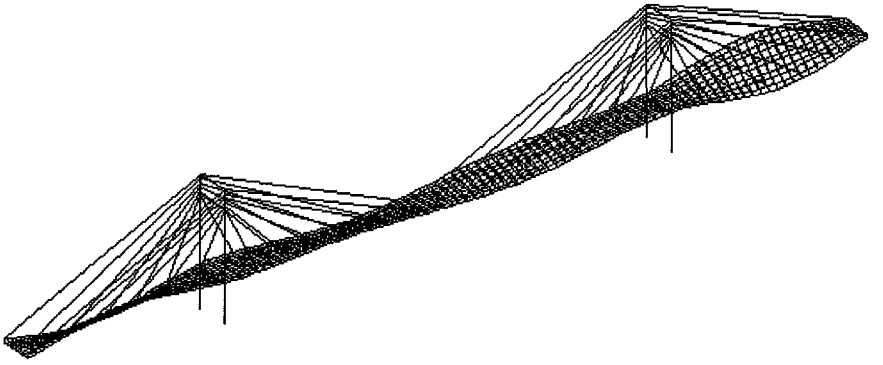

(i) Mode 9, Frequency = 0.88 Hz

FIGURE 4.18 MODE SHAPES OF CABLE-STAYED BRIDGE FOR CASE 3 (CONTINUED)

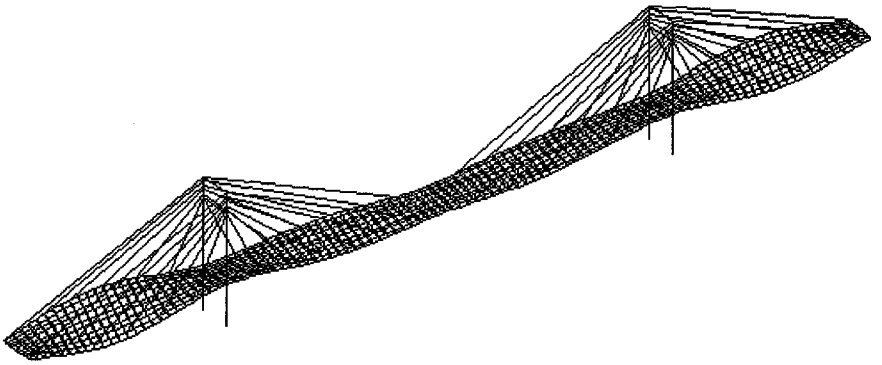

(j) Mode 10, Frequency = 0.90 Hz

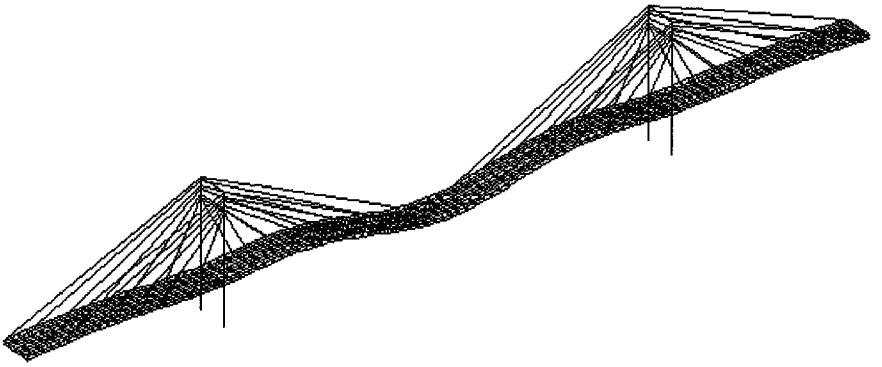

(k) Mode 11, Frequency = 0.94 Hz

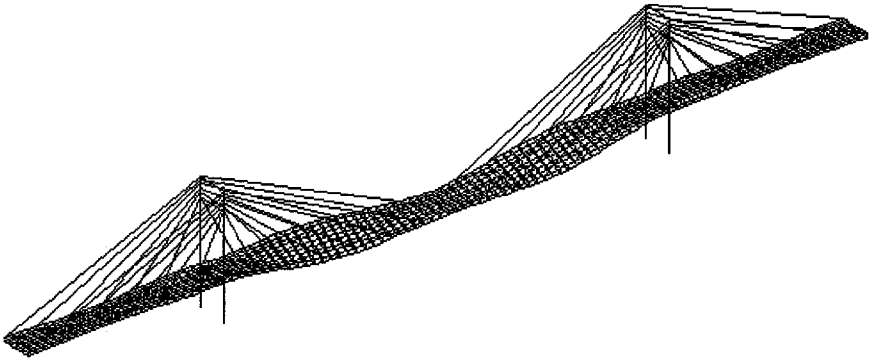

(l) Mode 12, Frequency = 1.11 Hz

FIGURE 4.18 MODE SHAPES OF CABLE-STAYED BRIDGE FOR CASE 3 (CONTINUED)

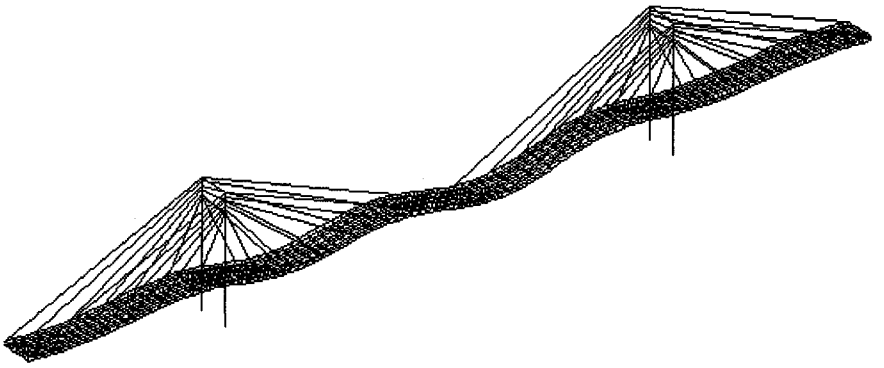

(m) Mode 13, Frequency = 1.47 Hz

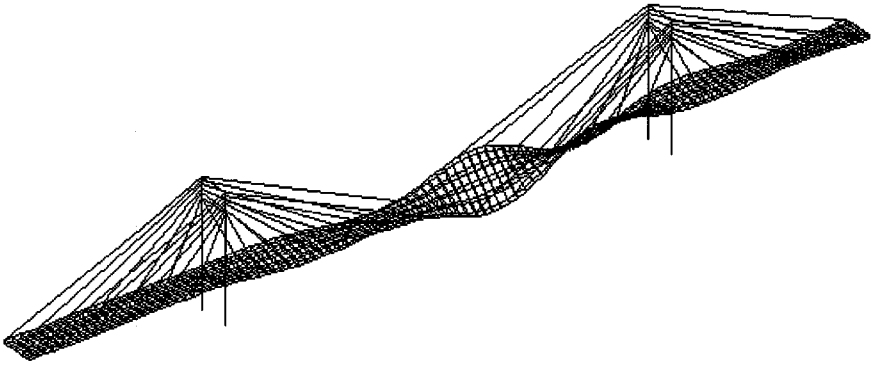

(n) Mode 14, Frequency = 1.54 Hz

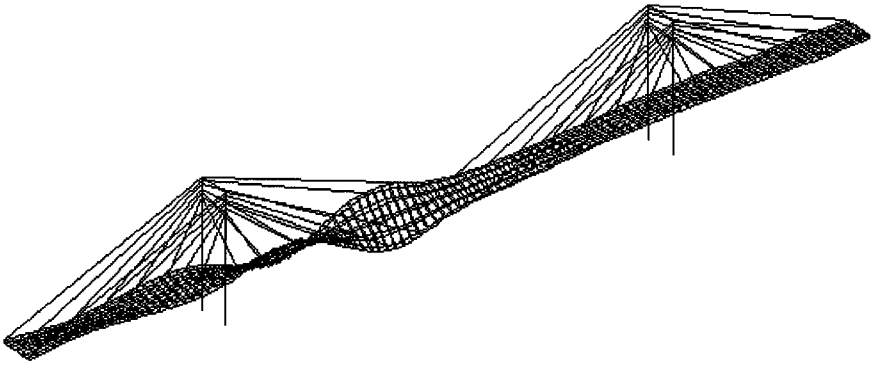

(o) Mode 15, Frequency = 1.62 Hz

FIGURE 4.18 MODE SHAPES OF CABLE-STAYED BRIDGE FOR CASE 3 (CONTINUED)

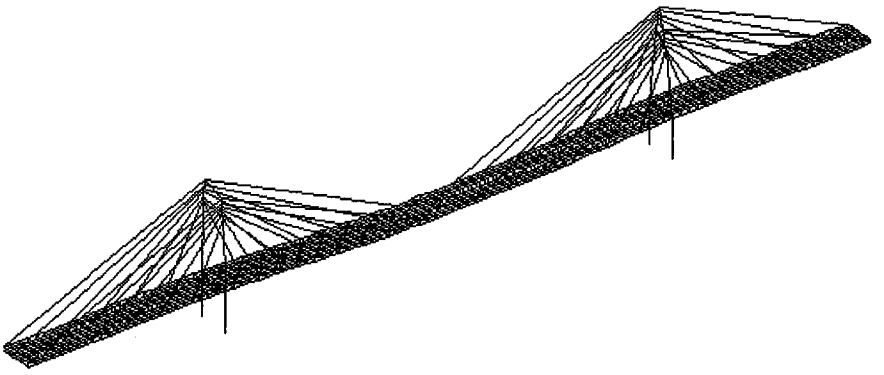

(p) Mode 16, Frequency = 1.72 Hz

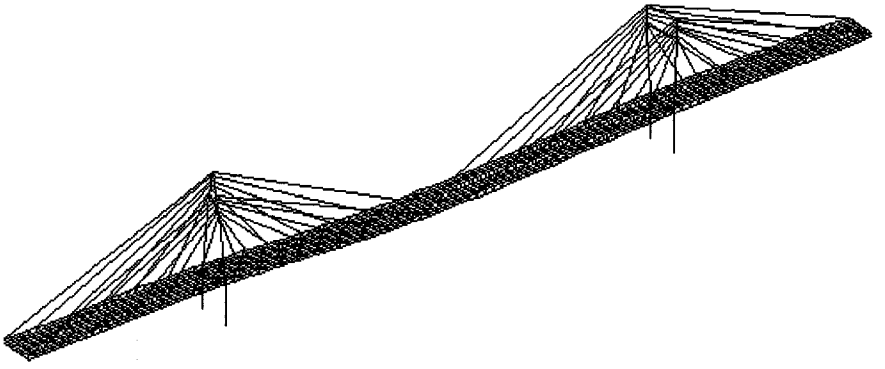

(q) Mode 17, Frequency = 1.72 Hz

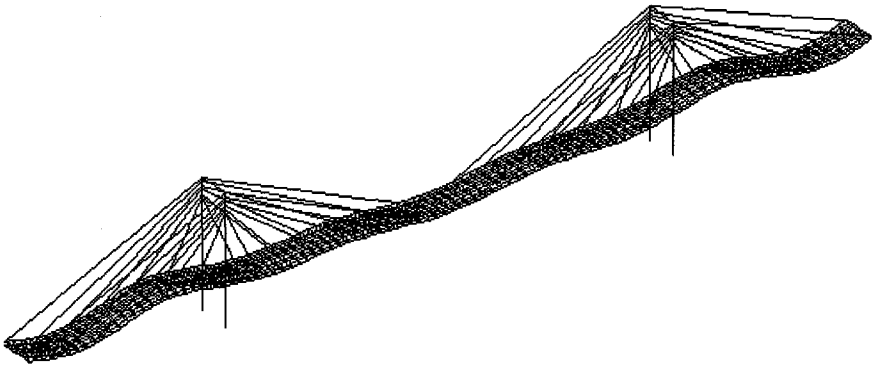

(r) Mode 18, Frequency = 1.90 Hz

FIGURE 4.18 MODE SHAPES OF CABLE-STAYED BRIDGE FOR CASE 3 (CONTINUED)

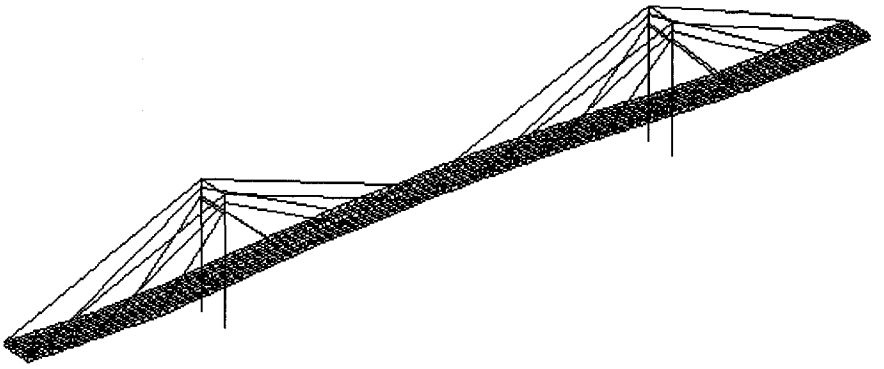

(a) Mode 1, Frequency = 0.33 Hz

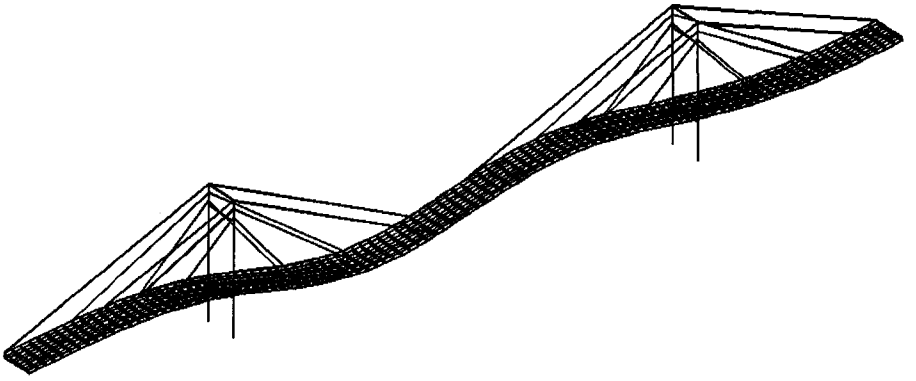

(b) Mode 2, Frequency = 0.44 Hz

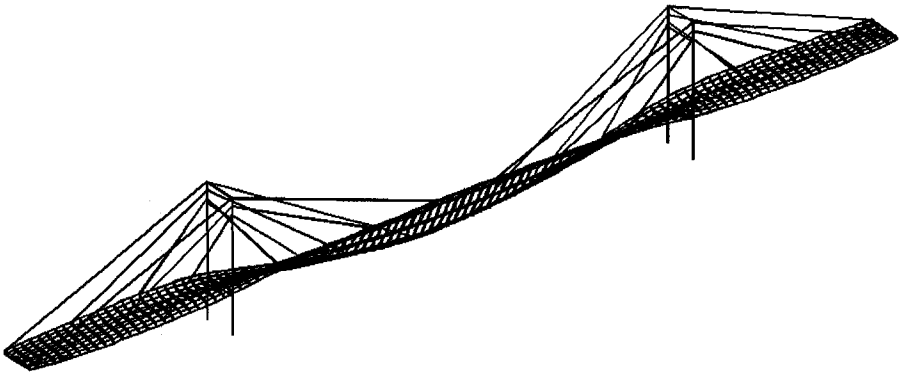

(c) Mode 3, Frequency = 0.57 Hz

FIGURE 4.19 MODE SHAPES OF CABLE-STAYED BRIDGE FOR CASE 5

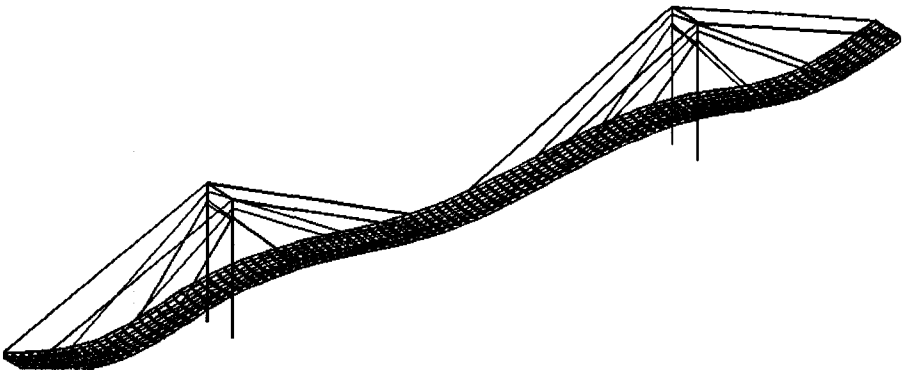

(d) Mode 4, Frequency = 0.63 Hz

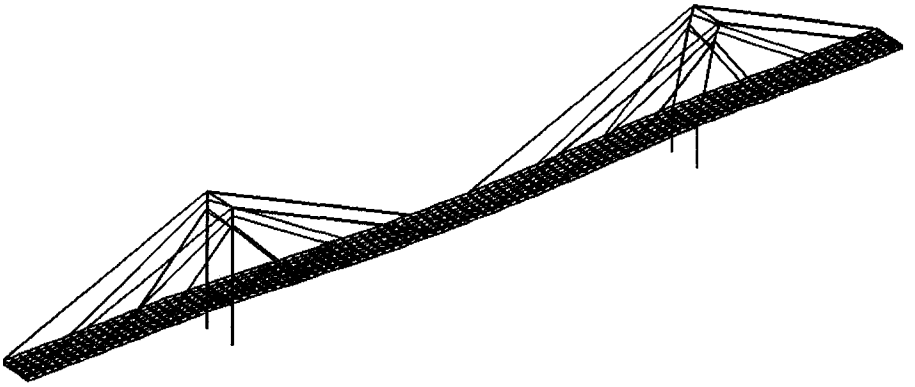

(e) Mode 5, Frequency = 0.64 Hz

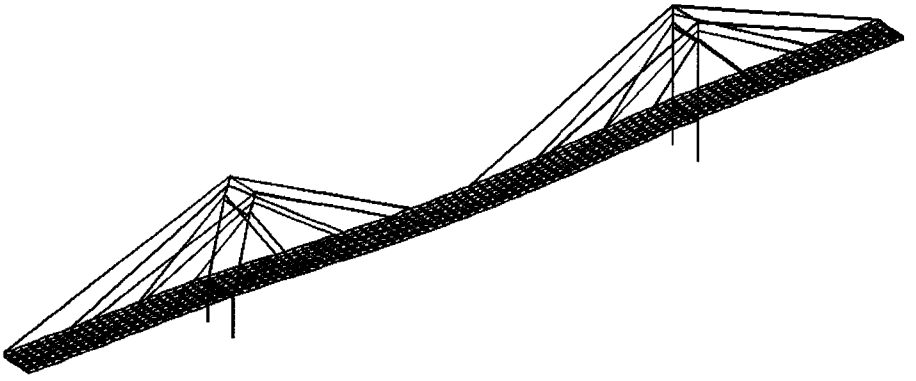

(f) Mode 6, Frequency = 0.64 Hz

FIGURE 4.19 MODE SHAPES OF CABLE-STAYED BRIDGE FOR CASE 5 (CONTINUED)

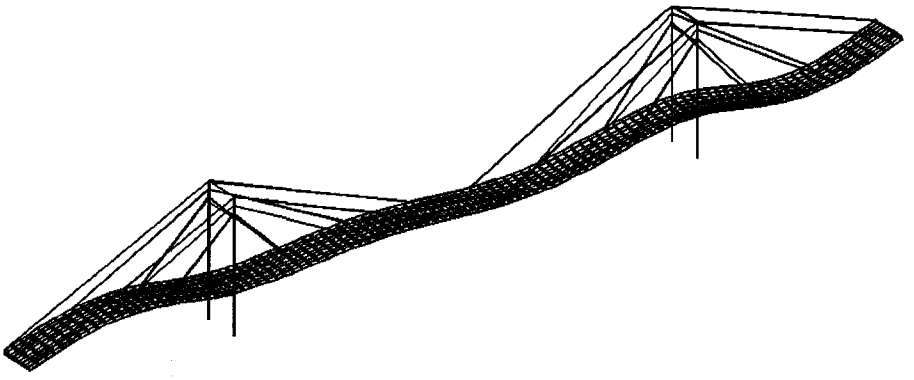

(g) Mode 7, Frequency = 0.66 Hz

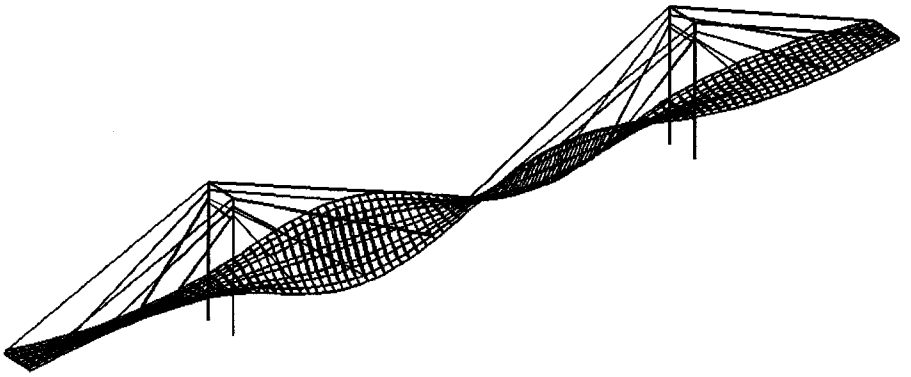

(h) Mode 8, Frequency = 0.73 Hz

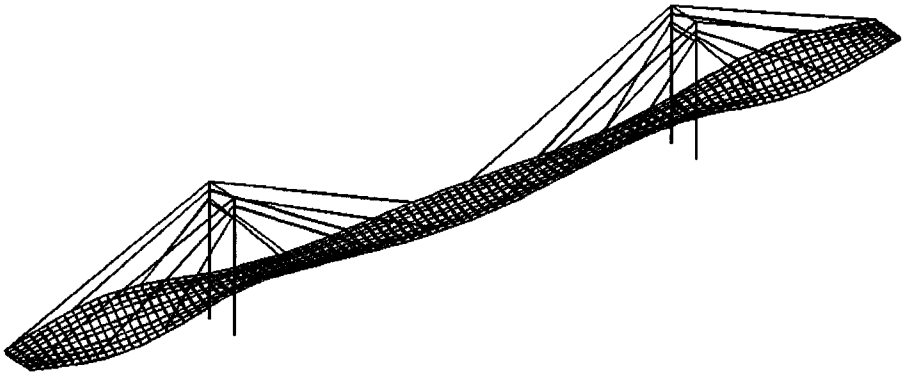

(i) Mode 9, Frequency = 0.85 Hz

FIGURE 4.19 MODE SHAPES OF CABLE-STAYED BRIDGE FOR CASE 5 (CONTINUED)

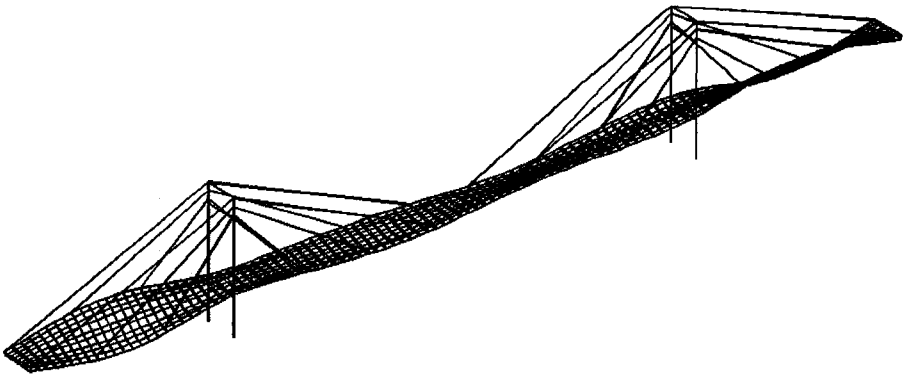

(j) Mode 10, Frequency = 0.89 Hz

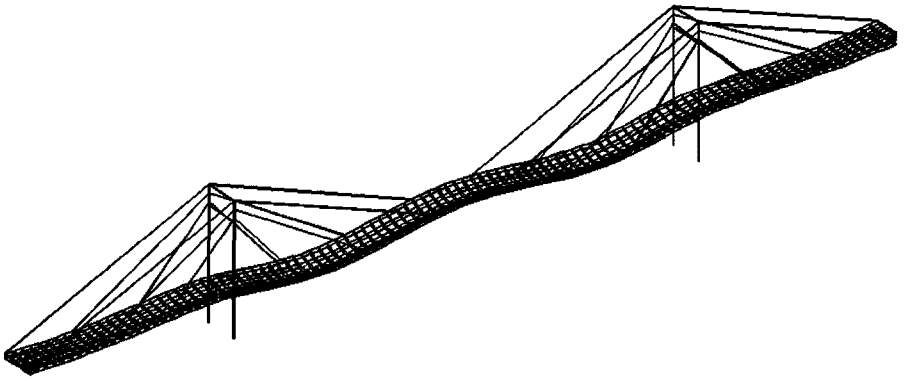

(k) Mode 11, Frequency = 0.92 Hz

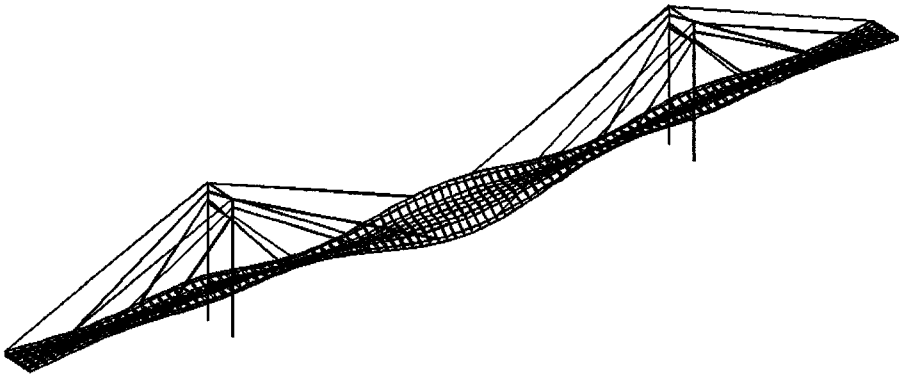

(l) Mode 12, Frequency = 1.03 Hz

FIGURE 4.19 MODE SHAPES OF CABLE-STAYED BRIDGE FOR CASE 5 (CONTINUED)

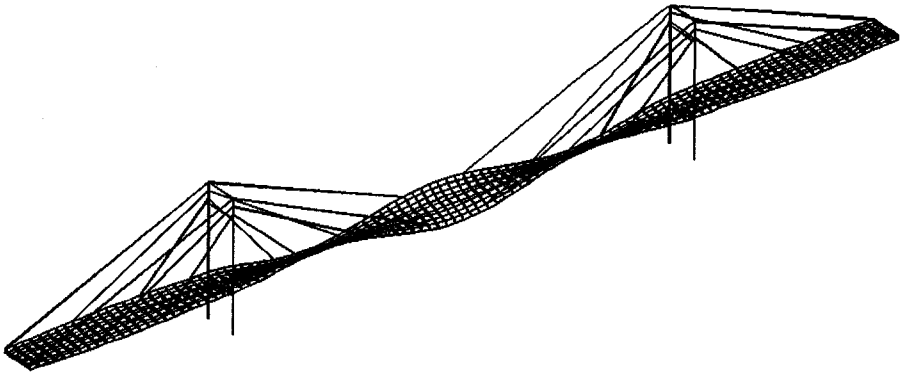

(m) Mode 13, Frequency = 1.05 Hz

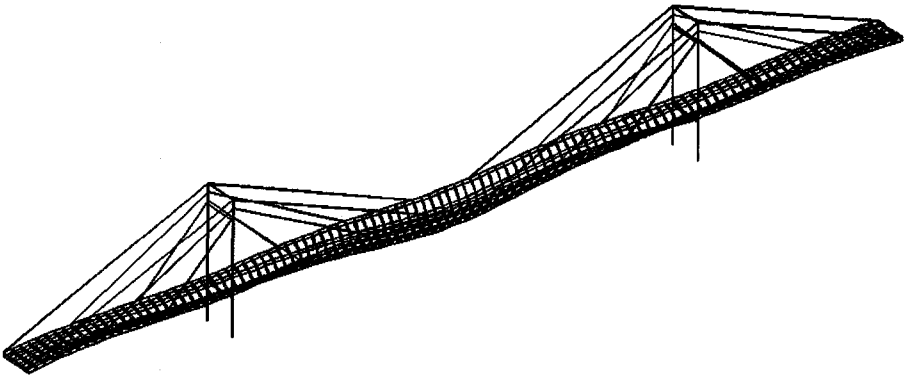

(n) Mode 14, Frequency = 1.28 Hz

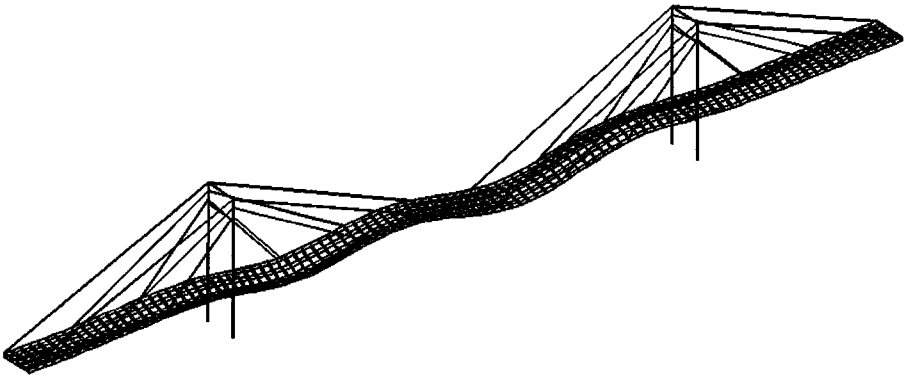

(o) Mode 15, Frequency = 1.44 Hz

FIGURE 4.19 MODE SHAPES OF CABLE-STAYED BRIDGE FOR CASE 5 (CONTINUED)

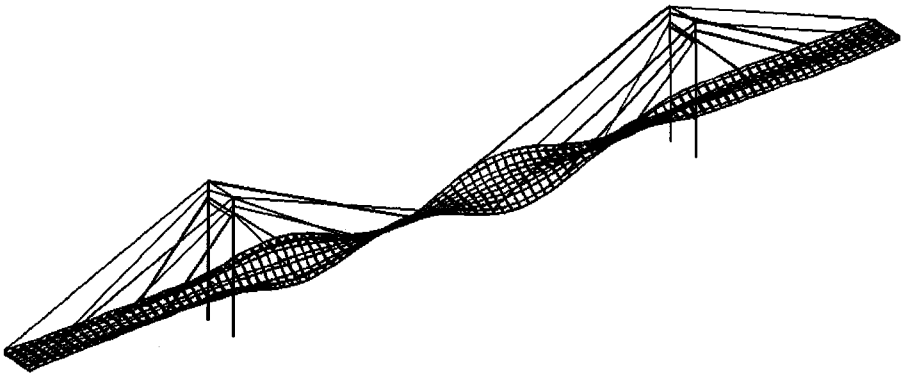

(p) Mode 16, Frequency = 1.52 Hz

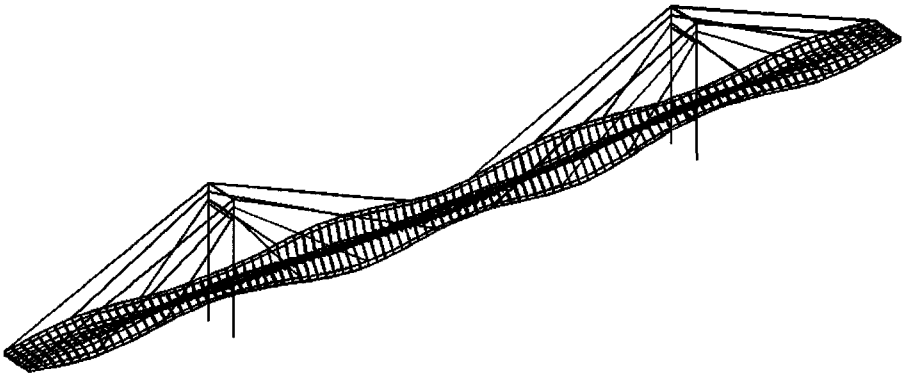

(q) Mode 17, Frequency = 1.55 Hz

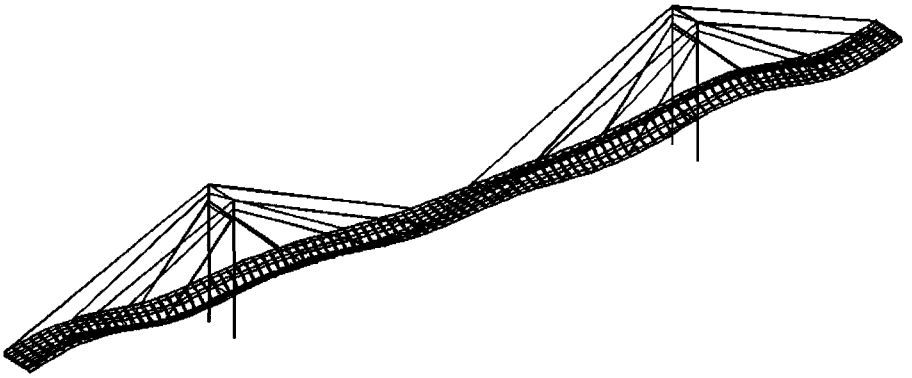

(r) Mode 18, Frequency = 1.72 Hz

FIGURE 4.19 MODE SHAPES OF CABLE-STAYED BRIDGE FOR CASE 5 (CONTINUED)

Chapter 5

VEHICLE MODEL AND BRIDGE-VEHICLE INTERACTION

5.1 Dynamic Model of the Vehicle

For the present analytical study of the bridge-vehicle system, the vehicle is modeled as a three axle, six wheel system as shown in Figure 5.1. The vehicle body consists of a tractor and a trailer, which are considered to be rigid and supported by a system of springs and dash-pots attached to the three axles. The trailer with concentrated mass m_2 is pin connected to the tractor with concentrated mass m_1 at point D. The dash-pots provide viscous damping. The mass of the axles, wheels driveshaft, brakes and the suspension system is supported by the wheels, which always remain in contact with the bridge surface.

There are five independent degrees of freedom (d.o.f.) in the vehicle system, namely translation d_{z1}, rotation θ_{x1} and rotation θ_{y1} of sprung mass m_1, and translation d_{z2} and rotation θ_{x2} of the sprung mass m_2 with respect to the longitudinal axis x along the direction of motion, the transverse axis y and the vertical axis z. The rotation about y of mass m_2, θ_{y2}, is related to the above five independent d.o.f.

The unsprung mass m_3, m_4 and m_5 are assumed to be concentrated at the centers of the three axles respectively. Mass m_3 can undergo vertical translation d_{z3} and a rotation θ_{x3}. Similarly,

mass m_4 has vertical translation d_{z4} and a rotation θ_{x4} and mass m_5 has vertical translation d_{z5} and a rotation θ_{x5}. Since mass m_3, m_4 and m_5 are not supported by springs and the wheels are summed to remain in contact with the bridge surface, d_{z3}, θ_{x3}, d_{z4}, θ_{x4}, d_{z5} and θ_{x5} are not independent but related to the vertical motions of the contact points between the wheels and the bridge surface. Thus, the total number of d.o.f. of the bridge-vehicle system is N+5, in which N is the number of d.o.f. of the bridge structure.

5.2 Formulation of the Equations of Motion

The following assumptions are made to model the bridge and vehicle:

- The materials used in the bridge are assumed to be linearly elastic.
- The damping in the bridge structure is assumed to be viscous.
- The supporting springs are assumed to be linearly elastic and the vehicle damping is assumed to be viscous.
- The surface roughness of the bridge is ignored.
- During the motion, the vehicle is assumed to remain in contact with the bridge.

The compatibility and equilibrium conditions must also be met for the interaction of bridge and vehicle at any contact point:

- Displacements of the bridge deck and the vehicle are equal.
- The external loads on the bridge are equal and opposite to the reactions on the vehicle.

The formulation deriving procedure adopted in this study is similar to that presented by Kashif (1992), who modeled a two-axle four-wheel truck. The equations of motions of the bridge-vehicle system are derived in three steps: 1) vehicle sprung mass motion, 2) the contact forces, and 3) bridge-vehicle interaction motion equations.

5.2.1 Vehicle Sprung Mass Motion

A free body diagram in Figure 5.2 shows the forces and moments acting on the sprung mass of the vehicle. Referring to Figure 5.1 and Figure 5.2, the following geometric relationships can be written:

$$\theta_{y2} = -\frac{1}{(a_3 - a_5)L_2} d_{z1} - \frac{a_2 L_1 + a_5 L_2}{(a_3 - a_5)L_2} \theta_{y1} + \frac{1}{(a_3 - a_5)L_2} d_{z2} \tag{5.1}$$

$$d_{z3} = \frac{1}{2}(w_1 + w_2) \;\; ; \;\; \theta_{x3} = \frac{1}{b}(w_2 - w_1) \tag{5.2}$$

$$d_{z4} = \frac{1}{2}(w_3 + w_4) \;\; ; \;\; \theta_{x4} = \frac{1}{b}(w_4 - w_3) \tag{5.3}$$

$$d_{z5} = \frac{1}{2}(w_5 + w_6) \;\; ; \;\; \theta_{x5} = \frac{1}{b}(w_6 - w_5) \tag{5.4}$$

in which a_2, a_3, a_5, α, L_1 and L_2 are defined in Figure 5.1, and w_1, w_2, w_3, w_4, w_5 and w_6 are the vertical displacements at contact points.

The deformations related to the spring and damping forces F_1, F_2, F_3, F_4, F_5 and F_6 are given by

$$\Delta_1 = d_{z1} - a_1 L_1 \theta_{y1} - \alpha b \theta_{x1} - (0.5 + \alpha) w_1 - (0.5 - \alpha) w_2 \tag{5.5}$$

$$\Delta_2 = d_{z1} - a_1 L_1 \theta_{y1} + \alpha b \theta_{x1} - (0.5 - \alpha) w_1 - (0.5 + \alpha) w_2 \tag{5.6}$$

$$\Delta_3 = d_{z1} + a_2 L_1 \theta_{y1} - \alpha b \theta_{x1} - (0.5 + \alpha) w_3 - (0.5 - \alpha) w_4 \tag{5.7}$$

$$\Delta_4 = d_{z1} + a_2 L_1 \theta_{y1} + \alpha b \theta_{x1} - (0.5 - \alpha) w_3 - (0.5 + \alpha) w_4 \tag{5.8}$$

$$\Delta_5 = -a_6 d_{z1} - a_7 L_1 \theta_{y1} + a_8 d_{z2} - \alpha b \theta_{x2} - (0.5 + \alpha) w_5 - (0.5 - \alpha) w_6 \tag{5.9}$$

$$\Delta_6 = -a_6 d_{z1} - a_7 L_1 \theta_{y1} + a_8 d_{z2} + \alpha b \theta_{x2} - (0.5 - \alpha) w_5 - (0.5 + \alpha) w_6 \tag{5.10}$$

where a_1 and a_4 are defined in Figure 5.1 and

$$a_6 = \frac{a_4}{a_3 - a_5} \;\; ; \;\; a_7 = \frac{(a_2 L_1 + a_5 L_2) a_4}{(a_3 - a_5) L_1} \;\; ; \;\; a_8 = \frac{1 - a_5}{a_3 - a_5} \tag{5.11}$$

Therefore,

$$F_1 = k_1 \Delta_1 + c_1 \dot{\Delta}_1 \;\; ; \;\; F_2 = k_1 \Delta_2 + c_1 \dot{\Delta}_2 \tag{5.12}$$

$$F_3 = k_2 \Delta_3 + c_2 \dot{\Delta}_3 \;\; ; \;\; F_4 = k_2 \Delta_4 + c_2 \dot{\Delta}_4 \tag{5.13}$$

$$F_5 = k_3\Delta_5 + c_3\dot{\Delta}_5 \quad ; \quad F_6 = k_3\Delta_6 + c_3\dot{\Delta}_6 \tag{5.14}$$

in which k_1, k_2 and k_3 are the stiffness of the axle springs; c_1, c_2 and c_3 are the viscous damping coefficients of the axle springs.

The total virtual work done is given by

$$m_1\ddot{d}_{z1}\delta d_{z1} + I_{x1}\ddot{\theta}_{x1}\delta\theta_{x1} + I_{y1}\ddot{\theta}_{y1}\delta\theta_{y1} + m_2\ddot{d}_{z2}\delta d_{z2} + I_{x2}\ddot{\theta}_{x2}\delta\theta_{x2} + I_{y2}\ddot{\theta}_{y2}\delta\theta_{y2} + \sum_{i=1}^{6} F_i\delta\Delta_i = 0 \tag{5.15}$$

where I_{x1} and I_{y1} are the mass moments of inertia of m_1 about axes x and y, and I_{x2} and I_{y2} are the mass moments of inertia of m_2 about axes x and y respectively.

Substituting Equations 5.1~5.14 to Equation 5.15 and according to virtual work principle, the equilibrium equations can be assembled in a matrix form:

$$\mathbf{m}\ddot{\mathbf{d}} + \mathbf{c}\dot{\mathbf{d}} + \mathbf{k}\mathbf{d} - \mathbf{q} = \mathbf{0} \tag{5.16}$$

where

$$\mathbf{d} = \{d_{z1} \quad b\theta_{x1} \quad L_1\theta_{y1} \quad d_{z2} \quad b\theta_{x2}\}^T \tag{5.17}$$

$$\mathbf{m} = \begin{bmatrix} m_1 + a_9\dfrac{I_{y2}}{L_2^2} & 0 & \dfrac{a_{10}I_{y2}}{L_1L_2} & -a_9\dfrac{I_{y2}}{L_2^2} & 0 \\ 0 & \dfrac{I_{x1}}{b^2} & 0 & 0 & 0 \\ a_{10}\dfrac{I_{y2}}{L_1L_2} & 0 & \dfrac{I_{y1}}{L_1^2} + \dfrac{a_{11}I_{y2}}{L_1^2} & -\dfrac{a_{10}I_{y2}}{L_1L_2} & 0 \\ -a_9\dfrac{I_{y2}}{L_2^2} & 0 & -\dfrac{a_{10}I_{y2}}{L_1L_2} & m_2 + a_9\dfrac{I_{y2}}{L_2^2} & 0 \\ 0 & 0 & 0 & 0 & \dfrac{I_{x2}}{L_2^2} \end{bmatrix} \tag{5.18}$$

$$\mathbf{k} = \begin{bmatrix} 2(k_1 + k_2 + a_6^2k_3) & 0 & 2(-a_1k_1 + a_2k_2 + a_6a_7k_3) & -2a_6a_8k_3 & 0 \\ 0 & 2\alpha^2(k_1 + k_2) & 0 & 0 & 0 \\ 2(-a_1k_1 + a_2k_2 + a_6a_7k_3) & 0 & 2(a_1^2k_1 + a_2^2k_2 + a_7^2k_3) & -2a_7a_8k_3 & 0 \\ -2a_6a_8k_3 & 0 & -2a_6a_8k_3 & 2a_8^2k_3 & 0 \\ 0 & 0 & 0 & 0 & 2\alpha^2k_3 \end{bmatrix} \tag{5.19}$$

$$\mathbf{c}=\begin{bmatrix} 2(c_1+c_2+a_6^2c_3) & 0 & 2(-a_1c_1+a_2c_2+a_6a_7c_3) & -2a_6a_8c_3 & 0 \\ 0 & 2\alpha^2(c_1+c_2) & 0 & 0 & 0 \\ 2(-a_1c_1+a_2c_2+a_6a_7c_3) & 0 & 2(a_1^2c_1+a_2^2c_2+a_7^2c_3) & -2a_7a_8c_3 & 0 \\ -2a_6a_8c_3 & 0 & -2a_7a_8c_3 & 2a_8^2c_3 & 0 \\ 0 & 0 & 0 & 0 & 2\alpha^2c_3 \end{bmatrix} \tag{5.20}$$

$$\mathbf{q}=\begin{bmatrix} -k_1(w_1+w_2)-k_2(w_3+w_4)+a_6k_3(w_5+w_6)+\cdots \\ -c_1(\dot{w}_1+\dot{w}_2)-c_2(\dot{w}_3+\dot{w}_4)+a_6c_3(\dot{w}_5+\dot{w}_6) \\ \\ 2\alpha^2k_1(w_1-w_2)+2\alpha^2k_2(w_3-w_4)+2\alpha^2c_1(\dot{w}_1-\dot{w}_2)+2\alpha^2c_2(\dot{w}_3-\dot{w}_4) \\ \\ a_1k_1(w_1+w_2)-a_2k_2(w_3+w_4)+a_7k_3(w_5+w_6)+\cdots \\ +a_1(\dot{w}_1+\dot{w}_2)-a_2c_2(\dot{w}_3+\dot{w}_4)+a_7c_3(\dot{w}_5+\dot{w}_6) \\ \\ -a_8k_3(w_5+w_6)-a_8c_3(\dot{w}_5+\dot{w}_6) \\ \\ -2\alpha^2k_3(w_5+w_6)-2\alpha^2c_3(\dot{w}_5+\dot{w}_6) \end{bmatrix} \tag{5.21}$$

$$a_9=\left(\frac{1}{a_3-a_5}\right)^2 \tag{5.22}$$

$$a_{10}=\frac{a_2L_1+a_5L_2}{(a_3-a_5)^2L_2} \tag{5.23}$$

$$a_{11}=\left(\frac{a_2L_1+a_5L_2}{(a_3-a_5)L_2}\right)^2 \tag{5.24}$$

5.2.2 Contact Forces

Considering equilibrium for each axle shown in Figure 5.2, the contact forces P_i at any point I can be derived as

$$P_1=\frac{1}{2}(F_1+F_2)+\alpha(F_1-F_2)-\frac{F_A}{2}-\frac{m_3g}{2}-\frac{m_3}{2}\ddot{d}_{z3}+\frac{I_{x3}}{b^2}(b\ddot{\theta}_{x3}) \tag{5.25}$$

$$P_2 = \frac{1}{2}(F_1 + F_2) - \alpha(F_1 - F_2) - \frac{F_A}{2} - \frac{m_3 g}{2} - \frac{m_3}{2}\ddot{d}_{z3} - \frac{I_{x3}}{b^2}(b\ddot{\theta}_{x3}) \tag{5.26}$$

$$P_3 = \frac{1}{2}(F_3 + F_4) + \alpha(F_3 - F_4) - \frac{F_B}{2} - \frac{m_4 g}{2} - \frac{m_4}{2}\ddot{d}_{z4} + \frac{I_{x4}}{b^2}(b\ddot{\theta}_{x4}) \tag{5.27}$$

$$P_4 = \frac{1}{2}(F_3 + F_4) - \alpha(F_3 - F_4) - \frac{F_B}{2} - \frac{m_4 g}{2} - \frac{m_4}{2}\ddot{d}_{z4} - \frac{I_{x4}}{b^2}(b\ddot{\theta}_{x4}) \tag{5.28}$$

$$P_5 = \frac{1}{2}(F_5 + F_6) + \alpha(F_5 - F_6) - \frac{F_C}{2} - \frac{m_5 g}{2} - \frac{m_5}{2}\ddot{d}_{z5} + \frac{I_{x4}}{b^2}(b\ddot{\theta}_{x5}) \tag{5.29}$$

$$P_6 = \frac{1}{2}(F_5 + F_6) - \alpha(F_5 - F_6) - \frac{F_C}{2} - \frac{m_5 g}{2} - \frac{m_5}{2}\ddot{d}_{z5} - \frac{I_{x5}}{b^2}(b\ddot{\theta}_{x5}) \tag{5.30}$$

where

m_3, m_4 and m_5 – concentrated mass of the three axles respectively;

I_{x3}, I_{x4} and I_{x5} – the mass moments of inertia of m_3, m_4 and m_5 about axis x;

$$F_A = m_1 g a_2 - \frac{a_4 a_5}{1 - a_5} \cdot \frac{L_2}{L_1} m_2 g \tag{5.31}$$

$$F_B = m_1 g a_1 + \frac{a_4 (L_1 + a_5 L_2)}{(1 - a_5) L_1} m_2 g \tag{5.32}$$

$$F_C = \frac{a_3 - a_5}{1 - a_5} m_2 g \tag{5.33}$$

The x-coordinates of contact points are given by

$$x_1 = x_2 = v_0 t + 0.5 a_0 t^2 + a_1 L_1 \tag{5.34a}$$

$$x_3 = x_4 = v_0 t + 0.5 a_0 t^2 - a_2 L_1 \tag{5.34b}$$

$$x_5 = x_6 = v_0 t + 0.5 a_0 t^2 - a_2 L_1 - a_3 L_2 \tag{5.34c}$$

$$\dot{x}_1 = \dot{x}_2 = \dot{x}_3 = \dot{x}_4 = \dot{x}_5 = \dot{x}_6 = v_0 + a_0 t \tag{5.34d}$$

$$\ddot{x}_1 = \ddot{x}_2 = \ddot{x}_3 = \ddot{x}_4 = \ddot{x}_5 = \ddot{x}_6 = a_0 \tag{5.34e}$$

in which v_0 is the velocity of the vehicle and v_0 is its acceleration. The vertical displacements of the contact points can be written in terms of the nodal d. o. f. of the bridge as

$$w_i = \mathbf{N}_i \mathbf{D} \tag{5.35}$$

where $\mathbf{N}_i$ is the shape function with nonzero terms only corresponding to the d. o. f. of the element in which wheel i is located and $\mathbf{D}$ is the vector of nodal d. o. f. of the bridge. The time derivatives of w are

$$\dot{w} = \frac{\partial \mathbf{N}}{\partial x}\mathbf{D}\dot{x} + \mathbf{N}\dot{\mathbf{D}} \tag{5.36}$$

$$\ddot{w} = \frac{\partial^2 \mathbf{N}}{\partial x^2}\mathbf{D}\dot{x}^2 + 2\frac{\partial \mathbf{N}}{\partial x}\dot{\mathbf{D}}\dot{x} + \frac{\partial \mathbf{N}}{\partial x}\mathbf{D}\ddot{x} + \mathbf{N}\ddot{\mathbf{D}} \tag{5.37}$$

Therefore contact forces P_i can be expressed in terms of the d. o. f. **d** and **D** and their derivatives as

$$P_1 = \mathbf{f}_1\mathbf{d} + \mathbf{g}_1\dot{\mathbf{d}} + \mathbf{G}_1\mathbf{D} + \mathbf{H}_1\dot{\mathbf{D}} + \mathbf{J}_1\ddot{\mathbf{D}} + (-\frac{F_A}{2} - \frac{m_3 g}{2}) \tag{5.38a}$$

$$P_2 = \mathbf{f}_2\mathbf{d} + \mathbf{g}_2\dot{\mathbf{d}} + \mathbf{G}_2\mathbf{D} + \mathbf{H}_2\dot{\mathbf{D}} + \mathbf{J}_2\ddot{\mathbf{D}} + (-\frac{F_A}{2} - \frac{m_3 g}{2}) \tag{5.38b}$$

$$P_3 = \mathbf{f}_3\mathbf{d} + \mathbf{g}_3\dot{\mathbf{d}} + \mathbf{G}_3\mathbf{D} + \mathbf{H}_3\dot{\mathbf{D}} + \mathbf{J}_3\ddot{\mathbf{D}} + (-\frac{F_B}{2} - \frac{m_4 g}{2}) \tag{5.38c}$$

$$P_4 = \mathbf{f}_4\mathbf{d} + \mathbf{g}_4\dot{\mathbf{d}} + \mathbf{G}_4\mathbf{D} + \mathbf{H}_4\dot{\mathbf{D}} + \mathbf{J}_4\ddot{\mathbf{D}} + (-\frac{F_B}{2} - \frac{m_4 g}{2}) \tag{5.38d}$$

$$P_5 = \mathbf{f}_5\mathbf{d} + \mathbf{g}_5\dot{\mathbf{d}} + \mathbf{G}_5\mathbf{D} + \mathbf{H}_5\dot{\mathbf{D}} + \mathbf{J}_5\ddot{\mathbf{D}} + (-\frac{F_C}{2} - \frac{m_5 g}{2}) \tag{5.38e}$$

$$P_6 = \mathbf{f}_6\mathbf{d} + \mathbf{g}_6\dot{\mathbf{d}} + \mathbf{G}_6\mathbf{D} + \mathbf{H}_6\dot{\mathbf{D}} + \mathbf{J}_6\ddot{\mathbf{D}} + (-\frac{F_C}{2} - \frac{m_5 g}{2}) \tag{5.38f}$$

where

$$\mathbf{f}_1 = \begin{bmatrix} k_1 & -2\alpha^2 k_1 & -a_1 k_1 & 0 & 0 \end{bmatrix} \tag{5.39a}$$

$$\mathbf{f}_2 = \begin{bmatrix} k_1 & 2\alpha^2 k_1 & -a_1 k_1 & 0 & 0 \end{bmatrix} \tag{5.39b}$$

$$\mathbf{f}_3 = \begin{bmatrix} k_2 & -2\alpha^2 k_2 & a_2 k_2 & 0 & 0 \end{bmatrix} \tag{5.39c}$$

$$\mathbf{f}_4 = \begin{bmatrix} k_2 & 2\alpha^2 k_2 & a_2 k_2 & 0 & 0 \end{bmatrix} \tag{5.39d}$$

$$\mathbf{f}_5 = \begin{bmatrix} -a_6 k_3 & 0 & -a_7 k_3 & a_8 k_3 & -2\alpha^2 k_3 \end{bmatrix} \tag{5.39e}$$

$$\mathbf{f}_6 = \begin{bmatrix} -a_6 k_3 & 0 & -a_7 k_3 & a_8 k_3 & 2\alpha^2 k_3 \end{bmatrix} \tag{5.39f}$$

$$\mathbf{g}_1 = \begin{bmatrix} c_1 & -2\alpha^2 c_1 & -a_1 c_1 & 0 & 0 \end{bmatrix} \tag{5.40a}$$

$$\mathbf{g}_2 = \begin{bmatrix} c_1 & 2\alpha^2 c_1 & -a_1 c_1 & 0 & 0 \end{bmatrix} \tag{5.40b}$$

$$\mathbf{g}_3 = \begin{bmatrix} c_2 & -2\alpha^2 c_2 & a_2 c_2 & 0 & 0 \end{bmatrix} \tag{5.40c}$$

$$\mathbf{g}_4 = \begin{bmatrix} c_2 & 2\alpha^2 c_2 & a_2 c_2 & 0 & 0 \end{bmatrix} \tag{5.40d}$$

$$\mathbf{g}_5 = \begin{bmatrix} -a_6 c_3 & 0 & -a_7 c_3 & a_8 c_3 & -2\alpha^2 c_3 \end{bmatrix} \tag{5.40e}$$

$$\mathbf{g}_6 = \begin{bmatrix} -a_6 c_3 & 0 & -a_7 c_3 & a_8 c_3 & 2\alpha^2 c_3 \end{bmatrix} \tag{5.40f}$$

$$\mathbf{G}_1 = \begin{bmatrix} k_1(-\frac{1}{2}-2\alpha^2)\mathbf{N}_1 + k_1(-\frac{1}{2}+2\alpha^2)\mathbf{N}_2 + \dot{x}_1 c_1(-\frac{1}{2}-2\alpha^2)\frac{\partial \mathbf{N}_1}{\partial x} + \dots \\ + \dot{x}_2 c_1(-\frac{1}{2}+2\alpha^2)\frac{\partial \mathbf{N}_2}{\partial x} + \ddot{x}_1(-\frac{m_3}{4}-\frac{I_{x3}}{b^2})\frac{\partial \mathbf{N}_1}{\partial x} + \ddot{x}_2(-\frac{m_3}{4}+\frac{I_{x3}}{b^2})\frac{\partial \mathbf{N}_2}{\partial x} + \dots \\ + \dot{x}_1^2(-\frac{m_3}{4}-\frac{I_{x3}}{b^2})\frac{\partial^2 \mathbf{N}_1}{\partial x^2} + \dot{x}_2^2(-\frac{m_3}{4}+\frac{I_{x3}}{b^2})\frac{\partial^2 \mathbf{N}_2}{\partial x^2} \end{bmatrix} \tag{5.41a}$$

$$\mathbf{G}_2 = \begin{bmatrix} k_1(-\frac{1}{2}+2\alpha^2)\mathbf{N}_1 + k_1(-\frac{1}{2}-2\alpha^2)\mathbf{N}_2 + \dot{x}_1 c_1(-\frac{1}{2}+2\alpha^2)\frac{\partial \mathbf{N}_1}{\partial x} + \dots \\ + \dot{x}_2 c_1(-\frac{1}{2}-2\alpha^2)\frac{\partial \mathbf{N}_2}{\partial x} + \ddot{x}_1(-\frac{m_3}{4}+\frac{I_{x3}}{b^2})\frac{\partial \mathbf{N}_1}{\partial x} + \ddot{x}_2(-\frac{m_3}{4}-\frac{I_{x3}}{b^2})\frac{\partial \mathbf{N}_2}{\partial x} + \dots \\ + \dot{x}_1^2(-\frac{m_3}{4}+\frac{I_{x3}}{b^2})\frac{\partial^2 \mathbf{N}_1}{\partial x^2} + \dot{x}_2^2(-\frac{m_3}{4}-\frac{I_{x3}}{b^2})\frac{\partial^2 \mathbf{N}_2}{\partial x^2} \end{bmatrix} \tag{5.41b}$$

$$\mathbf{G}_3 = \begin{bmatrix} k_2(-\frac{1}{2}-2\alpha^2)\mathbf{N}_3 + k_2(-\frac{1}{2}+2\alpha^2)\mathbf{N}_4 + \dot{x}_3 c_2(-\frac{1}{2}-2\alpha^2)\frac{\partial \mathbf{N}_3}{\partial x} + \dots \\ + \dot{x}_4 c_2(-\frac{1}{2}+2\alpha^2)\frac{\partial \mathbf{N}_4}{\partial x} + \ddot{x}_3(-\frac{m_4}{4}-\frac{I_{x4}}{b^2})\frac{\partial \mathbf{N}_3}{\partial x} + \ddot{x}_4(-\frac{m_4}{4}+\frac{I_{x4}}{b^2})\frac{\partial \mathbf{N}_4}{\partial x} + \dots \\ + \dot{x}_3^2(-\frac{m_4}{4}-\frac{I_{x4}}{b^2})\frac{\partial^2 \mathbf{N}_3}{\partial x^2} + \dot{x}_4^2(-\frac{m_4}{4}+\frac{I_{x4}}{b^2})\frac{\partial^2 \mathbf{N}_4}{\partial x^2} \end{bmatrix} \tag{5.41c}$$

$$\mathbf{G}_4 = \begin{bmatrix} k_2(-\frac{1}{2}+2\alpha^2)\mathbf{N}_3 + k_2(-\frac{1}{2}-2\alpha^2)\mathbf{N}_4 + \dot{x}_3 c_2(-\frac{1}{2}+2\alpha^2)\frac{\partial \mathbf{N}_3}{\partial x} + \dots \\ + \dot{x}_4 c_2(-\frac{1}{2}-2\alpha^2)\frac{\partial \mathbf{N}_4}{\partial x} + \ddot{x}_3(-\frac{m_4}{4}+\frac{I_{x4}}{b^2})\frac{\partial \mathbf{N}_3}{\partial x} + \ddot{x}_4(-\frac{m_4}{4}-\frac{I_{x4}}{b^2})\frac{\partial \mathbf{N}_4}{\partial x} + \dots \\ + \dot{x}_3^2(-\frac{m_4}{4}+\frac{I_{x4}}{b^2})\frac{\partial^2 \mathbf{N}_3}{\partial x^2} + \dot{x}_4^2(-\frac{m_4}{4}-\frac{I_{x4}}{b^2})\frac{\partial^2 \mathbf{N}_4}{\partial x^2} \end{bmatrix} \tag{5.41d}$$

$$\mathbf{G}_5 = \begin{bmatrix} k_3(-\frac{1}{2}-2\alpha^2)\mathbf{N}_5 + k_3(-\frac{1}{2}+2\alpha^2)\mathbf{N}_6 + \dot{x}_5 c_3(-\frac{1}{2}-2\alpha^2)\frac{\partial \mathbf{N}_5}{\partial x} + \dots \\ + \dot{x}_6 c_3(-\frac{1}{2}+2\alpha^2)\frac{\partial \mathbf{N}_6}{\partial x} + \ddot{x}_5(-\frac{m_5}{4}-\frac{I_{x5}}{b^2})\frac{\partial \mathbf{N}_5}{\partial x} + \ddot{x}_6(-\frac{m_5}{4}+\frac{I_{x5}}{b^2})\frac{\partial \mathbf{N}_6}{\partial x} + \dots \\ + \dot{x}_5^2(-\frac{m_5}{4}-\frac{I_{x5}}{b^2})\frac{\partial^2 \mathbf{N}_5}{\partial x^2} + \dot{x}_6^2(-\frac{m_5}{4}+\frac{I_{x5}}{b^2})\frac{\partial^2 \mathbf{N}_6}{\partial x^2} \end{bmatrix} \tag{5.41e}$$

$$\mathbf{G}_6=\begin{bmatrix} k_3(-\frac{1}{2}+2\alpha^2)\mathbf{N}_5+k_3(-\frac{1}{2}-2\alpha^2)\mathbf{N}_6+\dot{x}_5c_3(-\frac{1}{2}+2\alpha^2)\frac{\partial\mathbf{N}_5}{\partial x}+\dots \\ +\dot{x}_6c_3(-\frac{1}{2}-2\alpha^2)\frac{\partial\mathbf{N}_6}{\partial x}+\ddot{x}_5(-\frac{m_5}{4}+\frac{I_{x5}}{b^2})\frac{\partial\mathbf{N}_5}{\partial x}+\ddot{x}_6(-\frac{m_5}{4}-\frac{I_{x5}}{b^2})\frac{\partial\mathbf{N}_6}{\partial x}+\dots \\ +\dot{x}_5^2(-\frac{m_5}{4}+\frac{I_{x5}}{b^2})\frac{\partial^2\mathbf{N}_5}{\partial x^2}+\dot{x}_6^2(-\frac{m_5}{4}-\frac{I_{x5}}{b^2})\frac{\partial^2\mathbf{N}_6}{\partial x^2} \end{bmatrix} \tag{5.41f}$$

$$\mathbf{H}_1=\begin{bmatrix} c_1(-\frac{1}{2}-2\alpha^2)\mathbf{N}_1+c_1(-\frac{1}{2}+2\alpha^2)\mathbf{N}_2+\dots \\ +2\dot{x}_1(-\frac{m_3}{4}-\frac{I_{x3}}{b^2})\frac{\partial\mathbf{N}_1}{\partial x}+2\dot{x}_2(-\frac{m_3}{4}+\frac{I_{x3}}{b^2})\frac{\partial\mathbf{N}_2}{\partial x} \end{bmatrix} \tag{5.42a}$$

$$\mathbf{H}_2=\begin{bmatrix} c_1(-\frac{1}{2}+2\alpha^2)\mathbf{N}_1+c_1(-\frac{1}{2}-2\alpha^2)\mathbf{N}_2+\dots \\ +2\dot{x}_1(-\frac{m_3}{4}+\frac{I_{x3}}{b^2})\frac{\partial\mathbf{N}_1}{\partial x}+2\dot{x}_2(-\frac{m_3}{4}-\frac{I_{x3}}{b^2})\frac{\partial\mathbf{N}_2}{\partial x} \end{bmatrix} \tag{5.42b}$$

$$\mathbf{H}_3=\begin{bmatrix} c_2(-\frac{1}{2}-2\alpha^2)\mathbf{N}_3+c_2(-\frac{1}{2}+2\alpha^2)\mathbf{N}_4+\dots \\ +2\dot{x}_3(-\frac{m_4}{4}-\frac{I_{x4}}{b^2})\frac{\partial\mathbf{N}_3}{\partial x}+2\dot{x}_4(-\frac{m_4}{4}+\frac{I_{x4}}{b^2})\frac{\partial\mathbf{N}_4}{\partial x} \end{bmatrix} \tag{5.42c}$$

$$\mathbf{H}_4=\begin{bmatrix} c_2(-\frac{1}{2}+2\alpha^2)\mathbf{N}_3+c_2(-\frac{1}{2}-2\alpha^2)\mathbf{N}_4+\dots \\ +2\dot{x}_3(-\frac{m_4}{4}+\frac{I_{x4}}{b^2})\frac{\partial\mathbf{N}_3}{\partial x}+2\dot{x}_4(-\frac{m_4}{4}-\frac{I_{x4}}{b^2})\frac{\partial\mathbf{N}_4}{\partial x} \end{bmatrix} \tag{5.42d}$$

$$\mathbf{H}_5=\begin{bmatrix} c_3(-\frac{1}{2}-2\alpha^2)\mathbf{N}_5+c_3(-\frac{1}{2}+2\alpha^2)\mathbf{N}_6+\dots \\ +2\dot{x}_5(-\frac{m_5}{4}-\frac{I_{x5}}{b^2})\frac{\partial\mathbf{N}_5}{\partial x}+2\dot{x}_6(-\frac{m_5}{4}+\frac{I_{x5}}{b^2})\frac{\partial\mathbf{N}_6}{\partial x} \end{bmatrix} \tag{5.42e}$$

$$\mathbf{H}_6=\begin{bmatrix} c_3(-\frac{1}{2}+2\alpha^2)\mathbf{N}_5+c_3(-\frac{1}{2}-2\alpha^2)\mathbf{N}_6+\dots \\ +2\dot{x}_5(-\frac{m_5}{4}+\frac{I_{x5}}{b^2})\frac{\partial\mathbf{N}_5}{\partial x}+2\dot{x}_6(-\frac{m_5}{4}-\frac{I_{x5}}{b^2})\frac{\partial\mathbf{N}_6}{\partial x} \end{bmatrix} \tag{5.42f}$$

$$\mathbf{J}_1=\begin{bmatrix}(-\frac{m_3}{4}-\frac{I_{x3}}{b^2})\mathbf{N}_1+(-\frac{m_3}{4}+\frac{I_{x3}}{b^2})\mathbf{N}_2\end{bmatrix} \tag{5.43a}$$

$$\mathbf{J}_2=\begin{bmatrix}(-\frac{m_3}{4}+\frac{I_{x3}}{b^2})\mathbf{N}_1+(-\frac{m_3}{4}-\frac{I_{x3}}{b^2})\mathbf{N}_2\end{bmatrix} \tag{5.43b}$$

$$\mathbf{J}_3 = \left[(-\frac{m_4}{4} - \frac{I_{x4}}{b^2})\mathbf{N}_3 + (-\frac{m_4}{4} + \frac{I_{x4}}{b^2})\mathbf{N}_4 \right] \tag{5.43c}$$

$$\mathbf{J}_4 = \left[(-\frac{m_4}{4} + \frac{I_{x4}}{b^2})\mathbf{N}_3 + (-\frac{m_4}{4} - \frac{I_{x4}}{b^2})\mathbf{N}_4 \right] \tag{5.43d}$$

$$\mathbf{J}_5 = \left[(-\frac{m_5}{4} - \frac{I_{x5}}{b^2})\mathbf{N}_5 + (-\frac{m_5}{4} + \frac{I_{x5}}{b^2})\mathbf{N}_6 \right] \tag{5.43e}$$

$$\mathbf{J}_6 = \left[(-\frac{m_5}{4} + \frac{I_{x5}}{b^2})\mathbf{N}_5 + (-\frac{m_5}{4} - \frac{I_{x5}}{b^2})\mathbf{N}_6 \right] \tag{5.43f}$$

5.2.3 Equation of Motion of the Bridge-Vehicle System

With the contact forces P_i are converted to equivalent nodal forces using the principle of virtual work, the equations of motion of the bridge is

$$\begin{aligned} \mathbf{M}\ddot{\mathbf{D}} + \mathbf{C}\dot{\mathbf{D}} + \mathbf{K}\mathbf{D} &= \mathbf{N}_1^T P_1 + \mathbf{N}_2^T P_2 + \mathbf{N}_3^T P_3 + \mathbf{N}_4^T P_4 + \mathbf{N}_5^T P_5 + \mathbf{N}_6^T P_6 \\ &= \sum_{i=1}^{6} \mathbf{N}_i^T P_i \end{aligned} \tag{5.44}$$

where **M** is the mass matrix, **C** the damping matrix and **K** the stiffness matrix of the bridge structure. Substituting Equation 5.38, the right hand side of Equation 5.44 can be written as

$$\sum_{i=1}^{6} \mathbf{N}_i^T P_i = \sum_{i=1}^{6} \mathbf{N}_i^T \mathbf{f}_i \mathbf{d} + \mathbf{N}_i^T \mathbf{g}_i \dot{\mathbf{d}} + \mathbf{N}_i^T \mathbf{G}_i \mathbf{D} + \mathbf{N}_i^T \mathbf{H}_i \dot{\mathbf{D}} + \mathbf{N}_i^T \mathbf{J}_i \ddot{\mathbf{D}} + \mathbf{N}_i^T Q_i \tag{5.45}$$

where

$$Q_1 = Q_2 = -\frac{F_A}{2} - \frac{m_3 g}{2};\ Q_3 = Q_4 = -\frac{F_B}{2} - \frac{m_4 g}{2};\ Q_5 = Q_6 = -\frac{F_C}{2} - \frac{m_5 g}{2} \tag{5.46}$$

in which F_A, F_B and F_C are defined in Equations 5.31~5.33.

By substituting Equations 5.35~5.37 into Equation 5.21, it gives

$$\mathbf{q} = [\mathbf{q}_1 \quad \mathbf{q}_2 \quad \mathbf{q}_3 \quad \mathbf{q}_4 \quad \mathbf{q}_5]^T \tag{5.47}$$

where

$$\mathbf{q}_1 = [-k_1(\mathbf{N}_1+\mathbf{N}_2) - k_2(\mathbf{N}_3+\mathbf{N}_4) + a_6k_3(\mathbf{N}_5+\mathbf{N}_6) - c_1(\dot{x}_1\frac{\partial \mathbf{N}_1}{\partial x} + \dot{x}_2\frac{\partial \mathbf{N}_2}{\partial x}) - \ldots$$
$$- c_2(\dot{x}_3\frac{\partial \mathbf{N}_3}{\partial x} + \dot{x}_4\frac{\partial \mathbf{N}_4}{\partial x}) + a_6c_3(\dot{x}_5\frac{\partial \mathbf{N}_5}{\partial x} + \dot{x}_6\frac{\partial \mathbf{N}_6}{\partial x})]\mathbf{D} + \ldots \quad (5.48a)$$
$$+ [-c_1(\mathbf{N}_1+\mathbf{N}_2) - c_2(\mathbf{N}_3+\mathbf{N}_4) + a_6c_3(\mathbf{N}_5+\mathbf{N}_6)]\dot{\mathbf{D}}$$

$$\mathbf{q}_2 = [2\alpha^2k_1(\mathbf{N}_1-\mathbf{N}_2) + 2\alpha^2k_2(\mathbf{N}_3-\mathbf{N}_4) + 2\alpha^2c_1(\dot{x}_1\frac{\partial \mathbf{N}_1}{\partial x} - \dot{x}_2\frac{\partial \mathbf{N}_2}{\partial x}) + \ldots$$
$$+ 2\alpha^2c_2(\dot{x}_3\frac{\partial \mathbf{N}_3}{\partial x} - \dot{x}_4\frac{\partial \mathbf{N}_4}{\partial x})]\mathbf{D} + \ldots \quad (5.48b)$$
$$+ [2\alpha^2c_1(\mathbf{N}_1-\mathbf{N}_2) + 2\alpha^2c_2(\mathbf{N}_3-\mathbf{N}_4)]\dot{\mathbf{D}}$$

$$\mathbf{q}_3 = [a_1k_1(\mathbf{N}_1+\mathbf{N}_2) - a_2k_2(\mathbf{N}_3+\mathbf{N}_4) + a_7k_3(\mathbf{N}_5+\mathbf{N}_6) + \ldots$$
$$+ a_1c_1(\dot{x}_1\frac{\partial \mathbf{N}_1}{\partial x} + \dot{x}_2\frac{\partial \mathbf{N}_2}{\partial x}) - a_2c_2(\dot{x}_3\frac{\partial \mathbf{N}_3}{\partial x} + \dot{x}_4\frac{\partial \mathbf{N}_4}{\partial x}) + \ldots \quad (5.48c)$$
$$+ a_7c_3(\dot{x}_5\frac{\partial \mathbf{N}_5}{\partial x} + \dot{x}_6\frac{\partial \mathbf{N}_6}{\partial x})]\mathbf{D} + \ldots$$
$$+ [a_1c_1(\mathbf{N}_1+\mathbf{N}_2) - a_2c_2(\mathbf{N}_3+\mathbf{N}_4) + a_7c_3(\mathbf{N}_5+\mathbf{N}_6)]\dot{\mathbf{D}}$$

$$\mathbf{q}_4 = [-a_8k_3(\mathbf{N}_5+\mathbf{N}_6) - a_8c_3(\dot{x}_5\frac{\partial \mathbf{N}_5}{\partial x} + \dot{x}_6\frac{\partial \mathbf{N}_6}{\partial x})]\mathbf{D} + \ldots \quad (5.48d)$$
$$+ [-a_8c_3(\mathbf{N}_5+\mathbf{N}_6)]\dot{\mathbf{D}}$$

$$\mathbf{q}_5 = [-2\alpha^2k_3(\mathbf{N}_5+\mathbf{N}_6) - 2\alpha^2c_3(\dot{x}_5\frac{\partial \mathbf{N}_5}{\partial x} + \dot{x}_6\frac{\partial \mathbf{N}_6}{\partial x})]\mathbf{D} + \ldots \quad (5.48e)$$
$$+ [-2\alpha^2c_3(\mathbf{N}_5+\mathbf{N}_6)]\dot{\mathbf{D}}$$

Combining Equations 5.44 and 5.16, the equations of motions for bridge-vehicle system can be expressed as

$$\begin{bmatrix}\mathbf{m} & \mathbf{0}\\ \mathbf{0} & \mathbf{M}+\mathbf{m}^*\end{bmatrix}\begin{bmatrix}\ddot{\mathbf{d}}\\ \ddot{\mathbf{D}}\end{bmatrix} + \begin{bmatrix}\mathbf{c} & \mathbf{c}_h\\ \mathbf{c}_v & \mathbf{C}+\mathbf{c}^*\end{bmatrix}\begin{bmatrix}\dot{\mathbf{d}}\\ \dot{\mathbf{D}}\end{bmatrix} + \begin{bmatrix}\mathbf{k} & \mathbf{k}_h\\ \mathbf{k}_v & \mathbf{K}+\mathbf{k}^*\end{bmatrix}\begin{bmatrix}\mathbf{d}\\ \mathbf{D}\end{bmatrix} = \begin{bmatrix}\mathbf{0}\\ \mathbf{p}^*\end{bmatrix} \quad (5.49)$$

where

$$\mathbf{m}^*_{(NxN)} = -\sum_{i=1}^{6}\mathbf{N}_i^T\cdot\mathbf{J}_i \quad (5.50a)$$

$$\mathbf{c}^*_{(NxN)} = -\sum_{i=1}^{6}\mathbf{N}_i^T\cdot\mathbf{H}_i \quad (5.50b)$$

$$\mathbf{k}^*_{(NxN)} = -\sum_{i=1}^{6} \mathbf{N}_i^T \cdot \mathbf{G}_i \tag{5.50c}$$

$$\mathbf{c}_{\mathbf{v}(Nx5)} = -\sum_{i=1}^{6} \mathbf{N}_i^T \cdot \mathbf{g}_i \tag{5.50d}$$

$$\mathbf{k}_{\mathbf{v}(Nx5)} = -\sum_{i=1}^{6} \mathbf{N}_i^T \cdot \mathbf{f}_i \tag{5.50e}$$

$$\mathbf{p}^*_{(Nx1)} = \sum_{i=1}^{6} \mathbf{N}_i^T \cdot Q_i \tag{5.50f}$$

$$\mathbf{c}_{h(5xN)} = \begin{bmatrix} -c_1(\mathbf{N}_1+\mathbf{N}_2)-c_2(\mathbf{N}_3+\mathbf{N}_4)+a_6c_3(\mathbf{N}_5+\mathbf{N}_6) \\ 2\alpha^2c_1(\mathbf{N}_1-\mathbf{N}_2)+2\alpha^2c_2(\mathbf{N}_3-\mathbf{N}_4) \\ a_1c_1(\mathbf{N}_1+\mathbf{N}_2)-a_2c_2(\mathbf{N}_3+\mathbf{N}_4)+a_7c_3(\mathbf{N}_5+\mathbf{N}_6) \\ -a_8c_3(\mathbf{N}_5+\mathbf{N}_6) \\ -2\alpha^2c_3(\mathbf{N}_5+\mathbf{N}_6) \end{bmatrix} \tag{5.50g}$$

$$\mathbf{k}_{h(5xN)} = \begin{bmatrix} -k_1(\mathbf{N}_1+\mathbf{N}_2)-k_2(\mathbf{N}_3+\mathbf{N}_4)+a_6k_3(\mathbf{N}_5+\mathbf{N}_6) \\ 2\alpha^2k_1(\mathbf{N}_1-\mathbf{N}_2)+2\alpha^2k_2(\mathbf{N}_3-\mathbf{N}_4) \\ a_1k_1(\mathbf{N}_1+\mathbf{N}_2)-a_2k_2(\mathbf{N}_3+\mathbf{N}_4)+a_7k_3(\mathbf{N}_5+\mathbf{N}_6) \\ -a_8k_3(\mathbf{N}_5+\mathbf{N}_6) \\ -2\alpha^2k_3(\mathbf{N}_5+\mathbf{N}_6) \end{bmatrix} +$$

$$+ \begin{bmatrix} -c_1(\dot{x}_1\frac{\partial \mathbf{N}_1}{\partial x}+\dot{x}_2\frac{\partial \mathbf{N}_2}{\partial x})-c_2(\dot{x}_3\frac{\partial \mathbf{N}_3}{\partial x}+\dot{x}_4\frac{\partial \mathbf{N}_4}{\partial x})+a_6c_3(\dot{x}_5\frac{\partial \mathbf{N}_5}{\partial x}+\dot{x}_6\frac{\partial \mathbf{N}_6}{\partial x}) \\ 2\alpha^2c_1(\dot{x}_1\frac{\partial \mathbf{N}_1}{\partial x}-\dot{x}_2\frac{\partial \mathbf{N}_2}{\partial x})+2\alpha^2c_2(\dot{x}_3\frac{\partial \mathbf{N}_3}{\partial x}-\dot{x}_4\frac{\partial \mathbf{N}_4}{\partial x}) \\ a_1c_1(\dot{x}_1\frac{\partial \mathbf{N}_1}{\partial x}+\dot{x}_2\frac{\partial \mathbf{N}_2}{\partial x})-a_2c_2(\dot{x}_3\frac{\partial \mathbf{N}_3}{\partial x}+\dot{x}_4\frac{\partial \mathbf{N}_4}{\partial x})+a_7c_3(\dot{x}_5\frac{\partial \mathbf{N}_5}{\partial x}+\dot{x}_6\frac{\partial \mathbf{N}_6}{\partial x}) \\ -a_8c_3(\dot{x}_5\frac{\partial \mathbf{N}_5}{\partial x}+\dot{x}_6\frac{\partial \mathbf{N}_6}{\partial x}) \\ -2\alpha^2c_3(\dot{x}_5\frac{\partial \mathbf{N}_5}{\partial x}+\dot{x}_6\frac{\partial \mathbf{N}_6}{\partial x}) \end{bmatrix} \tag{5.50h}$$

The equations of motion 5.49 are valid at any time t. For nonlinear analysis these equations should be applied in an incremental form so that during the small incremental time step the

stiffness, damping and mass matrices can be assumed to be constant. Therefore, Equation 5.49 will be rewritten in the form:

$$\begin{bmatrix} \mathbf{m} & \mathbf{0} \\ \mathbf{0} & \mathbf{M}+\mathbf{m}^* \end{bmatrix} \begin{bmatrix} \Delta\ddot{\mathbf{d}} \\ \Delta\ddot{\mathbf{D}} \end{bmatrix} + \begin{bmatrix} \mathbf{c} & \mathbf{c}_h \\ \mathbf{c}_v & \mathbf{C}+\mathbf{c}^* \end{bmatrix} \begin{bmatrix} \Delta\dot{\mathbf{d}} \\ \Delta\dot{\mathbf{D}} \end{bmatrix} + \begin{bmatrix} \mathbf{k} & \mathbf{k}_h \\ \mathbf{k}_v & \mathbf{K}+\mathbf{k}^* \end{bmatrix} \begin{bmatrix} \Delta\mathbf{d} \\ \Delta\mathbf{D} \end{bmatrix} = \begin{bmatrix} \mathbf{0} \\ \Delta\mathbf{p}^* \end{bmatrix} \tag{5.51}$$

5.3 Solution of the Equations of Motion

Previous investigations (Chen and Xiang, 1988) have shown that the main effect on the nonlinear behavior of cable-stayed bridges caused by the interaction of axial and bending deformations is due to the axial force created by dead loads. The effect of axial forces caused by the vehicle on the cables and girders can be neglected. Fleming and Egeseli (1980) also concluded that nonlinear dynamic analysis of a cable-stayed bridge almost yields the same results throughout the time loading as linear dynamic analysis using the stiffness matrix obtained from nonlinear analysis of dead load state. A linear dynamic analysis of the structure is far less complicated and requires far less computer time than a non-linear dynamic analysis. Considering the dynamic characteristics of the system, the modal method (Humar, 1990) and the step-by-step integration method are adopted in the solution of the equations of motion. The overall scheme of the procedure is as follows:

5.3.1 Modal Method

The free vibration analysis is first performed for both the bridge structure and the vehicle system to calculate the natural frequencies and the mode shapes. Both the bridge and the vehicle nodal displacements can be expressed in terms of modal coordinates as

$$\mathbf{D} = \mathbf{\Phi}_b \mathbf{Y}_b \tag{5.52a}$$

$$\mathbf{d} = \Phi_v \mathbf{Y}_v \tag{5.52b}$$

Similarly, the displacement increments are

$$\Delta\mathbf{D} = \mathbf{\Phi}_b \mathbf{Y}_b \tag{5.53a}$$

$$\Delta \mathbf{d} = \Phi_v \mathbf{Y}_v \tag{5.53b}$$

where $\mathbf{\Phi}_b$ is an N × J matrix (J <= N) , referred as the modal matrix of the bridge system. This matrix comprises J mass-orthonormal mode shapes ϕ_b placed side by side in the following form

$$\Phi = [\phi_1 \quad \phi_2 \quad \cdots \quad \phi_J] \tag{5.54}$$

Matrix $\mathbf{\Phi}_v$ is the 5 × 5 modal matrix of the vehicle. The orthogonality property of the mode shape gives

$$\begin{aligned} \mathbf{\Phi}_b^T \mathbf{M} \mathbf{\Phi}_b &= \mathbf{I} \quad ; \quad \mathbf{\Phi}_v^T \mathbf{m} \mathbf{\Phi}_v = \mathbf{I} \\ \mathbf{\Phi}_b^T \mathbf{K} \mathbf{\Phi}_b &= \mathbf{\Lambda}_b \quad ; \quad \mathbf{\Phi}_v^T \mathbf{k} \mathbf{\Phi}_v = \mathbf{\Lambda}_v \\ \mathbf{\Phi}_b^T \mathbf{C} \mathbf{\Phi}_b &= \mathbf{\Psi}_b \quad ; \quad \mathbf{\Phi}_v^T \mathbf{c} \mathbf{\Phi}_v = \mathbf{\Psi}_v \end{aligned} \tag{5.55}$$

where $\mathbf{\Lambda}_b$ and $\mathbf{\Lambda}_v$ are the diagonal spectral matrices of the bridge and the vehicle with eigenvalues λ; and $\mathbf{\Psi}_b$ and $\mathbf{\Psi}_v$ are the diagonal transformed damping matrices of the bridge and vehicle respectively, in which the i^{th} term is $2\zeta_i\omega_i$ (ζ_i and ω_i are the i^{th} mode damping ratio and natural frequency).

Applying normal coordinate transformation to Equation 5.51, it gives

$$\begin{aligned} \hat{\mathbf{m}} \Delta \ddot{\mathbf{Y}}_v + \hat{\mathbf{c}} \Delta \dot{\mathbf{Y}}_v + \hat{\mathbf{k}} \Delta \mathbf{Y}_v + \hat{\mathbf{c}}_h \Delta \dot{\mathbf{Y}}_b + \hat{\mathbf{k}}_h \Delta \mathbf{Y}_b &= 0 \\ \hat{\mathbf{M}} \Delta \ddot{\mathbf{Y}}_b + \hat{\mathbf{C}} \Delta \dot{\mathbf{Y}}_b + \hat{\mathbf{K}} \Delta \mathbf{Y}_b + \hat{\mathbf{c}}_v \Delta \dot{\mathbf{Y}}_v + \hat{\mathbf{k}}_v \Delta \mathbf{Y}_v &= \hat{\mathbf{P}} \end{aligned} \tag{5.56}$$

where

$$\hat{\mathbf{m}}_{5\times5} = \mathbf{I}_{5\times5} \tag{5.57a}$$

$$\hat{\mathbf{c}}_{5\times5} = \mathbf{\Psi}_{v\ 5\times5} \tag{5.57b}$$

$$\hat{\mathbf{k}}_{5\times5} = \mathbf{\Lambda}_{v\ 5\times5} \tag{5.57c}$$

$$\hat{\mathbf{M}}_{J\times J} = \mathbf{\Phi}^T_{b\ J\times N} \mathbf{m}^*_{N\times N} \mathbf{\Phi}_{b\ N\times J} + \mathbf{I}_{J\times J} \tag{5.57d}$$

$$\hat{\mathbf{C}}_{J\times J} = \mathbf{\Phi}^T_{b\ J\times N} \mathbf{c}^*_{N\times N} \mathbf{\Phi}_{b\ N\times J} + \mathbf{\Psi}_{b\ J\times J} \tag{5.57e}$$

$$\hat{\mathbf{K}}_{J\times J} = \mathbf{\Phi}^T_{b\ J\times N} \mathbf{k}^*_{N\times N} \mathbf{\Phi}_{b\ N\times J} + \mathbf{\Lambda}_{b\ J\times J} \tag{5.57f}$$

$$\hat{\mathbf{c}}_{h\ 5\times J} = \mathbf{\Phi}^T_{v\ 5\times5} \mathbf{c}_{h\ 5\times N} \mathbf{\Phi}_{b\ N\times J} \tag{5.57g}$$

$$\hat{\mathbf{k}}_{h\ 5\times J} = \mathbf{\Phi}^T_{v\ 5\times5} \mathbf{k}_{h\ 5\times N} \mathbf{\Phi}_{b\ N\times J} \tag{5.57h}$$

$$\hat{\mathbf{c}}_{v\ J\times 5} = \mathbf{\Phi}^T_{b\ J\times N}\mathbf{c}_{v\ N\times 5}\mathbf{\Phi}_{v\ 5\times 5} \tag{5.57i}$$

$$\hat{\mathbf{k}}_{v\ J\times 5} = \mathbf{\Phi}^T_{b\ J\times N}\mathbf{k}_{h\ N\times 5}\mathbf{\Phi}_{v\ 5\times 5} \tag{5.57j}$$

$$\hat{\mathbf{P}}_{J\times 1} = \mathbf{\Phi}^T_{b\ J\times N}\Delta\mathbf{P}^*_{N\times 1} \tag{5.57k}$$

Equation 5.56 can also be expressed as

$$\mathbf{M}_T\Delta\ddot{\mathbf{U}} + \mathbf{C}_T\Delta\dot{\mathbf{U}} + \mathbf{K}_T\Delta\mathbf{U} = \mathbf{P}_T \tag{5.58}$$

where

$$\mathbf{M}_T = \begin{bmatrix} \hat{\mathbf{m}} & 0 \\ 0 & \hat{\mathbf{M}} \end{bmatrix} \tag{5.59a}$$

$$\mathbf{C}_T = \begin{bmatrix} \hat{\mathbf{c}} & \hat{\mathbf{c}}_h \\ \hat{\mathbf{c}}_v & \hat{\mathbf{C}} \end{bmatrix} \tag{5.59b}$$

$$\mathbf{K}_T = \begin{bmatrix} \hat{\mathbf{k}} & \hat{\mathbf{k}}_h \\ \hat{\mathbf{k}}_v & \hat{\mathbf{K}} \end{bmatrix} \tag{5.59c}$$

$$\Delta\mathbf{U} = \begin{bmatrix} \Delta\mathbf{Y}_v \\ \Delta\mathbf{Y}_b \end{bmatrix} \tag{5.59d}$$

$$\mathbf{P}_T = \begin{bmatrix} \mathbf{0} \\ \hat{\mathbf{P}} \end{bmatrix} \tag{5.59e}$$

5.3.2 Newmark Direct Integration

In the Newmark integration scheme the following assumptions are used (Bathe, 1996):

$$\dot{\mathbf{U}}_{t+\Delta t} = \dot{\mathbf{U}}_t + [(1-\delta)\ddot{\mathbf{U}}_t + \delta\ddot{\mathbf{U}}_{t+\Delta t}]\Delta t \tag{5.60}$$

$$\mathbf{U}_{t+\Delta t} = \mathbf{U}_t + \dot{\mathbf{U}}_t\Delta t + [(\frac{1}{2}-\alpha)\ddot{\mathbf{U}}_t + \alpha\ddot{\mathbf{U}}_{t+\Delta t}]\Delta t^2 \tag{5.61}$$

where $\delta = \frac{1}{2}$ and $\alpha = \frac{1}{4}$ correspond to an unconditionally stable scheme, the constant – average – acceleration method. From Equations 5.60 and 5.61, it gives

$$\Delta\dot{\mathbf{U}} = \dot{\mathbf{U}}_{t+\Delta t} - \dot{\mathbf{U}}_t = (\ddot{\mathbf{U}}_t + \frac{1}{2}\Delta\ddot{\mathbf{U}})\Delta t \tag{5.62}$$

$$\Delta \mathbf{U} = \mathbf{U}_{t+\Delta t} - \mathbf{U}_t = \dot{\mathbf{U}}_t \Delta t + (\frac{1}{2}\ddot{\mathbf{U}}_t + \frac{1}{4}\Delta\ddot{\mathbf{U}})\Delta t^2 \tag{5.63}$$

Solving Equations 5.62 and 5.63, the following expressions are obtained:

$$\Delta\ddot{\mathbf{U}} = \frac{4}{\Delta t^2}\Delta\mathbf{U} - \frac{4}{\Delta t}\dot{\mathbf{U}}_t - 2\ddot{\mathbf{U}}_t \tag{5.64}$$

$$\Delta\dot{\mathbf{U}} = \frac{2}{\Delta t}\Delta\mathbf{U} - 2\dot{\mathbf{U}}_t \tag{5.65}$$

Substitution of Equations 5.64 and 5.65 in Equation 5.58 gives

$$(\frac{4}{\Delta t^2}\mathbf{M}_T + \frac{2}{\Delta t}\mathbf{C}_T + \mathbf{K}_T)\Delta\mathbf{U} = \mathbf{P}_T + \mathbf{M}_T(\frac{4}{\Delta t}\dot{\mathbf{U}}_t + 2\ddot{\mathbf{U}}_t) + \mathbf{C}_T(2\dot{\mathbf{U}}_t) \tag{5.66}$$

Having obtained the incremental displacements from Equation 5.66, the incremental velocity and acceleration can be obtained from Equations 5.64 and 5.65. The displacement, velocity and acceleration at $t + \Delta t$ can also be obtained by

$$\begin{aligned} \mathbf{U}_{t+\Delta t} &= \mathbf{U}_t + \Delta\mathbf{U} \\ \dot{\mathbf{U}}_{t+\Delta t} &= \dot{\mathbf{U}}_t + \Delta\dot{\mathbf{U}} \\ \ddot{\mathbf{U}}_{t+\Delta t} &= \ddot{\mathbf{U}}_t + \Delta\ddot{\mathbf{U}} \end{aligned} \tag{5.67}$$

5.4 Numerical Example of Vehicle

A numerical example of three-axle vehicle is presented in Figure 6.3 corresponding to the vehicle model defined in Figure 5.1. The physical properties of the vehicle were obtained and modified from FWHA test vehicle (Kashif, 1992) to simulate an AASHTO HS20-44 design loading.

The natural frequencies of the truck and the corresponding mode shapes are listed in Table 5.1. It can be noted that the mode shapes are uncoupled for θ_{x1} and θ_{x2}, while the rest are coupled mode shapes.

TABLE 5.1 NATURAL FREQUENCIES AND MODE SHAPES OF THE TRUCK DEFINED IN FIGURE 5.3

Degree of freedom		Mode 1	Mode 2	Mode 3	Mode 4	Mode 5
Mode Shape	d_{z1}	1.00	0	0.78	0.19	0.00
	θ_{x1}	0.00	1.00	0.00	0.00	0.00
	θ_{y1}	-2.74	0.00	1.00	0.60	0.00
	d_{z2}	-1.61	0.00	1.20	1.00	0.00
	θ_{x2}	0.00	0.00	0.00	0.00	1.00
Frequency (Hz)		1.77	2.03	1.98	4.95	6.74

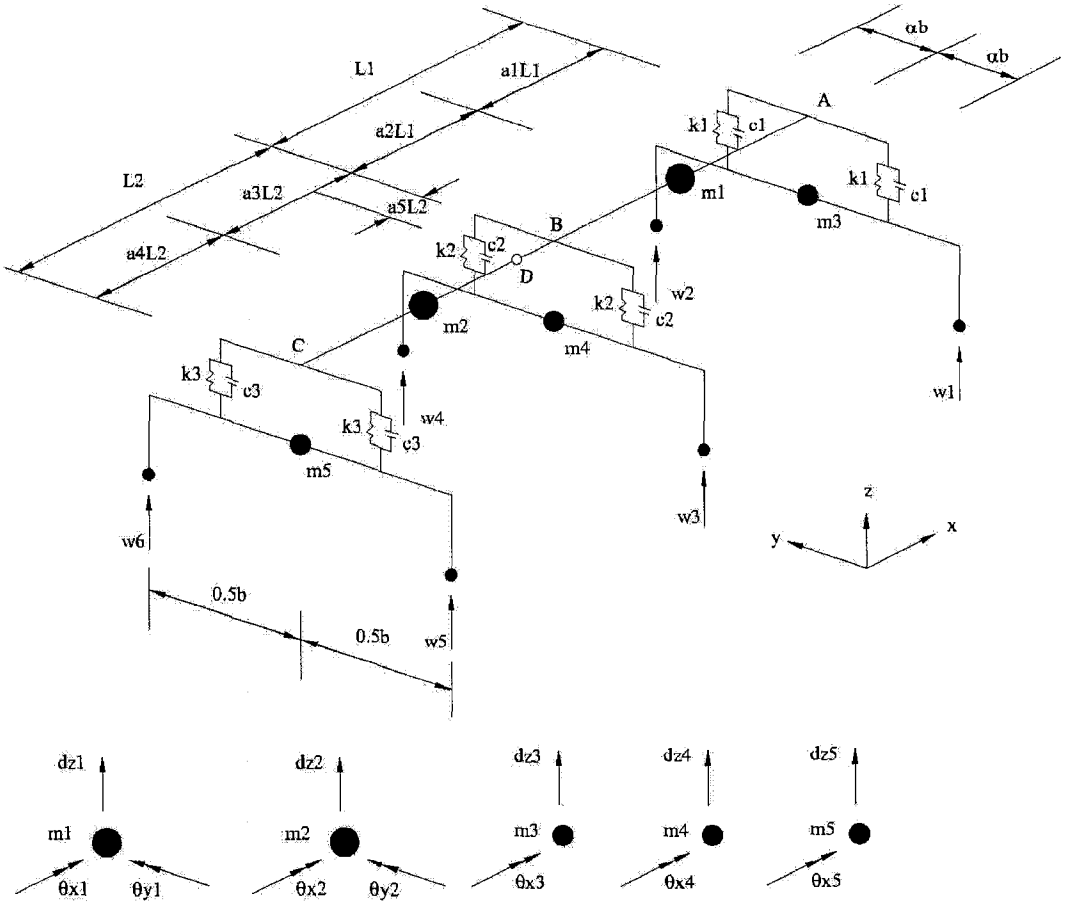

FIGURE 5.1 DYNAMIC MODEL OF THREE – AXLE VEHICLE

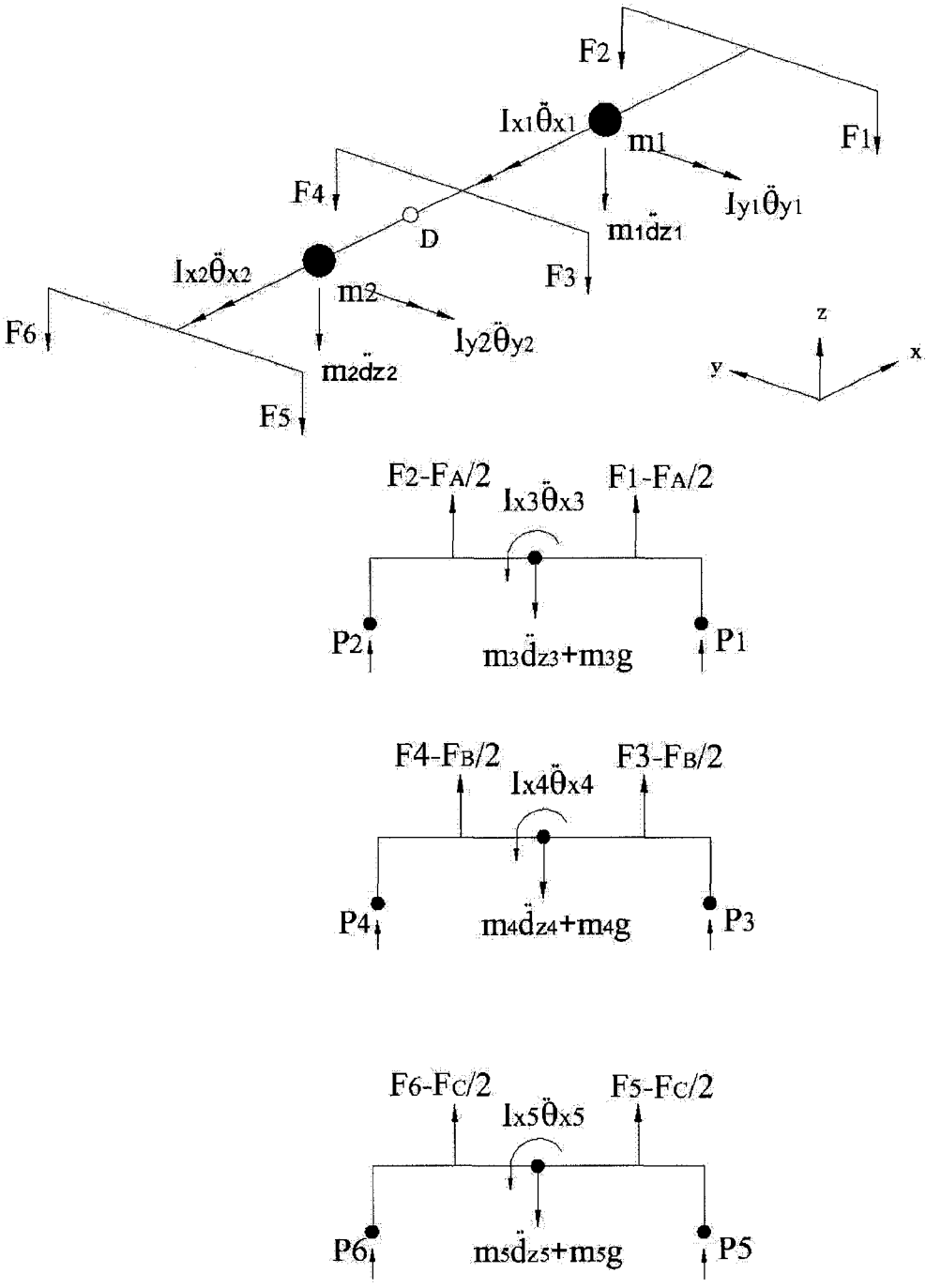

FIGURE 5.2 FREE BODY DIAGRAMS OF THREE-AXLE VEHICLE

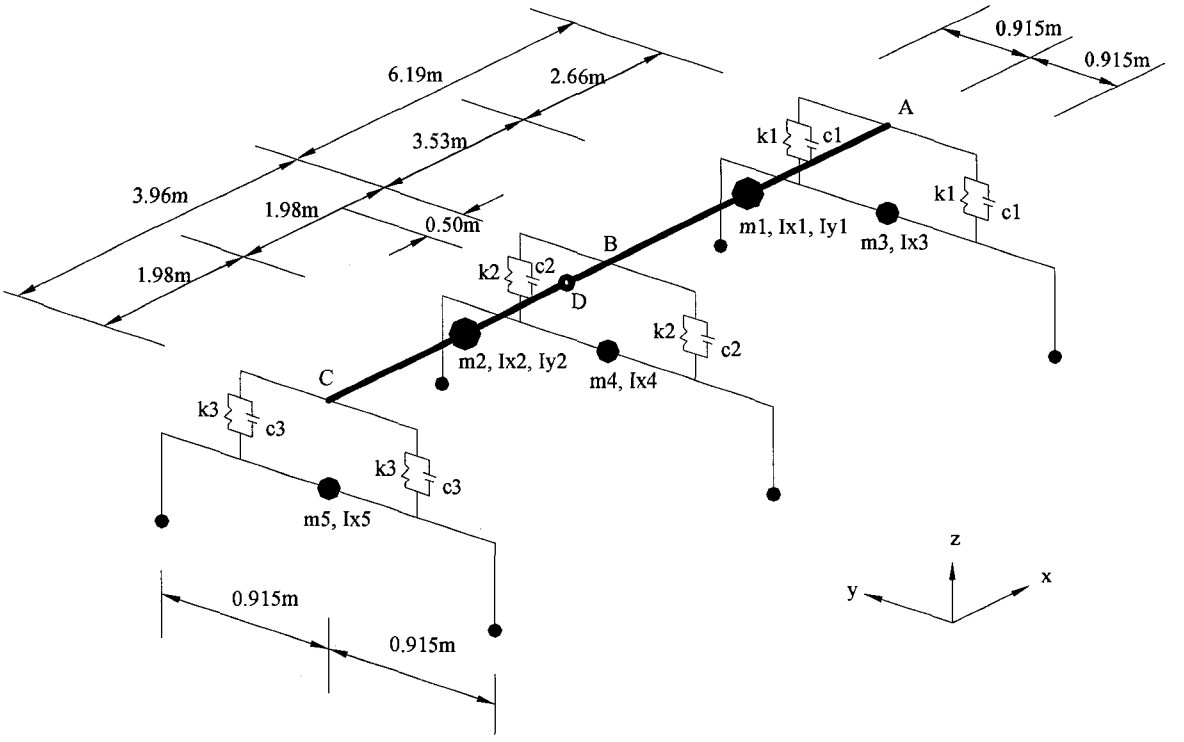

Trailer sprung mass m_1 = 28038kg
Tractor sprung mass m_2 = 2804kg
Trailer rear axle mass m_3 = 1752kg
Trailer front axle mass m_4 = 1402kg
Tractor front axle mass m_5 = 1051kg
Mass moment inertia I_{x1} = 23448 kg.m^2, I_{y1} = 263052 kg.m^2
I_{x2} = 4982 kg.m^2, I_{y2} = 26305 kg.m^2
I_{x3} = 4982 kg.m^2, I_{x4} = 879 kg.m^2, I_{x5} = 879 kg.m^2
Front axle stiffness k_1 = rear axle stiffness k_2 = 1138300 N/m
Tractor axle stiffness k_3 = 1138300 N/m
Viscous damping $c_1 = c_2 = c_3 = 0.0$

FIGURE 5.3 3-AXLE VEHICLE MODEL

Chapter 6

DYNAMIC ANALYSIS OF BOX-GIRDER BRIDGES SUBJECTED TO TRAFFIC LOADING

6.1 Introduction

The purpose of this part of the thesis is to study the dynamic response of a 3D model of box-girder bridges subjected to vehicle loading. The 3-D idealization is adopted for adequate representation of box-girder bridges. Chapter 3 presents the equations and detailed derivation. Confederation Bridge with single cell and super long span has been used in Chapter 3 to study the mode shapes and natural frequencies. The same bridge is also adopted in this chapter for dynamic analysis due to vehicle traverse.

The three-axle vehicle is represented by a sophisticated model with multiple degrees of freedom corresponding to bounce, pitch and roll of the vehicle, which has been described earlier in Chapter 5. The physical properties of the vehicle used in the following parametric study are shown in Figure 5.3.

The equation solver described in Chapter 5 is utilized for solving the nonlinear equations associated with the analysis of the complex bridge-vehicle system. The analysis performed in the present chapter is focused on parametric study of the response of simple span box-girder

bridge including the effect of vehicle. The parameters investigated in this paper are given in the following sections with a brief definition of each of them.

1. Number of vehicles on the bridge and traveling path
2. Traveling speed

   The traveling speed has been varying from 20 km/h to 120 km/h in the study.
3. Vehicle mass
4. Damping ratio of vehicle
5. Impact factor

   The response of bridge and vehicle interaction system can be evaluated by impact factor defined as the ratio of the maximum dynamic response to the maximum static response under moving vehicle. Deflection amplification factor is defined as

$$DI_{\max} = \frac{Peak\ dynamic\ vertical\ deflection}{Peak\ static\ vertical\ deflection}$$

   And longitudinal moment amplification factor is defined as

$$MI_{\max} = \frac{Peak\ dynamic\ longitudinal\ moment}{Peak\ static\ longitudinal\ moment}$$

6.2 Results and Discussion

Different analyses have been carried out using the bridge model of Confederation Bridge with central span of 250 m and total length of 442m. Two diaphragms are located at the cross sections above the piers to avoid distortion modes. Several key parameters have been investigated in this study.

The bridge contains two traffic lanes. Four load patterns representing various number of trucks and traveling path have been considered, including: (1) one truck traveling along the centerline of bridge; (2) one truck traveling along the center of lane; (3) two trucks traveling simultaneously side by side along the center of lanes; and (4) four trucks traveling along the

center of lanes with two trucks tailgating on each lane. Dynamic responses of the bridge, namely mid-span deflections, accelerations and longitudinal moments have been calculated at five locations along the top slab of bridge, which are defined in Figures 6.1(a) through 6.1(d). For comparison purposes, the corresponding static deflections and longitudinal moments due to equivalent truck load have also been calculated.

Numerical results are shown in Figures 6.2 through 6.12 and organized as follows:

1. Figures 6.2 through 6.5: mid-span responses of Confederation Bridge during the passage of truck at traveling speed of 70 km/h subjected to four load patterns.
2. Figures 6.6: dynamic amplification factor of simply supported beam with respect to speed of moving force.
3. Figures 6.7: effect of vehicle speed on mid-span responses of Confederation Bridge subjected to Loads 1 through Load 4
4. Figures 6.8 through 6.10: effect of vehicle mass on mid-span responses of Confederation Bridge subjected to Loads 1 through 3 respectively.
5. Figures 6.11: effect of vehicle damping ratio on mid-span responses of Confederation Bridge under Load 1.
6. Figure 6.12: convergence of deflection results of Confederation Bridge under load pattern 1.

6.2.1 Effect of Load Patterns

The study of the effect of load patterns has been conducted using the bridge model of Confederation Bridge during the passage of trucks at constant traveling speed of 70 km/h. The four load patterns are shown in Figure 6.1. The responses are obtained by moving a single vehicle or multiple vehicles along either the center line of the bridges or the center of the lanes and recording the deflections, bending moments and accelerations along the mid-span cross section from the front wheels loading on till the rear wheels loading off the bridge deck.

Figure 6.2 presents the time histories of mid-span deflections and the transverse distributions of peak deflections subjected to Loads 1 through 4. It can be seen that the maximum deflection are obtained at the location close to the traveling truck for each load pattern. At locations farthest away from the truck, the deflections are the lowest. The mid-span deflection due to bridge-vehicle interaction is larger than that obtained by the equivalent static loads for all four loading cases. The lowest deflections are experienced under Load 2 when one truck traveling along the center of the lane, which is probably because the center of the lane is located closely to the vertical wall of the cell acting as a local support to the top slab and thus resulting in reduced deflection. However, the amplification factor of deflection for Load 2 is larger than that for Load 1. Increasing the number of trucks results in the significant increase of amplification factor. Further inspection indicates that the peak dynamic and static deflection do not occur simultaneously, which is due to the multi-mode contribution. For Confederation Bridge, although longitudinal flexure governs the bridge vibration, it is also coupled with torsional or transverse modes at relatively low frequency range, i.e., between 2 and 3 Hz.

The time histories of mid-span acceleration have been calculated for the five locations indicated in Figure 6.1. Since the accelerations at Locations 2 and 4 are relatively low, only the time histories at Positions 1, 3 and 5 are plotted in Figure 6.3. Three groups of spikes can be visualized from Figures 6.3(a) and 6.3(b), which are associated with impacts as the truck enters the mid-span, leaves the frame and the bridge respectively. Each group has three spikes

representing the impacts induced by the three axles of the truck. Similar observation can be obtained in Figure 6.3(c) since two truck move side by side simultaneously. There are also three groups of spikes presented in Figure 6.3(d) but each group contains six spikes associated with the six axles of the two tailgating trucks. Contrary to the amplification factor, Load 1 produces the largest acceleration and increasing the number of trucks doesn't necessarily increase the acceleration.

In order to better understand the bridge-vehicle interaction, it is important to obtain the frequency contents in the oscillation curves of the acceleration. The time histories of accelerations have been processed using Welch's average modified periodogram method of spectral estimation. The rectangular window was selected to filter the records for easier identification of the modal frequencies. Power spectral density is plotted for frequencies from 0 to 5 Hz and illustrated in Figures 6.4(a) through 6.4(d) for the four load cases respectively.

As can be noted from the curves of power spectral density that there are two ranges of predominant frequencies in the vertical vibrations of the deck, i.e., between 0 and 1 Hz and at 4 Hz. It can be seen from Figures 6.4(a) and 6.4(b) that the predominant frequencies of the vibration at mid-span are about 1Hz with one truck moving along centrally or eccentrically, which is in good agreement with the field test (Naumoski, et. al., 2004). The frequency of 1.0 Hz is identified as the fourth vertical modal frequency of the bridge (see Figure 3.7 and Table 3.4). Figure 6.4(c) shows the power spectral density obtained under Load 3 with two trucks moving side by side. The predominant frequency excited by the trucks is 0.7 Hz which is identified as the third modal frequency of the bridge. Figure 6.4(d) shows the power spectral density excited by Load 4 for four trucks with two trucks tailgating on each lane. The predominant frequency is 0.55 Hz which is consistent with the second modal frequency of the bridge. All the above observation indicates that increasing the number of the trucks results in exciting lower predominant frequency, which brings great concern of bridge safety since the forced frequency is close to the fundamental frequency of the bridge. The results also imply that the position of truck, whether central or eccentric, has little effect on the predominant frequency.

Figure 6.5 presents the amplification factor of longitudinal moment at mid-span. It reveals that the peak *MI* is generally less than the corresponding *DI*. It implies that the amplification magnitude of internal forces is less pronounced than that of deflection due to traffic excitation.

6.2.2 Effect of Traveling Speed

Vehicle speed is an important parameter which affects the dynamic response of bridge. In previous study, the effect of vehicle speed was investigated using a simplest model of a bridge-vehicle system consisting of a beam with a moving force (Humar, 1990; and Humar and Kashif, 1992). Considering that the beam vibrates in its first sinusoidal mode the amplification factor is given by

$$DI(\frac{L}{2},t)=\left[\frac{1}{1-\alpha^2}\sin(\alpha\omega_b t)-\frac{\alpha}{1-\alpha^2}\sin(\omega_b t)\right] \tag{6.1}$$

where

ω_b - the fundamental frequency of the bridge structure, equal to $\pi^2\sqrt{\frac{EI}{\bar{m}L^4}}$;

$\bar{m}$ - the mass of the bridge per unit length;

α - speed parameter, equal to $\frac{\pi v}{\omega_b L}$;

L - length of bridge span;

v - speed of the vehicle.

Equation 6.1 can be rewritten in the form

$$DI(\frac{L}{2},t)=\left[\frac{1}{1-\alpha^2}\sin(2\pi\alpha\frac{t}{T_b})-\frac{\alpha}{1-\alpha^2}\sin(2\pi\frac{t}{T_b})\right] \tag{6.2}$$

and

$$\alpha=\frac{vT_b}{2L} \tag{6.3}$$

where T_b is the fundamental period of the bridge structure. By equating the differential of Equation 6.2 to zero, the maximum deflection occurs when

$$\frac{t}{T_b} = \frac{n}{1+\alpha} \tag{6.4}$$

where n is an integer. In selecting n, t shouldn't exceed the traversing time, L/v. In other words, t/T_b shouldn't exceed $1/(2\alpha)$. By substituting Equation 6.4 to 6.2, the maximum dynamic amplification factor is obtained as

$$DI_{\max} = \frac{1}{1-\alpha}\sin\frac{2\pi n\alpha}{1+\alpha} \tag{6.5}$$

For simply supported beam, the maximum deflection occurs at mid-span. When $t = \frac{L}{2v}$, the value of n is the integer of $\frac{1+\alpha}{4\alpha}$. The parameter DI_{max} has been plotted in terms of α in Figure 6.6.

Effect of vehicle speed and load pattern have been studied in the present study using the bridge model of Confederation Bridge. Various vehicle speeds from 20 km/h to 120 km/h have been involved in the analysis. The corresponding speed parameter α varies from 0.02 to 0.14. Four load patterns representing various number of trucks and traveling path have been considered. The results are presented in Figure 6.7.

The amplification factor of deflection DI_{max} is plotted as a function of vehicle speed and shown in Figure 6.7a. Similar to the curve shown in Figure 6.6, periodically oscillating curves represent DI_{max} – vehicle speed relationship of box-girder bridges. In general, the peak value of DI_{max} tends to increase with the truck speed going up. The dynamic amplification factors due to bridge-vehicle interaction associated with lower vehicle speed are less pronounced than those corresponding to higher vehicle speed. Therefore, it is very important to set speed limit especially for long span bridges. It can identify that in some cases bridge-vehicle interaction reduces the response, while in others it increases the response, and the changes can be significant. However, the moving load model only enhance the dynamic response where the DI_{max} curve in Figure 6.6 is always larger than 1.0. The oscillation period of the curves increases with the increase of vehicle speed. Little difference is observed between the curves for Load 1 and Load 2. The two curves exhibit almost identical period. The peak amplification

factor generally increases with the increase of number of trucks. The period of the oscillation of the curves also increase with more trucks, especially with higher vehicle speed. It emphasizes the importance of interaction between bridge and vehicle.

The MI_{max} values are plotted with respect to varying vehicle speed and illustrated in Figure 6.7(b). It can be noted that the peak value of MI_{max} tends to increase with the increase of truck speed. The peak amplification factor generally increases with the increase of number of trucks. For Load 2, the MI_{max} is always lower than 1.0, which indicates that the bridge-vehicle interaction reduce the moment response of the bridge under off-center loading.

The amplification factor of deflection reaches as high as 1.41 at about 105 km/h. By limiting the vehicle speed at 80 km/h, which is the posted maximum allowed speed on the bridge, the amplification factor is reduced to 1.35. The maximum amplification factor of moment is about 1.27 at 115 km/h. This value agrees with formulation of the AASHTO (1998) LRFD specifications to consider a simple one multiplier equal to 33% applied to the truck model only. The representation of the DLF as a function of span length in AASHTO (1992) (impact factor = 0.13 for Confederation Bridge, see Equation 2.1) or natural frequency in OHBDC (1991) (see Equation 2.2) does not fully address the complexity of bridge-vehicle interaction.

It can be observed from Figure 6.7(c) that the accelerations tend to increase with the increase of truck speed. For all the bridges investigated, load pattern 1 always generates the largest acceleration curve. The difference between the curves under other load patterns is relatively minor.

6.2.3 Effect of Vehicle Mass

The effect of mass ratio has been investigated by analyzing the response of Confederation Bridge under load patterns 1, 2 and 3. Two cases of truck weight, namely Mass1 and Mass 2, have been calculated. Mass 1 uses the exact physical properties shown in Figure 5.3. Mass 2

adopts most of the properties of Figure 6.1 but doubling the truck weight proportionally. The weight of the bridge deck structure is approximately 17.5×10^6 kg. Therefore, the mass ratios for mass1 and mass2 to the weight of bridge superstructure are 0.002 and 0.004 respectively. The results are presented in Figures 6.8 through 6.10 including DI_{max}, MI_{max} and accelerations plotted as functions of truck speed corresponding to mass 1 and mass 2.

By comparing the response curves of the two truck weight cases, two important features have been revealed. First, increasing truck weight can result in significant increase of MI_{max} and acceleration of the bridge. Second, increasing truck weight might either enlarge or reduce the DI_{max} . At higher truck speed, mass 2 tend to produce higher DI_{max} than mass 1. Generally speaking, truck mass does not affect DI_{max} as much as MI_{max} and accelerations in the approaches.

6.2.4 Effect of Vehicle Damping Ratio

The effect of damping ratio has been studied by analyzing the responses of Confederation Bridge when one truck traveling along the centerline of the bridge. The truck model shown in Figure 5.3 has been used in the analysis. Field investigations indicate that the vehicle damping ratio is fairly low. For a 10-ton dump truck the average damping ratio is 2.2% (Humar and Kashif, 1994). Hence, the vehicle damping for the current study is taken from 0.0 to 0.1.

Figure 6.11 displays the effect of vehicle damping on bridge response. DI_{max}, MI_{max} and acceleration are drawn for three levels of vehicle damping ratio from 0.0 to 0.1. It is observed that vehicle damping reduce the response of bridge. The reduction becomes less pronounced with higher vehicle speed. Further more, introduce of vehicle damping does not change the nature of the variation of response with variation of truck speed.

6.2.5 Convergence of Analysis Results

Since the finite element method is a numerical procedure for solving complex engineering problems, important considerations pertain to the accuracy of the analysis results and the convergence of the numerical solution. Some sources of errors that affect the finite element solution results, such as the selection of element type and the number of elements, have been discussed in previous chapters. Modal method described in Chapter 5 has been used for dynamic solutions. The bridge natural frequencies and mode shapes are the governing parameters in this method. Therefore, the number of frequencies and corresponding mode shape selected in the integration is an important element that affects the accuracy and convergence of the results.

The effect of natural frequencies and mode shapes on result convergence has been investigated by analyzing the mid-span deflection of Confederation Bridge under load pattern 1. Different numbers of natural frequencies and mode shapes varying from 100 to 550 are selected for the integration of dynamic equations. The results are plotted in Figure 6.14. It can be seen that the curves are converging with the increase of the number frequencies involved in the integration. It indicates that the bridge vibration due to traffic loads are not only controlled by lower frequencies but also affected significantly by higher frequencies.

6.3 Summary

A series of analytical studies have been conducted on 3-dimensional model of simple span box-girder bridge to determine its forced responses due to traffic loads. The effects of several parameters on the dynamic responses have been investigated. Some conclusions can be drawn as follows.

1. Bridge-vehicle interaction can either increase or reduce bridge responses and the change can be significant. Long-span bridges are more pronounced to interaction than short-span bridges.
2. Increasing vehicle damping reduces the response of bridge but the reduction is not significant, especially for high vehicle speed. Further more, introduce of vehicle damping does not change the nature of the variation of response with variation of truck speed.
3. In general, the dynamic responses of bridge tend to increase with the increase of vehicle speed. The dynamic amplification factors due to bridge-vehicle interaction associated with higher vehicle speed are much more pronounced than lower vehicle speed.
4. The traffic load patterns play an important role in simulating the dynamic responses of box-girder bridges. Eccentric traffic load tends to produce larger amplification factor than central traffic load. Increasing the number of trucks can result in the increase of dynamic response. Distributing the trucks on multiple lanes can reduce the bridge responses.
5. Good agreement is obtained on the frequency contents of the forced vibration induced by traffic load when comparing the results of current study and field measurements.
6. Increasing the number of the trucks results in exciting lower predominant frequency, which brings great concern of bridge safety since the forced frequency is close to the fundamental frequency of the bridge. However the position of truck, whether central or eccentric, has little effect on the predominant frequency.
7. The results in present study agree with formulation of the AASHTO (1998) LRFD specifications to consider a simple one multiplier equal to 33% applied to the truck model only. The representation of the impact factor as a function of span length in AASHTO

(1992) or natural frequency in OHBDC (1991) does not fully address the complexity of bridge-vehicle interaction.

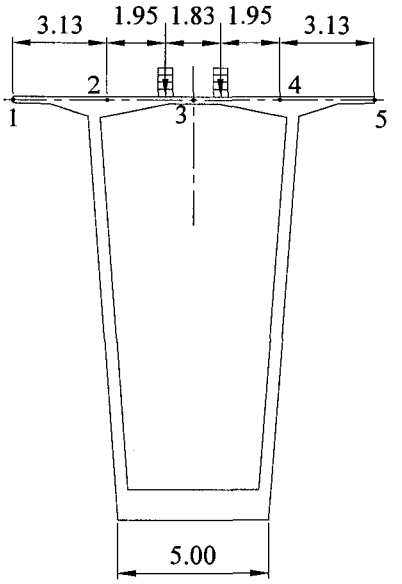

(a) Truck Traveling in the Centerline of the Bridge

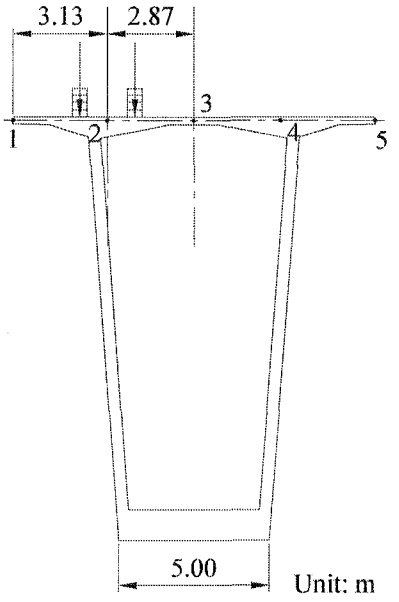

(b) One Truck Traveling in the Center of Lane

FIGURE 6.1 TRANVERSE TRAVELING POSITION OF 3-AXLE VEHICLE ON CONFEDERATION BRIDGE

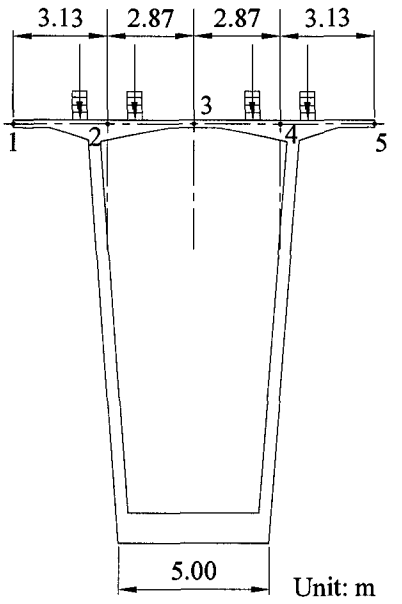

(c) Two Trucks Traveling in the Center of Lanes

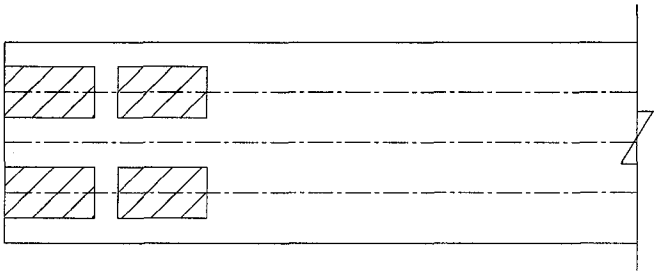

(d) Four Trucks Traveling in the Center of Lanes

FIGURE 6.1 TRANVERSE TRAVELING POSITION OF 3-AXLE VEHICLE ON CONFEDERATION BRIDGE (CONTINUED)

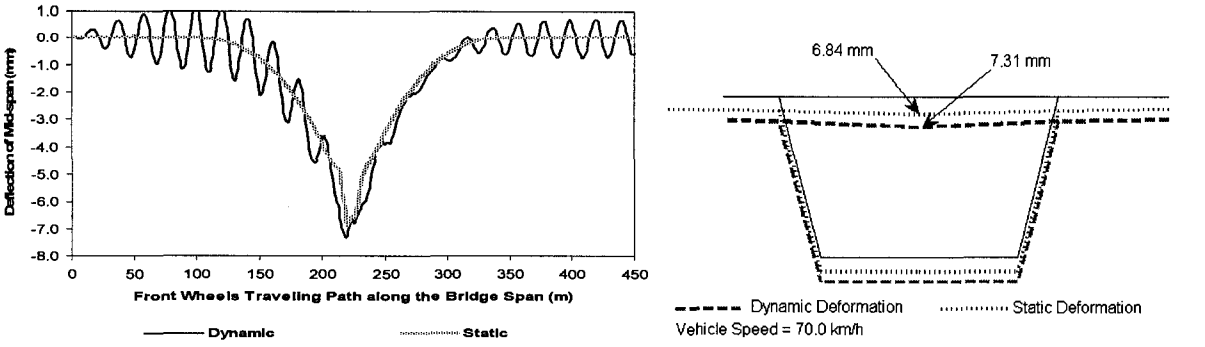

(a) Load 1, $DI = 1.069$

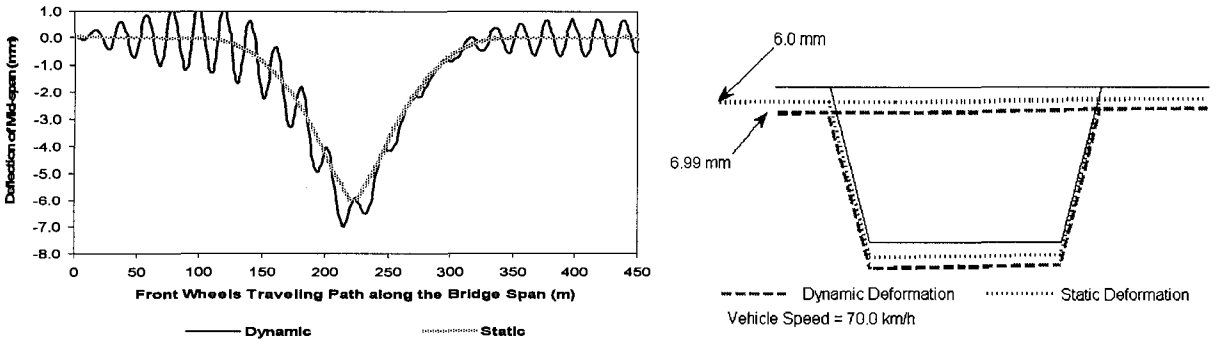

(b) Load 2, $DI = 1.165$

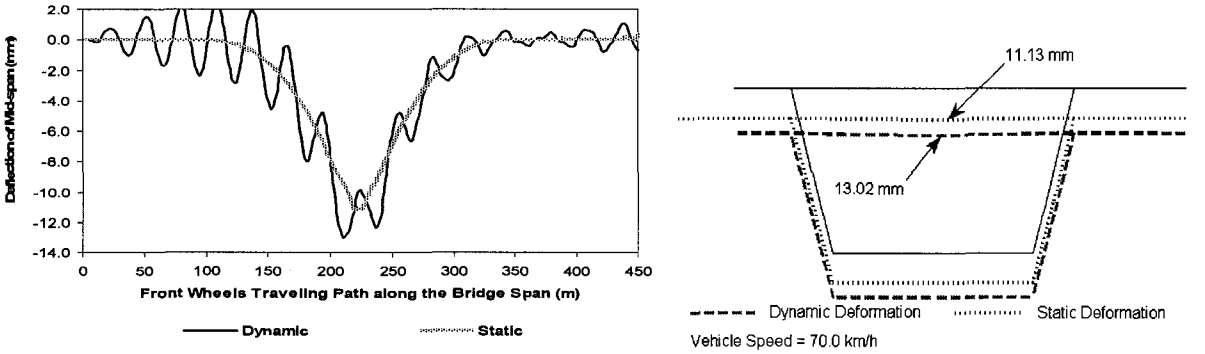

(c) Load 3, $DI = 1.170$

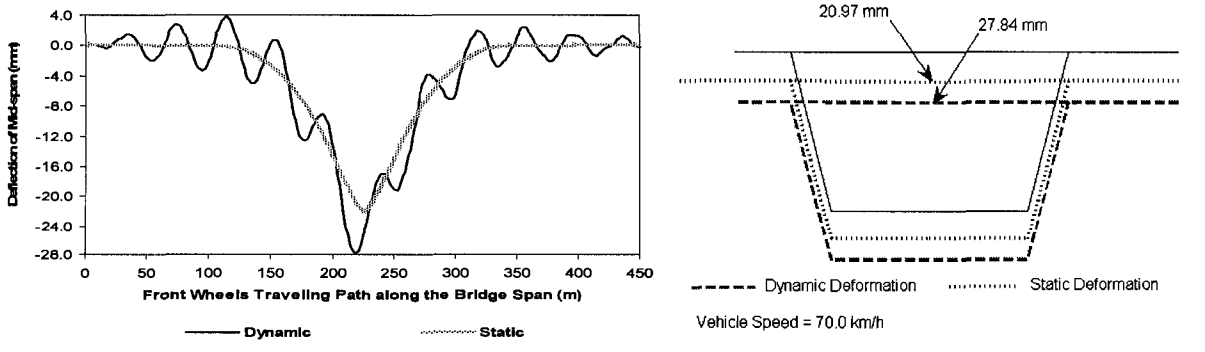

(d) Load 4, $DI = 1.328$

FIGURE 6.2 MID-SPAN DEFLECTION OF CONFEDERATION BRIDGE AT VEHICLE SPEED 70KM/H

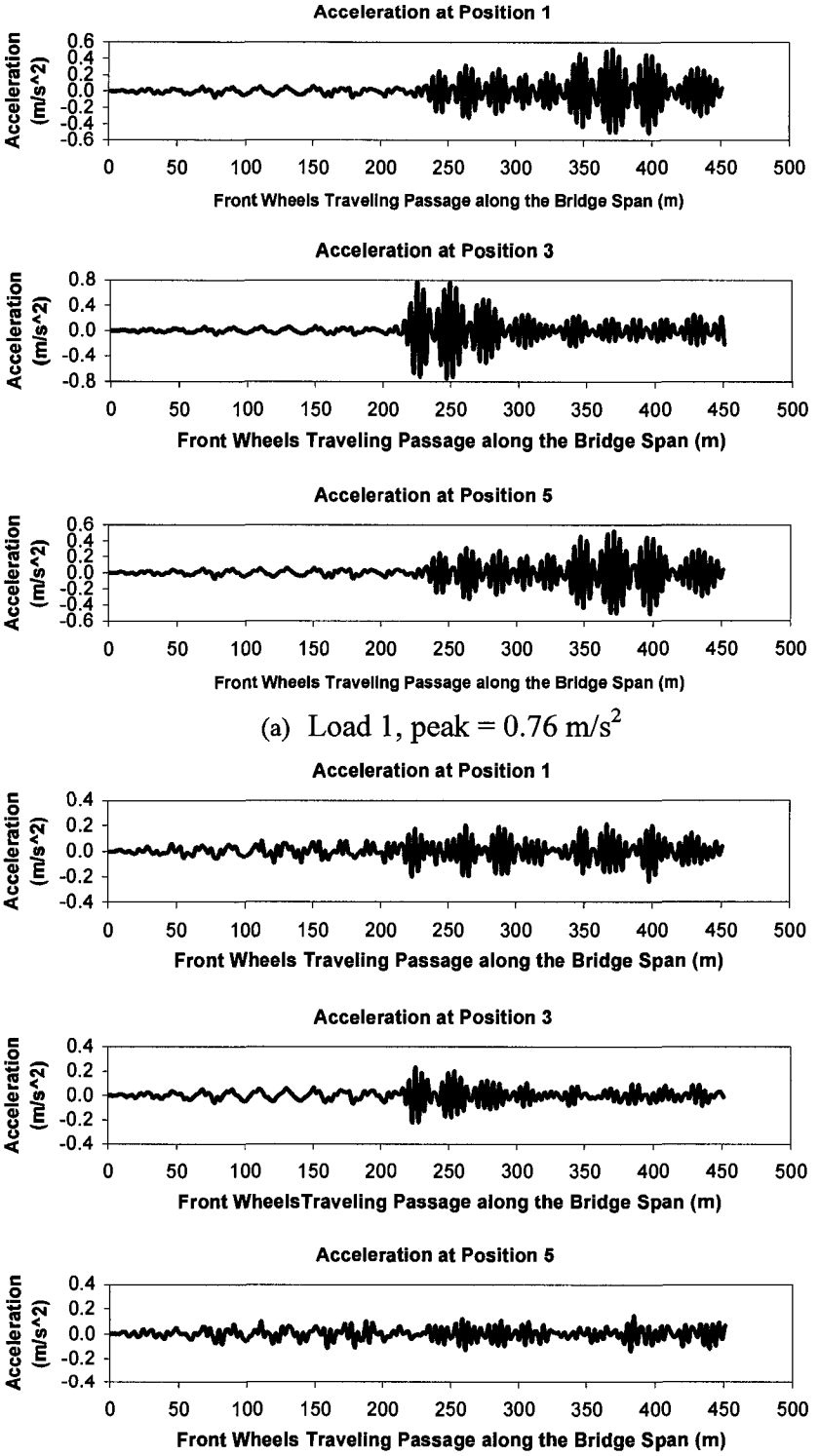

(a) Load 1, peak = 0.76 m/s^2

(b) Load 2, peak = 0.24 m/s^2

FIGURE 6.3 MID-SPAN ACCELERATION OF CONFEDERATION BRIDGE AT VEHICLE SPEED 70KM/H

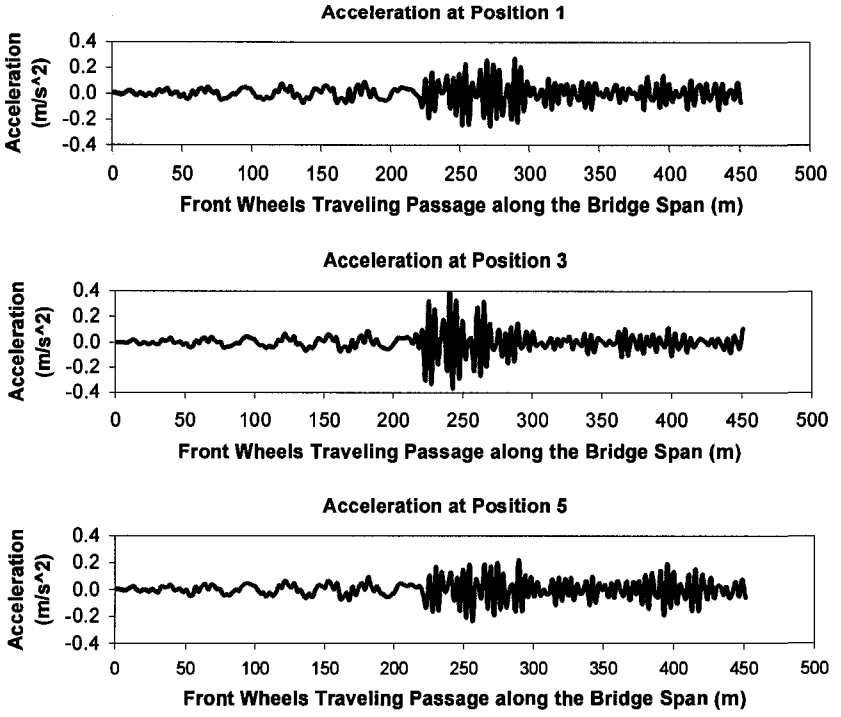

(c) Load 3, peak = 0.41 m/s^2

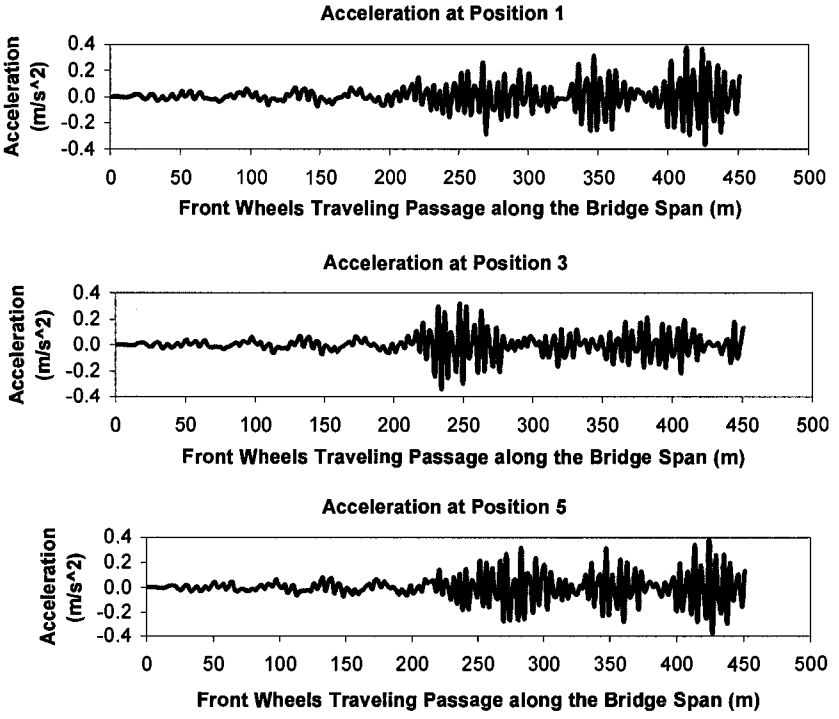

(d) Load 3, peak = 0.39 m/s^2

FIGURE 6.3 MID-SPAN ACCELERATION OF CONFEDERATION BRIDGE AT VEHICLE SPEED 70KM/H (CONTINUED)

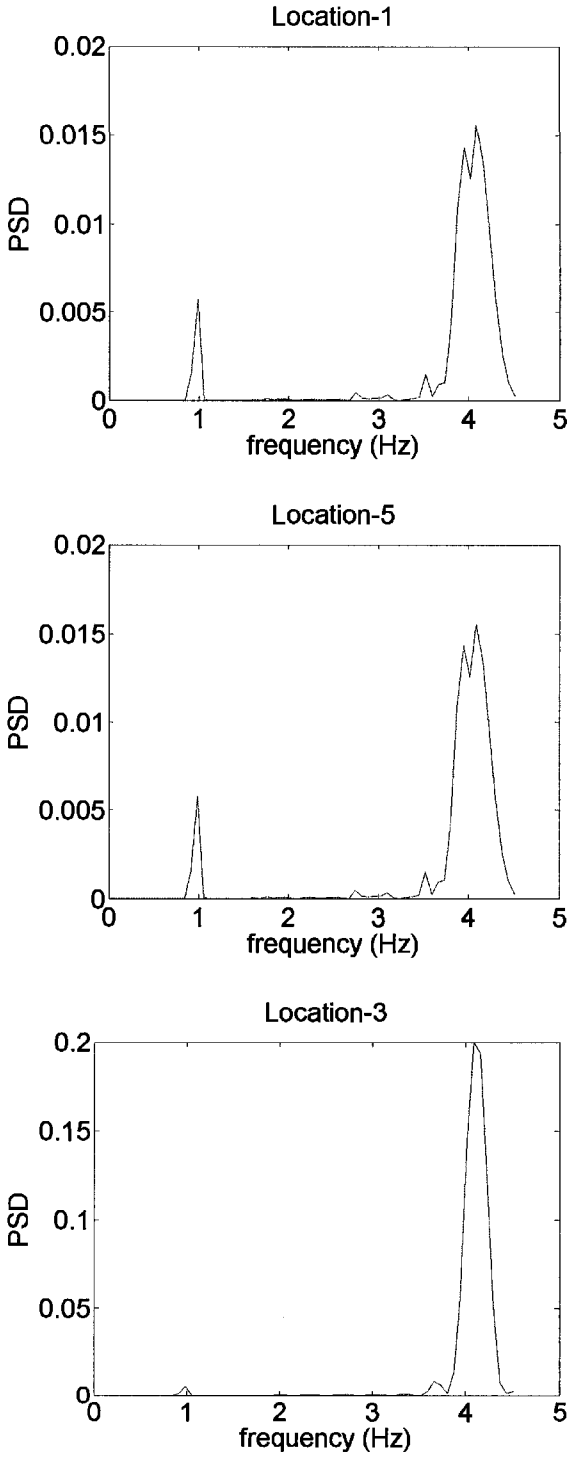

(a) Load 1

FIGURE 6.4 POWER SPECTRAL DENSITY OF ACCELERATION FOR CONFEDERATION BRIDGE AT VEHICLE SPEED 70KM/H

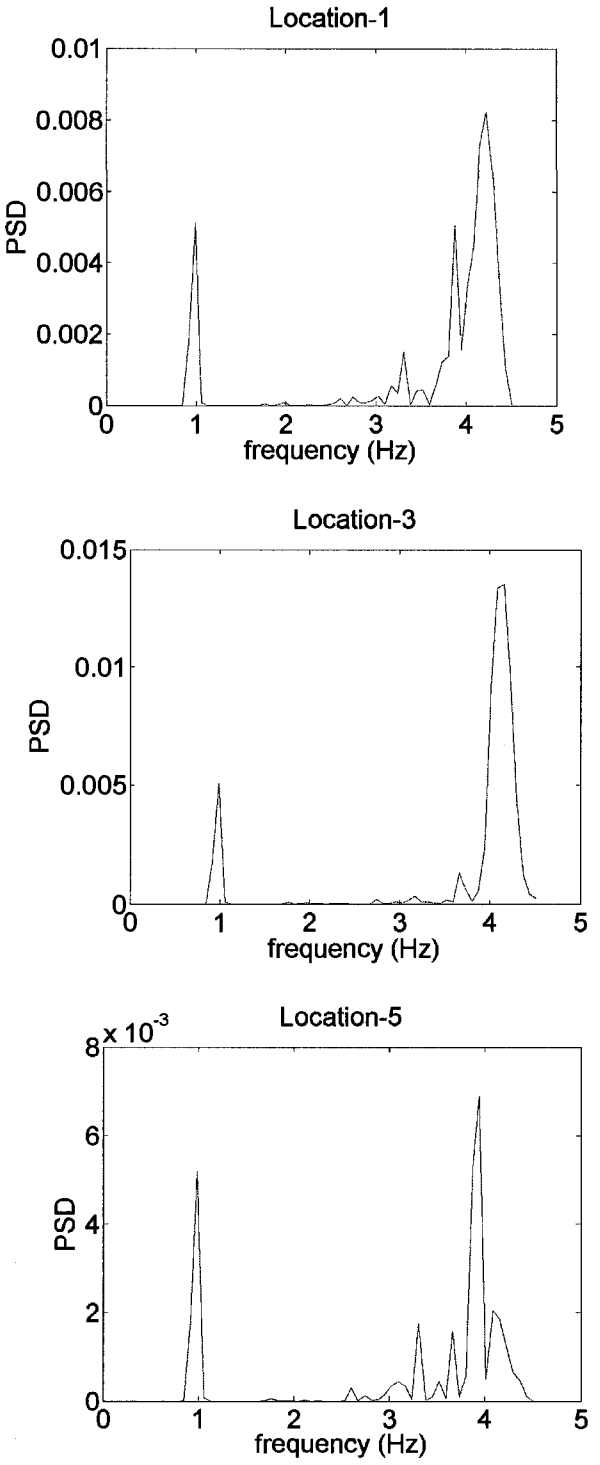

(b) Load 2

FIGURE 6.4 POWER SPECTRAL DENSITY OF ACCELERATION FOR CONFEDERATION BRIDGE AT VEHICLE SPEED 70KM/H (CONTINUED)

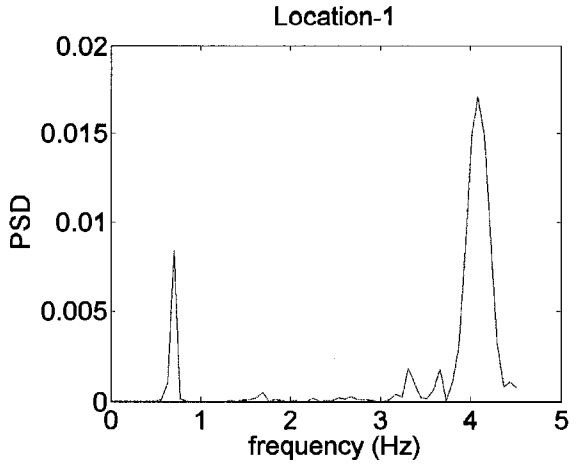

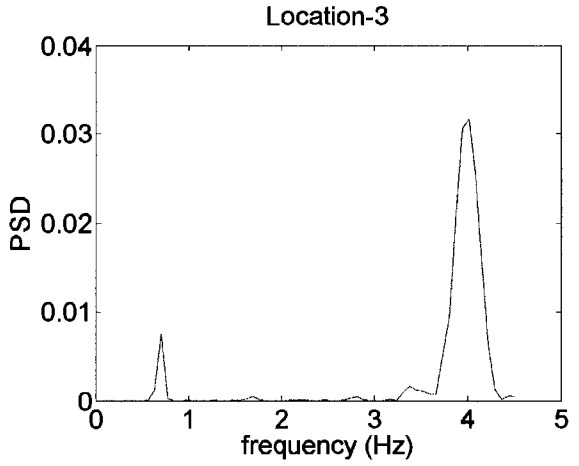

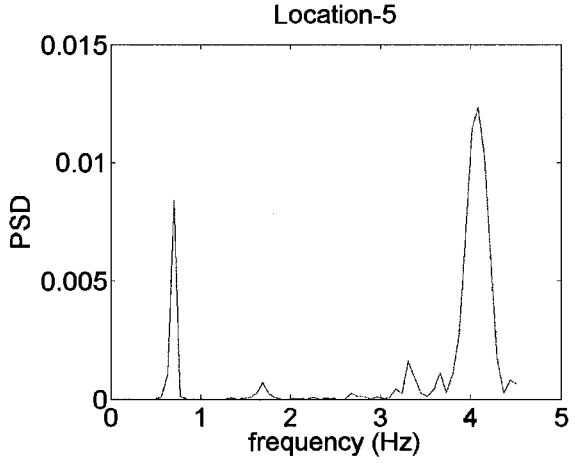

(c) Load 3

FIGURE 6.4 POWER SPECTRAL DENSITY OF ACCELERATION FOR CONFEDERATION BRIDGE AT VEHICLE SPEED 70KM/H (CONTINUED)

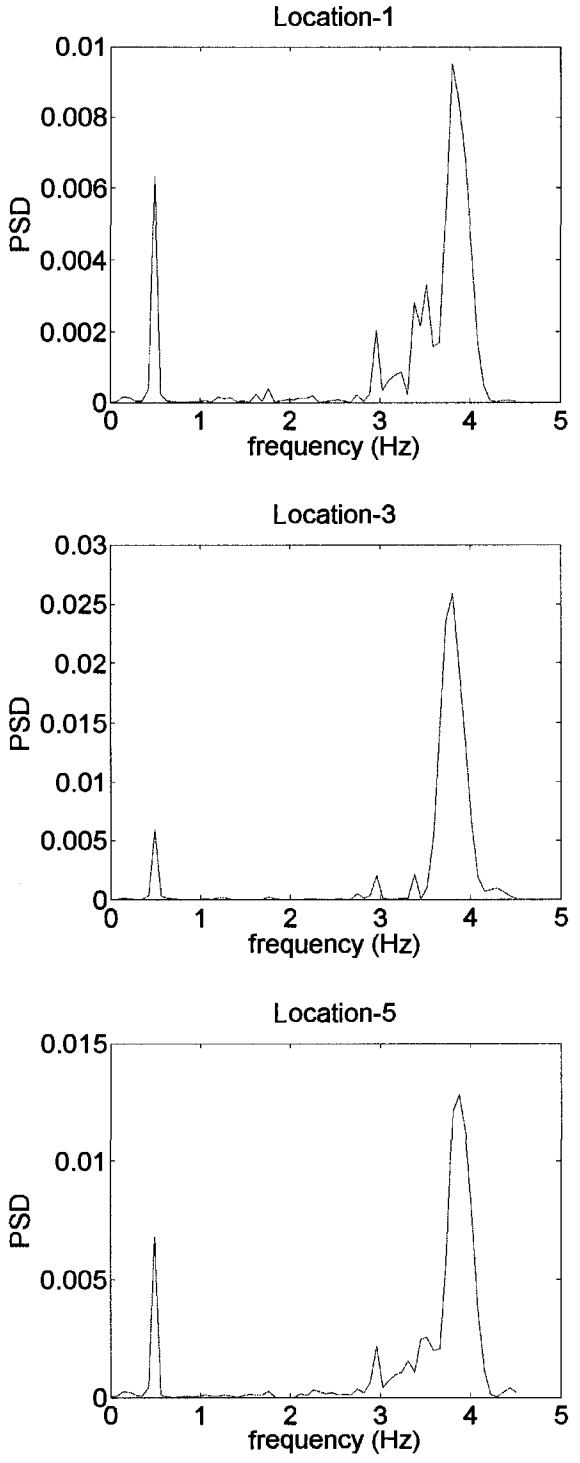

(d) Load 4

FIGURE 6.4 POWER SPECTRAL DENSITY OF ACCELERATION FOR CONFEDERATION BRIDGE AT VEHICLE SPEED 70KM/H (CONTINUED)

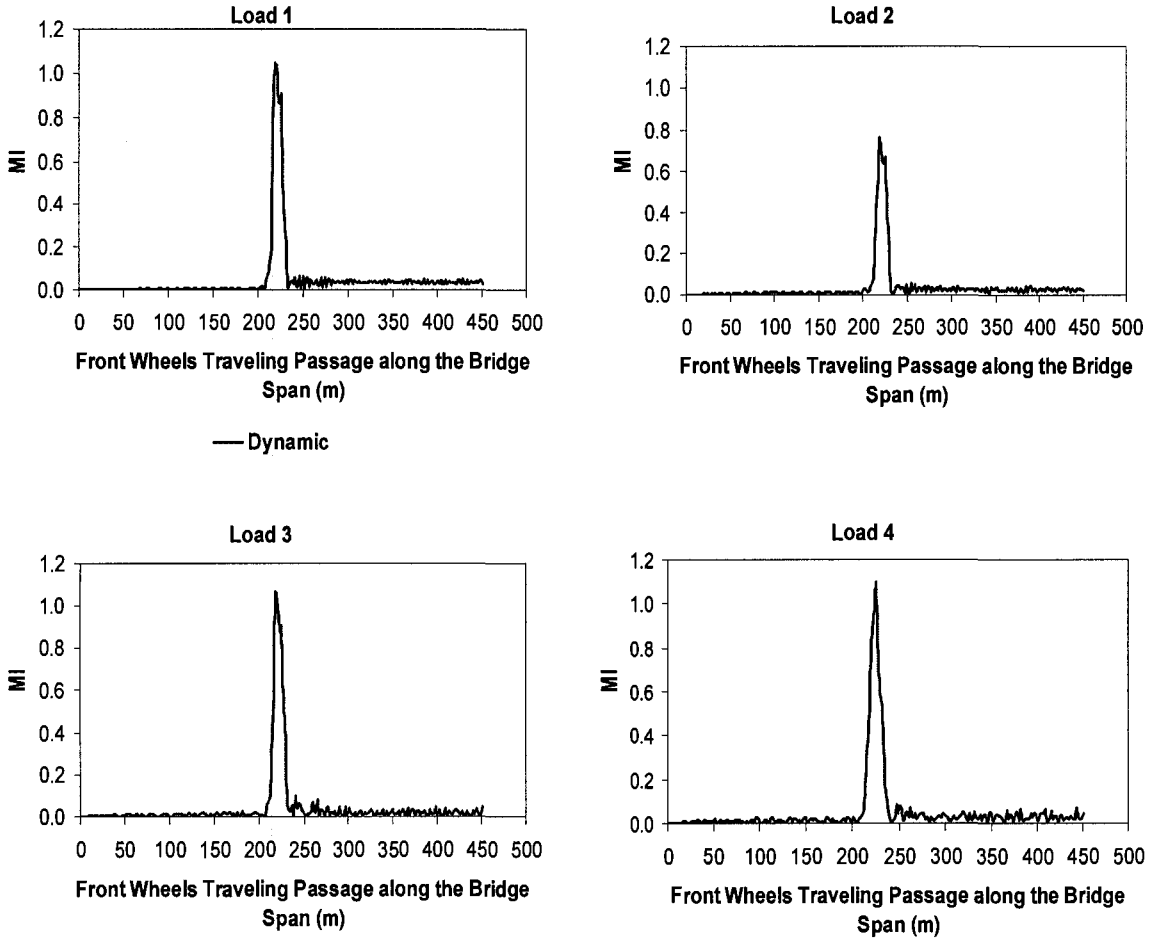

FIGURE 6.5 AMPLIFICATION FACTOR OF MID-SPAN LONGITUDINAL MOMENT FOR CONFEDERATION BRIDGE AT VEHICLE SPEED 70KM/H

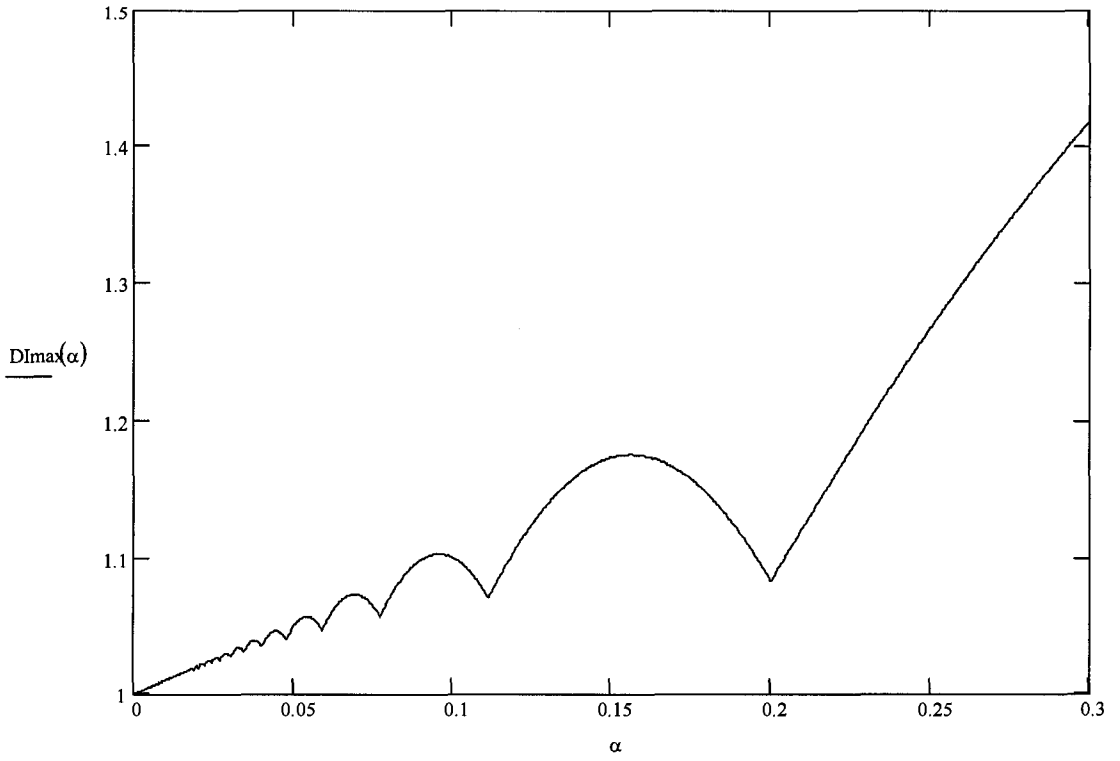

6.6 DYNAMIC AMPLIFICATION FACTOR OF SIMPLY SUPPORTED BEAM WITH RESPECT TO SPEED OF MOVING FORCE

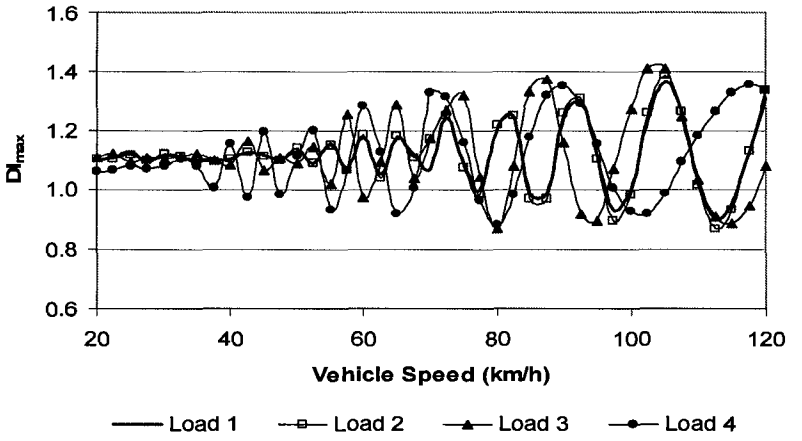

(a) Mid-span Deflection Amplification Factor

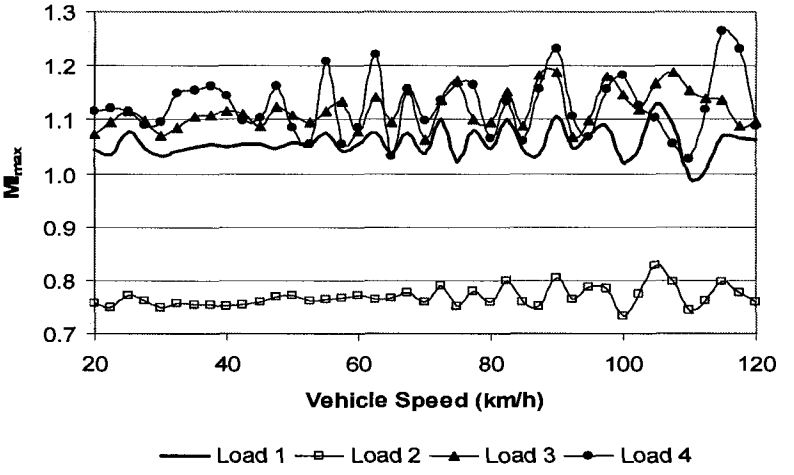

(b) Mid-span Longitudinal Moment Amplification Factor

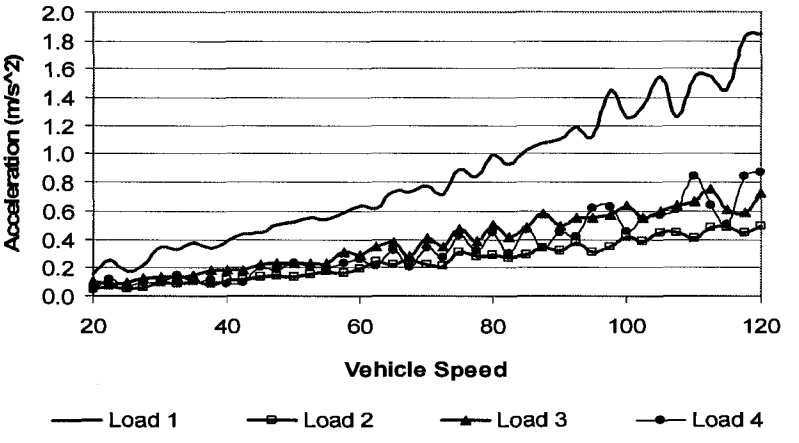

(c) Peak Acceleration of Mid-span

FIGURE 6.7 EFFECT OF VEHICLE SPEED ON MID-SPAN RESPONSES OF CONFEDERATION BRIDGE SUBJECTED TO LOADS 1 THROUGH 4

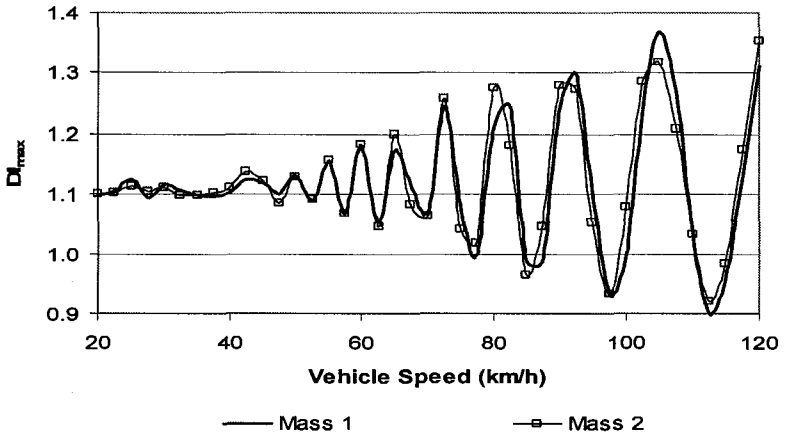

(a) Mid-span Deflection Amplification Factor

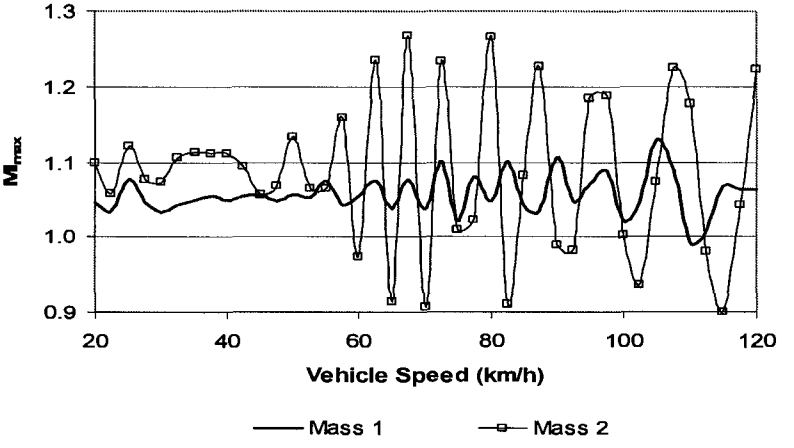

(b) Mid-span Longitudinal Moment Amplification Factor

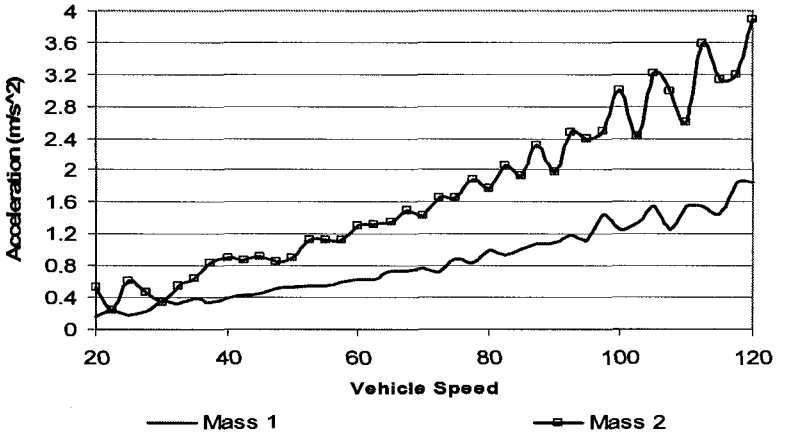

(c) Peak Acceleration of Mid-span

FIGURE 6.8 EFECT OF VEHICLE MASS ON MID-SPAN RESPONSES OF CONFEDERATION BRIDGE SUBJECTED TO LOAD 1

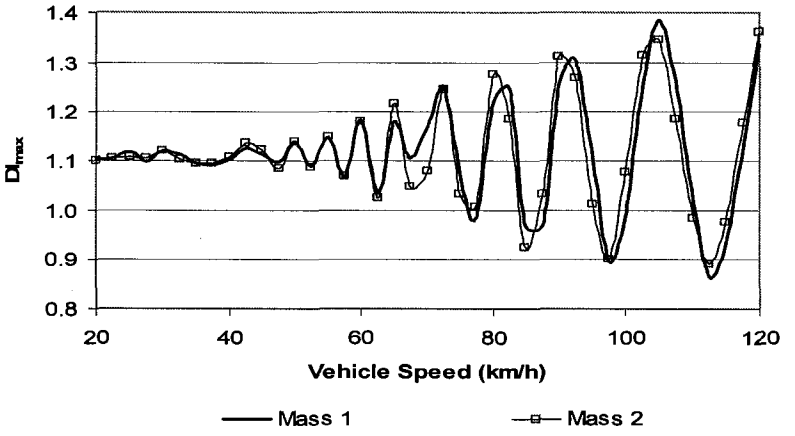

(a) Mid-span Deflection Amplification Factor

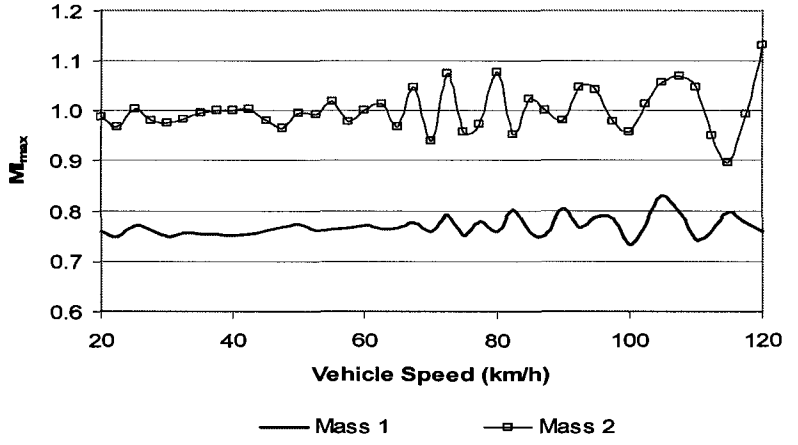

(b) Mid-span Longitudinal Moment Amplification Factor

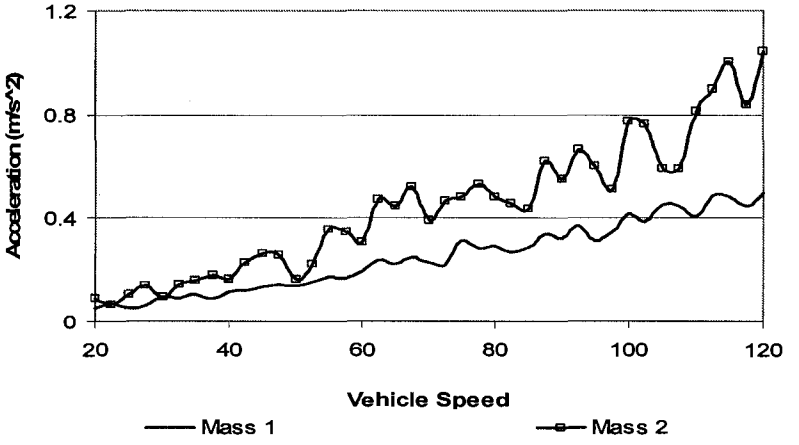

(c) Peak Acceleration of Mid-span

FIGURE 6.9 EFECT OF VEHICLE MASS ON MID-SPAN RESPONSES OF CONFEDERATION BRIDGE SUBJECTED TO LOAD 2

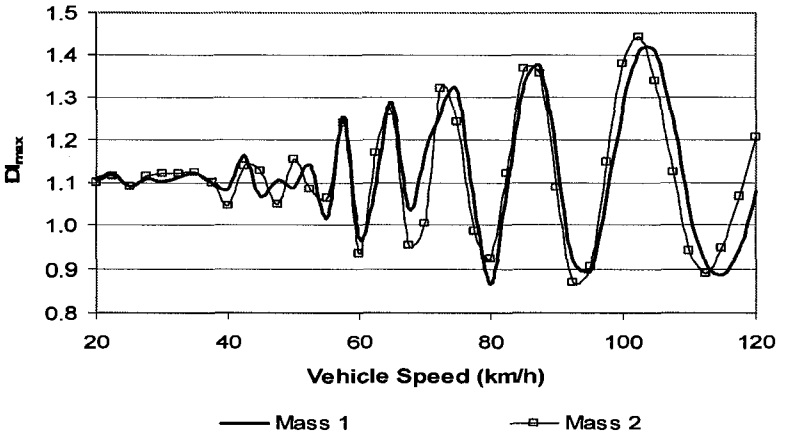

(a) Mid-span Deflection Amplification Factor

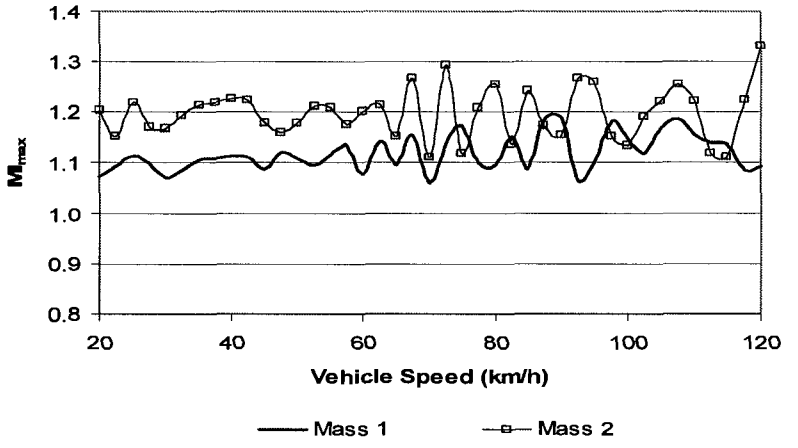

(b) Mid-span Longitudinal Moment Amplification Factor

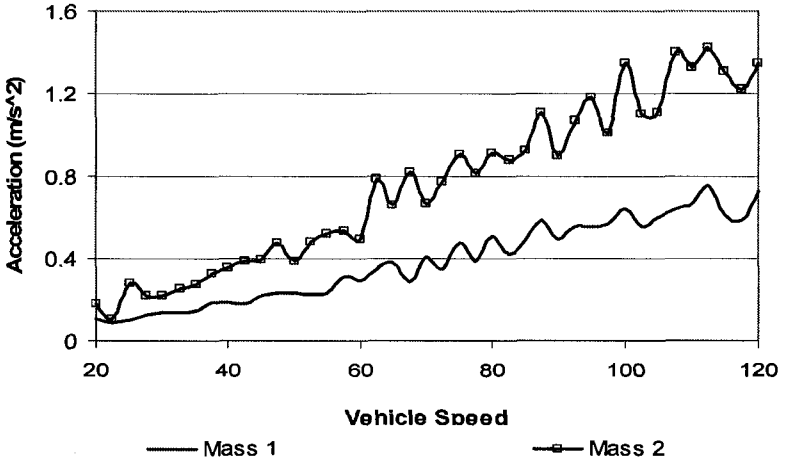

(c) Peak Acceleration of Mid-span

FIGURE 6.10 EFECT OF VEHICLE MASS ON MID-SPAN RESPONSES OF CONFEDERATION BRIDGE SUBJECTED TO LOAD 3

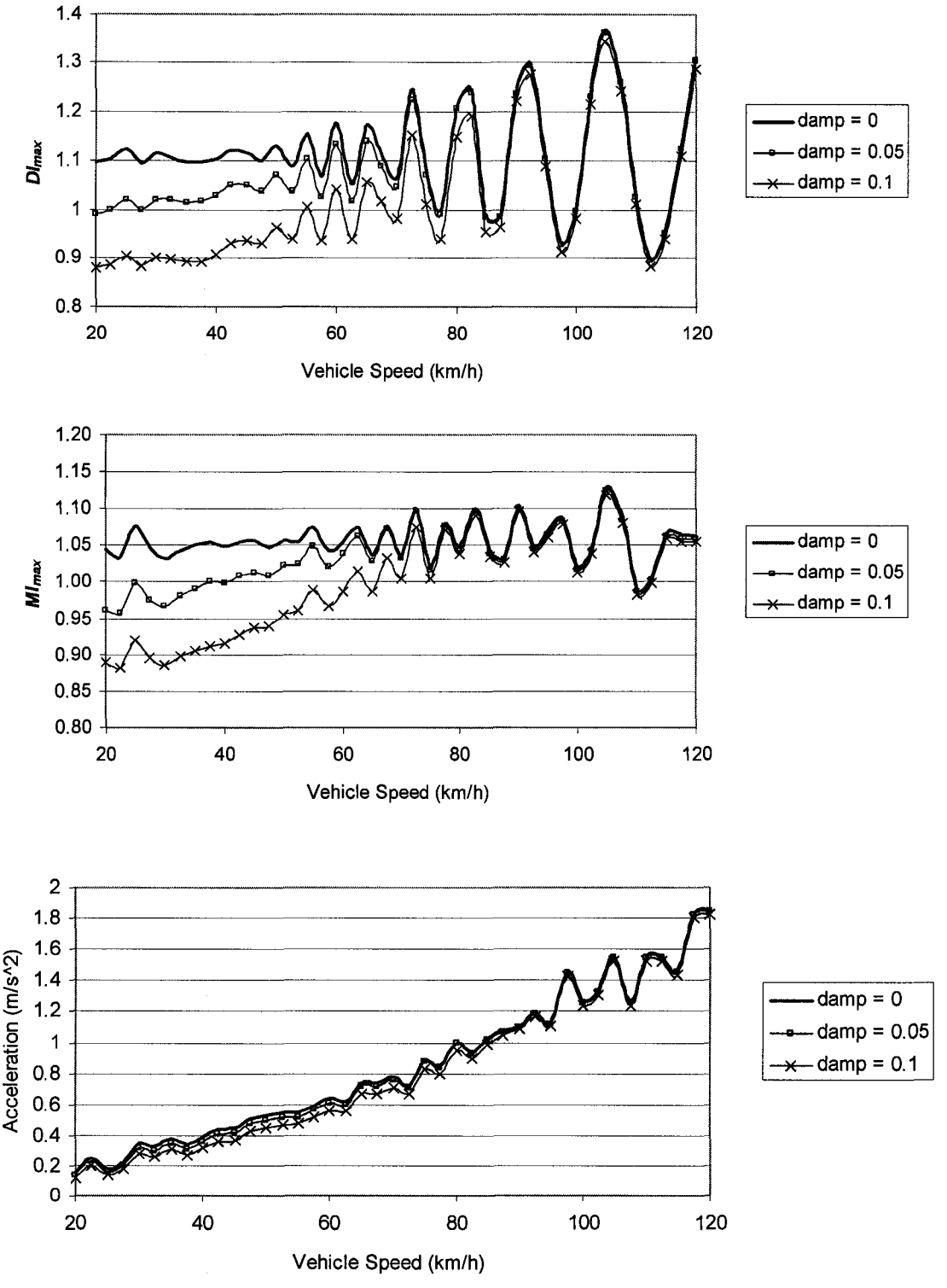

FIGURE 6.11 EFECT OF VEHICLE DAMPING ON MID-SPAN RESPONSES OF CONFEDERATION BRIDGE SUBJECTED TO LOAD 1

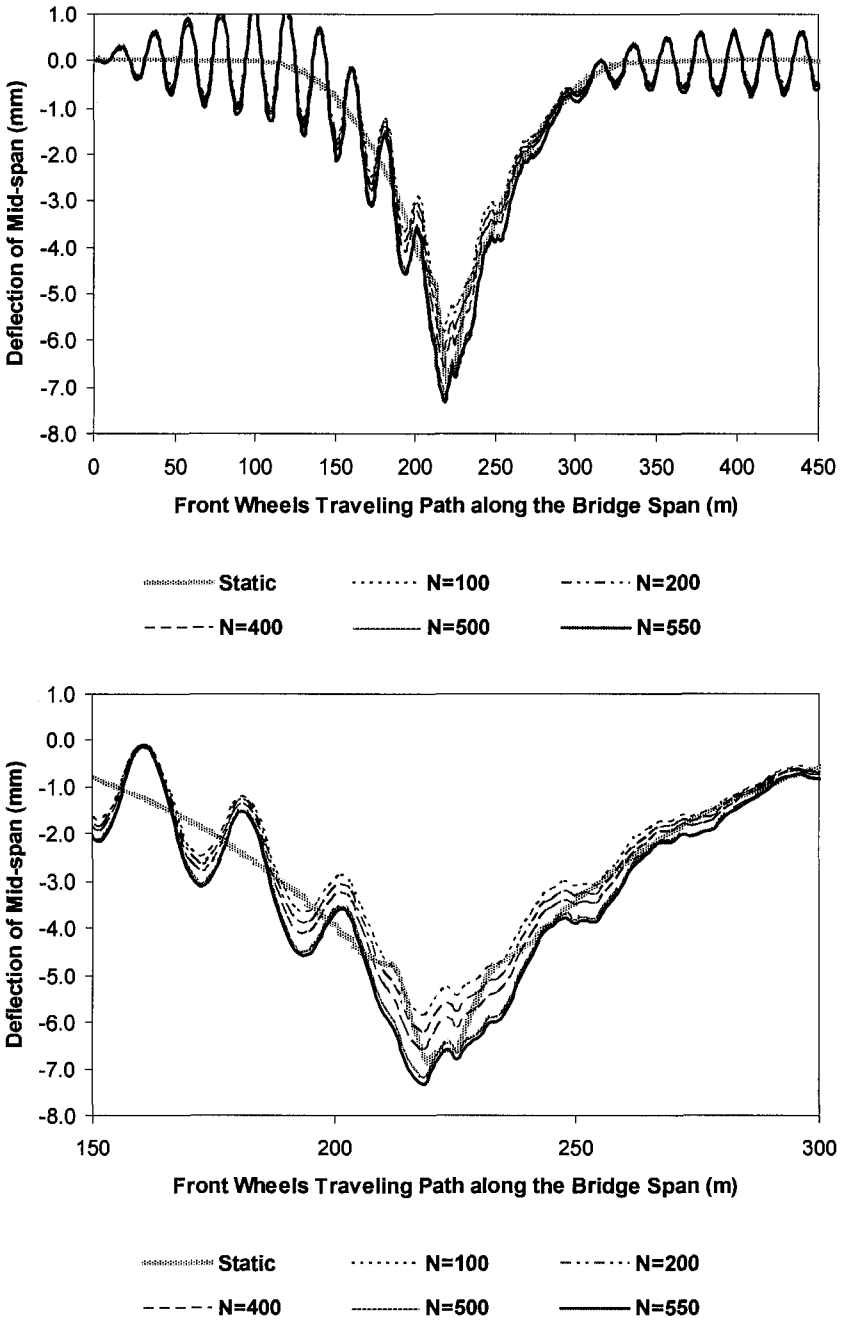

FIGURE 6.12 MID-SPAN DEFLECTIONS OF CONFEDERATION BRIDGE UNDER LOAD 1 CORRESPONDING TO SELECTED NUMBER OF BRIDGE NATURAL FREQUENCIES AND MODE SHAPES

Chapter 7

DYNAMIC ANALYSIS OF CABLE-STAYED BRIDGES SUBJECTED TO TRAFFIC LOADING

7.1 Introduction

Cable-stayed bridges are very important lifetime structures. It is well known that large deflections and vibrations caused by dynamic forces of heavy vehicles can lead to bridge deterioration and eventually increasing maintenance costs and decreasing service life of bridge structure. Nowadays, very long-span slender cable-stayed bridges are being built, however, little is known about their dynamic behavior under the action of moving vehicles. The dynamic responses of bridges subjected to traffic loads are complicated because the dynamic effect induced by moving vehicles is basically influenced by the interaction between the bridge and the moving vehicle. The bridge-vehicle interaction is affected by many factors, such as vehicle speed, road roughness, damping of bridge and vehicle, dynamic characteristics of bridge, and etc.

In this part of the thesis, the dynamic responses of 3D model of cable-stayed box-girder bridges subjected to vehicle loading are studied. Nonlinear geometric effects, exact cable behavior and bridge damping are considered. Because of the non-separable nature of the parameters, it might be difficult to isolate any single parameter to investigate its effect on the behavior of the bridge.

However it is also impossible to incorporate the effect of all parameters at one time. Thus, parametric study is necessary because it gives the idea of the effect of the various parameters on forces and displacements in cable-stayed bridges. The present study focuses on the following aspects that influence the bridge responses:

1. Number of vehicles on the bridge and traveling path
2. Effect of diaphragms at bridge deck
3. Traveling speed of vehicle
4. Damping ratio of bridge
5. The mass of vehicle
6. Types of cable arrangement – fan-type and harp-type

7.2 Numerical Examples and Discussion

7.2.1 Finite Element Modeling

Two models of cable-stayed box-girder bridge, referred as Model 1 (fan layout) and Model 2 (harp layout) shown in Figures 7.1a and 7.1b have been adopted for this investigation. The two models have the same physical properties listed in Table 4.1, except for their cable arrangement. The bridge models have one main span between the reinforced concrete pylons and two side spans with total length of 627.8 m. The bridge deck with total width of 23.5 m is divided into four traffic lanes. Steel box-girders with four cells are adopted for the bridge deck. Two basic solid plate diaphragms are placed at both ends of the bridge within the box cells. Each model has two stayed cable planes parallel to each other with either fan-type (Model 1) or harp-type (Model 2) configuration. There are 24 pairs of stayed cables laying out from each side of the pylon. The spacing between two adjacent points of attachment of the cables on the box-girder is typically 6.1 m.

Finite element method has been used to model the bridge structure. The bridge deck has been modeled as 8-node shell elements and is assumed to be pinned at the ends and elastically connected to the pylons by vertical links. The pylons are modeled as beam elements and are assumed to be rigidly fixed to the piers. The cables are modeled as catenary cable elements and are assumed fixed to the pylons and to the deck at their joints of attachment.

The vehicle is modeled as three-axle truck with multiple degrees of freedom corresponding to bounce, pitch and roll of the vehicle, which has been described earlier in Chapter 5. The physical properties of the vehicle shown in Figure 5.3 are used in the analysis. Six load cases, shown in Figure 7.2, representing various number of vehicles and traffic path are considered in the analyses.

The Traffic loading module of the program GLBA is employed to perform the dynamic analysis of bridge-vehicle interaction. The algorithm of this part of program has been described in details in Chapter 5. All the responses of the bridges subjected traffic load are based on the equilibrium conditions under dead load which have been analyzed and discussed in Chapter 4. The dynamic responses are calculated by using the bridge-vehicle interaction equations derived in Chapter 5, while the static deflections and forces are calculated by assuming the truck weight as static forces acting on the bridge deck through the wheels.

7.2.2 List of Numerical Results

Parametric studies have been carried out on the dynamic responses of cable-stayed bridges. All the responses of the bridges subjected to traffic loading are based on the equilibrium conditions under dead load. The results are evaluated by: i) vertical deflection of mid-span; ii) mid-span acceleration; iii) mid-span longitudinal bending moment; iv) cable tension; and v) amplification factors (the ratio of the maximum dynamic response to the maximum equivalent static response under moving vehicles). Numerical results are shown in Figures 7.3 through 7.8 and organized as follows:

1. Figures 7.3(a) through 7.3(g): effect of traffic load patterns on dynamic responses of Model 1;
2. Figures 7.4(a) through 7.4(g): effect of diaphragms on dynamic responses of Model 1;
3. Figures 7.5(a) through 7.5(g): effect of bridge damping on dynamic responses of Model 1;
4. Figures 7.6(a) through 7.6(d): effect of vehicle speed on dynamic responses of Model 1;
5. Figures 7.7(a) through 7.7(e): effect of vehicle-bridge mass ratio on dynamic responses of Model 1;
6. Figures 7.8(a) through 7.8(e): effect of cable arrangement on dynamic responses of Model 1 and Model 2.

7.2.3 Effect of Traffic Load Patterns

The effect of traffic load patterns has been studied by analyzing the responses of Model 1 with five diaphragms at ends of the bridge, at mid-span and at the pylons within the box-girder. The damping ratio of the bridge was assumed to be 0.02. Six load cases shown in Figure 7.2 have been considered including various number of vehicles and vehicle traveling path. The bridge model was then subjected to one to eight trucks moving from the left to the right on a smooth road surface at the constant speed of 80 km/h. The results are presented in Figures 7.3(a) through 7.3(j).

Figure 7.3(a) shows the time history of mid-span deflection subjected to traffic loading only. Both dynamic and static normalized deflections are plotted as the truck (or trucks) moving along the bridge span. The dynamic amplification factors of deflections *DI* (the ratio of the absolute dynamic deflection to the absolute maximum static deflection) have also been calculated and are shown in Figure 7.3(b). It can be seen that the peak deflections occur when the trucks are close to the middle of the bridge span. In all the load cases, the peak dynamic deflections are larger than the peak static deflections. As expected, increasing the number of trucks on the bridge results in the increase of the peak deflection at mid-span. Eccentric traffic

loads produce larger deflection than central traffic loads. From Figure 7.3(b), it can be noticed that the dynamic amplification factor *DI* can be significantly increased by increasing the number of trucks, i.e. load 3 versus load 4. Comparing the results of load 4, load 5 and load 6, where eight trucks are involved in each case, it has been found that the peak deflection significantly decreases when the trucks distributing on multiple lanes (i.e. load 4), however the change in *DI* is not pronounced.

Figure 7.3(c) shows the time history of mid-span acceleration subjected to Load 1 through Load 6 respectively. It can be visualized that the records has high frequency content after the front wheels of the first truck passing 150 m. Load 1 with one truck moving along the center of the bridge gives the lowest peak acceleration of 0.048 m/s^2, while Load 6 with eight trucks moving along the outer lane of the bridge gives the highest peak acceleration of 0.248 m/s^2. The accelerations of load 2, 3, 4 and 5 fall in between.

Figure 7.3(d) presents power spectral density of mid-span acceleration corresponding to the time histories shown in Figure 7.3(c). The time histories have been processed using Welch's average modified periodogram method of spectral estimation. The rectangular window was selected to filter the records for easier identification of the modal frequencies. The power spectral density is plotted for frequencies from 0 to 6 Hz, which is the range of interest in this study. The six spectral curves correspond to the six load cases. Figure 7.3(d) shows two ranges of predominant frequencies in the vertical vibrations of the deck, i.e., between 0 and 1 Hz and between 2 and 5 Hz. For frequencies below 1 Hz, the spectral curves have similar shape which is characterized with three peaks. Since the response consists of modal vibrations, the spectral peaks are associated with the predominant modes of the bridge, where the frequencies of the 1^{st}, 2^{nd} and 3^{rd} vertical modes of the bridge are 0.33, 0.44 and 0.57 Hz. The frequency components between 2 and 5 Hz correspond essentially to higher modes of the bridge. Further examination of Figure 7.3(d) shows that higher frequency range dominants the maximum responses of Loads 1 through 4, while lower frequency range governs the responses of Loads 5 and 6. Furthermore, increasing the number of trucks generally results in response peaks occurring at lower frequencies. It can therefore be concluded that the increase of number of

trucks and eccentric loading path will trigger low frequency vibration, which is more significant to bridge safety since it is close to the fundamental frequency of the bridge.

Figure 7.3(e) displays the time history of normalized cable tension of Cable #12, the longest cable, at the connection of pylon. The normalization is done by dividing the cable tension caused by traffic load only by the cable tension caused by dead load. Both dynamic and static cable tension are plotted. The dynamic cable tension is larger than static tension for all the load cases. The dynamic cable tension under load 1 is only 1.2% of the cable tension under dead load, while the cable tension under load 6 is as high as 19%. It appears that eccentric loads cause much higher cable tension than central or evenly distributed loads. On comparing the results under load 3 and load 4, in which the distribution patterns of the trucks are similar but load 4 has twice number of trucks as load 3, it can be noticed that the static tension under load 4 is twice as much as that under load 3, while the dynamic tension under load 4 is almost three time as much as that under load 3. It is believed that this difference in response occurs as the result of bridge-vehicle interaction and the nonlinear behavior of cable-stayed bridge.

The amplification factor of cable tension, which is defined as the dynamic cable tension divided by the maximum static cable tension, is shown in Figure 7.3(f). The distribution of cable tension amplification factor is in general similar to that of deflection, but is more peaked. The peak amplification factor of cable tension increases tremendously when increasing the total number of trucks. However, only slight change can be found by changing the path of truck when the total number of truck remains the same.

The amplification factor of mid-span longitudinal bending moment MI, which is defined as the ratio of the dynamic bending moment to the maximum static bending moment, is displayed in Figure 7.3(g). It can be seen that the amplification factor associate with eccentric traffic load is larger than that with central traffic load. The peak moment at mid-span occurs when the trucks pass through the mid-span, and then mid-span vibration continues due to bridge-vehicle interaction but with much less magnitude. It is interesting to be noted that there is post-peak oscillation for all the cases and the post-peak oscillation appears most significant under Load 5 and Load 6. It implies that the vehicle-bridge interaction still trigger significant vibration at

mid-span even if the trucks are far away from that point. It is believed that the post-peak oscillation is associated with the low frequency range of the bridge. The excitation triggered by Load 5 and Load 6 exhibits higher energy than other cases (see Figure 7.3(d)).

7.2.4 Effect of Diaphragms

The main purpose of providing diaphragms within the bridge deck boxes is to increase the torsional resistance of the bridge. As in Chapter 4, the effect of diaphragms is studied for the following diaphragm locations with Model 1:

- Diaphragms at each end of the bridge within the box-girder;
- Diaphragms at ends, at mid-span and at the pylons within the box-girder.

The bridge is assumed to have damping ratio of 0.02 subjected to two load cases – load 4 and load 5. The trucks are assumed to be moving at a constant speed of 80 km/h.

Figure 7.4(a) shows the dynamic vertical deflection of mid-span bridge deck. As can be noticed, the deflection of the bridge deck is reduced by approximately 20% for both load cases due to the presence of extra diaphragms. Further examination of Figure 7.4(a) indicates that the effect of diaphragms is more pronounced when bridge is subjected to eccentric traffic load.

Figure 7.4(b) shows the deflection amplification factors. It can be noted that the bridge with diaphragms located at mid-span, at ends and at pylons exhibits higher amplification factor than those observed in the bridge with diaphragms only at ends.

Figure 7.4(c) shows the time histories of mid-span accelerations for Bridge 1 with two diaphragms only. Comparison between Figure 7.3(c) and Figure 7.4(c) corresponding to the same load case indicates that providing extra diaphragms at mid-span and at pylons can significantly reduce the accelerations of bridge deck.

Figure 7.4(d) presents the power spectral density obtained from Figure 7.4(c), in which the curves are quite similar to the corresponding cases shown in Figure 7.3(d) but with much less

magnitude. It can be noted that the peaks correspond to almost the same frequency components as those with five diaphragms. This observation verifies that the frequency components excited by the vehicles are associated with bridge natural frequencies based on the fact that providing additional diaphragms does not make much difference on vertical modes but influence torsional modes (see Table 4.3).

Figures 7.4(e) and 7.4(f) present the normalized cable tensions of Cable #12 and the corresponding dynamic amplification factor under load 4 and load 5 respectively. It can be seen that the amplification factors for the bridge with five diaphragms and with two diaphragms are quite close. The improvement made by the extra diaphragms is much more pronounced under load 5 than under load 4.

Figure 7.4(g) shows the amplification factor of mid-span longitudinal bending moments. The results shown in this figure further indicate that the additional diaphragms at mid- span and at pylons can provide significant improvement on bridge dynamic responses.

7.2.5 Effect of Damping Ratio of Bridge

The effect of bridge damping ratio has been investigated on Model 1 with diaphragms located at ends, at mid-span and at pylons. Load 4 is applied in the analysis. The trucks are assumed to move on a smooth road surface at the constant speed of 80 km/h. Three levels of bridge damping ratio are used including 0.02, 0.01 and no damping.

Figures 7.5(a) and 7.5(b) present the normalized vertical deflection of mid-span and the corresponding amplification factor. Figures 7.5(c) and 7.5(d) present the mid-span accelerations and the corresponding power spectral density. Figures 7.5(e) and 7.5(f) present the normalized cable tension of Cable #12 and the corresponding dynamic amplification factor. Figure 7.5(g) presents the amplification factor of mid-span longitudinal bending moments.

It can be concluded form the results shown in those figures that bridge damping can reduce the overall dynamic responses of cable-stayed bridges. It has a significant effect upon the response and should therefore always be considered if accurate representation of the true dynamic response is required.

7.2.6 Effect of Traveling Speed of Vehicle

The effect of vehicle speed has been studied by analyzing the dynamic responses of Model 1 with diaphragms located at ends, at mid-span and at pylons. The damping ratio of the bridge is assumed to be 0.02. Load 4 is adopted, in which eight trucks traveling side by side in four groups of two trucks along the center of the four traffic lanes. The vehicle speed is ranging form 20 km/h to 120 km/h with an increment of 5km/h.

Figures 7.6(a) through 7.6(d) characterize the dynamic response of Model 1 in terms of the amplification factor of mid-span vertical deflection, peak mid-span acceleration, tension in stay cable #12, as well as the amplification factor of mid-span longitudinal bending moment respectively as functions of vehicle speed. As can be seen, the amplification factors of deflection and cable tension increase as the vehicle speed increases and exhibit a peak value at a speed around 90 km/h. Furthermore, the amplification factor of cable tension is slightly larger than mid-span vertical deflection, but the two curves are quite similar. Examining the motion equation 5.51 and the detailed equations for each parameter, it can be noted that the variation of vehicle speed only influence the matrix $\mathbf{k}^*$ and $\mathbf{c}^*$ with the assumption of constant vehicle speed and zero damping of vehicle. The effect of vehicle speed on bridge vibration depends on the contribution of $\mathbf{k}^*$ and $\mathbf{c}^*$, which provide correction to the stiffness matrix $\mathbf{K}$ and the damping matrix $\mathbf{C}$ of the bridge respectively during bridge-vehicle interaction. Therefore, the peaks of the amplification curves at 90 km/h indicate the occurrence of the vehicle-bridge resonance at that speed.

The amplification factor of mid-span moment *MI* tends to increase with the increase of vehicle speed. Similar behavior occurs for mid-span acceleration. Unlike the displacement and cable tension amplification factors reaching a peak at the resonant speed of 90 km/h, such a peak does not exist for the moment. It implies that the extent of amplification for moment is smaller than that for the displacement and cable tension at resonant speeds.

7.2.7 Effect of Mass of Vehicle

Another task of this part of study is to investigate the effect of mass of vehicle on the dynamic responses. It has been carried out on the dynamic analysis of Model 1 under load 4. The damping ratio of the bridge is assumed as 0.02. Two cases of truck weight, namely mass 1 and mass 2, have been considered. Mass 1 uses the exact physical properties shown in Figure 5.3. Mass 2 adopts most of the properties of Figure 5.3 but doubling the truck weight proportionally.

Figure 7.7(a) shows the dynamic amplification factor of mid-span vertical deflection during the passage of vehicles. It can be seen that the peak amplification factor of mass 2 is slightly larger than that of mass 1.

Figure 7.7(d) shows the time history of normalized cable tension for Cable #12 and the corresponding amplification factor of cable tension. It can be noticed that the peak normalized cable tension for mass 2 is approximately twice as much as that for mass 1. Therefore, only slight difference is observed from the curves of cable tension amplification factors for mass 1 and mass 2.

Figure 7.22(e) shows the amplification factor of mid-span longitudinal bending moment. Similar to the observation from Figure 7.21(a) and (c), the moment amplification factor of mass 2 is very close to that of mass 1.

The time history of mid-span accelerations for mass 1 and mass 2 are plotted in Figure 7.7(b). As expected, the peak acceleration increases with the increase of vehicle mass. The acceleration for mass 2 is 2.6 times as much as that for mass 1. Evidently, the increase of acceleration is not linearly proportional to the increase of vehicle mass, which emphasizes the importance of bridge vehicle interaction. Figure 7.7(c) illustrates the power spectral density corresponding to the time histories shown in Figure 7.7(b). Doubling vehicle mass results in the decrease of the natural frequencies of vehicle. However, the curves for mass 1 and mass 2 presented in Figure 7.7(c) apparently have the same frequency components, which verify that both peak ranges are associated with bridge natural frequencies.

Form the above discussion, it can be concluded that increasing the mass of vehicle can result in the increase of dynamic responses of bridge but proportional to the increase of static responses including deflection, moment and cable tension. It implies that heavy vehicles have minor influence on the amplification factors of bridge-vehicle interaction.

7.2.8 Effect of Cable Arrangement

There are four basic longitudinal cable configurations: harp-type, fan-type, radiating-type and star-type. The harp-type cable arrangement has the cable parallel and spaced along the girder and the pylon. The radiating-type is a converging system where the cables intersect at a common point at the top of the pylon. The fan type cable arrangement combines the radiating-type and the harp-type. In the star-type arrangement, the cables are placed along the pylon and converge at a common point on the girder. Only two of these are considered in the present study, the fan-type and harp-type configurations.

The general configurations of Model 1 and Model 2, representing fan-type and harp-type respectively, are shown in Figure 7.1 and adopted in the analysis. It is assumed that Model 1 and Model 2 have the same properties except for their cable arrangement. Each bridge has

diaphragms installed at ends. The bridge damping ratio is taken as 0.02. Load 4 is applied as traffic loading.

Figures 7.8(a), 7.8(d) and 7.8(e) present the amplification factors of mid-span vertical deflection, cable tension and mid-span moment for Model 1 and Model 2 respectively. Figures 7.8(b) and 7.8(c) present the mid-span accelerations for the two models and the corresponding power spectral density. Little difference can be observed for the curves of amplification factors between harp type and fan type. The bridge with harp-type cable arrangement experiences larger accelerations than the bridge with fan-type cable arrangement, however, the two models almost have identical predominant frequencies. These observations are due the fact that fan type and harp type models have close natural frequencies for longitudinal vertical modes, but harp type model has more torsional and transverse coupling modes in lower frequency range (see Table 4.3).

7.3 Summary

This chapter has presented the analysis of cable-stayed bridges subjected to moving vehicles. Bridge damping, cable behavior and cable arrangement, effect of diaphragms and nonlinear geometric effects have been considered when analyzing the linear dynamic responses. Influences associated with moving vehicles have been discussed, such as the effect of traffic load patterns, vehicle speed, and mass of vehicle. Based on the above investigations, the following conclusions and remarks can be made:

1. The dynamic responses induced by bridge-vehicle interaction are generally larger than the static responses due to equivalent static traffic load. In other wards, the peak amplification factors of cable-stayed bridge are mostly larger than 1.0.
2. In general, the amplification factors of mid-span deflection and cable tension are higher than the amplification factor of mid-span longitudinal bending moment.

3. Generally, a large number of modes are essential to obtain the realistic response. Because of adopting the 3-dimensional model of bridge and vehicle, traffic excitations may introduce special features into bridge response due to the complicated interaction between vehicle and bridge. For example, vertical vibrations of the bridge are introduced to a great extent by both lateral and torsional modes in addition to the longitudinal vertical modes. Modal coupling can not be captured in any 2-D analysis.
4. The traffic load patterns play an important role in simulating the dynamic responses of cable stayed bridge. Eccentric traffic load tends to produce larger bridge response than central traffic load, but the change in amplification factors is not pronounced. Increasing the number of trucks can result in the increase of both dynamic response and the amplification factors. Distributing the trucks on multiple lanes can reduce the bridge responses. Fewer and evenly distributed trucks excite bridge vibration with higher frequency, while more and eccentric trucks trigger low frequency vibration, which is more significant to bridge safety since it is close to the fundamental frequency of the bridge.
5. Bridge damping has a significant effect upon the responses and should be always considered in the analysis. Increasing the bridge damping can result in decrease of the bridge responses.
6. In general, the dynamic responses of bridge tend to increase with the increase of vehicle speed. The dynamic amplification factors due to bridge-interaction associated with higher vehicle speed are much more pronounced than lower vehicle speed. Resonance can occur on the interaction system as the vehicle speed and frequencies of the bridge meet some specific relations, which can result in dramatic amplification of the response of each component.
7. Proving solid plate diaphragms can significantly improve the dynamic responses of box-girder cable-stayed bridge, especially at the ends of bridge, at pylons and at mid-span.
8. Cable arrangement and increase of vehicle weight have minor influence on the amplification factors. However, larger mid-span acceleration is observed in harp-type than in fan-type.

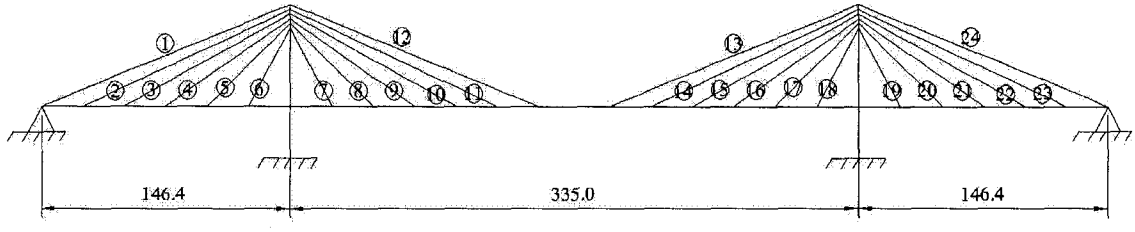

(a) Model 1: Fan-type

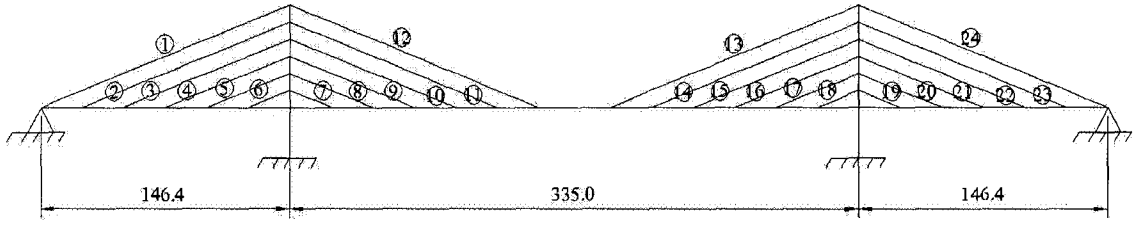

(b) Model 2: Harp-type

FIGURE 7.1 CONFIGURATION OF CABLE-STAYED BRIDGE FOR CASE 1 AND CASE 2

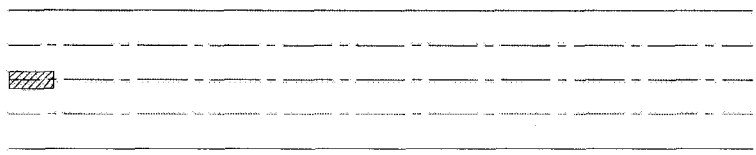

(a) Load 1

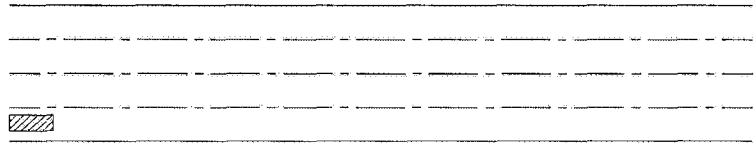

(b) Load 2

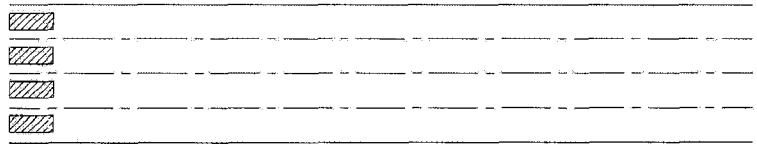

(c) Load 3

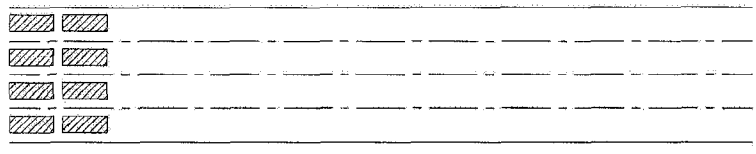

(d) Load 4

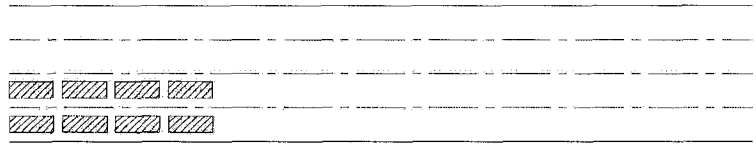

(e) Load 5

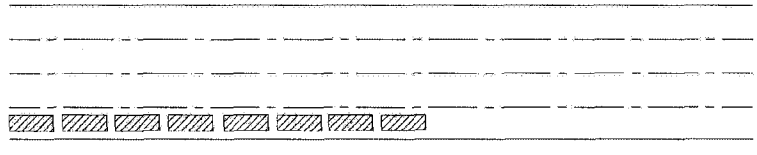

(f) Load 6

FIGURE 7.2 TRAFFIC LOAD CASES

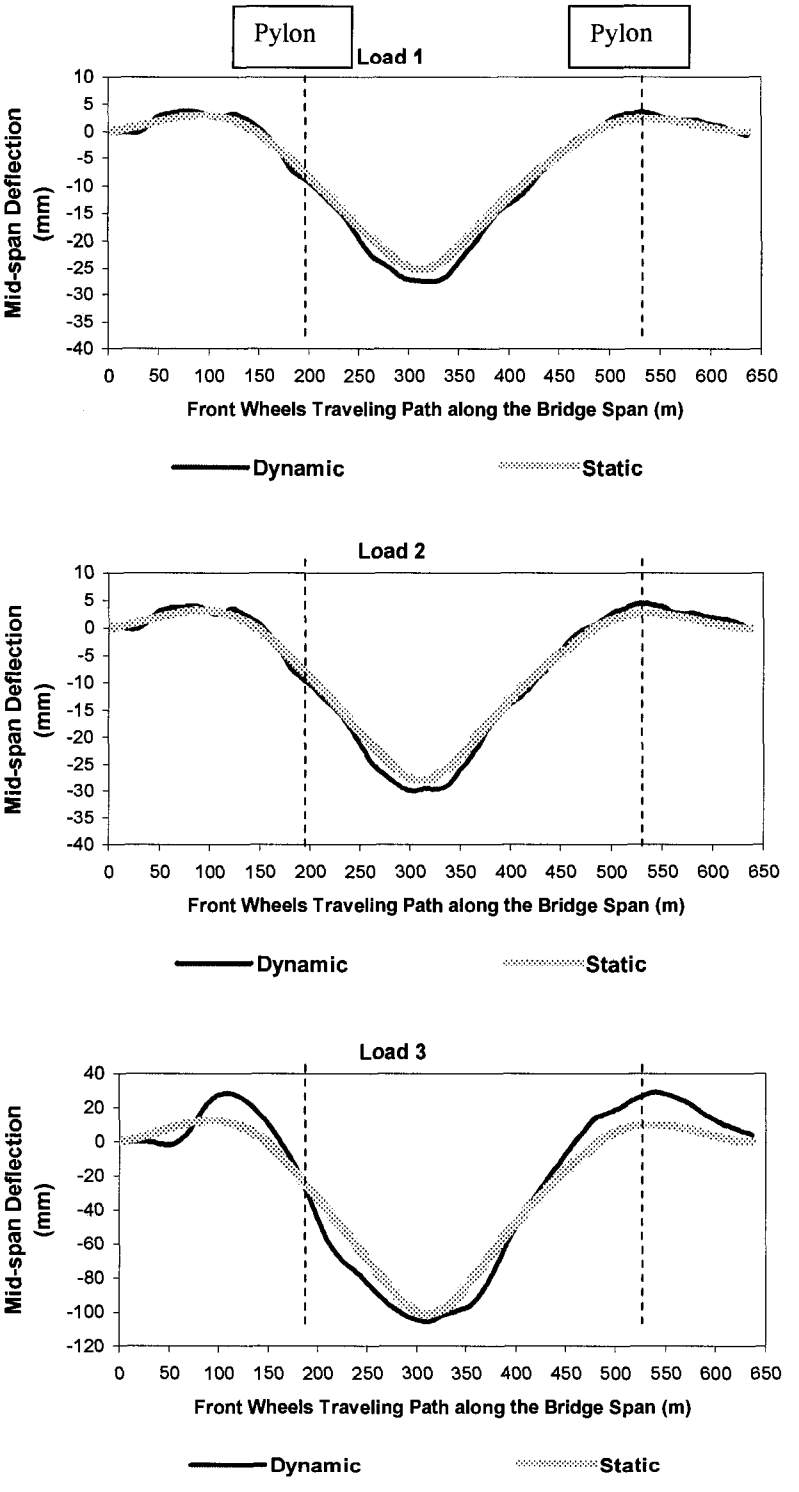

(a) Vertical Deflection of Mid-span

FIGURE 7.3 DYNAMIC RESPONSES OF MODEL 1 WITH FIVE DIAPHRAGMS UNDER LOAD 1 THROUGH LOAD 6, VEHICLE SPEED = 80KM/H

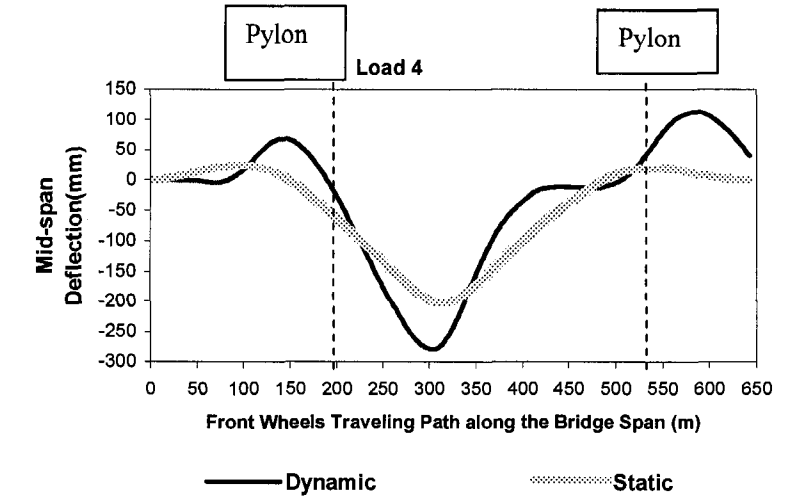

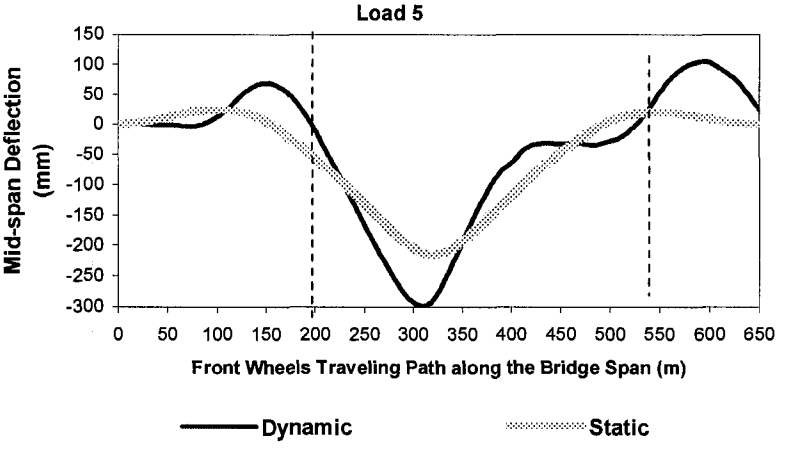

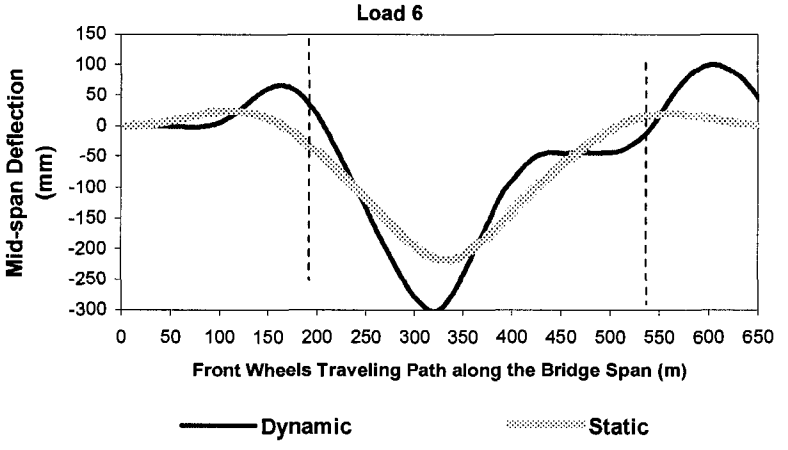

(a) Vertical Deflection of Mid-span (continued)

FIGURE 7.3 DYNAMIC RESPONSES OF MODEL 1 WITH FIVE DIAPHRAGMS UNDER LOAD 1 THROUGH LOAD 6, VEHICLE SPEED = 80KM/H (CONTINUED)

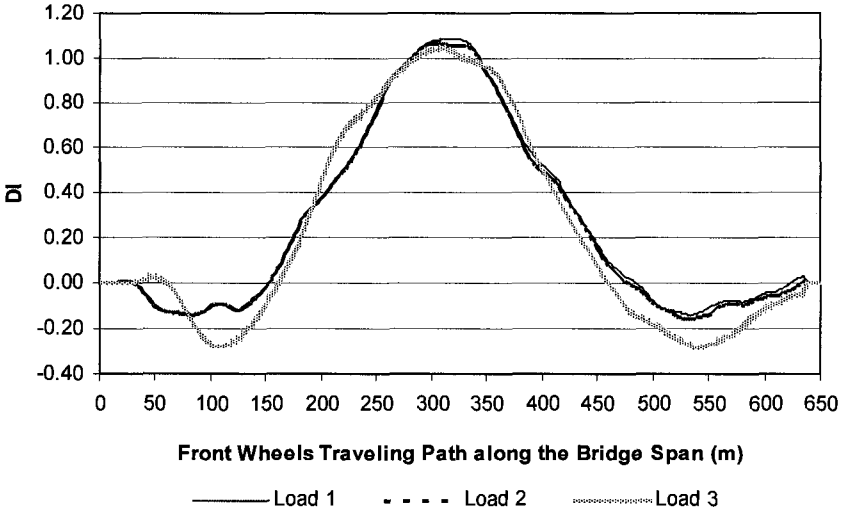

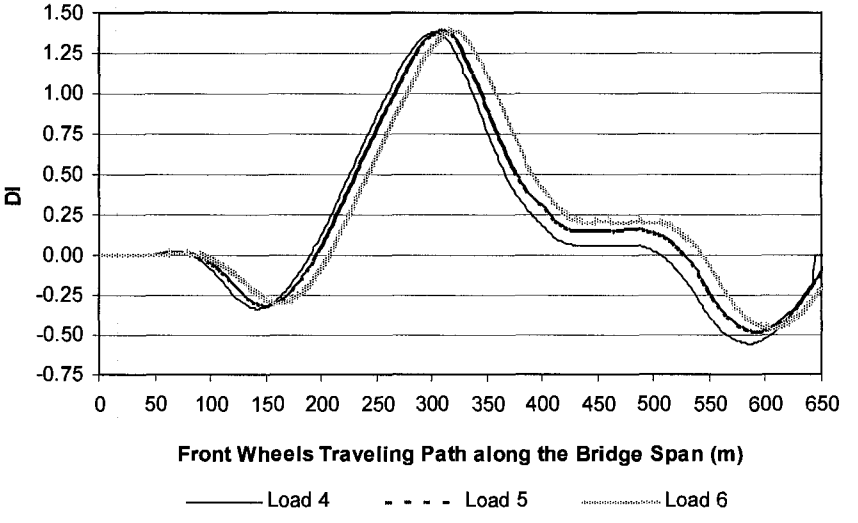

(b) Amplification factor of vertical deflection

FIGURE 7.3 DYNAMIC RESPONSES OF MODEL 1 WITH FIVE DIAPHRAGMS UNDER LOAD 1 THROUGH LOAD 6, VEHICLE SPEED = 80KM/H (CONTINUED)

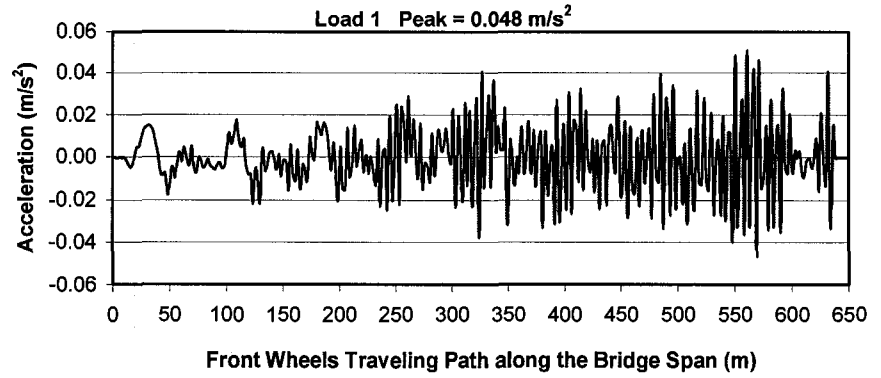

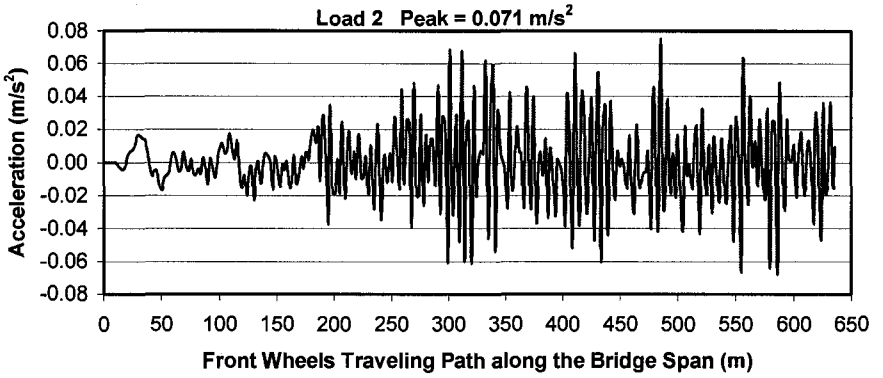

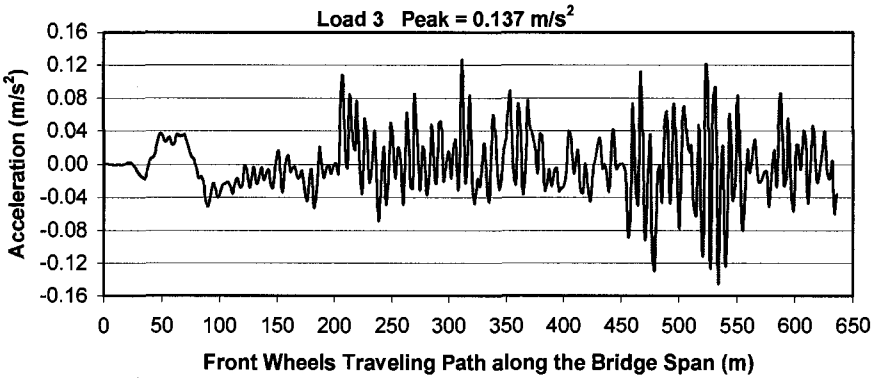

(c) Mid-span Acceleration

FIGURE 7.3 DYNAMIC RESPONSES OF MODEL 1 WITH FIVE DIAPHRAGMS UNDER LOAD 1 THROUGH LOAD 6, VEHICLE SPEED = 80KM/H (CONTINUED)

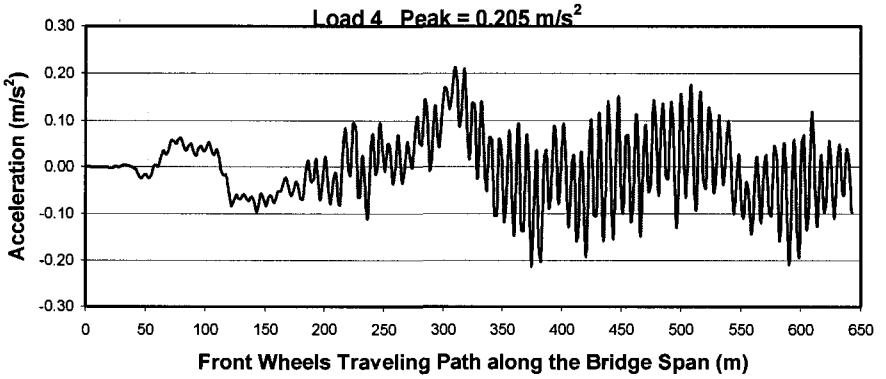

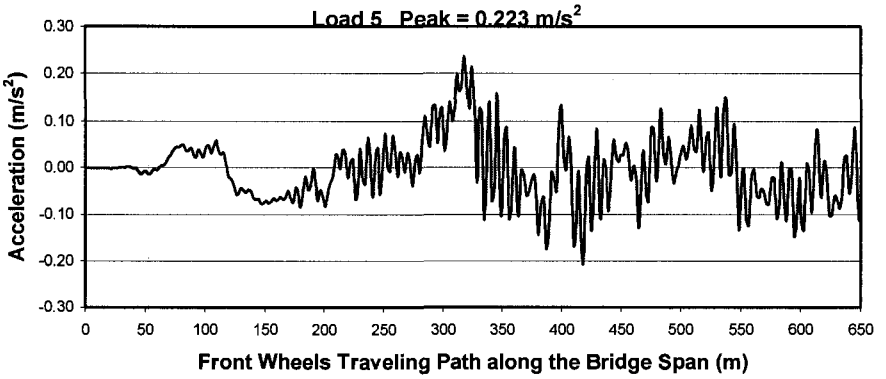

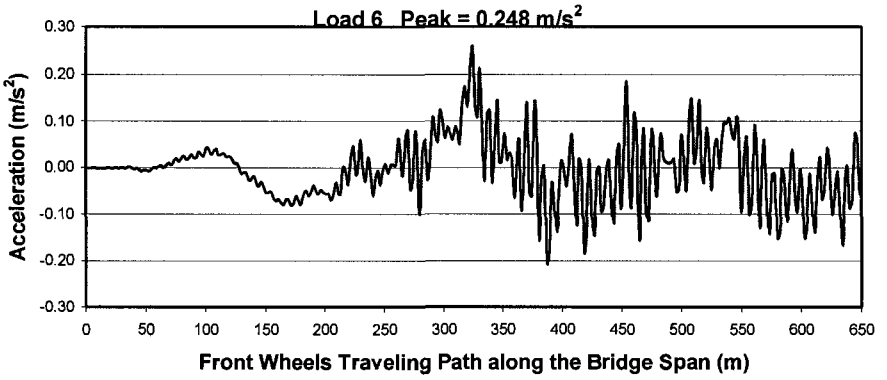

(c) Mid-span Acceleration (continued)

FIGURE 7.3 DYNAMIC RESPONSES OF MODEL 1 WITH FIVE DIAPHRAGMS UNDER LOAD 1 THROUGH LOAD 6, VEHICLE SPEED = 80KM/H (CONTINUED)

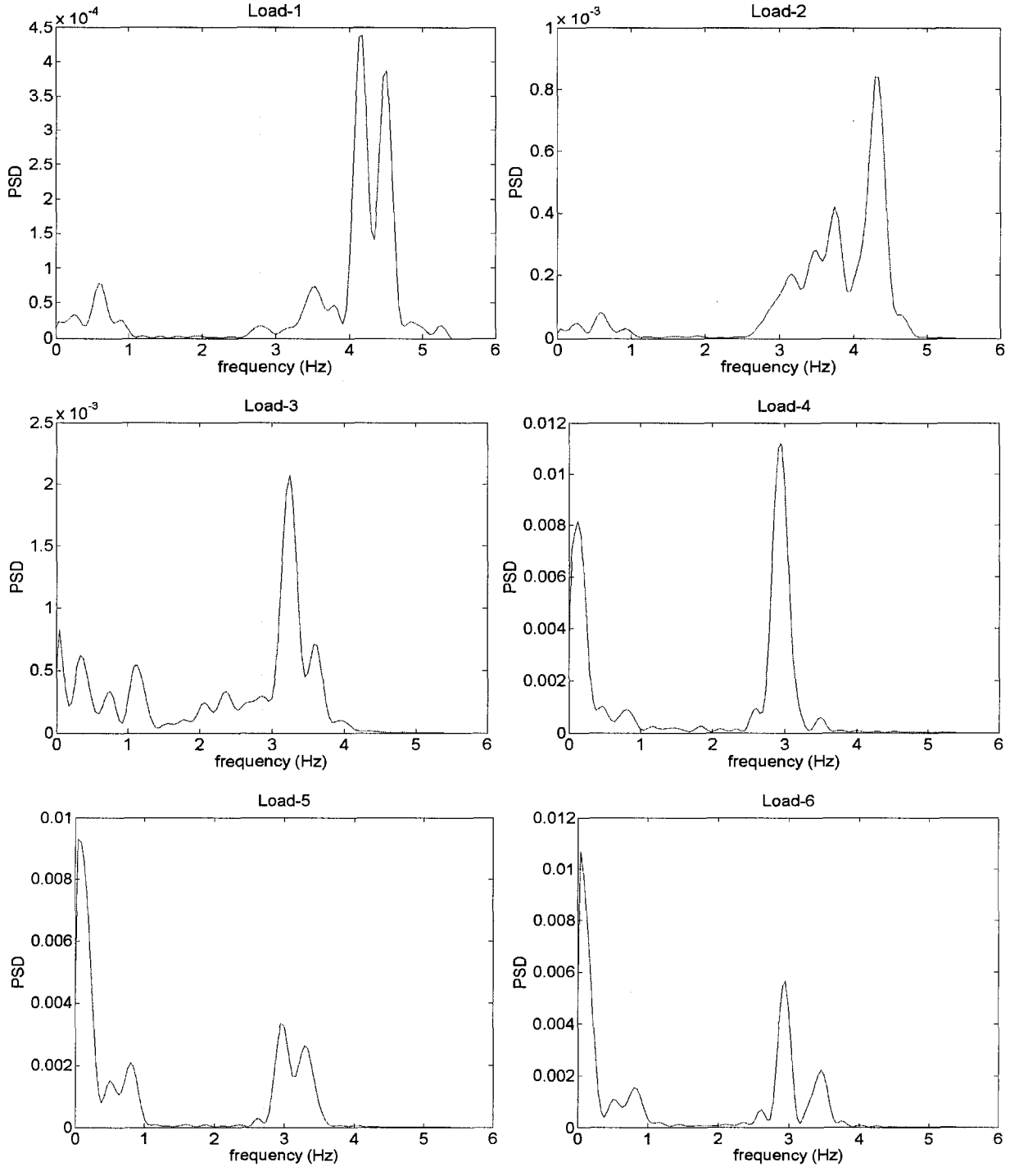

(d) Power spectral density of mid-span acceleration

FIGURE 7.3 DYNAMIC RESPONSES OF MODEL 1 WITH FIVE DIAPHRAGMS UNDER LOAD 1 THROUGH LOAD 6, VEHICLE SPEED = 80KM/H (CONTINUED)

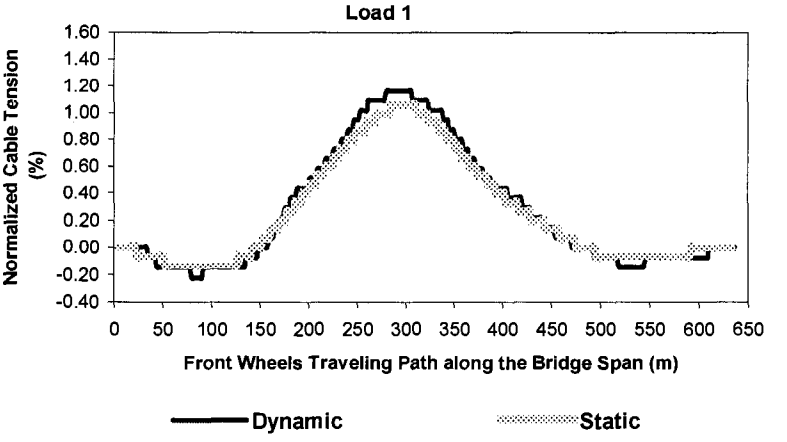

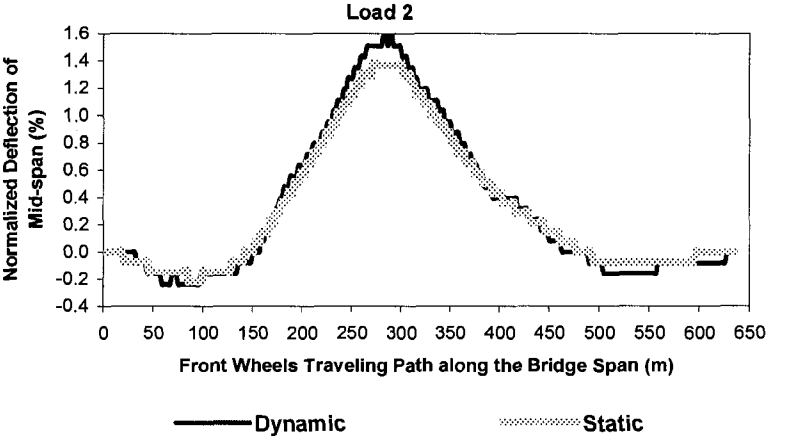

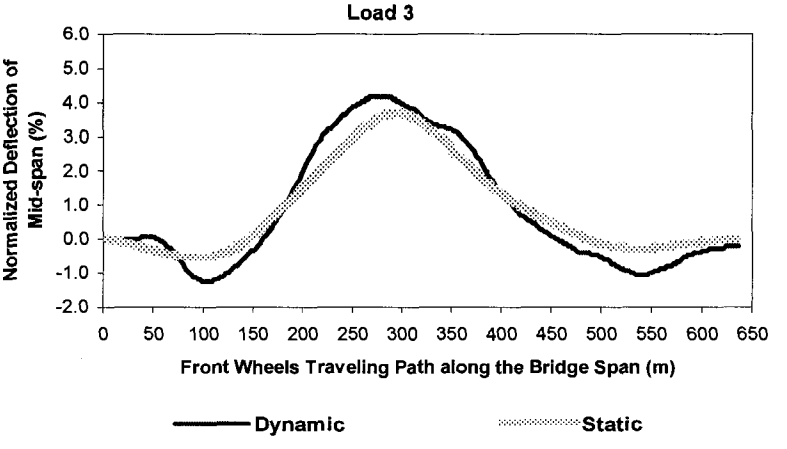

(e) Normalized tension of cable #12

FIGURE 7.3 DYNAMIC RESPONSES OF MODEL 1 WITH FIVE DIAPHRAGMS UNDER LOAD 1 THROUGH LOAD 6, VEHICLE SPEED = 80KM/H (CONTINUED)

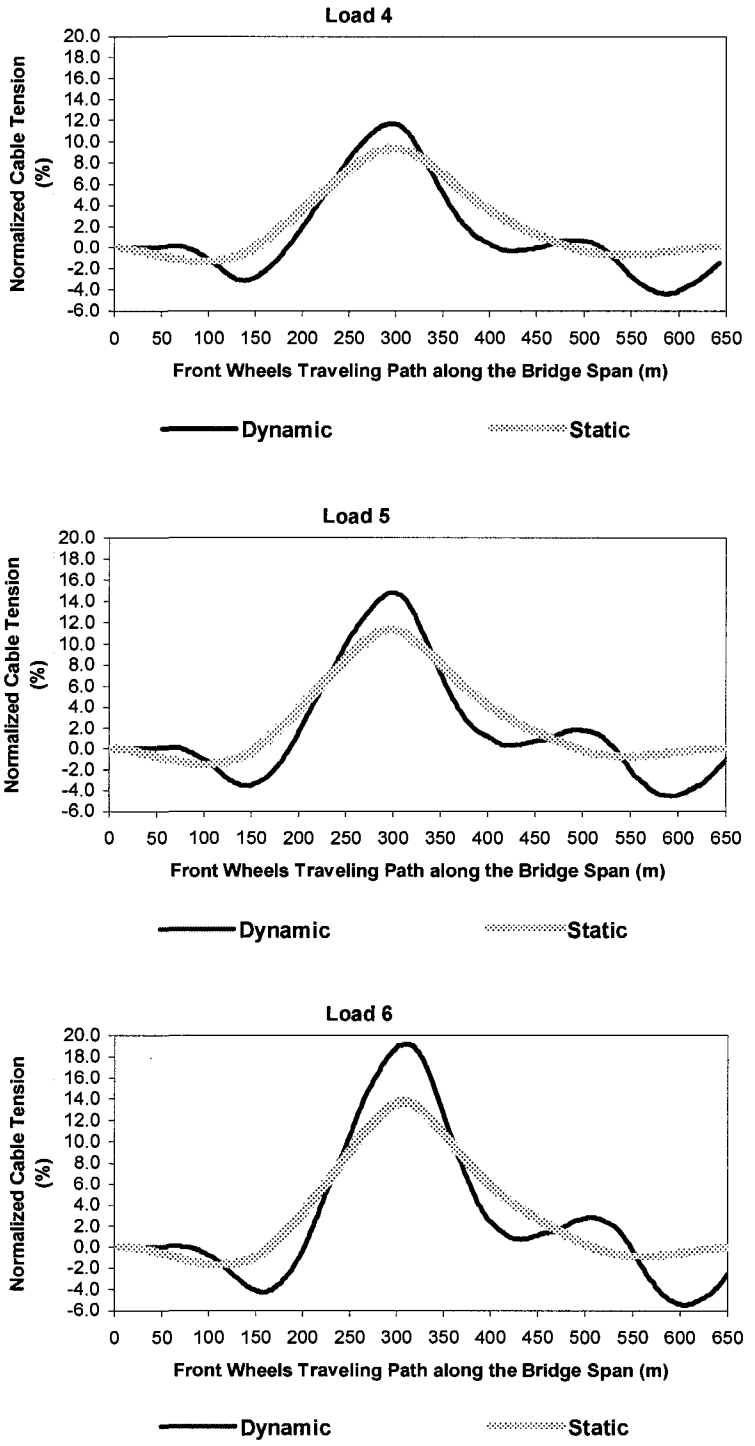

(e) Normalized tension of cable #12 (continued)

FIGURE 7.3 DYNAMIC RESPONSES OF MODEL 1 WITH FIVE DIAPHRAGMS UNDER LOAD 1 THROUGH LOAD 6, VEHICLE SPEED = 80KM/H (CONTINUED)

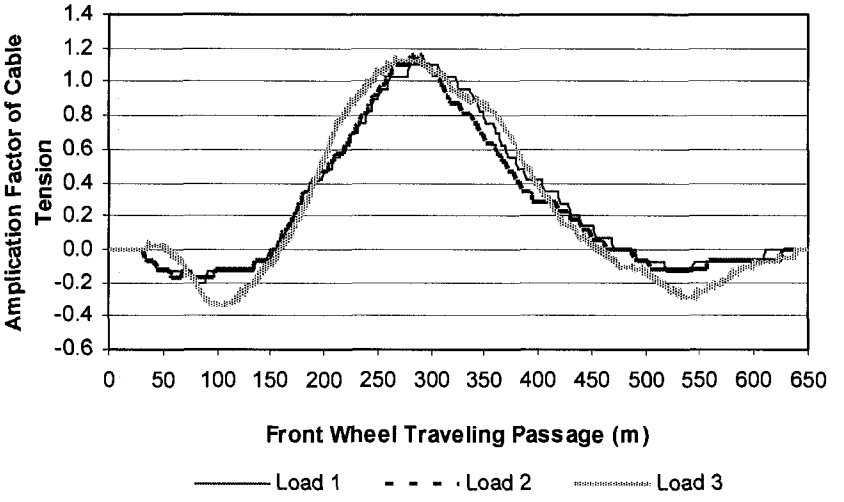

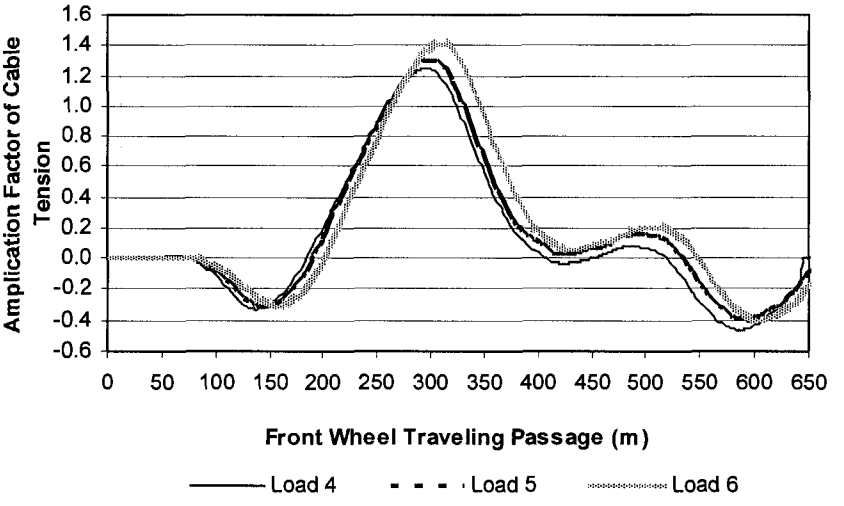

(f) Amplification factor of cable tension for cable #12

FIGURE 7.3 DYNAMIC RESPONSES OF MODEL 1 WITH FIVE DIAPHRAGMS UNDER LOAD 1 THROUGH LOAD 6, VEHICLE SPEED = 80KM/H (CONTINUED)

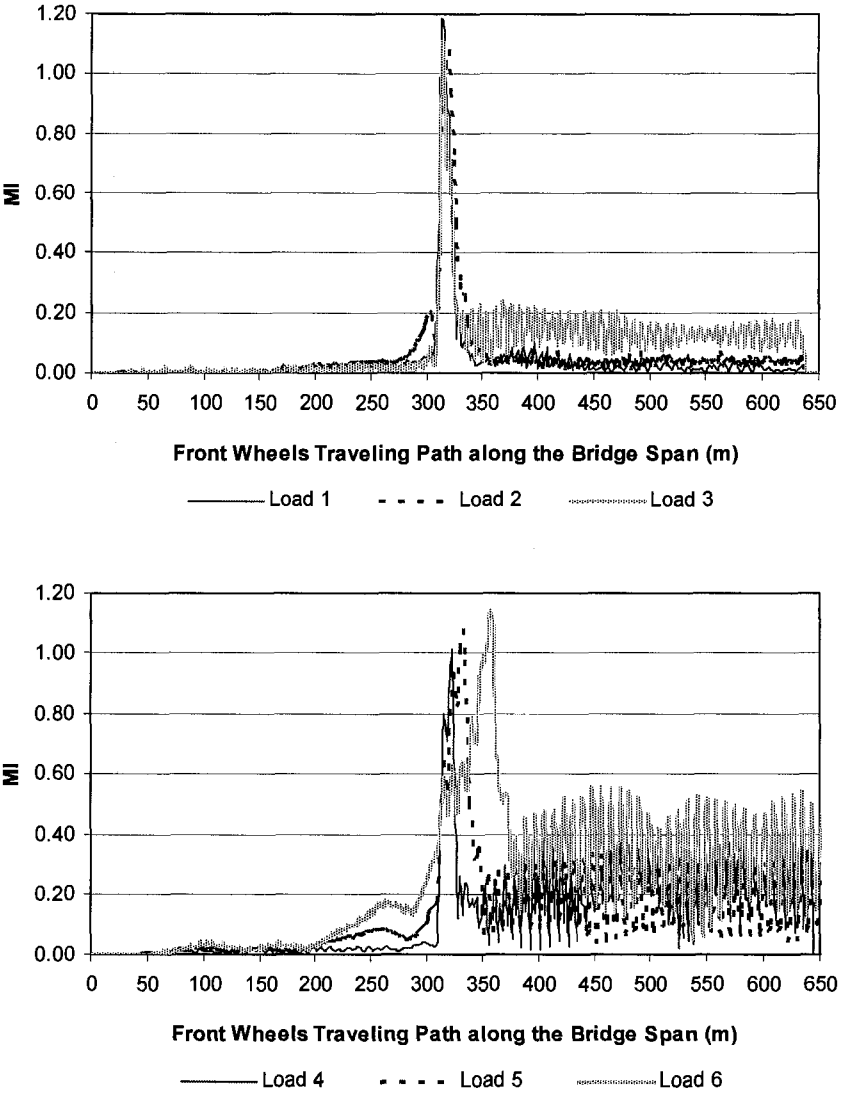

(g) Amplification factor of mid-span longitudinal bending moments

FIGURE 7.3 DYNAMIC RESPONSES OF MODEL 1 WITH FIVE DIAPHRAGMS UNDER LOAD 1 THROUGH LOAD 6, VEHICLE SPEED = 80KM/H (CONTINUED)

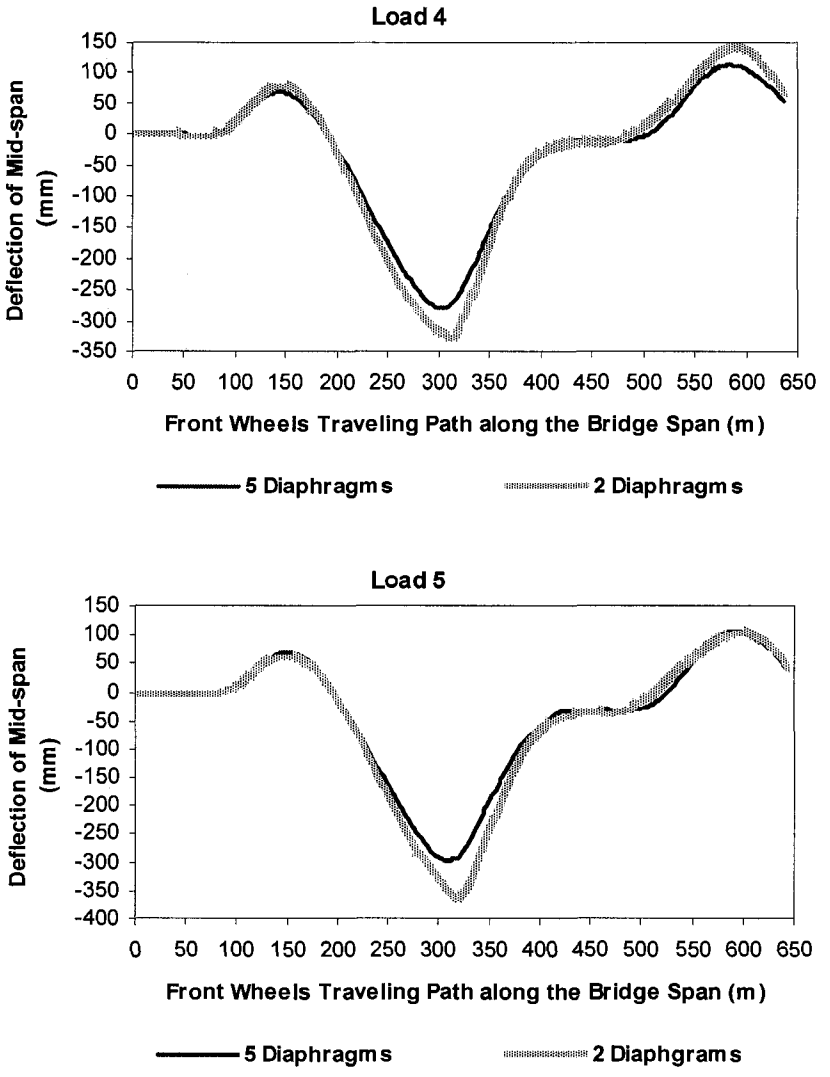

(a) Vertical Deflection of Mid-span

FIGURE 7.4 DYNAMIC RESPONSES OF MID-SPAN FOR MODEL 1 WITH FIVE DIAPHRAGMS AND TWO DIAPHRAGMS UNDER LOAD 4 AND LOAD 5, VEHICLE SPEED = 80KM/H

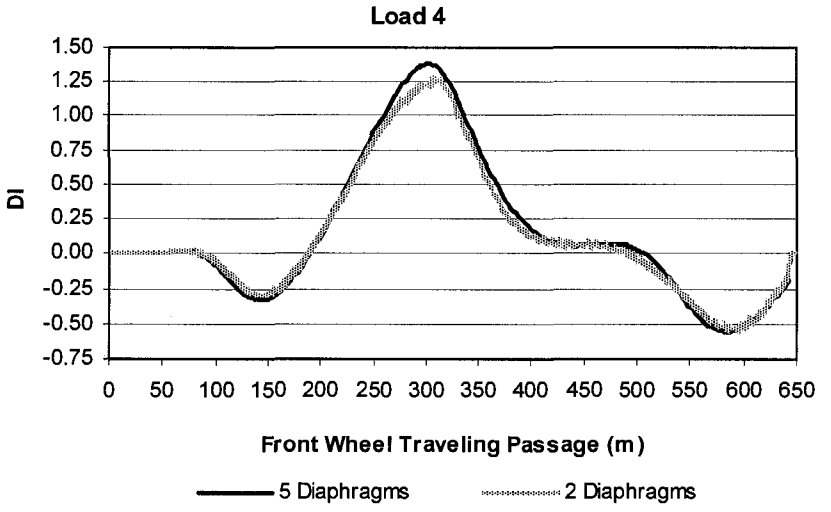

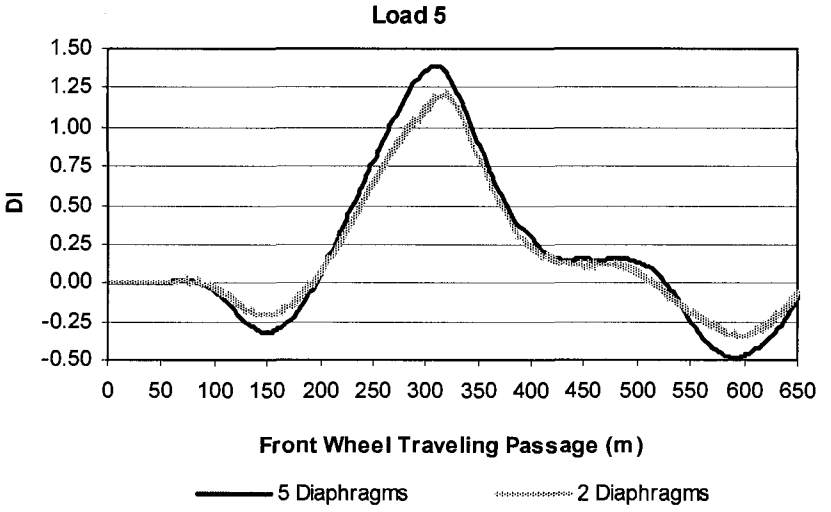

(b) Amplification factor of mid-span deflection

FIGURE 7.4 DYNAMIC RESPONSES OF MID-SPAN FOR MODEL 1 WITH FIVE DIAPHRAGMS AND TWO DIAPHRAGMS UNDER LOAD 4 AND LOAD 5, VEHICLE SPEED = 80KM/H

(CONTINUED)

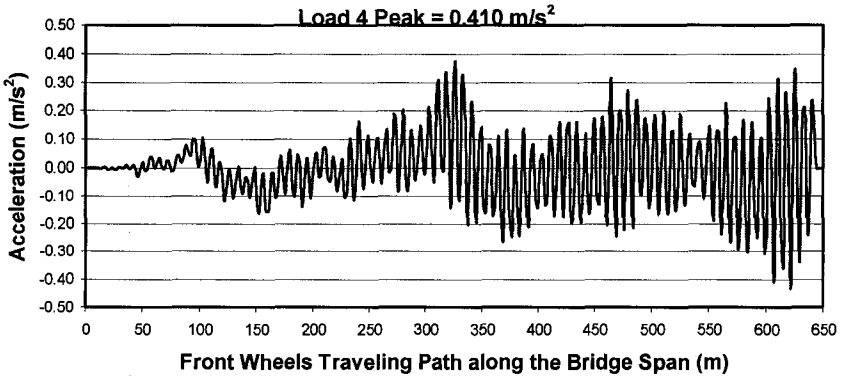

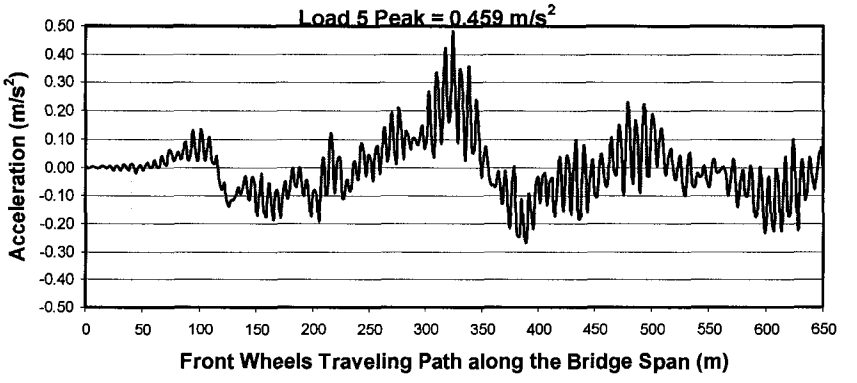

(c) Mid-span acceleration for Model 1 with two diaphragms

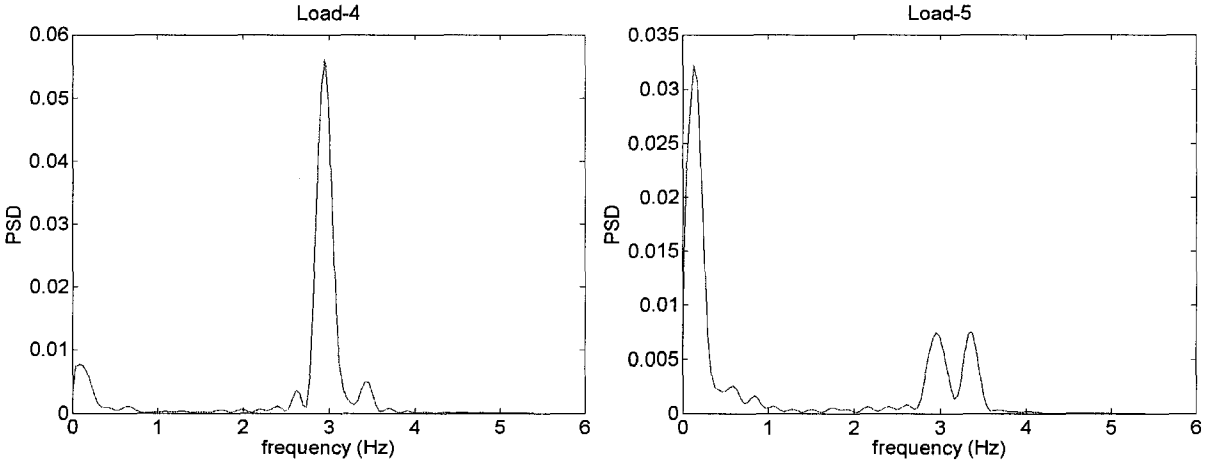

(d) Power spectral density of mid-span acceleration for Model 1 with two diaphragms

FIGURE 7.4 DYNAMIC RESPONSES OF MID-SPAN FOR MODEL 1 WITH FIVE DIAPHRAGMS AND TWO DIAPHRAGMS UNDER LOAD 4 AND LOAD 5, VEHICLE SPEED = 80KM/H

(CONTINUED)

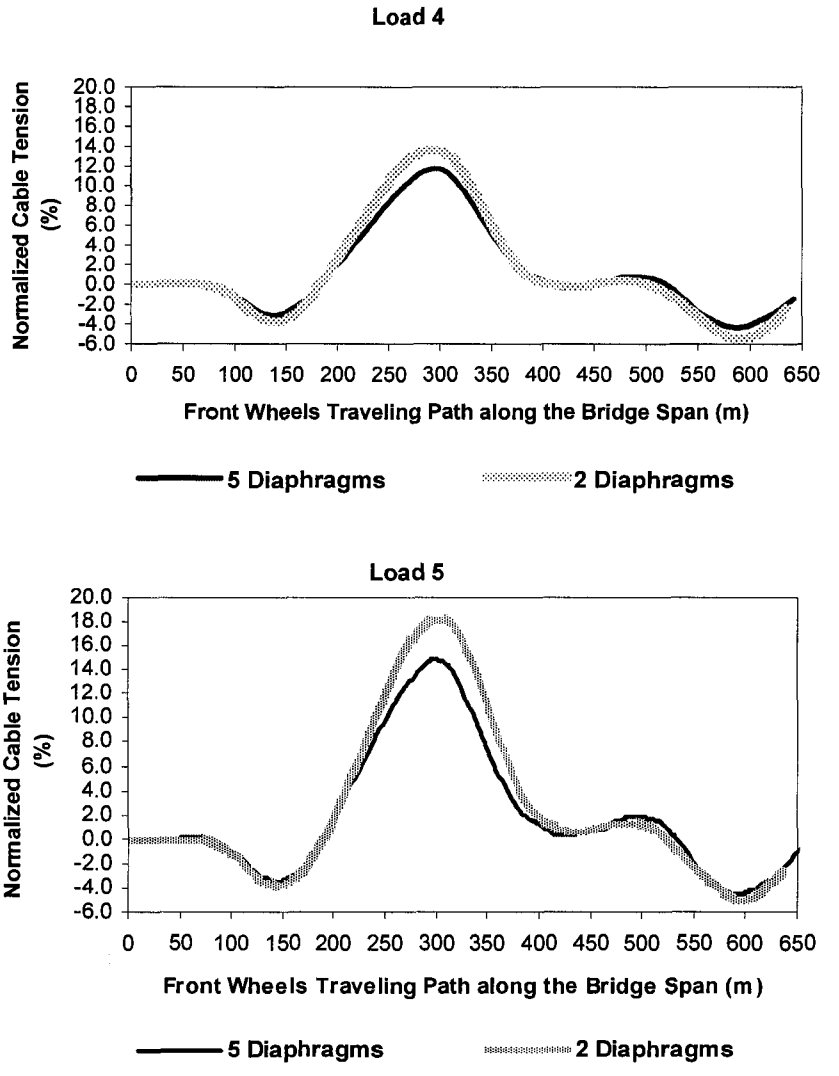

(e) Normalized tension of Cable #12

FIGURE 7.4 DYNAMIC RESPONSES OF MID-SPAN FOR MODEL 1 WITH FIVE DIAPHRAGMS AND TWO DIAPHRAGMS UNDER LOAD 4 AND LOAD 5, VEHICLE SPEED = 80KM/H (CONTINUED)

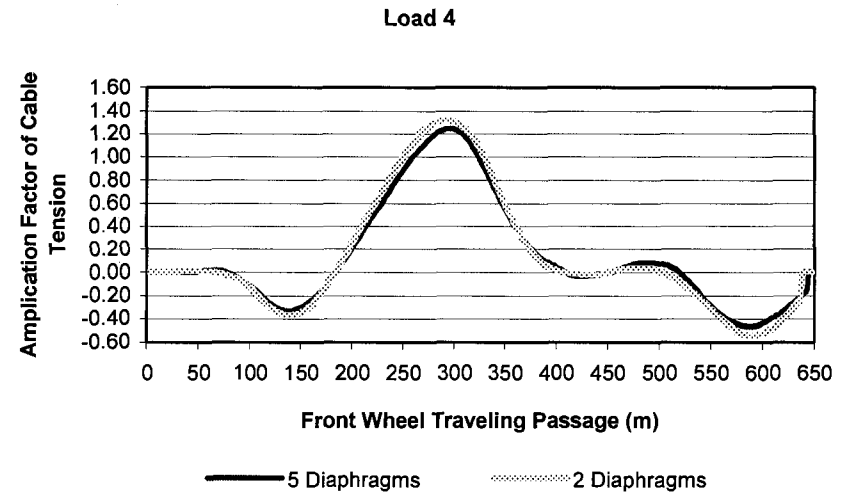

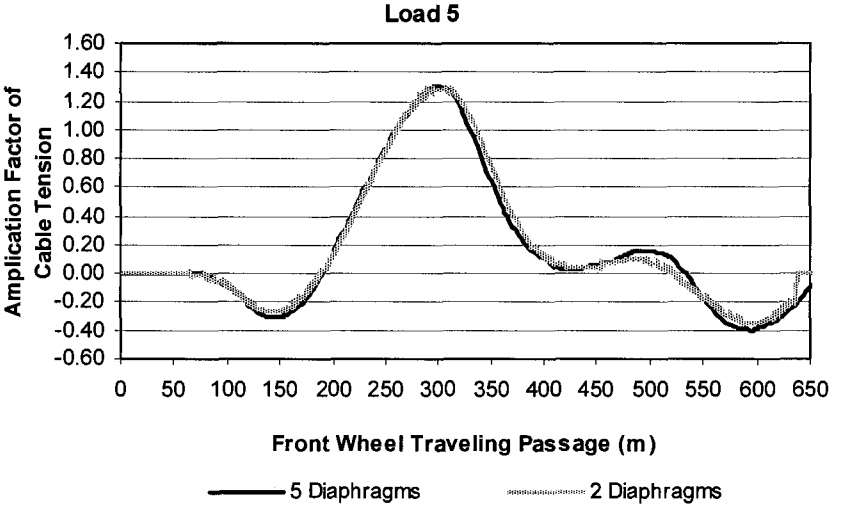

(f) Amplification factor of cable tension for cable #12

FIGURE 7.4 DYNAMIC RESPONSES OF MID-SPAN FOR MODEL 1 WITH FIVE DIAPHRAGMS AND TWO DIAPHRAGMS UNDER LOAD 4 AND LOAD 5, VEHICLE SPEED = 80KM/H (CONTINUED)

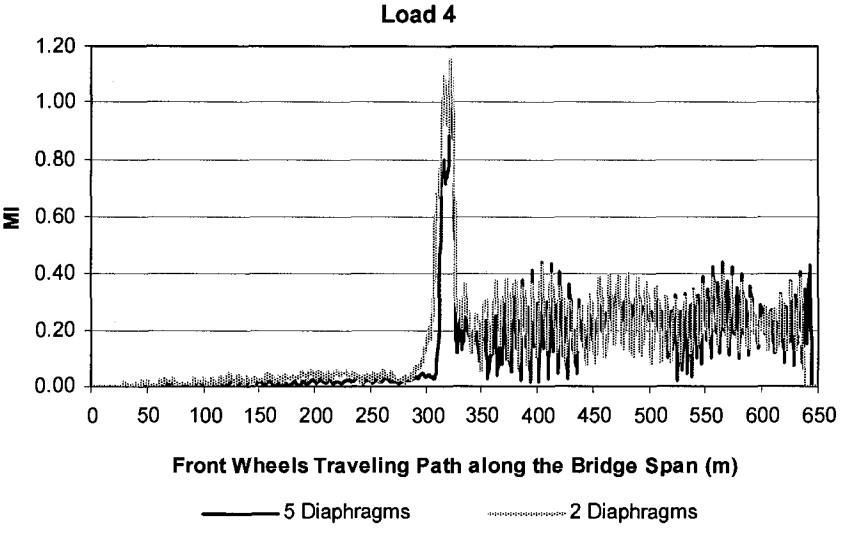

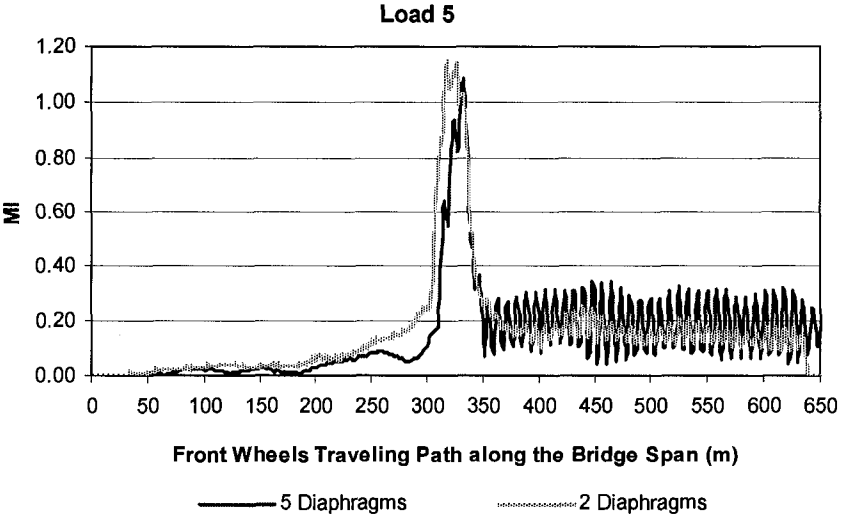

(g) Amplification factor of mid-span longitudinal bending moments

FIGURE 7.4 DYNAMIC RESPONSES OF MID-SPAN FOR MODEL 1 WITH FIVE DIAPHRAGMS AND TWO DIAPHRAGMS UNDER LOAD 4 AND LOAD 5, VEHICLE SPEED = 80KM/H (CONTINUED)

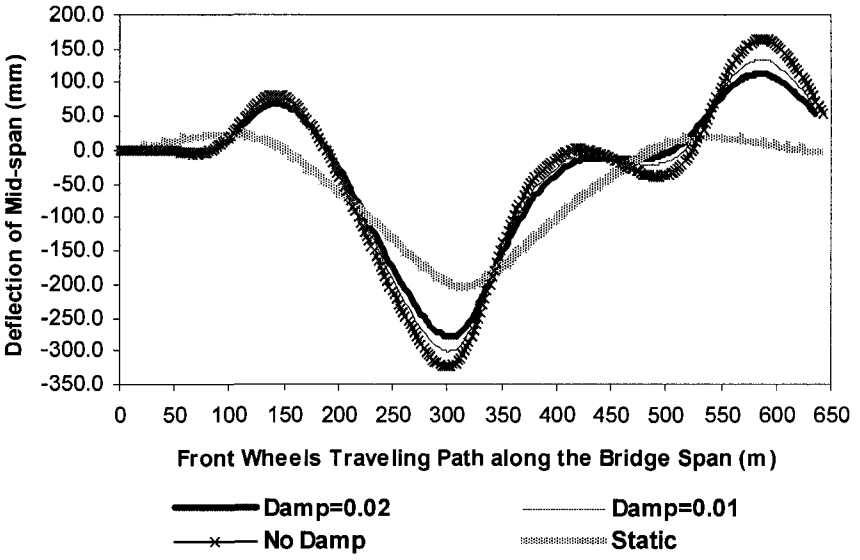

(a) Vertical Deflection of Mid-span

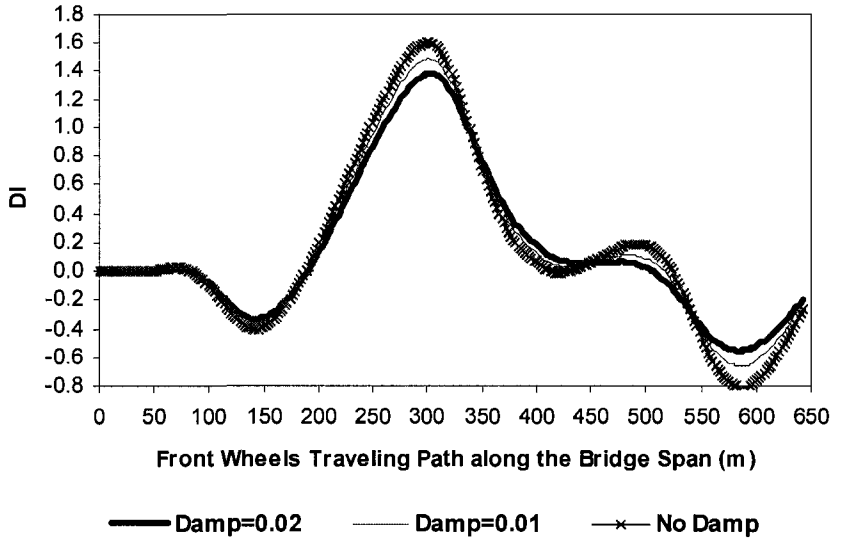

(b) Amplification Factor of Mid-span Deflection

FIGURE 7.5 EFFECT OF BRIDGE DAMPING RATIO FOR MODEL 1 WITH FIVE DIAPHRAGMS UNDER LOAD 4, VEHICLE SPEED = 80KM/H BRIDGE DAMPING RATIO = 0.02, 0.01 AND 0.00

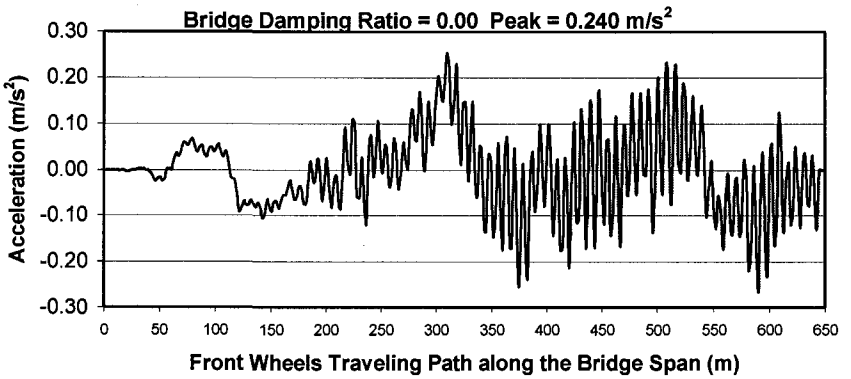

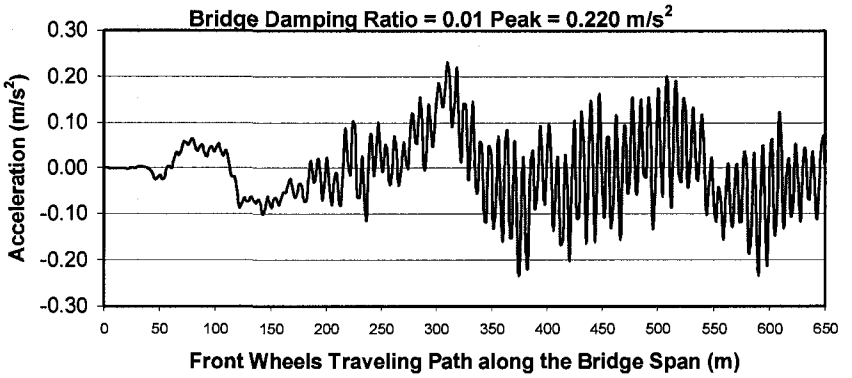

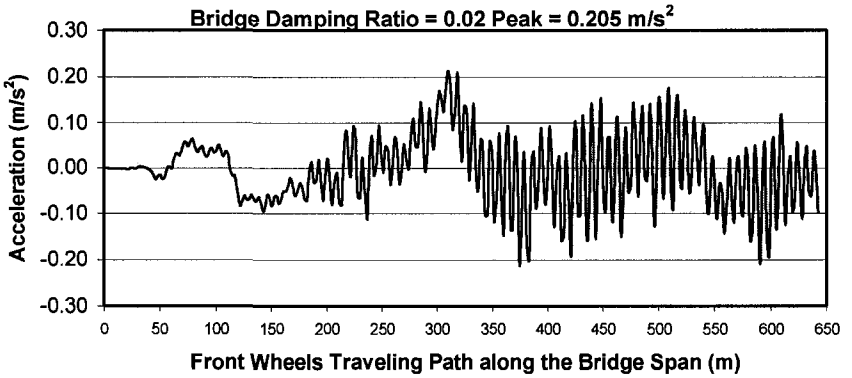

(c) Bridge mid-span acceleration

FIGURE 7.5 EFFECT OF BRIDGE DAMPING RATIO FOR MODEL 1 WITH FIVE DIAPHRAGMS UNDER LOAD 4, VEHICLE SPEED = 80KM/H BRIDGE DAMPING RATIO = 0.02, 0.01 AND 0.00 (CONTINUED)

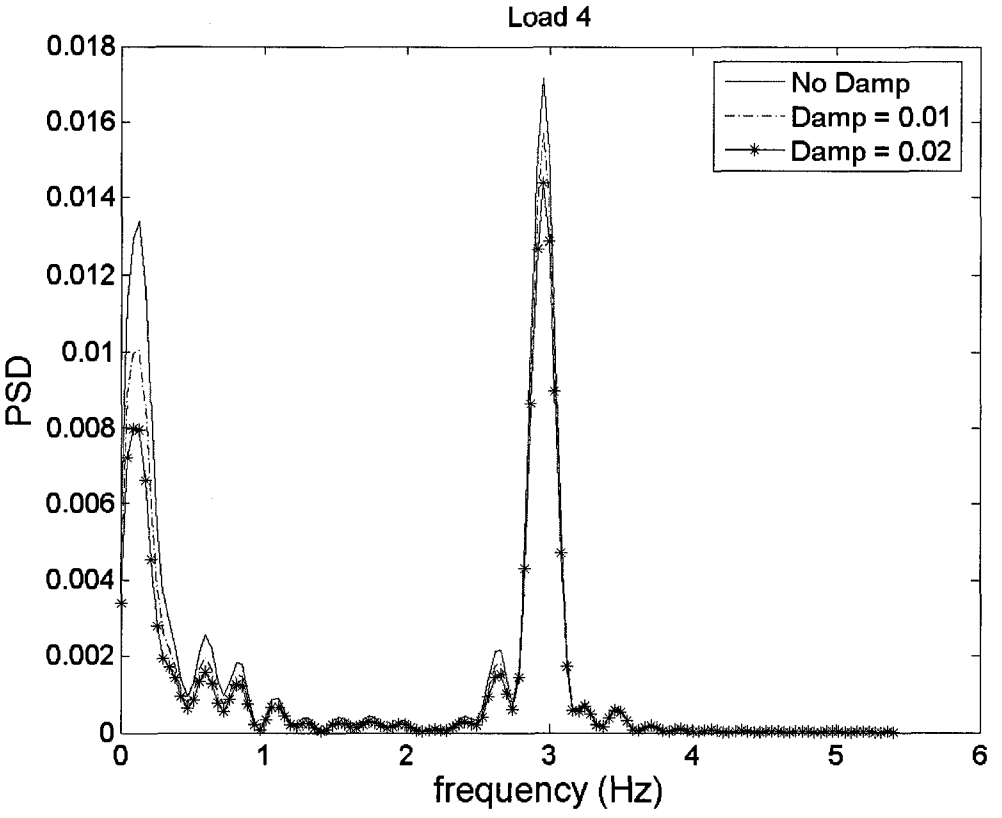

(d) Power spectral density of mid-span acceleration

FIGURE 7.5 EFFECT OF BRIDGE DAMPING RATIO FOR MODEL 1 WITH FIVE DIAPHRAGMS UNDER LOAD 4, VEHICLE SPEED = 80KM/H BRIDGE DAMPING RATIO = 0.02, 0.01 AND 0.00 (CONTINUED)

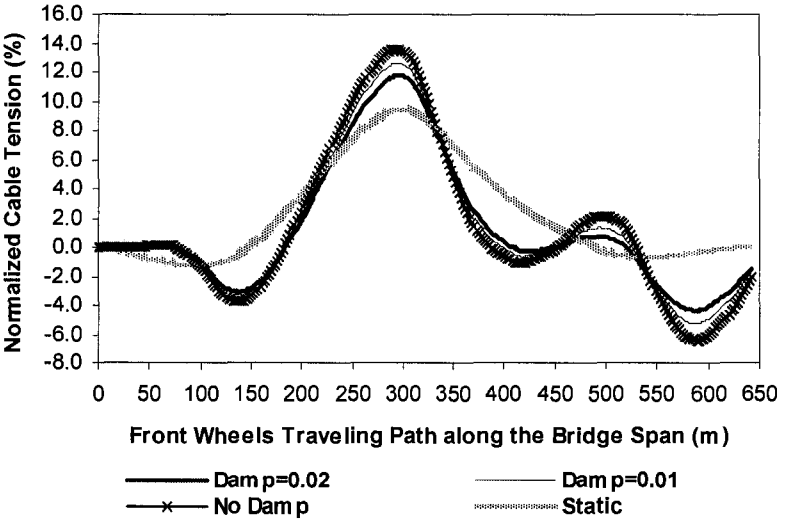

(e) Normalized Cable Tension of Cable #12

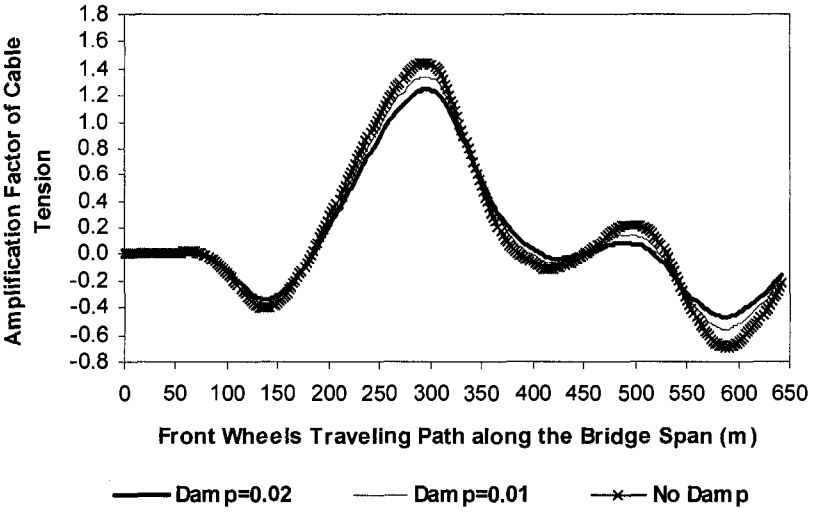

(f) Amplification Factor of Cable Tension for Cable #12

FIGURE 7.5 EFFECT OF BRIDGE DAMPING RATIO FOR MODEL 1 WITH FIVE DIAPHRAGMS UNDER LOAD 4, VEHICLE SPEED = 80KM/H BRIDGE DAMPING RATIO = 0.02, 0.01 AND 0.00 (CONTINUED)

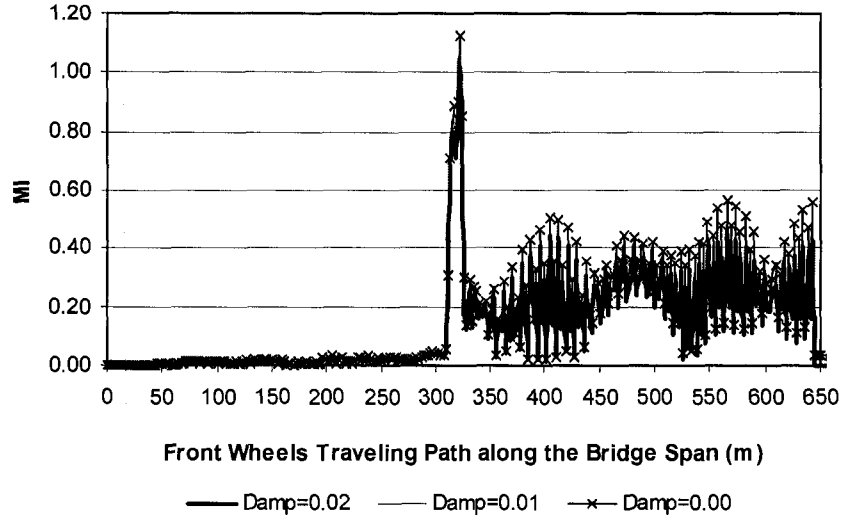

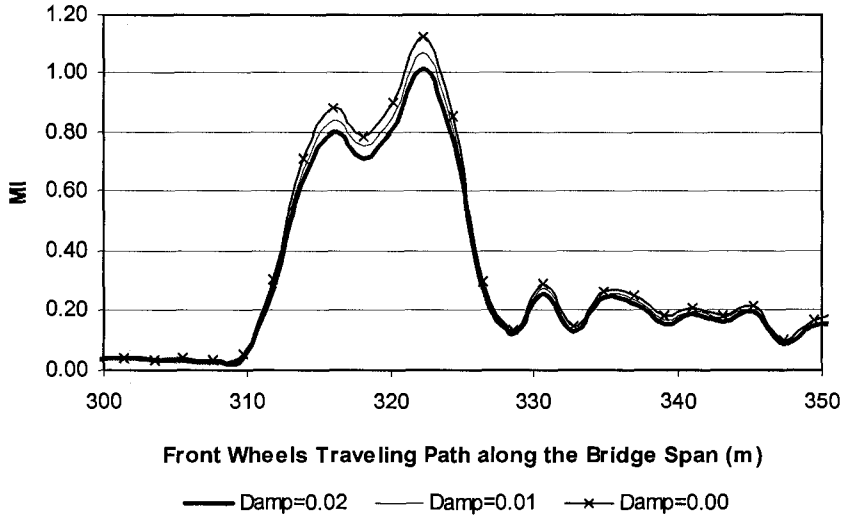

(g) Amplification Factor of mid-span longitudinal moment

FIGURE 7.5 EFFECT OF BRIDGE DAMPING RATIO FOR MODEL 1 WITH FIVE DIAPHRAGMS UNDER LOAD 4, VEHICLE SPEED = 80KM/H BRIDGE DAMPING RATIO = 0.02, 0.01 AND 0.00 (CONTINUED)

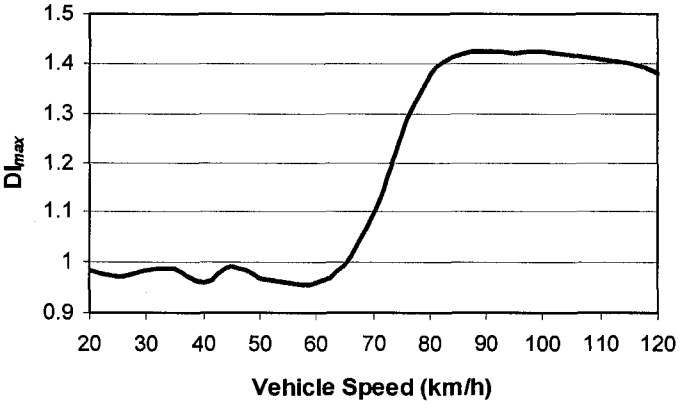

(a) Amplification Factor of Mid-Span Vertical Deflection

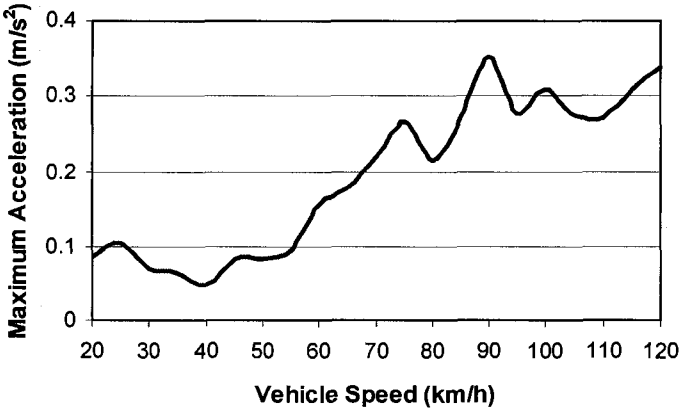

(b) Maximum Acceleration of Mid-Span

FIGURE 7.6 DYNAMIC RESPONSES OF MODEL 1 WITH FIVE DIAPHRAGMS UNDER LOAD 4, VEHICLE SPEED = 20 ~ 120 KM/H

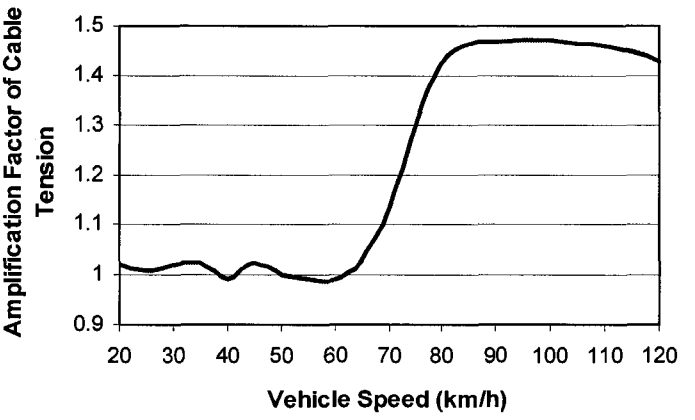

(c) Amplification Factor of Cable Tension for Cable #12

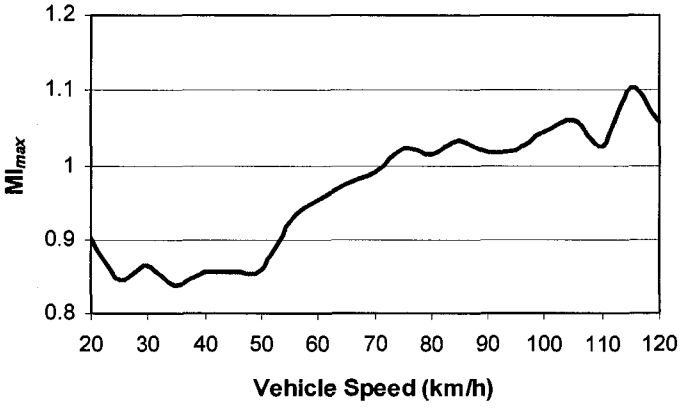

(d) Amplification Factor of Mid-span Longitudinal Bending Moment

FIGURE 7.6 DYNAMIC RESPONSES OF MODEL 1 WITH FIVE DIAPHRAGMS UNDER LOAD 4, VEHICLE SPEED = 20 ~ 120 KM/H (CONTINUED)

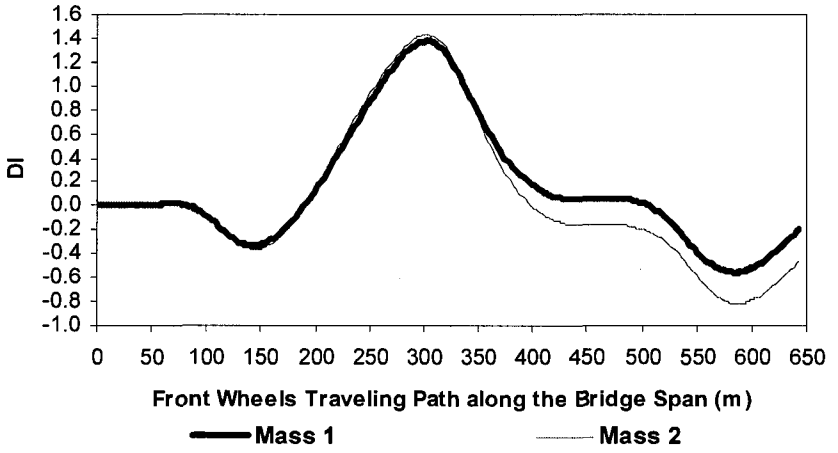

(a) Amplification Factor of Mid-Span Vertical Deflection

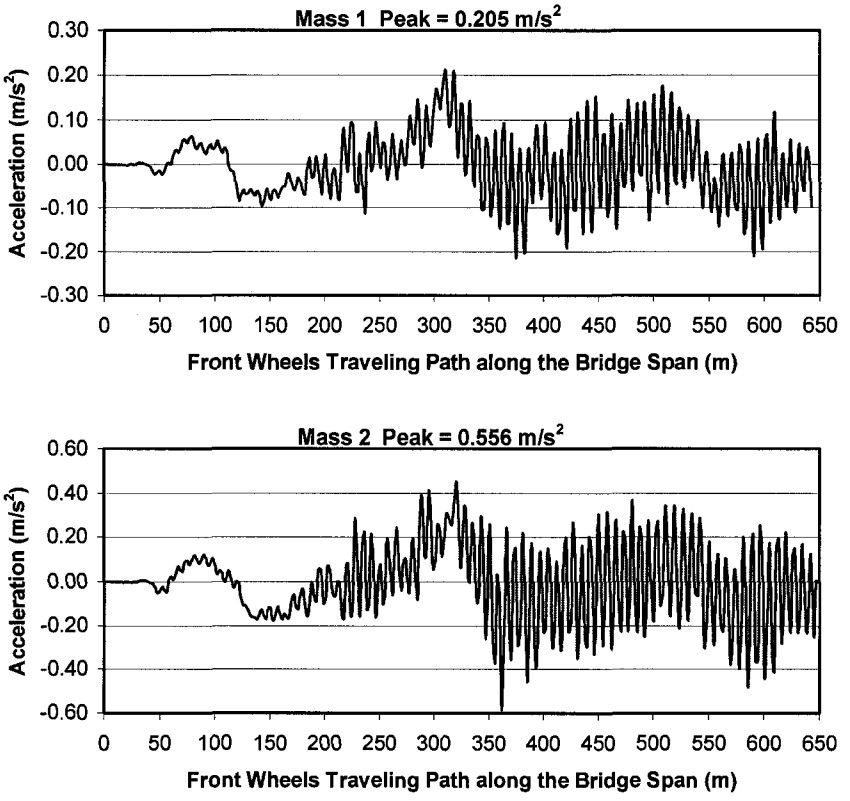

(b) Mid-span Acceleration

FIGURE 7.7 EFFECT OF VEHICLE-BRIDGE MASS RATIO ON DYNAMIC RESPONSES OF CABLE-STAYED BRIDGE

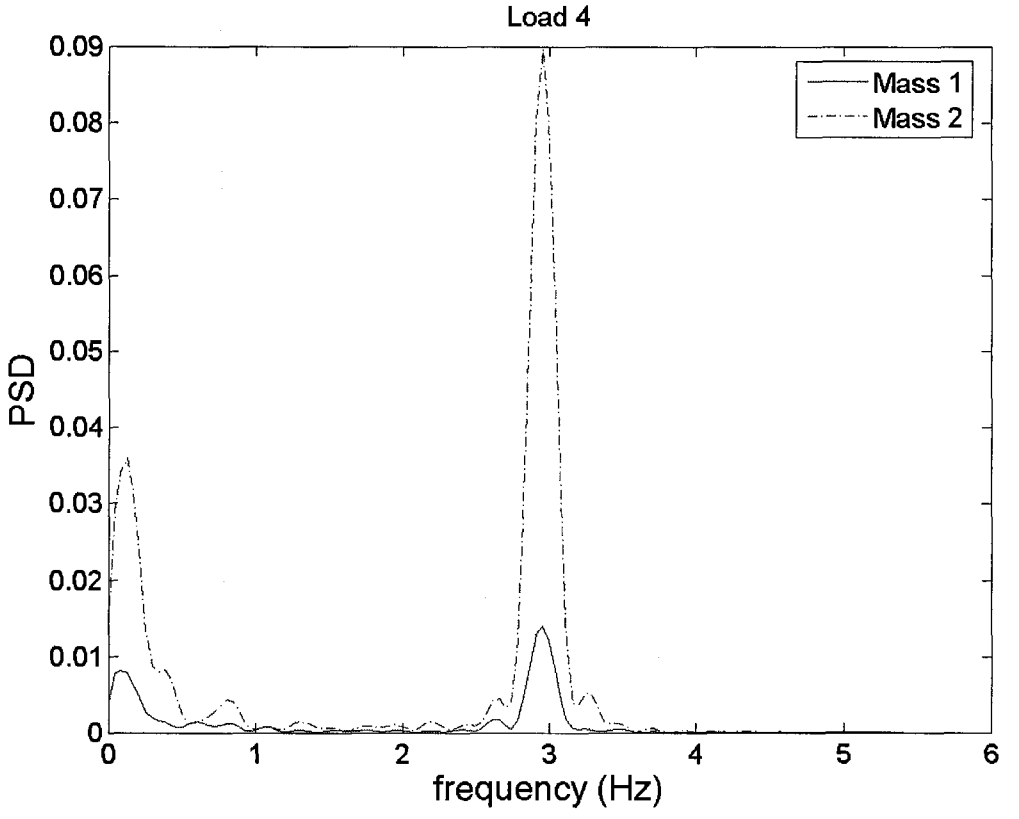

(c) Power spectral density of mid-span acceleration

FIGURE 7.7 EFFECT OF VEHICLE-BRIDGE MASS RATIO ON DYNAMIC RESPONSES OF CABLE-STAYED BRIDGE (CONTINUED)

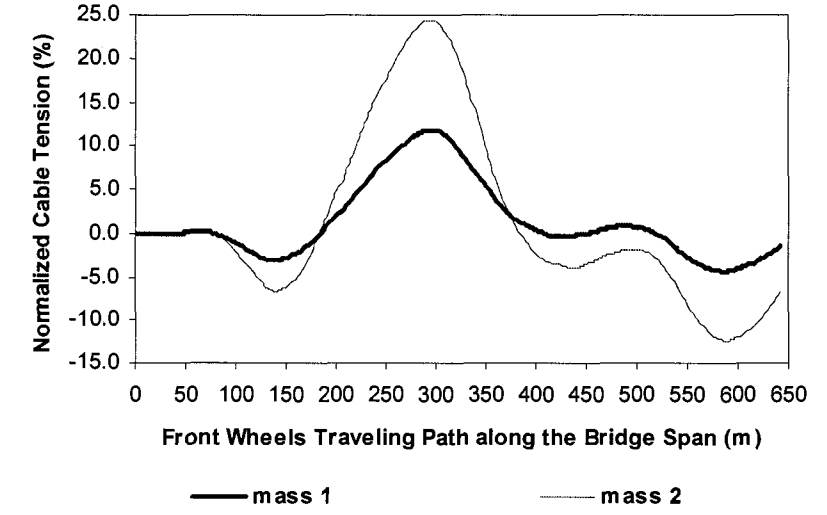

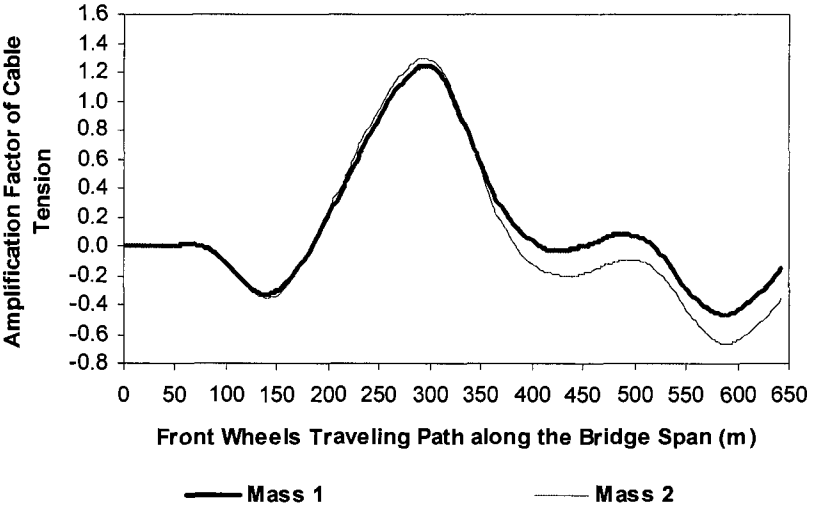

(d) Cable Tension of Cable #12

FIGURE 7.7 EFFECT OF VEHICLE-BRIDGE MASS RATIO ON DYNAMIC RESPONSES OF CABLE-STAYED BRIDGE (CONTINUED)

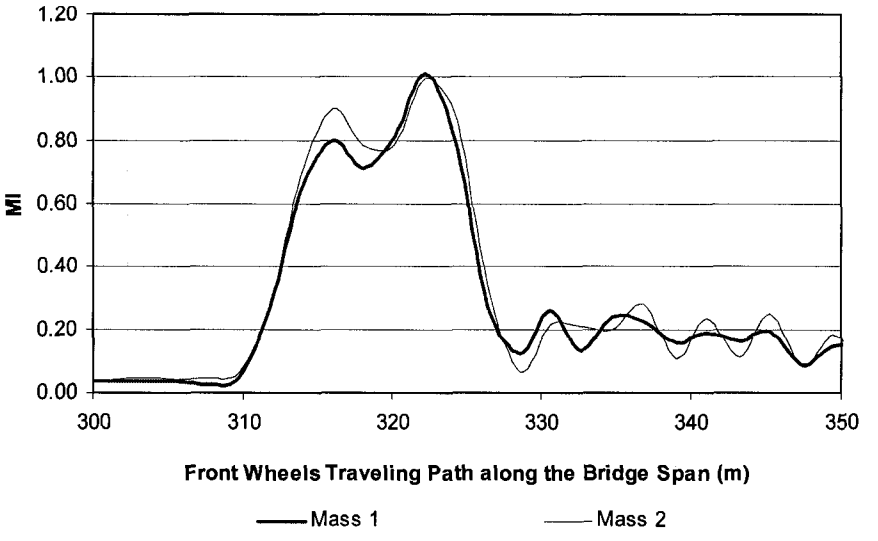

(e) Amplification Factor of Mid-span Longitudinal Bending Moment

FIGURE 7.7 EFFECT OF VEHICLE-BRIDGE MASS RATIO ON DYNAMIC RESPONSES OF CABLE-STAYED BRIDGE (CONTINUED)

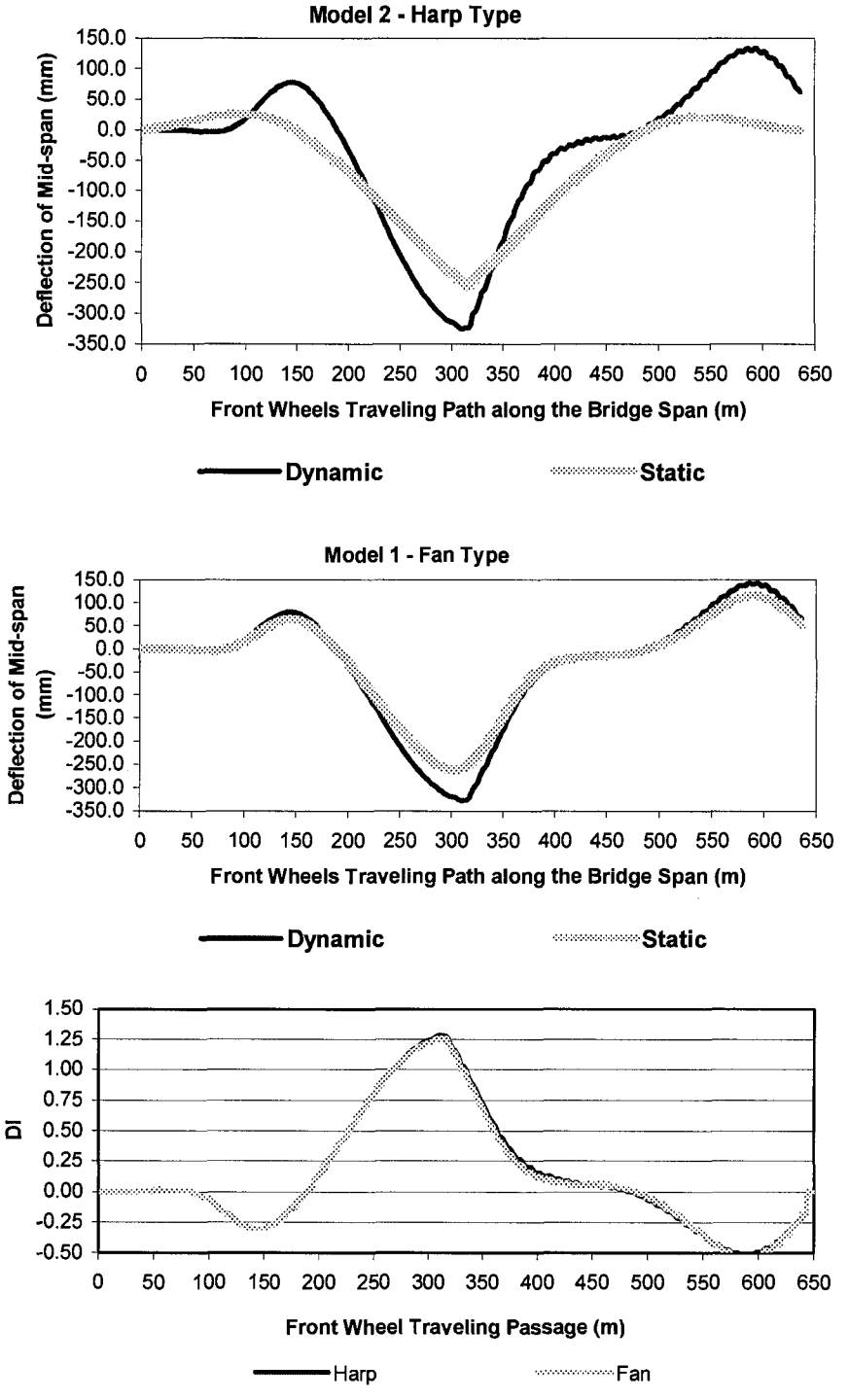

(a) Vertical Deflection of Mid-Span

FIGURE 7.8 EFFECT OF CABLE ARRANGEMENT ON DYNAMIC RESPONSES OF CABLE-STAYED BRIDGE

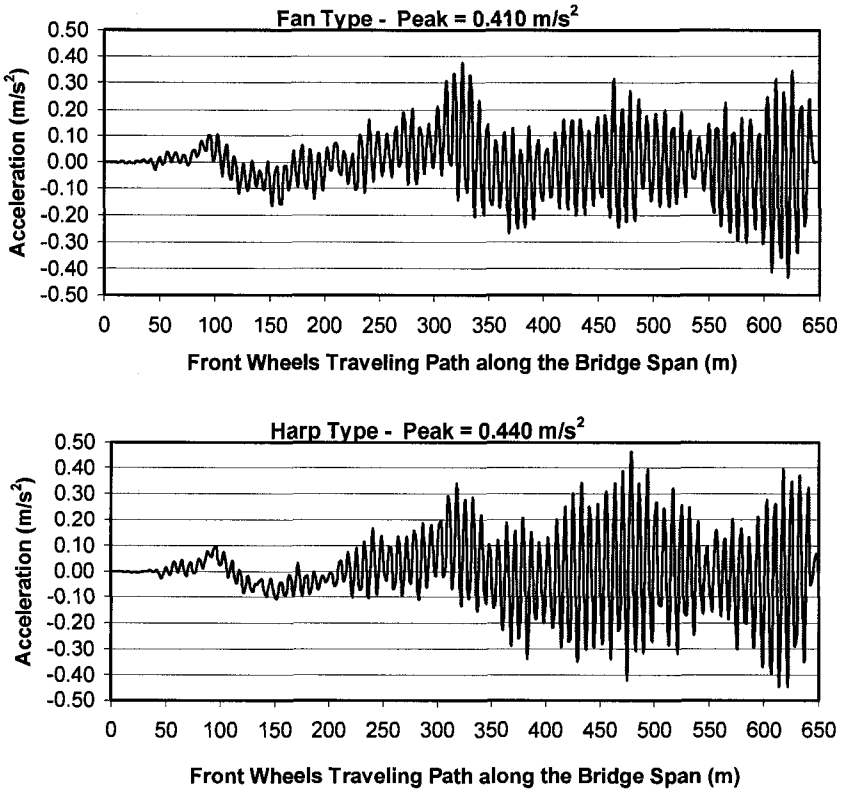

(b) Acceleration of Mid-span

FIGURE 7.8 EFFECT OF CABLE ARRANGEMENT ON DYNAMIC RESPONSES OF CABLE-STAYED BRIDGE (CONTINUED)

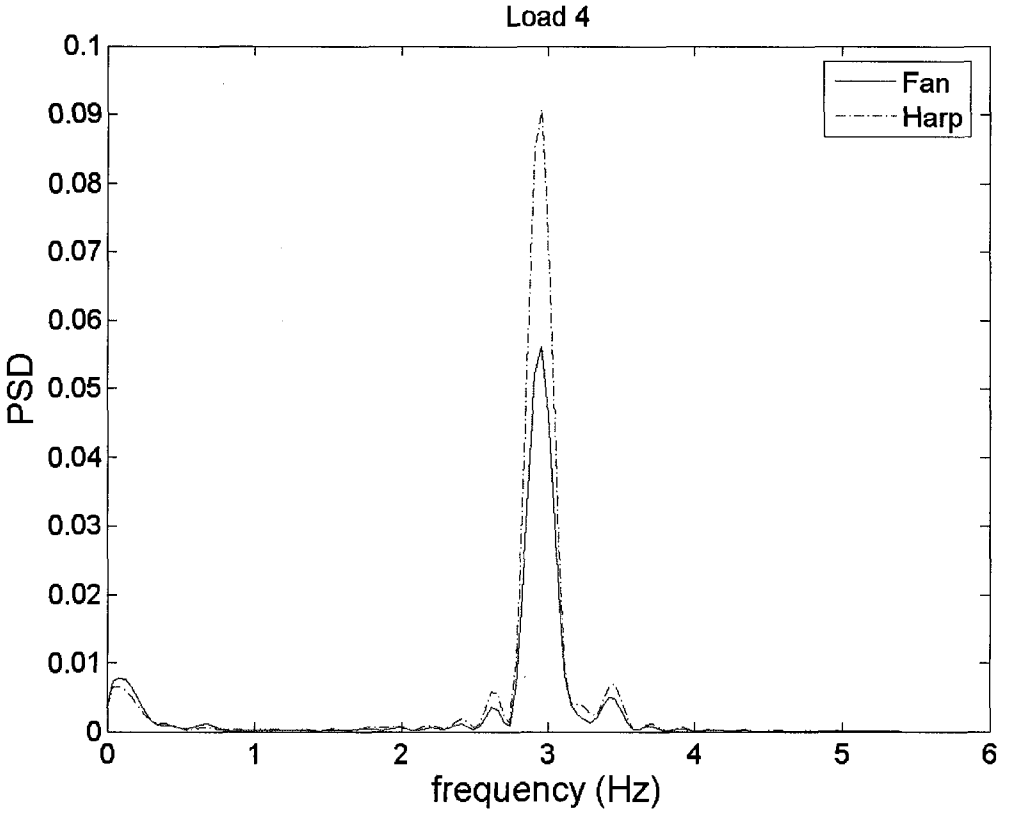

(c) Power spectral density of mid-span acceleration

FIGURE 7.8 EFFECT OF CABLE ARRANGEMENT ON DYNAMIC RESPONSES OF CABLE-STAYED BRIDGE (CONTINUED)

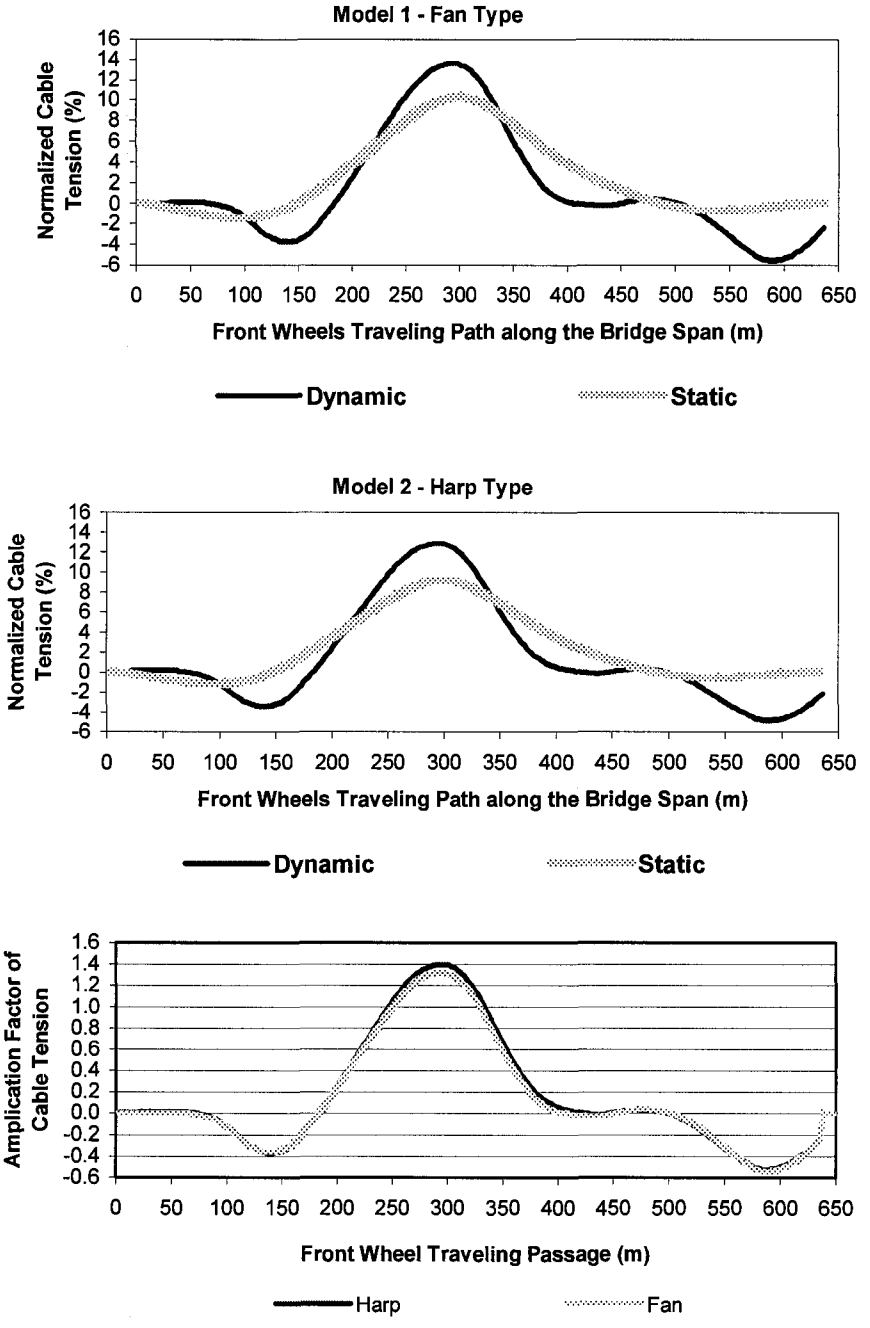

(d) Cable Tension of Cable #12

FIGURE 7.8 EFFECT OF CABLE ARRANGEMENT ON DYNAMIC RESPONSES OF CABLE-STAYED BRIDGE (CONTINUED)

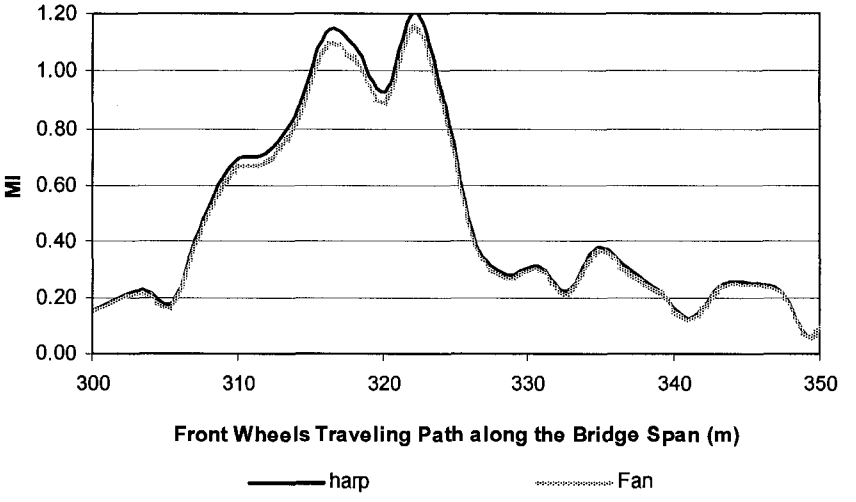

(e) Amplification Factor of Mid-span Longitudinal Bending Moment

FIGURE 7.8 EFFECT OF CABLE ARRANGEMENT ON DYNAMIC RESPONSES OF CABLE-STAYED BRIDGE (CONTINUED)

Chapter 8

CONCLUSIONS AND FURTHER WORK

8.1 Conclusions

The main objective of the current study is to investigate the nature and mechanics of the dynamic system of vehicle moving on a bridge, particular for long-span box-girder bridges and cable-stayed bridges. 3-D finite-element models have been developed for both box-girder bridge and cable-stayed bridge. A 3-D vehicle model is developed with a three-axle, six -wheel system. A computer program GLBA has been developed and employed in the analysis. Parametric studies are conducted to investigate the effect of several key parameters on the forced dynamic responses of box-girder bridge and cable-stayed bridge. In this work, each chapter is followed by a brief summary and conclusions. The main conclusions are rewritten and organized as follows.

Conclusions pertaining to box-girder bridges

Free Vibration analysis

1. In general, the proposed 8-node isoparametric shell element gives the best results. It is also the most efficient in convergence. Hence, the 8-node isoparametric shell element is chosen for the present study.

2. For bridges with long span, the lower modes are pure longitudinal flexure. The governing deformation in higher modes is also longitudinal flexure but occasionally combined with lateral flexure and torsion.

Forced Vibration analysis

1. Bridge-vehicle interaction can either increase or reduce bridge responses and the change can be significant. Long-span bridges are more pronounced to interaction than short-span bridges.
2. Increasing vehicle damping reduces the response of bridge but the reduction is not significant, especially for high vehicle speed. Further more, introduce of vehicle damping does not change the nature of the variation of response with variation of truck speed.
3. In general, the dynamic responses of bridge tend to increase with the increase of vehicle speed. The dynamic amplification factors due to bridge-vehicle interaction associated with higher vehicle speed are much more pronounced than lower vehicle speed.
4. The traffic load patterns play an important role in simulating the dynamic responses of box-girder bridges. Eccentric traffic load tends to produce larger amplification factor than central traffic load. Increasing the number of trucks can result in the increase of dynamic response. Distributing the trucks on multiple lanes can reduce the bridge responses.
5. Good agreement is obtained on the frequency contents of the forced vibration induced by traffic load when comparing the results of current study and field measurements.
6. Increasing the number of the trucks results in exciting lower predominant frequency, which brings great concern of bridge safety since the forced frequency is close to the fundamental frequency of the bridge. However the position of truck, whether central or eccentric, has little effect on the predominant frequency.
7. The results in present study agree with formulation of the AASHTO (1998) LRFD specifications to consider a simple one multiplier equal to 33% applied to the truck model only. The representation of the impact factor as a function of span length in

AASHTO (1992) or natural frequency in OHBDC (1991) does not fully address the complexity of bridge-vehicle interaction.

Conclusions pertaining to cable-stayed bridges

Free Vibration analysis

1. The elastic catenary cable element realistically reflects the dynamic characteristics of a stayed cable.
2. There is strong coupling in the three orthogonal directions, especially for torsion and flexure. It indicates that a three dimensional model can better reflect the dynamic characteristics of cable-stayed bridges than a two dimensional model. It is also evident that the close spacing of the natural frequencies is another feature in each case.
3. Solid plate diaphragms play an important role on the structural behavior of box-girder cable-stayed bridge. Providing diaphragms not only at ends but also at pylons and mid-span within the box can improve the torsional and lateral resistance, decrease the mid-span deflection and increase the torsional frequency.
4. Cable arrangement is an important parameter for cable-stayed bridge. The deck is more heavily stressed in a bridge of harp pattern than in a bridge of fan pattern under dead load. For lower modes, the natural frequencies in harp type are lower than in fan type, while for higher modes, both natural frequencies and mode shapes appear similar. Moreover, the harp type appears to have more torsional modes for lower frequencies.
5. The cumulative axial force under dead load increases as the number of cables increases. The structural stiffness may be changed if the axial force increases. For the two-pylon bridge, the bridge girder around the pylon is subjected to more compressive axial loads with more cables. Large compressive axial forces may reduce the stiffness of the bridge girder and lead to stability problems. On the other hand, the midpoint of the main span of the bridge is subjected to stronger tensile axial forces with the increase of number of cables. Strongly tensile axial forces may enhance the stiffness at the midpoint of the main span. However the number of stayed cables has minor influence on the dynamic characteristics of cable-stayed bridges.

6. Increasing deck inertia will attract considerable bending moments without appreciably reducing the forces in the cables and the deformation of mid-span under dead load. The natural frequencies do not increase proportionally with the increase of deck inertia. It indicates that the tension of stays play an important role for the stiffness of the entire structural system. It also reflects the non-linear characteristics of cable-stayed bridges.
7. Cable vibrations are basically induced by vortex shedding, rain vibration and wake galloping. Several methods can be adopted to restrain the stay movements. Few observation of cable vibration excited by traffic loads were reported in the literature. Therefore, dynamic interaction between the vibrating cables and the vibrating deck-tower system are not considered in the present study. Further studies will be conducted in the future to account for the combination effects of cable vibration coupled with deck-tower system by modeling each cable with multiple catenary elements.

Forced Vibration analysis

1. The dynamic responses induced by bridge-vehicle interaction are generally larger than the static responses due to equivalent static traffic load. In other wards, the peak amplification factors of cable-stayed bridge are mostly larger than 1.0.
2. In general, the amplification factors of mid-span deflection and cable tension are higher than the amplification factor of mid-span longitudinal bending moment.
3. Generally, a large number of modes are essential to obtain the realistic response. Because of adopting the 3-dimensional model of bridge and vehicle, traffic excitations may introduce special features into bridge response due to the complicated interaction between vehicle and bridge. For example, vertical vibrations of the bridge are introduced to a great extent by both lateral and torsional modes in addition to the longitudinal vertical modes. Modal coupling can not be captured in any 2-D analysis.
4. The traffic load patterns play an important role in simulating the dynamic responses of cable stayed bridge. Eccentric traffic load tends to produce larger bridge response than central traffic load, but the change in amplification factors is not pronounced. Increasing the number of trucks can result in the increase of both dynamic response and the amplification factors. Distributing the trucks on multiple lanes can reduce the bridge

responses. Fewer and evenly distributed trucks excite bridge vibration with higher frequency, while more and eccentric trucks trigger low frequency vibration, which is more significant to bridge safety since it is close to the fundamental frequency of the bridge.

5. Bridge damping has a significant effect upon the responses and should be always considered in the analysis. Increasing the bridge damping can result in decrease of the bridge responses.
6. In general, the dynamic responses of bridge tend to increase with the increase of vehicle speed. The dynamic amplification factors due to bridge-interaction associated with higher vehicle speed are much more pronounced than lower vehicle speed. Resonance can occur on the interaction system as the vehicle speed and frequencies of the bridge meet some specific relations, which can result in dramatic amplification of the response of each component.
7. Proving solid plate diaphragms can significantly improve the dynamic responses of box-girder cable-stayed bridge, especially at the ends of bridge, at pylons and at mid-span.
8. Cable arrangement and increase of vehicle weight have minor influence on the amplification factors. However, larger mid-span acceleration is observed in harp-type than in fan-type.

8.2 Future Work

The following investigations need to be carried out to have a more thorough understanding of dynamic responses of long-span bridges subjected to traffic loading:

1. Considering using finite strip method to model the bridges in order to reduce the number of elements and save CPU time;
2. Comparing different stiffness ductility model for non-linear inelastic analysis;
3. Developing a mathematic model to analyze moving road vehicles on a long-span bridge under crosswind;
4. Considering road roughness.

References

1. AASHTO (1992). ''Standard specifications for highway bridges", Washington, D.C.
2. AASHTO (1998). LRFD Bridge Design Specifications, 3rd edition, American Association of State Highway and Transportation Officials, Washington, D.C.
3. Abdel-Ghaffar, A.M. and Khalifa, M.A. (1991). "Importance of cable vibration in dynamic of cable-stayed bridges", J. Eng. Mechanics, ASCE, 117 (11), 2571-2589.
4. Abdel-Ghaffar, A.M. and Nazmy, A.S. (1991). '2-D nonlinear seismic behavior of cable-stayed bridges', J. Struct. Eng., ASCE, 117 (11), 3456-3476.
5. Akin, J. E. and Mofid, M. (1989). "Numerical solution for response of beams with moving mass", J. Struct. Eng., ASCE, 94 (3), 761-781.
6. Ali, H.M. and Abdel-Ghaffar, A.M. (1995). "Modeling the nonlinear seismic behavior of cable-stayed bridges", Computers and Structures, 54, pp. 461-492.
7. Bathe KJ. (1996). "Finite element procedures", Englewood Cliffs, New Jersey: Prentice-Hall.
8. Blejwas, T. E., Feng, C. C. and Ayre, R. S. (1979). "Dynamic interaction of moving vehicles and structures", J. Sound and Vibration, 67 (4), 513-521.
9. Brownjohn, J. M. W. and Xia, P. Q. (2000). "Dynamic assessment of curved cable-stayed bridge by model updating", J. Struct. Eng., ASCE, 126 (2), 252-260.
10. Calcada, R., Cunha, A. and Delgado, R. (2005). "Analysis of traffic-induced vibrations in a cable-stayed bridge. Part II: numerical modeling and stochastic simulation", J. Bridge Eng., ASCE, 10(4), 386-397.
11. CHBDC (2000). "The Canadian Highway Bridge Design Code", CSA-S6-00.
12. Chang, D. and Lee, H. (1994). "Impact factor for simple-span highway girder bridges", J. Struct. Eng., ASCE, 120 (3), 704-715.
13. Chang, C. C., Chang, T.Y.P., and Zhang, Q. W. (2001). "Ambient vibration of long-span cable-stayed bridge", J. Bridge Eng., ASCE, 6 (1), 46-53.

14. Chen, D. W. and Xiang, H. F. (1988). "Practical method of the second order theory of cable-stayed bridges" (in Chinese). Journal of Urban Road Bridge and Flood Control, 1(1), 1-12.
15. Cheung, M.S. and Megnounit, A. (1991). "Parametric study of design variations on the vibration modes of box girder bridges". Can. J. Civ. Eng., 18, 789-798.
16. Cheung, M.S., Tadros, G.S., Brown, T., Dilger, W.H., Dilger, W.H., Ghali, A. and Lau, D.T. (1997). "Field monitoring and research on performance of the Confederation Bridge". Can. J. Civ. Eng., 24, 951-962.
17. Chu, K. H., Garg, V. K., and Wang, T. L. (1986). "Impact in railway prestressed concrete bridges", J. Struct. Engrg., ASCE, 112 (5), 1036-1051.
18. Croce, P. and Salvatore, W. (2001). "Stochastic model for multilane traffic effects on bridges", J. Bridge Eng., ASCE, 6 (2), 136-143.
19. Cunha, A., Caetano, E., and Delgado, R. (2001). "Dynamic tests on large cable-stayed bridge", J. Bridge Eng., ASCE, 6 (1), 54-62.
20. Ernst, J. H. (1965). "Der E-Modul von Seilen unter Berucksichtiguns des Durchanges", Der Bauingenieur, 40, No. 2.
21. Fleming, J. F. and Egeseli, E. (1980). "Dynamic behavior of cable-stayed bridges", J. Earthquake Engrg. & Struct. Dynamics, 8 (1), 1-16.
22. Galdos, N. H., Schelling, D. R. and Sahin, M. A. (1993). "Methodology for impact factor of horizontally curved box bridges", J. Struct. Engrg., ASCE, 119 (6), 1917-1934.
23. Gambhir ML and Batchelor B. A. (1977). "Finite element for 3-D pre-stressed cablenets", Int J Numer Meth Engng, 11, 1699-718.
24. George, H. W. (1999). "Influence of deck material on response of cable-stayed bridge to live loads", J. Bridge Engrg., ASCE, 4 (2), 136-142.
25. Gorman, D. J. (1982). "Free vibrations analysis of rectangular plates", Elsevier North Holland Inc.
26. Hinton, E. and Owen, D. R. J. (1984). "Finite element software for plates and shells", Swansea, U.K. : Pineridge Press.
27. Hutton, S. G. and Cheung, Y. K. (1979). "Dynamic response of single highway bridges", J. Earthquake Eng. and Struct. Dynamics, 7 (6), 543-554.

28. Hwang, E. S., and Nowak, A. S. (1991). "Simulation of dynamic load for bridges", J. Struct. Engrg., ASCE, 117 (5), 1413-1434.
29. Huang, D., Wang, T. L. and Shahawy, M. (1992). "Impact analysis of continuous multigirder bridges due to moving vehicles", J. Struct. Eng., ASCE, 118 (12), 3427-3443.
30. Humar, J. L. (1990). "Dynamics of structures", Englewood Cliffs, N.J., Prentice Hall.
31. Humar, J. L. and Kashif, A. M. (1992). "Dynamic response of bridges under travelling loads", Can. J. Civ. Eng., Ottawa, Canada, 20 (2), 287-298.
32. Humar, J. L. and Kashif, A. M. (1995). "Dynamic response analysis of slab-type bridges", J. Struct. Engrg., ASCE, 121 (1), 48-62.
33. Huang, D., Wang, T. L. and Shahawy, M. (1995). "Vibration of thin-walled box-girder bridges excited by vehicles", J. Struct. Eng., ASCE, 121 (9), 1330-1337.
34. Inbanathan, M. J. and Wieland, M. (1987). "Bridge vibrations due to vehicle moving over rough surface", J. Struct. Engrg., ASCE, 113 (9), 1994-2008.
35. Irvine, H.M. (1981). "Cable structures", The MIT Press, Cambridge, Massachusetts, and London, England.
36. Jayaraman, HB and Knudson, WC. A (1981). "Curved element for the analysis of cable structures", Computers and Structures, 14 (3-4).
37. Jeffcott, H. H. (1929). "On the vibration beams under the action of moving loads", Phil. Mag., 7 (8), 66.
38. Karoumi, R. (1996). "Dynamic response of cable-stayed bridges subjected to moving vehicles", IABSE 15th Congress, Danmark, 87-92.
39. Karoumi, R. (1999). "Some modeling aspects in the nonlinear finite element analysis of cable supported bridges", Computers and Structures, Vol. 71, No. 4, pp. 397 – 412.
40. Karoumi, R. (2000). "Modeling of Cable Stayed Bridges for Analysis of Traffic InducedVibrations", IMAC-XVIII Conference on Structural Dynamics, San Antonio, Texas USA.
41. Kashif, A. H. (1992). "Dynamic response of highway bridges to moving vehicles", PhD thesis, Carleton University, Canada.
42. Kou, J.W., and DeWolf, J.T. (1997). "Vibrational behavior of continuous span highway bridge- influencing variables", J. Struct. Eng., ASCE, 123 (3), 333-344.

43. Morris, N.F. (1974). "Dynamic analysis of cable-stiffened structures", J. Struct. Eng., ASCE, 100 (5), 971-981.
44. Morris, N. F. (1976). "Analysis of cable-stiffened space structures", J. Struct. Eng., ASCE, 102 (3), 501-513.
45. Naumoski, N., Cheung, S. and Foo, S. (2004). "Dynamic performance of the Confederation Bridge due to traffic and wind", Can. J. Civ. Eng. 31: 487-498.
46. Nassif, H.H., Liu, M., and Ertekin, O. (2003). "Model validation for bridge-road-vehicle dynamic interaction system", J. Bridge Eng., ASCE, 8(2), 112-120.
47. Nazmy, A.S. and Abdel-Ghaffar, A.M. (1990). "Three-dimensional nonlinear static analysis of cable-stayed bridges", Computers & structures, Vol. 34, No. 2, pp. 257 – 271.
48. O'Brien, W.T. and Francis, A.J. (1964). "Cable movements under two-dimensional loads", J. Struct. Division, ASCE, 90 (3), 89-123.
49. O'Brien, W.T. (1967). "General solution of suspended cable problems", J. Struct. Division, ASCE, 93 (1), 1-26.
50. Ohashi, M. (1991). "Cables for cable-stayed bridges", Cable-Stayed Bridges - Recent Developments and their Future, M. Ito et al. (Editors), Elsevier Science Publishers B.V.
51. Ozdemir H.A. (1979). "Finite element approach for cable problems", Int J. Solids Structures, 15, 427-37.
52. Pan, T. C., and Li, J. (2002). "Dynamic vehicle element method for transient response of coupled vehicle-structure systems", J. Struct. Eng., ASCE, 128 (2), 333-344.
53. Peyrot, A.H. and Goulois A.M. (1978). "Analysis of flexible transmission lines", J. Struct. Division, ASCE, 194 (5), 763-779.
54. Peyrot, A.H. and Goulois A.M. (1979). "Analysis of cable structures", Computers & structures, Vol. 10.
55. Rasoul, M. (1981). "Dynamic analysis of cable-stayed bridges", PhD thesis, Purdue University, Lafayette, Ind.
56. Ren, W. X. (1999). "Ultimate behavior of long-span cable-stayed bridges", J. Bridge Engrg., ASCE, 4 (1), 30-37.
57. Shu, H.S. and Yang, Y.C. (2001). "Stability analysis of box-girder cable-stayed bridges", J. Bridge Eng., ASCE, 6(1), 63-68.

58. Sridharan, N. and Mallik, A. K. (1979). "Numerical analysis of vibration of beams subjected to moving loads", J. Sound and Vibration, 65 (1), 147-150.
59. Tadros, G. (1997). "The Confederation Bridge: an overview". Can. J. Civ. Eng., 24, 850-866.
60. Tan, C. P. and Shore, S. (1968a). "Dynamic response of a horizontally curved bridge", J. Struct. Engrg., ASCE, 94 (3), 761-781.
61. Tan, C. P. and Shore, S. (1968b). "Response of horizontally curved bridge to moving load", J. Struct. Engrg., ASCE, 94 (3), 761-781.
62. Timoshenko, S., Young, D. H. and Weaver, W. Jr. (1974). "Vibration problems in engineering", 4th Ed., Wiley, New York, NY.
63. Trahair, N.S. (1993). "Flexural Torsional Bucking of Structures", CRC Press, Boca Raton, FL, USA.
64. Walther, R., Isler, W. and Moia, P. (1985). "Cable stayed bridges", Thomas Telford, London.
65. Warburton, G. B. (1976). "The dynamic behavior of structures", 2th Ed., Pergamon Press, Oxford, England.
66. Wang, T.L., Garg, V. K., and Chu, K. H. (1991). "Railway bridge / vehicle interaction studies with new vehicle model", J. Struct. Eng., ASCE, 117 (7), 2099-2116.
67. Wang, T.L., and Huang, D. (1992). "Cable-stayed bridge vibration due to road surface roughness", J. Struct. Eng., ASCE, 118 (5), 1354-1374.
68. Wang, Y.C. (1999). "Number of cable effects on buckling analysis of cable-stayed bridges". J. Bridge Eng., ASCE, 4(4), 242-248.
69. Weaver, W. Jr. and Gere, J. (1980). "Matrix Analysis of Framed Structures", 2nd Edn. D. Van Nostrand, New York.
70. Xu, Y.L. and Guo, W.H. (2003). "Dynamic analysis of coupled road vehicle and cable-stayed bridge systems under turbulent wind", Elsevier Engineering Structures, 25, 473-486.
71. Yang, F.H. and Fonder, G.A. (1998). "Dynamic response of cable-stayed bridges under moving loads", J. Eng. Mechanics, ASCE, 124(7), 741-747.
72. Yang, Y. B., and Yau, J. D. (1997). "Vehicle-bridge interaction element for dynamic analysis", J. Struct. Eng., ASCE, 123 (11), 1512-1518.

73. Yang, Y. B., and Lin, B. H. (1995). "Vehicle-bridge interaction analysis by dynamic condensation method", J. Struct. Eng., ASCE, 121 (11), 1636-1643.
74. Zhang, Q. W., Chang, T.Y.P., and Chang, C. C. (2001). "Finite-element model updating for the Kap Shui Mun cable-stayed bridge", J. Bridge Eng., ASCE, 6 (4), 285-293.
75. Zhang, Q. W., Fan, L.C., and Yuan, W. C. (2002). "Traffic-induced variability in dynamic properties of cable-stayed bridge", Earthquake Engineering and Structural Dynamics, 31, 2015-2021.